

# Nonstandard heavy mesons and baryons: Experimental evidence


Stephen Lars Olsen\*

*Center for Underground Physics, Institute for Basic Science, Daejeon 34126 Korea*

Tomasz Skwarnicki†

*Department of Physics, Syracuse University, Syracuse, New York 13244, USA*

Daria Zieminska‡

*Department of Physics, Indiana University, Bloomington, Indiana 47405-71055, USA*
 (published 8 February 2018)

Quantum chromodynamics (QCD), the generally accepted theory for strong interactions, describes the interactions between quarks and gluons. The strongly interacting particles that are seen in nature are hadrons, which are composites of quarks and gluons. Since QCD is a strongly coupled theory at distance scales that are characteristic of observable hadrons, there are no rigorous, first-principle methods to derive the spectrum and properties of the hadrons from the QCD Lagrangian, except for lattice QCD simulations that are not yet able to cope with all aspects of complex and short-lived states. Instead, a variety of “QCD inspired” phenomenological models have been proposed. Common features of these models are predictions for the existence of hadrons with substructures that are more complex than the standard quark-antiquark mesons and the three-quark baryons of the original quark model that provides a concise description of most of the low-mass hadrons. Recently, an assortment of candidates for nonstandard multi-quark mesons, meson-gluon hybrids, and pentaquark baryons that contain heavy (charm or bottom) quarks has been discovered. Here the experimental evidence for these states is reviewed and some general comparisons of their measured properties with standard quark model expectations and predictions of various models for nonstandard hadrons are made. The conclusion is that the spectroscopy of all but the simplest hadrons is not yet understood.

DOI: 10.1103/RevModPhys.90.015003

## CONTENTS

I. Introduction	2	C. Lattice QCD	12
A. Color charges, gluons, and QCD	2	III. Heavy Flavor Experiments	13
1. Asymptotic freedom and confinement	2	IV. Heavy-light Exotic Hadron Candidates	18
B. The QCD dilemma	3	V. Neutral Exotic Hadron Candidates	21
C. Searches for light “nonstandard” hadrons	4	A. $X(3872)$	21
D. Heavy quarks and the quarkonium spectra	5	B. $X(3915)$	25
1. The $b$ quark and the spectrum of bottomonium mesons	5	1. Is the $X(3915)$ the $\chi_{c0}$ charmonium state?	26
2. Nonstandard quarkoniumlike mesons and quarkonium pentaquarks	5	2. Is the $X(3915)$ a $c\bar{c}s\bar{s}$ four-quark state?	26
3. Comments on units, terminology, and notation	6	3. Discussion	27
II. Models for Nonstandard Hadrons	8	C. $Y(4260)$ and other $J^{PC} = 1^{--}$ states	27
A. QCD-color-motivated models	9	1. BESIII as a “ $Y(4260)$ factory”	28
1. QCD diquarks	9	2. Discussion	30
2. QCD hybrids	9	D. $X(4140)$ and other $J/\psi\phi$ structures	30
B. Other models	10	1. The six-dimensional LHCb amplitude analysis	32
1. Hadronic molecules	10	2. Charmonium assignments for the $J/\psi\phi$ states?	33
2. Hadrocharmonium	10	E. $X^*(3860)$ , $X(3940)$ , and $X(4160)$	34
3. Born-Oppenheimer model	10	1. $X^*(3860) \rightarrow D\bar{D}$ , an alternative $\chi_{c0}(2P)$ candidate?	34
4. Kinematically induced resonancelike mass peaks	11	2. $X(3940) \rightarrow D\bar{D}^*$	34
		3. $X(4160) \rightarrow D^*\bar{D}^*$	35
		4. Discussion	35
		VI. Charged Nonstandard Hadron Candidates	35
		A. $Z(4430)^+$ and similar structures in $B$ decays	36
		1. The $Z(4430)^+ \rightarrow \psi'\pi^+$ in $B \rightarrow \psi'\pi^+K$ decays	36
		2. The $Z(4200)^+ \rightarrow J/\psi\pi^+$ in $\bar{B}^0 \rightarrow J/\psi\pi^+K^-$ decays	37

\*solsen@ibs.re.kr

†tskwarni@syr.edu

‡daria@indiana.edu

3. Charged $\chi_{c1}\pi^+$ resonances in $\bar{B}^0 \rightarrow \chi_{c1}\pi^+ K^-$ decays	37
4. Discussion	38
B. Charged $Z_b^+$ and $Z_c^+$ states produced in $e^+e^-$ processes	38
1. The $Z_b$ charged bottomoniumlike mesons	38
2. The $Z_c$ charged charmoniumlike mesons	41
VII. Pentaquark Candidates	43
VIII. Summary and Future Prospects	46
A. Theory	46
1. Molecules	46
2. Diquarks	49
3. QCD hybrids	51
4. Hadrocharmonium	51
5. Kinematically induced resonancelike peaks	51
6. Comments	51
B. Experiment	52
C. Final remark	53
Acknowledgments	53
References	53

## I. INTRODUCTION

The major breakthrough in our understanding of the spectrum of subatomic hadrons was the nearly simultaneous realization by Gell-Mann (1964) and Zweig (1964) that hadrons could be succinctly described as composites of fractionally charged fermions with baryon number  $B = 1/3$ , called “quarks” by Gell-Mann and “aces” by Zweig. The original quark model had three different flavored quarks:  $q = u^{+2/3}$ ,  $d^{-1/3}$ , and  $s^{-1/3}$  (now called the light flavors)<sup>1</sup> and their  $B = -1/3$  antiparticles  $\bar{q} = \bar{u}^{-2/3}$ ,  $\bar{d}^{+1/3}$ , and  $\bar{s}^{+1/3}$ . The most economical quark combinations for producing  $B = 0$  mesons and  $B = 1$  baryons are  $q\bar{q}$  and  $qqq$ ,<sup>2</sup> respectively, and these combinations reproduce the pseudoscalar and vector meson octets and the spin-1/2 and spin-3/2 baryon octet and decuplet that were known at that time. Nevertheless, both authors noted in their original papers that more complex structures with integer charges and  $B = 0$  or  $B = 1$  could exist, such as  $qqq\bar{q}$  “tetraquark” mesons and  $qqq\bar{q}q$  “pentaquark” baryons. However, no candidates for these more complicated configurations were known at the time.

### A. Color charges, gluons, and QCD

The original quark model implied violations of the Pauli exclusion principle. For example, the quark model identifies the  $J = 3/2$   $\Omega^-$  baryon as a state that contains three  $s$  quarks that are all in a relative  $S$  wave and with parallel spins; i.e., the three  $s$  quarks occupy the same quantum state, in violation of Pauli’s principle. This inspired a suggestion by Greenberg (1964) that quarks were not fermions but, instead,

<sup>1</sup>The  $u$  and  $d$  quarks form an isospin doublet:  $u$  with  $I_3 = 1/2$  and  $d$  with  $I_3 = -1/2$ . The  $s$  quark has a nonzero additive flavor quantum number called strangeness; for historical reasons the  $s$  quark has negative strangeness  $S = -1$  and the  $\bar{s}$  quark has positive strangeness  $S = +1$ .

<sup>2</sup>For simplicity of notation, flavor indices are suppressed. In combinations such as  $qqq$  and  $q\bar{q}$ , it is implicitly assumed that each  $q$  can have any one of the three light-quark flavors.

“parafermions” of the order of 3, with an additional hidden quantum number that made them distinct. In this picture, the three  $s$  quarks in the  $\Omega^-$  have different values of this hidden quantum number and are, therefore, nonidentical particles.

In the following year, Han and Nambu (1965) proposed a model in which each of the quarks are  $SU(3)$  triplets in flavor space (and with integer electric charges) with strong-interaction “charges” that are a triplet in another  $SU(3)$  space. They identified Greenberg’s hidden quantum numbers with three different varieties of strong charges  $q \rightarrow q_i$ ,  $i = 1, 2$ , and 3, and associated the observable hadrons as singlets in the space of this additional  $SU(3)$  symmetry group. This can be done with three-quark combinations in which each quark has a different strong charge (baryons =  $\epsilon_{ijk}q_iq_jq_k$ ) or quark-antiquark combinations, where the quark’s strong charge and the antiquark’s strong anticharge are the same type (mesons =  $\delta^i_jq_i\bar{q}^j$ ). Because of the correspondence between these prescriptions with the rules for human color perception, where white can be produced either by triplets of three primary colors or by color plus complementary-color pairs, the strong-interaction charges were soon named “color” charges: red, green, and blue, with anticharges that are the corresponding complementary colors: cyan, magenta, and yellow. The color neutral combinations that form baryons, antibaryons, and mesons are illustrated in Fig. 1(a).

Measurements of the total cross section for  $e^+e^- \rightarrow$  hadrons were consistent with the existence of the 3 color degrees of freedom (Litke *et al.*, 1973). The generalization of the Han-Nambu idea to a gauge theory with quarks of fractional electric charge was done in 1973 (Bardeen, Fritsch, and Gell-Mann, 1972) and is called quantum chromodynamics (QCD). This is now the generally accepted theory for the strong interactions.

### 1. Asymptotic freedom and confinement

In QCD, the color force is mediated by eight massless vector particles called gluons, which are the generalization of the photon in quantum electrodynamics (QED). Unlike QED in which the photons are electrically neutral and do not interact with each other, the gluons of QCD have color charges and, thus, interact with each other. Figure 1(b) shows a single gluon exchange between two colored quarks. In QED, the vacuum polarization diagram, shown in Fig. 2(a), results in a modification of the QED coupling strength  $\alpha_{\text{QED}}$  that makes it

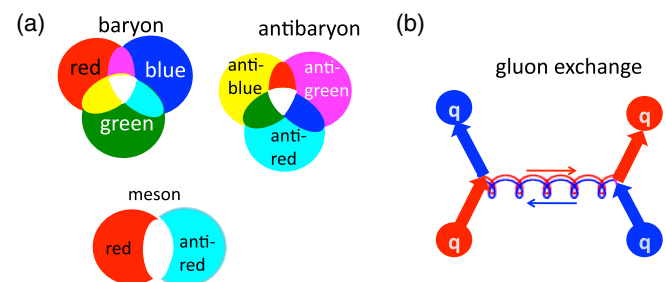


FIG. 1. (a) The color makeup of baryons, antibaryons, and a meson. (b) Single gluon exchange between two quarks. Gluons have two color indices that can be viewed as two color charges that propagate in opposite directions.

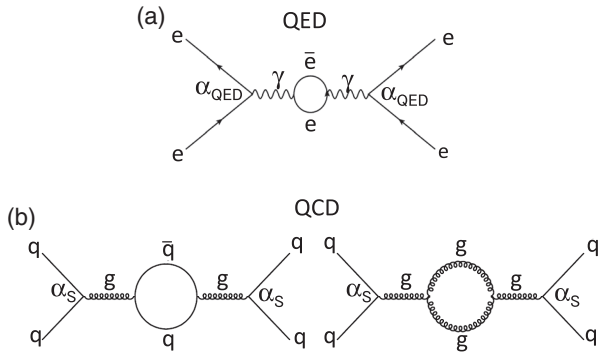


FIG. 2. (a) The lowest-order QED vacuum polarization diagram for electron-electron scattering. (b) The lowest-order QCD vacuum polarization diagrams for quark-quark scattering.

decrease with increasing distance. For distance scales of the order of 1 m,  $\alpha_{\text{QED}} \approx 1/137$ ; at a distance scale of 0.002 fm, comparable to the Compton wavelength of the  $Z^0$  weak vector boson,  $\alpha_{\text{QED}} \approx 1/128$ .

In QCD, the gluon-gluon interaction includes additional vacuum polarization diagrams that have virtual gluon loops as shown in Fig. 2(b). These gluon loops modify the QCD coupling strength  $\alpha_s$  in a way that is opposite to that of its QED counterpart: they cause  $\alpha_s$  to *decrease* at short distances and *increase* at long distances (Gross and Wilczek, 1973; Politzer, 1973) as illustrated in Fig. 3. The relatively small value of the coupling strength at short distances,  $\alpha_s = 0.1185 \pm 0.0006$  at  $r \approx 0.002$  fm, results in what is called “asymptotic freedom” and facilitates the use of perturbation expansions to make reliable (albeit difficult) first-principle calculations for short-distance, high-momentum-transfer processes such as those studied in the high- $p_T$  detectors at CERN’s Large Hadron Collider (LHC). In contrast, for distance scales of that approach  $r \sim 1$  fm, which are characteristic of the sizes of hadrons,  $\alpha_s \sim \mathcal{O}(1)$  and perturbation expansions do not converge. This increase in the coupling strength for large quark separations is the source of “confinement,” i.e., the reason that isolated colored particles, be they quarks or gluons, are never seen. The only strongly interacting particles that can exist in isolation are color-charge-neutral (i.e., white) hadrons.

## B. The QCD dilemma

In QCD, the component of the standard model (SM) of elementary processes that deals with the strong interaction, the elementary particles are the color-charged quarks and gluons. However, a consequence of confinement is that these particles are never seen in experiments. Although the QCD Lagrangian is expected, in principle, to completely describe the spectrum of hadrons and all of their properties, there is no rigorous first-principle translation of this into any useful mathematical expressions.

The quark and gluon composition of hadrons can be hopelessly complex, as illustrated in the inset on the right side of Fig. 3. For distance scales on the order of 1 fm, the typical size of a hadron  $\alpha_s \sim 1$  and the pattern illustrated in the figure is just one of an infinite number of possible quark-gluon configurations that are subject only to the constraints that they

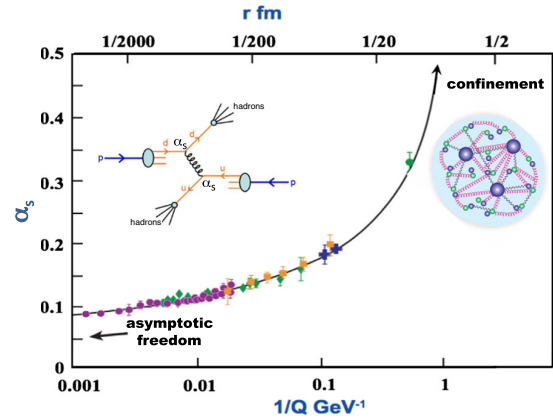


FIG. 3. The behavior of the QCD coupling strength  $\alpha_s$  as a function of the inverse momentum transfer  $1/Q$  or, equivalently, the quark separation distance  $r$ . Descriptions of the data points and the associated references are provided in Patrignani *et al.* (2016).

have appropriate quantum numbers and are color neutral. In fact, while the traditional three quarks form baryons and quark-antiquark pairs form mesons the prescription works well for the meson octets and the baryon octet and decuplet that were known at the time quarks were first introduced, it fails in a number of other areas. Soon after the quark model was proposed, it was realized that these simple rules failed to provide a satisfactory explanation for the properties of the lowest-mass scalar-meson octet (Jaffe, 1977a) and were unable to provide a simple explanation for the positive parity of the lowest-lying excitation of the proton, the  $J^P = 1/2^+ N^*(1440)$  (the “Roper resonance”) (Alvarez-Ruso, 2010) or the mass of the lowest-lying excitation of the  $\Lambda$  hyperon, the  $J^P = 1/2^- \Lambda(1405)$  (Close and Dalitz, 1980).

A fundamental process that can be computed with perturbative QCD is quark-quark elastic scattering at high-momentum transfer. This shows up in high-energy  $pp$  collider experiments as events with two high transverse momentum jets of hadrons that are nearly back to back in azimuth. The theoretical description of this process is based on calculations of the diagram shown in the inset on the left side of Fig. 3. Here, in lieu of a beam or target of isolated quarks, the beam and target particles are quarks contained inside the colliding protons. The momentum distribution of quarks inside the proton is governed by long-distance QCD and approximated by universal parton distribution functions that are taken from fits to data from hadron-collider measurements at lower center of mass (c.m.) energies, deep-inelastic lepton-proton scattering experiments, etc. The fundamental QCD  $qq \rightarrow qq$  process at the core of the diagram has been computed up to  $\mathcal{O}(\alpha_s^3)$ , but the properties of the final-state quarks cannot be directly measured and, instead, have to be inferred from the jets of hadrons that they produce; for this, empirical “fragmentation functions” are employed. Thus, even processes that are amenable to perturbative QCD calculations involve significant long-distance QCD effects in both the initial and final states.

This nearly total disconnect between the hadrons that we observe in experiments and the quarks and gluons that appear

in the theory is a problem of large proportions in particle physics.<sup>3</sup> This is what we refer to as the “QCD dilemma.” In addition to the intellectual dissatisfaction with a theory that is not directly applicable to the particles that are used and detected in experiments, there is also a practical problem in that many SM tests and searches for new physics (NP) involve strongly interacting hadrons in the initial and/or final states of the associated measurements. Even experiments that do not use initial or final states that contain hadrons are still subject to their effects from virtual quantum fluctuations. As a result, the sensitivities of many NP search experiments are ultimately limited by hadron-related theoretical uncertainties. Because of this, as the experimental sensitivities of NP searches improve, commensurate improvements in our understanding of long-distance QCD become more and more important. An example of the latter is hadronic contributions to the predicted value of the muon anomalous magnetic moment (Jegerlehner and Nyffeler, 2009).

### C. Searches for light “nonstandard” hadrons

A possible way experiments may be able to contribute to these improvements is by identifying patterns in hadron physics that may help guide the development of improved theoretical models. One peculiar pattern, and a long-standing puzzle, has been the lack of any evidence for light-flavored hadrons with substructures that are more complex than the three-quark baryons and quark-antiquark mesons of the original quark model. During the 50 years that have ensued since the birth of the quark idea, numerous experiments have searched for pentaquark baryons and light-flavored mesons with  $J^{PC}$  quantum numbers that are not accessible in  $q\bar{q}$  systems. Although during the same time period a large number of additional  $qqq$  baryon and  $q\bar{q}$  meson resonances were found, no unambiguous examples of light hadrons with nonstandard structures have emerged.

In particular, from the very earliest days of the quark model,  $K^+p$  and  $K^+d$  cross-section data were scoured for evidence of resonances with positive strangeness ( $S = +1$ ) quantum numbers in either the isospin  $I = 1$  or  $I = 0$  channels that would necessarily contain an  $\bar{s}$  quark in a minimal  $qu\bar{d}s$  ( $q = u$  or  $d$ ) five-quark (pentaquark) array.<sup>4</sup> Candidates for baryon states with positive strangeness, two with  $I = 0$ , named the  $Z_0(1780)$  and  $Z_0(1865)$ , and three with  $I = 1$ , the  $Z_1(1900)$ ,  $Z_1(2150)$ , and  $Z_1(2500)$ , appeared in the 1976 Particle Data Group (PDG) tables (Trippe *et al.*, 1976), but were absent by the time of the 1994 (Montanet *et al.*, 1994) and subsequent versions. History repeated itself in 2003, when an experiment studying  $\gamma n \rightarrow K^+K^-n$  reactions using a beam of energy-tagged  $\gamma$  rays impinging on a  $^{12}\text{C}$  target, reported a “sharp baryon resonance peak” in the

$K^+n$  invariant mass distribution with a mass and width  $M = 1.54 \pm 0.01$  GeV and  $\Gamma < 25$  MeV (Nakano *et al.*, 2003) that closely matched the 1.53 GeV mass and 15 MeV width that was predicted for an  $S = +1$  pentaquark by Diakonov, Petrov, and Polyakov (1997). The observation of this peak, which was called the  $\Theta^+$ , started a great flurry of activity that produced a number of conflicting experimental results. This ended three years later when results from some definitive experiments became available. Based on these, the PDG 2006 report (Yao *et al.*, 2006) declared that “The conclusion that pentaquarks in general, and the  $\Theta^+$ , in particular, do not exist, appears compelling.” Instructive reviews of this recent pentaquark episode and references to the many related experimental reports are provided in Dzierba, Meyer, and Szczepaniak (2005), Schumacher (2006), and Hicks (2012).

Searches for nonstandard mesons have mostly concentrated on looking for meson resonances with “exotic” quantum numbers, i.e.,  $J^{PC}$  values that cannot be formed from a fermion-antifermion pair, namely,  $0^{--}$  and  $0^{+-}$ ,  $1^{++}$ ,  $2^{+-}$ , etc. A number of experiments have reported evidence for resonancelike behavior with  $J^{PC} = 1^{+-}$ , but their interpretations as true resonances remain a subject of some dispute. The situation is summarized in Meyer and Van Haarlem (2010) and Meyer and Swanson (2015).

On the other hand, the scalar mesons with masses below 1 GeV,  $f_0(500)$ ,  $K_0^*(800)$ ,  $a_0(980)$ , and  $f_0(980)$ , which have nonexotic  $J^{PC} = 0^{++}$  quantum numbers that can be accessed by a spin-singlet ( $S = 0$ )  $q\bar{q}$  pair in a  $P$  wave, have frequently been cited as candidates for multi-quark states (Achasov, Kiselev, and Shestakov, 2008). In  $q\bar{q}$  systems, the lowest-lying  $J = 0$   $P$ -wave  $q\bar{q}$  states are expected to have masses that are above 1.2 GeV, close to those of the  $J^P = 1^+$  and  $J^P = 2^+$   $P$ -wave mesons, such as the  $a_1(1260)$  and  $a_2(1320)$  resonances. In fact, an octet of  $0^{++}$  states with the expected masses [i.e., the  $a_0(1450)$ ,  $K_0^*(1430)$ , etc.] has been identified, and this makes the lighter scalar octet supernumerary. An especially puzzling feature of the low-mass scalars is their mass hierarchy, which is inverted with respect to what would be expected from the quark model: the strange state  $K_0^*(800) = \bar{d}s$  is lighter than the  $I = 1$   $a_0(980)$ , which is nominally comprised of  $q\bar{q}$  pairs ( $q = u$  or  $d$ ), and the  $f_0(500)$ , which, in the standard meson scheme would be an  $s\bar{s}$  state, is the lightest member of the octet. This is contrary to the well-established quark model feature of other mesons and baryons, where states with more  $s$  quarks are heavier. These peculiar features led to speculation that the lightest  $0^{++}$  mesons are comprised of some kind of four quark configuration (Jaffe, 1977a, 2005; Weinstein and Isgur, 1982). The isosinglet scalar mesons with masses above 1 GeV,  $f_0(1370)$ ,  $f_0(1500)$ , and  $f_0(1710)$ , are also supernumerary since at most two can be attributed to the  $1^3P_0$   $q\bar{q}$  ( $q = u, d, s$ ) states. They fall into the region of the lightest predicted glueball, i.e., a meson comprised only of gluons, with no quarks. However, these can mix with conventional  $q\bar{q}$  states, thereby making a clear cut experimental identification of a glue-glue bound state component difficult. Detailed discussion of glueballs and other light exotic hadron candidates can be found in Patrignani *et al.* (2016).

<sup>3</sup>As Frank Wilczek put it in a recent interview (Wilczek, 2016): “We have something called a standard model, but its foundations are kind of scandalous. We have not known how to define an important part of it mathematically rigorously....”

<sup>4</sup>Since the  $s$  quark has  $S = -1$ , conventional three quark baryons that contain one or more  $s$  quarks have negative strangeness; the  $K^+$  meson contains an  $\bar{s}$  quark and has  $S = +1$ .

## D. Heavy quarks and the quarkonium spectra

During the decade that immediately followed the introduction of the notion of fractionally charged quarks, and when the role of confinement was not understood, their actual existence was met with considerable skepticism. Although fractionally charged particles produced in high-energy particle collisions would have very distinct experimental signatures and should be relatively easy to observe, numerous searches at accelerators and in cosmic rays all reported negative results. The conservation of electric charge ensures that at least one of the fractionally charged quark types should be stable, in which case there could be a fractionally charged component of ordinary matter. Searches in minerals, deep sea water, meteorites, moon rocks, etc., all failed to find any sign of this. Reviews of this interesting era of quark search experiments are provided by Jones (1977) and Lyons (1981).

Thus, while the usefulness of the quark idea as an effective classifier of the spectrum of hadronic particles and for describing the results of deep-inelastic electron-nucleon scattering experiments was without question, their existence as real physical entities as opposed to a useful mathematical mnemonic aid, was strongly debated. However, this debate was put to rest in 1974 and 1975 with the discovery of the  $J/\psi$  (Aubert *et al.*, 1974; Augustin *et al.*, 1974),  $\psi'$  (Abrams *et al.*, 1974), and  $\chi_{c0,1,2}$  (Feldman *et al.*, 1975) mesons<sup>5</sup> with masses between 3 and 4 GeV. These new resonance states, all of which are strikingly narrow, were accurately described by Appelquist and Politzer as bound states of a  $c$  and a  $\bar{c}$  quark (Appelquist and Politzer, 1975), where  $c$  denotes the charge =  $+2/3$  “charmed quark” with charm flavor  $C = +1$ . The assortment of possible  $c\bar{c}$  mesons is collectively known as charmonium. The large  $c$  quark mass ( $m_c \approx 1.3$  GeV) ensures that the  $c$  quark motion in bound  $c\bar{c}$  systems is nearly nonrelativistic and the spectrum of observed states can be reasonably well described by the Schrödinger equation with a potential that is Coulombic at short distances (in accord with the notion of asymptotic freedom) and joined to a linearly increasing “confining” term at large distances (Eichten *et al.*, 1978; Necco and Sommer, 2002). The charmonium spectrum of states, which have a one-to-one correspondence to the allowed atomic levels in the hydrogen atom, is indicated in Fig. 4. All of the states below the  $M = 2m_D (= 3730$  MeV) open-charm threshold<sup>6</sup> have been experimentally identified and found to have masses and other properties that are in good agreement with potential model expectations. The simplicity and dramatic success of the charmonium model resulted in a rapid and almost universal acceptance in the particle physics community that quarks are real, physical entities. A systematic theoretical framework for implementing corrections to the static potential approach was later developed in the form of nonrelativistic quantum chromodynamics (NRQCD) (Brambilla *et al.*, 2000, 2014).

<sup>5</sup>The  $\psi'$  and  $\chi_{cJ}$  are commonly used names for the spin-triplet  $\psi(2S)$  and  $\chi_{cJ}(1P)$  charmonium states.

<sup>6</sup>Here  $m_D$  is the mass of the  $D^0$ , the lightest “open-charm” meson with quark content  $c\bar{u}$  and charm quantum number  $C = 1$ .

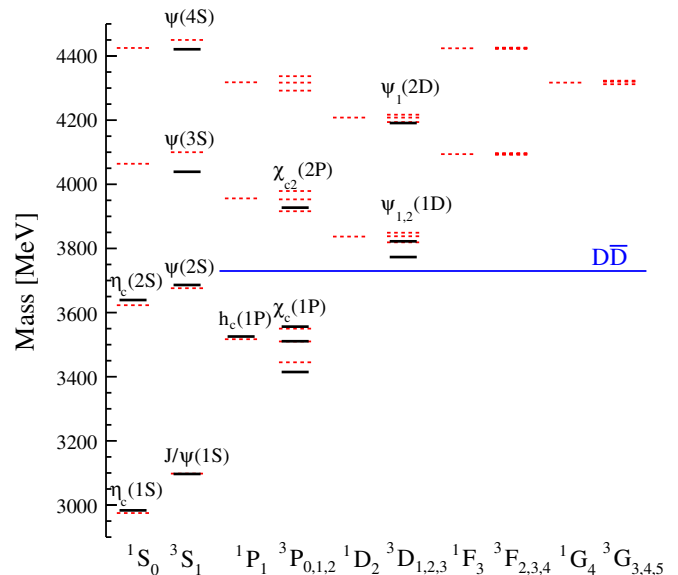


FIG. 4. The current status of the charmonium spectrum. The dashed (red) lines indicate the expected states and their masses based on recent calculations (Barnes, Godfrey, and Swanson, 2005) based on the Godfrey-Isgur relativized potential model (Godfrey and Isgur, 1985). The solid (black) lines indicate the experimentally established charmonium states with masses and spin-parity ( $J^{PC}$ ) quantum number assignments taken from Patrignani *et al.* (2016), and labeled by their spectroscopic designations. The open-flavor threshold is also indicated (blue line).

### 1. The $b$ quark and the spectrum of bottomonium mesons

Three years later, in 1977, a similar family of narrow meson resonances (the  $\Upsilon$ ,  $\Upsilon'$ , and  $\Upsilon''$ ) was discovered in the 9.4 to 10.4 GeV mass region (Herb *et al.*, 1977; Ueno *et al.*, 1979; Andrews *et al.*, 1980). These states were identified as  $b\bar{b}$  bound states, where  $b$  designates the charge =  $-1/3$  “bottom,” or “beauty” quark with beauty quantum number  $B = -1$  and are now called the bottomonium mesons. It was found that the application of the same potential that was used for charmonium, with a  $b$  quark mass of  $m_b \approx 4.2$  GeV, could produce a reasonable description of the bottomonium system (see Fig. 5). In this case there are more states below the  $M = 2m_B (= 10.56$  GeV) open-bottom threshold,<sup>7</sup> and most of these have been identified and found to have masses and other properties that are in good agreement with potential model expectations. The  $c$  and  $b$  quarks are known as “heavy quarks” and often denoted as  $Q$  ( $Q = c$  or  $b$ ); likewise charmonium and bottomonium mesons are collectively referred to as “quarkonium” mesons and denoted as  $Q\bar{Q}$ .

### 2. Nonstandard quarkoniumlike mesons and quarkonium pentaquarks

The large heavy-quark masses strongly suppress the production of  $Q\bar{Q}$  pairs from the vacuum during the

<sup>7</sup>To conform to the nomenclature of charge =  $-1/3$   $s$  quark system,  $B$  mesons contain a  $\bar{b}$  quark and have “beauty flavor”  $B = +1$  while  $\bar{B}$  mesons contain a  $b$  quark and have  $B = -1$ ; i.e.,  $B = \bar{b}q$  and  $\bar{B} = b\bar{q}$ , where  $q = u$  or  $d$

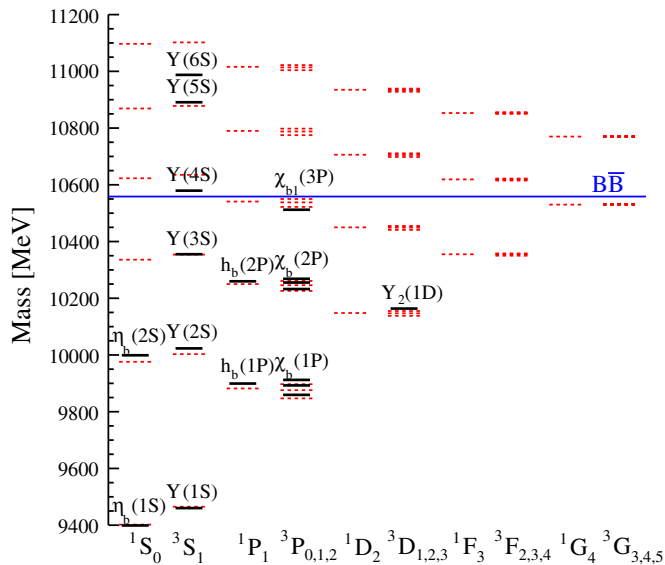


FIG. 5. The current status of the bottomonium spectrum. The dashed lines indicate the expected states and their masses based on recent calculations (Godfrey and Moats, 2015) based on the Godfrey-Isgur relativized potential model (Godfrey and Isgur, 1985). The solid lines indicate the experimentally established bottomonium states, with masses and spin-parity ( $J^{PC}$ ) quantum number assignments from Patrignani *et al.* (2016) and labeled by their spectroscopic designations. The open-flavor threshold is also indicated (blue line).

quark-to-hadron fragmentation process. Thus, if a  $Q$  and a  $\bar{Q}$  quark are found among the decay products of a previously unseen meson resonance, they must have been present as constituents of the meson itself. If the  $Q$  and  $\bar{Q}$  quarks are the parent meson's only constituents, it must be a  $Q\bar{Q}$  quarkonium state and, thus, have properties that match those of one of the as yet unassigned allowed quarkonium levels. If it does not fit into one of the available levels, it must have a substructure that is more complex than just  $Q\bar{Q}$  and, thus, qualify as a nonstandard hadron. The limited number of unassigned charmonium states with masses below 4.5 GeV and the theoretical expectation that most of the unassigned charmonium states will be relatively narrow and have nonoverlapping widths make the identification of nonstandard charmonium-like mesons less ambiguous than is the case for light-quark hadrons. For similar reasons, a baryon resonance that decays to a final state containing a  $Q$  and a  $\bar{Q}$  quark must contain a  $Q\bar{Q}$  pair among its constituents and, thus, have a valence configuration that contains at least five quarks.

In contrast to experiments in the light-quark sector, recent searches for nonstandard hadrons containing heavy quark pairs, i.e., hadrons that contain a  $c\bar{c}$  quark pair, have uncovered a number of intriguing states including the  $Z(4430)^\pm$ , which is electrically charged and evidence<sup>8</sup> for a four-quark meson that decays to  $\psi'\pi^\pm$  (Choi *et al.*, 2008; Aaij *et al.*, 2014b), and two strong candidates for pentaquark states,

<sup>8</sup>Since the  $Z(4430)^\pm$  decays to a final state that contains a  $\psi'$ , it must have constituent  $c$  and  $\bar{c}$  quarks plus additional light quarks to account for its nonzero electric charge.

the  $P_c(4380)$  and  $P_c(4450)$  that both decay to  $J/\psi p$  (Aaij *et al.*, 2015c). In addition to these, about 20 other candidate nonstandard hadron states containing  $c\bar{c}$  quarks have been found and studied by the BESIII experiment at the BEPCII  $\tau$ -charm factory in Beijing, the Belle and BABAR experiments at the KEKB and PEP-II  $B$  factories, the CDF and D0 experiments at the Tevatron, and the LHCb, ATLAS, and CMS experiments at the LHC. In addition, two nonstandard bottomoniumlike meson candidates were seen by Belle and a candidate for a mixed-flavor  $\bar{b}s\bar{d}u$  was reported by D0 (Abazov *et al.*, 2016). The nonstandard hadron candidates and some of their properties are listed in Tables I and II, where the charmed pentaquark candidates are labeled as  $P_c$ , the charged ( $I = 1$ ) meson states as  $Z$ , the  $J^{PC} = 1^{--}$  states as  $Y$ , and all the rest as  $X$ .

In this review, we summarize the results from this large amount of experimental activity and discuss how these findings reflect on theoretical ideas concerning long-distance QCD. The emphasis is on the experimental evidence; for recent reviews that have more focus on theoretical issues, see Esposito, Pilloni, and Polosa (2017), Ali, Lange, and Stone (2017), Lebed, Mitchell, and Swanson (2017), and Guo *et al.* (2018).

### 3. Comments on units, terminology, and notation

In this review we use “natural units” where  $\hbar = c = 1$ ; energy, momentum, and mass are expressed in units of either MeV or GeV. In the case of MeV, the units of both length ( $[L]$ ) and time ( $[T]$ ) are  $1 \text{ MeV}^{-1}$ . These can be related to conventional units by  $[L] = \hbar c / (1 \text{ MeV}) = 197 \text{ fm}$  and  $[T] = [L] / c = \hbar / (1 \text{ MeV}) = 6.58 \times 10^{-22} \text{ s}$ . Also, when an experimental number is quoted, we usually list the quadrature sum of the statistical and systematic errors.

The spectra of  $c\bar{c}$  charmonium and  $b\bar{b}$  bottomonium mesons are shown in Figs. 4 and 5, respectively, where their  $J^{PC}$  quantum numbers and commonly used names are listed. Sometimes it is convenient to describe these states using spectroscopic notation:  $n_r^{2S+1}L_J$ , where  $n_r$  is the  $Q\bar{Q}$  radial quantum number,  $S = 0$  or  $1$  is their combined spin,  $L = S, P, D$ , etc. denotes their relative orbital angular momentum and  $J$  is the total angular momentum. Thus, for example, the  $J/\psi$  and  $\psi'$  states shown in Fig. 4 are the  $1^3S_1$  and  $2^3S_1$   $c\bar{c}$  states, respectively, while the  $\chi_{c0}$ ,  $\chi_{c1}$ , and  $\chi_{c2}$  are the  $1^3P_{0,1,2}$  triplet states.

The charmonium (bottomonium) states contain  $c\bar{c}$  ( $b\bar{b}$ ) pairs and, thus, have a zero net charm (beauty) quantum number; these are sometimes referred to as hidden-charm (hidden-beauty) states. Particles with a single charmed (bottom) quark are referred to as open-charm (open-bottom) states. Properties of the lowest-lying open-charm and open-bottom mesons and baryons mentioned in this review are listed in Table III.

Limits on the electric dipole moment of the neutron confirm that QCD is matter-antimatter symmetric to a high degree of confidence (Pendlebury *et al.*, 2015). In addition, the experimental environments of the measurements discussed in this review are also mostly matter-antimatter symmetric. Thus, the data samples that are used for these measurements usually

TABLE I. Recently discovered nonstandard hadron candidates with hidden charm or beauty. The masses  $M$  and widths  $\Gamma$  are averages of measurements with uncertainties added in quadrature, except for  $X(4140)$ ,  $X(4274)$  [ $Z^+(4200)$ ], where Aaij *et al.* (2017a, 2017d) (Chilikin *et al.*, 2014) values are listed. See Sec. V.D (Sec. VI.A) for more detailed discussion. The errors on the average values include scale factors in case of tensions between individual measurements (Patrignani *et al.*, 2016). We do not quote a mass or width for the  $Y(4260)$  structure, since the latest precision data revealed its double-peak composition (Ablikim *et al.*, 2017c), with the main component listed under  $Y(4220)$  and its high-mass shoulder under  $Y(4360)$ . The results from single-peak fits to the  $Y(4260)$  structure are not included when determining the  $Y(4220)$  parameters. For  $X(3872)$ , only  $\pi^+\pi^-J/\psi$  decays are used in the mass average. Ellipses indicate an inclusive reaction. Question marks indicate informed guesses at  $J^{PC}$  values or no information. For charged states,  $C$  refers to the neutral isospin partner. See Table II for a continuation.

State	$M$ (MeV)	$\Gamma$ (MeV)	$J^{PC}$	Process (decay mode)	Experiment
$X(3872)$	$3871.69 \pm 0.17$	$< 1.2$	$1^{++}$	$B \rightarrow K(J/\psi\pi^+\pi^-)$ $p\bar{p} \rightarrow (J/\psi\pi^+\pi^-) + \dots$ $B \rightarrow K(J/\psi\pi^+\pi^-\pi^0)$ $B \rightarrow K(D^0\bar{D}^0\pi^0)$ $B \rightarrow K(J/\psi\gamma)$ $B \rightarrow K(\psi'\gamma)$ $pp \rightarrow (J/\psi\pi^+\pi^-) + \dots$ $e^+e^- \rightarrow \gamma(J/\psi\pi^+\pi^-)$	Belle (Choi <i>et al.</i> , 2003, 2011), BABAR (Aubert <i>et al.</i> , 2005c), LHCb (Aaij <i>et al.</i> , 2013a, 2015d) CDF (Acosta <i>et al.</i> , 2004; Abulencia <i>et al.</i> , 2006; Aaltonen <i>et al.</i> , 2009b), D0 (Abazov <i>et al.</i> , 2004) Belle (Abe <i>et al.</i> , 2005), BABAR (del Amo Sanchez <i>et al.</i> , 2010a) Belle (Gokhroo <i>et al.</i> , 2006; Aushev <i>et al.</i> , 2010b), BABAR (Aubert <i>et al.</i> , 2008c) BABAR (del Amo Sanchez <i>et al.</i> , 2010a), Belle (Bhardwaj <i>et al.</i> , 2011), LHCb (Aaij <i>et al.</i> , 2012a) BABAR (Aubert <i>et al.</i> , 2009b), Belle (Bhardwaj <i>et al.</i> , 2011), LHCb (Aaij <i>et al.</i> , 2014a) LHCb (Aaij <i>et al.</i> , 2012a), CMS (Chatrchyan <i>et al.</i> , 2013a), ATLAS (Aaboud <i>et al.</i> , 2017) BESIII (Ablikim <i>et al.</i> , 2014d)
$X(3915)$	$3918.4 \pm 1.9$	$20 \pm 5$	$0^{++}$	$B \rightarrow K(J/\psi\omega)$ $e^+e^- \rightarrow e^+e^-(J/\psi\omega)$	Belle (Choi <i>et al.</i> , 2005), BABAR (Aubert <i>et al.</i> , 2008b; del Amo Sanchez <i>et al.</i> , 2010a) Belle (Uehara <i>et al.</i> , 2010), BABAR (Lees <i>et al.</i> , 2012c)
$X(3940)$	$3942_{-8}^{+9}$	$37_{-17}^{+27}$	$0^{-+} (?)$	$e^+e^- \rightarrow J/\psi(D^*\bar{D})$ $e^+e^- \rightarrow J/\psi(\dots)$	Belle (Pakhlov <i>et al.</i> , 2008) Belle (Abe <i>et al.</i> , 2007)
$X(4140)$	$4146.5_{-5.3}^{+6.4}$	$83_{-25}^{+27}$	$1^{++}$	$B \rightarrow K(J/\psi\phi)$ $p\bar{p} \rightarrow (J/\psi\phi) + \dots$	CDF (Aaltonen <i>et al.</i> , 2009a), CMS (Chatrchyan <i>et al.</i> , 2014), D0 (Abazov <i>et al.</i> , 2014), LHCb (Aaij <i>et al.</i> , 2017a, 2017d) D0 (Abazov <i>et al.</i> , 2015)
$X(4160)$	$4156_{-25}^{+29}$	$139_{-65}^{+113}$	$0^{-+} (?)$	$e^+e^- \rightarrow J/\psi(D^*\bar{D}^*)$	Belle (Pakhlov <i>et al.</i> , 2008)
$Y(4260)$	See $Y(4220)$ entry		$1^{--}$	$e^+e^- \rightarrow \gamma(J/\psi\pi^+\pi^-)$	BABAR (Aubert <i>et al.</i> , 2005a; Lees <i>et al.</i> , 2012b), CLEO (He <i>et al.</i> , 2006), Belle (Yuan <i>et al.</i> , 2007; Liu <i>et al.</i> , 2013)
$Y(4220)$	$4222 \pm 3$	$48 \pm 7$	$1^{--}$	$e^+e^- \rightarrow (J/\psi\pi^+\pi^-)$ $e^+e^- \rightarrow (h_c\pi^+\pi^-)$ $e^+e^- \rightarrow (\chi_{c0}\omega)$ $e^+e^- \rightarrow (J/\psi\eta)$ $e^+e^- \rightarrow (\gamma X(3872))$ $e^+e^- \rightarrow (\pi^- Z_c^+(3900))$ $e^+e^- \rightarrow (\pi^- Z_c^+(4020))$	BESIII (Ablikim <i>et al.</i> , 2017c) BESIII (Ablikim <i>et al.</i> , 2017a) BESIII (Ablikim <i>et al.</i> , 2015g) BESIII (Ablikim <i>et al.</i> , 2015c) BESIII (Ablikim <i>et al.</i> , 2014d) BESIII (Ablikim <i>et al.</i> , 2013a), Belle (Liu <i>et al.</i> , 2013) BESIII (Ablikim <i>et al.</i> , 2013b)
$X(4274)$	$4273_{-9}^{+19}$	$56_{-16}^{+14}$	$1^{++}$	$B \rightarrow K(J/\psi\phi)$	CDF (Aaltonen <i>et al.</i> , 2017), CMS (Chatrchyan <i>et al.</i> , 2014), LHCb (Aaij <i>et al.</i> , 2017a, 2017d)
$X(4350)$	$4350.6_{-5.1}^{+4.6}$	$13.3_{-10.0}^{+18.4}$	$(0/2)^{++}$	$e^+e^- \rightarrow e^+e^-(J/\psi\phi)$	Belle (Shen <i>et al.</i> , 2010)
$Y(4360)$	$4341 \pm 8$	$102 \pm 9$	$1^{--}$	$e^+e^- \rightarrow \gamma(\psi'\pi^+\pi^-)$ $e^+e^- \rightarrow (J/\psi\pi^+\pi^-)$	BABAR (Aubert <i>et al.</i> , 2007; Lees <i>et al.</i> , 2014), Belle (Wang <i>et al.</i> , 2007, 2015) BESIII (Ablikim <i>et al.</i> , 2017c)
$Y(4390)$	$4392 \pm 6$	$140 \pm 16$	$1^{--}$	$e^+e^- \rightarrow (h_c\pi^+\pi^-)$	BESIII (Ablikim <i>et al.</i> , 2017a)
$X(4500)$	$4506_{-19}^{+16}$	$92_{-21}^{+30}$	$0^{++}$	$B \rightarrow K(J/\psi\phi)$	LHCb (Aaij <i>et al.</i> , 2017a, 2017d)
$X(4700)$	$4704_{-26}^{+17}$	$120_{-45}^{+52}$	$0^{++}$	$B \rightarrow K(J/\psi\phi)$	LHCb (Aaij <i>et al.</i> , 2017a, 2017d)
$Y(4660)$	$4643 \pm 9$	$72 \pm 11$	$1^{--}$	$e^+e^- \rightarrow \gamma(\psi'\pi^+\pi^-)$ $e^+e^- \rightarrow \gamma(\Lambda_c^+\Lambda_c^-)$	Belle (Wang <i>et al.</i> , 2007, 2015), BABAR (Aubert <i>et al.</i> , 2007; Lees <i>et al.</i> , 2014) Belle (Pakhlova <i>et al.</i> , 2008)

TABLE II. See the caption of Table I.

State	$M$ (MeV)	$\Gamma$ (MeV)	$J^{PC}$	Process (decay mode)	Experiment
$Z_c^{+0}(3900)$	$3886.6 \pm 2.4$	$28.1 \pm 2.6$	$1^{++}$	$e^+e^- \rightarrow \pi^{-0}(J/\psi\pi^{+0})$ $e^+e^- \rightarrow \pi^{-0}(D\bar{D}^*)^{+0}$	BESIII (Ablikim <i>et al.</i> , 2013a, 2015f), Belle (Liu <i>et al.</i> , 2013) BESIII (Ablikim <i>et al.</i> , 2014b, 2015e)
$Z_c^{+0}(4020)$	$4024.1 \pm 1.9$	$13 \pm 5$	$1^{++} (?)$	$e^+e^- \rightarrow \pi^{-0}(h_c\pi^{+0})$ $e^+e^- \rightarrow \pi^{-0}(D^*\bar{D}^*)^{+0}$	BESIII (Ablikim <i>et al.</i> , 2013b, 2014c) BESIII (Ablikim <i>et al.</i> , 2014a, 2015d)
$Z^+(4050)$	$4051_{-43}^{+24}$	$82_{-55}^{+51}$	$?^{?+}$	$B \rightarrow K(\chi_{c1}\pi^+)$	Belle (Mizuk <i>et al.</i> , 2008), BABAR (Lees <i>et al.</i> , 2012a)
$Z^+(4200)$	$4196_{-32}^{+35}$	$370_{-149}^{+99}$	$1^+$	$B \rightarrow K(J/\psi\pi^+)$ $B \rightarrow K(\psi'\pi^+)$	Belle (Chilikin <i>et al.</i> , 2014) LHCb (Aaij <i>et al.</i> , 2014b)
$Z^+(4250)$	$4248_{-45}^{+185}$	$177_{-72}^{+321}$	$?^{?+}$	$B \rightarrow K(\chi_{c1}\pi^+)$	Belle (Mizuk <i>et al.</i> , 2008), BABAR (Lees <i>et al.</i> , 2012a)
$Z^+(4430)$	$4477 \pm 20$	$181 \pm 31$	$1^+$	$B \rightarrow K(\psi'\pi^+)$ $B \rightarrow K(J\psi\pi^+)$	Belle (Choi <i>et al.</i> , 2008; Mizuk <i>et al.</i> , 2009), Belle (Chilikin <i>et al.</i> , 2013), LHCb (Aaij <i>et al.</i> , 2014b, 2015b) Belle (Chilikin <i>et al.</i> , 2014)
$P_c^+(4380)$	$4380 \pm 30$	$205 \pm 88$	$(\frac{3}{2}/\frac{5}{2})^\mp$	$\Lambda_b^0 \rightarrow K(J/\psi p)$	LHCb (Aaij <i>et al.</i> , 2015c)
$P_c^+(4450)$	$4450 \pm 3$	$39 \pm 20$	$(\frac{5}{2}/\frac{3}{2})^\pm$	$\Lambda_b^0 \rightarrow K(J/\psi p)$	LHCb (Aaij <i>et al.</i> , 2015c)
$Y_b(10860)$	$10891.1_{-3.8}^{+3.4}$	$53.7_{-7.8}^{+7.2}$	$1^{--}$	$e^+e^- \rightarrow (\Upsilon(nS)\pi^+\pi^-)$	Belle (Chen <i>et al.</i> , 2008; Santel <i>et al.</i> , 2016)
$Z_b^{+0}(10610)$	$10607.2 \pm 2.0$	$18.4 \pm 2.4$	$1^{++}$	$Y_b(10860) \rightarrow \pi^{-0}(\Upsilon(nS)\pi^{+0})$ $Y_b(10860) \rightarrow \pi^-(h_b(nP)\pi^+)$ $Y_b(10860) \rightarrow \pi^-(B\bar{B}^*)^+$	Belle (Bondar <i>et al.</i> , 2012; Garmash <i>et al.</i> , 2015), Belle (Krokovny <i>et al.</i> , 2013) Belle (Bondar <i>et al.</i> , 2012) Belle (Garmash <i>et al.</i> , 2016)
$Z_b^+(10650)$	$10652.2 \pm 1.5$	$11.5 \pm 2.2$	$1^{++}$	$Y_b(10860) \rightarrow \pi^-(\Upsilon(nS)\pi^+)$ $Y_b(10860) \rightarrow \pi^-(h_b(nP)\pi^+)$ $Y_b(10860) \rightarrow \pi^-(B^*\bar{B}^*)^+$	Belle (Bondar <i>et al.</i> , 2012; Garmash <i>et al.</i> , 2015) Belle (Bondar <i>et al.</i> , 2012) Belle (Garmash <i>et al.</i> , 2016)

include charge-conjugate reactions. For example, a measurement of a  $\pi D\bar{D}^*$  system will use a combined set of  $\pi^+D\bar{D}^*$ ,  $\pi^+D^*\bar{D}$ ,  $\pi^-D\bar{D}^*$ , and  $\pi^-D^*\bar{D}$  events. In this review for

TABLE III. Properties of the lowest-lying open-charm and open-bottom particles. Here  $I:I_3$  denote the total and third components of the isospin and  $S$ ,  $C$ , and  $B$  are the strangeness, charm, and beauty quantum numbers.

Particle	Quark content	$J^P$	$I:I_3$	$S$	$C$	$B$	$M$ (MeV)	$c\tau$ ( $\mu\text{m}$ )
$D^+$	$c\bar{d}$	$0^-$	$1/2:1/2$	0	1	0	1869.6	312
$D^0$	$c\bar{u}$	$0^-$	$1/2:-1/2$	0	1	0	1864.8	123
$D^{*+}$	$c\bar{d}$	$1^-$	$1/2:1/2$	0	1	0	2010.3	$\sim 0$
$D^{*0}$	$c\bar{u}$	$1^-$	$1/2:-1/2$	0	1	0	2007.0	$\sim 0$
$D_s^+$	$c\bar{s}$	$0^-$	$0:0$	1	1	0	1968.3	150
$\Lambda_c^+$	$cud$	$(1/2)^+$	$0:0$	0	1	0	2286.5	60
$\Sigma_c^{++}$	$cuu$	$(1/2)^+$	$1:1$	0	1	0	2454.0	$\sim 0$
$\Sigma_c^+$	$cud$	$(1/2)^+$	$1:0$	0	1	0	2452.9	$\sim 0$
$\Sigma_c^0$	$cdd$	$(1/2)^+$	$1:-1$	0	1	0	2453.8	$\sim 0$
$\bar{B}^0$	$b\bar{d}$	$0^-$	$1/2:1/2$	0	0	-1	5279.6	455
$B^-$	$b\bar{u}$	$0^-$	$1/2:-1/2$	0	0	-1	5279.3	491
$\bar{B}^{*0}$	$b\bar{d}$	$1^-$	$1/2:1/2$	0	0	-1	5325.2	$\sim 0$
$B^{*-}$	$b\bar{u}$	$1^-$	$1/2:-1/2$	0	0	-1	5325.2	$\sim 0$
$\bar{B}_s^0$	$b\bar{s}$	$0^-$	$0:0$	1	0	-1	5366.8	453
$\Lambda_b$	$bud$	$(1/2)^+$	$0:0$	0	0	-1	5619.5	435

simplicity and readability we abbreviate this to  $\pi^+D\bar{D}^*$  with the implicit assumption that charge-conjugate combinations are included. For similar reasons, when we discuss meson-antimeson moleculelike possibilities, we abbreviate combinations such as  $(D\bar{D}^* \pm \bar{D}D^*)/\sqrt{2}$  to simply  $D\bar{D}^*$ .

## II. MODELS FOR NONSTANDARD HADRONS

In the absence of any rigorous analytical method for making first-principle calculations of the spectrum of nonstandard hadrons, simplified models that are motivated by the color structure and other general features of QCD have been developed. The current best hope for a rigorous, first-principle treatment for some of the issues here is lattice QCD, which is discussed later in this section.

The color structure of QCD suggests the existence of three types of nonstandard hadronic particles. These include multi-quark hadrons (tetraquark mesons and pentaquark baryons) formed from tightly bound colored diquarks, hybrid mesons and baryons comprised of color-singlet combinations of quarks and one or more ‘‘valence’’ gluons, and glueball mesons that are comprised only of gluons (with no quarks). Other possible forms of multi-quark states are meson-meson and/or meson-baryon moleculelike systems that are bound (or nearly bound) via Yukawa-like nuclear forces and bound states comprised of quarkonium cores surrounded by clouds of light quarks and gluons.



## A. QCD-color-motivated models

### 1. QCD diquarks

It is well known that the combination of a  $q = u, d, s$  light-quark triplet with a  $\bar{q} = \bar{u}, \bar{d}, \bar{s}$  antiquark antitriplet gives the familiar meson nonets (an octet plus a singlet) of flavor  $SU(3)$ . Using similar considerations based on QCD (Jaffe, 1977a), a red and a blue quark triplet can be combined to form a magenta (antigreen) antitriplet of  $qq'$  “diquarks” that is antisymmetric in both color and flavor, and a magenta flavor-symmetric sextet, as illustrated in Fig. 6(a). The Pauli principle restricts the spin state of antitriplet quarks to  $S = 0$  and that of the sextet quarks to  $S = 1$ . Since the single-gluon-exchange color force between the quarks in an  $S = 0$  antitriplet diquark is attractive, Jaffe designated these as “good” diquarks and those in an  $S = 1$  sextet, where the short-range force is repulsive, as “bad” diquarks (Jaffe, 2005). From the nucleon and  $\Delta^0$ -baryon mass difference he estimated the difference in binding between light bad and good diquarks to be  $\sim(2/3)(m_\Delta - m_N) \sim 200$  MeV.

Likewise, green-red and blue-green diquarks form yellow (antiblue) and cyan (antired) antitriplets as shown in Fig. 6(b). Thus, in color space, a good diquark antitriplet looks like an antiquark triplet with baryon number  $B = +2/3$  and spin = 0.

Since these diquarks are not color singlets, they cannot exist as free particles but, instead, they should be able to combine with other colored objects in a manner similar to antiquark antitriplets, thereby forming multiquark color-singlet states with a more complex substructure than the  $q\bar{q}$  mesons and  $qqq$  baryons of the original quark model. Jaffe proposed that the puzzles associated with the low-mass  $0^{++}$  mesons, discussed in Sec. I.C, could be explained by identifying them as four-quark combinations of a diquark and a diantiquark. In

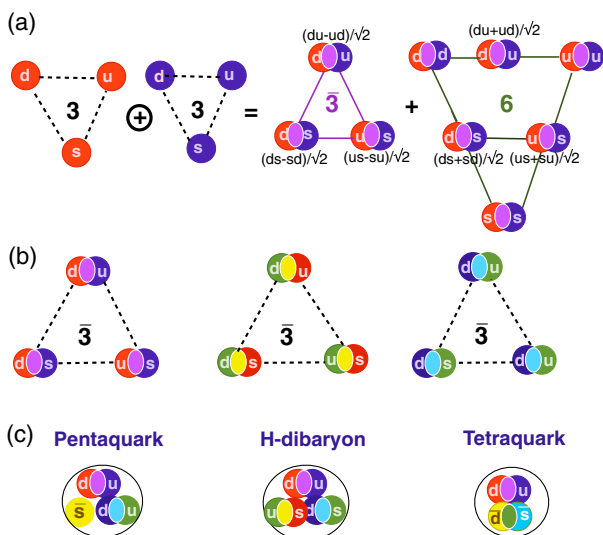


FIG. 6. (a) Combining a red and a blue quark triplet produces a magenta (antigreen) antitriplet and sextet. The antitriplet is antisymmetric in color and flavor while the sextet is color antisymmetric and flavor symmetric. (b) The three anticorelated diquark antitriplets. (c) Some of the multiquark, color-singlet states that can be formed from quarks, antiquarks, diquarks, and diantiquarks.

this scheme, the  $a_0(980)$  isotriplet mesons are formed from  $[qs]-[\bar{q}\bar{s}]$  ( $q = u$  or  $d$ ) configurations and their large mass relative to other octet members is due to the two  $s$  quarks among its constituents (Jaffe, 1977b; Maiani *et al.*, 2004; 't Hooft *et al.*, 2008). In addition to the light scalar mesons, diquarks and/or diantiquarks could be constituents of other octets of tetraquark mesons, as well as pentaquark baryons and six-quark  $H$  dibaryons, as illustrated in Fig. 6(c).

These considerations are expanded to include heavy-light diquarks ( $Qq$ ) and diantiquarks ( $\bar{Q}\bar{q}$ ) (Maiani *et al.*, 2005; Terasaki, 2004). The  $Qq$  ( $\bar{Q}\bar{q}$ ) combinations are color- $SU(3)$  antitriplets (triplets) and flavor- $SU(3)$  triplets (antitriplets). In this case, since the spin-spin force between the quarks is reduced by a factor of  $m_q/m_Q$ , the mass difference between bad and good diquarks is reduced. As a result  $S = 1$   $Qq$  diquarks are not so bad and both  $S = 0$  and 1 diquarks could be expected to play important roles in hadron spectroscopy (Manohar and Wise, 2000). More detailed discussions of diquark models are provided by Esposito, Guerrieri, Piccinini *et al.* (2015) and Esposito, Piloni, and Polosa (2017).

### 2. QCD hybrids

The linear confining term in the color-force potential produces a force between a meson's constituent quark and antiquark that is constant with increasing separation. As a result, unlike the electric field lines between opposite charges in QED, which spread out in space, the color field lines are configured in a tightly confined “flux tube” that runs between  $q$  and  $\bar{q}$  (Isgur and Paton, 1983).

In their lowest-mass configurations, the flux tube is in a ground state with angular momentum quantum numbers  $L = 0$  and  $S = 0$ , and only the relative orbital angular momentum of the quarks and their net spin determine the quantum numbers of a state; the gluonic degrees of freedom do not play any role. As a result, the  $J^{PC}$  quantum numbers of these ground-state or “conventional” mesons, where  $\vec{J} = \vec{L} + \vec{S}$ ,  $P = (-1)^{L+1}$ , and  $C = (-1)^{L+S}$  are restricted to values that can be accessed by a quark-antiquark pair  $J^{PC} = 0^{++}, 0^{-+}, 1^{++}, 1^{-+}, 1^{--}, 2^{++}, 2^{-+}, 2^{--}, \dots$ ; other quantum number combinations, namely,  $J^{PC} = 0^{-+}, 0^{+-}, 1^{-+}, 2^{+-}, \dots$  are inaccessible and are called “exotic.” However, if the flux tube is in an excited state, its orbital angular momentum and/or spin can be nonzero and contribute  $L$  and  $S$  values that are consistent with one or more gluons. In this case they contribute to the overall quantum numbers of the state and can form mesons with exotic quantum number assignments (Horn and Mandula, 1978). Since gluons have zero isospin, quarkonium hybrids, i.e.,  $Q\bar{Q} - g$  states, are necessarily isospin singlets.

Models for the decays of hybrids find that decays to identical mesons are strongly suppressed, while decays to two different mesons where one is a  $q\bar{q}$  in an  $S$  wave and the other a  $q\bar{q}$  in a  $P$  wave are enhanced (Isgur, Kokoski, and Paton, 1985; Page, Swanson, and Szczepaniak, 1999). The predicted widths for  $\pi\pi$  or  $K\bar{K}$  final states for light-quark hybrids are small, as are the  $D\bar{D}$  and  $B\bar{B}$  decay widths for quarkonium hybrids. In contrast, light hybrid decays to  $a_1\pi$ ,  $b_1\pi$ , and  $K_1(1400)\bar{K}$  decays, where  $a_1$ ,  $b_1$ , and  $K_1$

are axial-vector mesons, in which the  $q\bar{q}$  pair is in a relative  $P$  wave, are expected to be strong. Likewise, quarkonium hybrids are expected to have strong decay widths for  $D^{**}\bar{D}^{(*)}$  and  $B^{**}\bar{B}^{(*)}$  final states, where  $D^{**}$  and  $B^{**}$  denote open charm ( $c\bar{q}$ ) and beauty ( $b\bar{q}$ ) ( $q = u, d$ )  $P$ -wave states, respectively.

A recent review of hybrid mesons by Meyer and Swanson (2015) points out limitations in this naive but useful 30-year old picture and provides references to current computations based on the lattice gauge theory.

## B. Other models

### 1. Hadronic molecules

The idea that Yukawa-type meson-exchange forces could produce deuteronlike bound states of ordinary, color-singlet hadrons, as illustrated in Figs. 7(a) and 7(b), has been around for a long time (Bander *et al.*, 1976; Voloshin and Okun, 1976; De Rujula, Georgi, and Glashow, 1977; Manohar and Wise, 1993). These “molecular” states are expected to have masses that are near the constituent particles’ mass threshold and to have spin-parity ( $J^{PC}$ ) quantum numbers that correspond to an  $S$ -wave combination of the constituent particles. For the deuteron, single-pion exchange is the most important contributor to its binding. Tornqvist studied the possibility for forming deuteronlike  $B\bar{B}^*$  and  $B^*\bar{B}^*$  states, which he called “deusons,” using a single-pion exchange potential and concluded that such states “certainly must exist” (Tornqvist, 1994); he also predicted that if some small additional attraction was provided by shorter range exchanges, bound  $D\bar{D}^*$  and  $D^*\bar{D}^*$  systems would also exist.

Since three-pseudoscalar couplings such as  $D\bar{D}\pi$  and  $B\bar{B}\pi$  are forbidden by rotation plus parity invariance, single-pion exchange forces do not contribute to  $D\bar{D}$  or  $B\bar{B}$  binding and, thus, moleculelike structures in these systems are not expected to occur.

In moleculelike states formed from pairs of open-charm or open-beauty mesons that are primarily bound by single  $\pi$ -meson exchange, the heavy  $Q$  and  $\bar{Q}$  quarks are typically well separated in space with very little overlap. This suggests that “fall-apart” decay modes to pairs of open-flavor mesons would be dominant, while decays to final states in which the  $Q$  and  $\bar{Q}$  quarks coalesce to form a hidden-flavor quarkonium state would be rather strongly suppressed. More detailed discussions of molecular models have been provided by Swanson (2006), Polosa (2015), Lebed, Mitchell, and Swanson (2017), and Guo *et al.* (2018).

### 2. Hadrocharmonium

For conventional charmonium states with masses above the open-charm (i.e.,  $D\bar{D}^{(*)}$ ) threshold, the branching fractions for fall-apart decays to pairs of open-charm mesons are measured to be 2 or 3 orders of magnitude higher than decays to hidden-charm final states.<sup>9</sup> This is not the case for many of the nonstandard hadrons discussed here, where hidden

<sup>9</sup>For example,  $\mathcal{B}(\psi(3770) \rightarrow D\bar{D}) = (93^{+8}_{-9})\%$  while  $\mathcal{B}(\psi(3770) \rightarrow \pi^+\pi^-J/\psi) = (0.193 \pm 0.028)\%$  (Patrignani *et al.*, 2016).

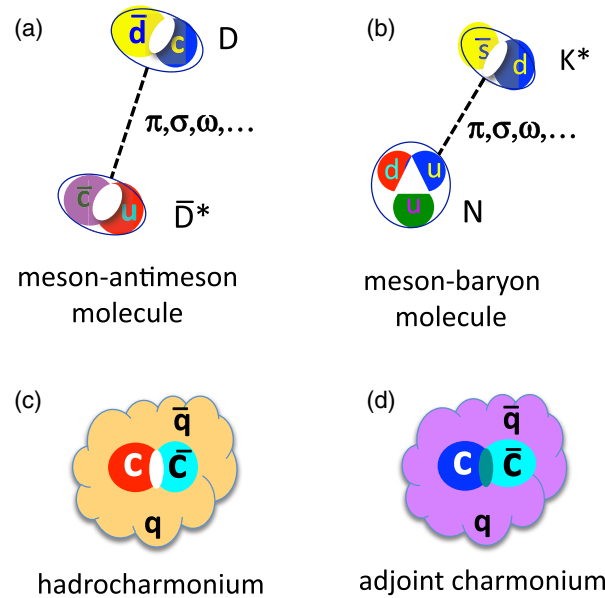


FIG. 7. (a) A meson-meson and (b) a meson-baryon molecular-like structure bound by Yukawa-type meson-exchange forces. (c) A sketch of the hadrocharmonium configuration of multi-quark states. Here a color-singlet  $Q\bar{Q}$  core state interacts with a surrounding “blob” of gluons and light quarks via QCD versions of van der Waals-type forces. (d) In adjoint charmonium states, a color-octet  $Q\bar{Q}$  pair interacts with surrounding gluons and light quarks via color forces.

quarkonium modes are a common discovery channel with branching fractions that are lower than open-flavor fall-apart modes, but only by factors of 10 or less. The hadrocharmonium model was proposed by Dubynskiy and Voloshin (2008) in order to account for this property. In this model, a compact color-singlet  $Q\bar{Q}$  charmonium core state is embedded in a spatially extended “blob” of light hadronic matter. These two components interact via QCD versions of the van der Waals force. They found that the mutual forces in this configuration are strong enough to form bound states if the light hadronic matter is a highly excited resonant state. In this model, decays to the hidden charmonium core state are enhanced to a level where they are competitive with those for fall-apart modes (Dubynskiy, Gorsky, and Voloshin, 2009). Allowing for a sizable branching fraction into open-charm modes requires a careful tuning of the model parameters.

### 3. Born-Oppenheimer model

An “all of the above” approach that incorporates all of the configurations previously discussed, plus the adjoint charmonium configuration illustrated in Fig. 7(d), which is like hadrocharmonium except with an allowance for the possibility that the  $Q\bar{Q}$  core state has nonzero color, has been advocated by Braaten (2013) and Braaten, Langmack, and Smith (2014). This is modeled on the Born-Oppenheimer approximation that is used in atomic and molecular physics to treat the binding of atoms into molecules. In this approach, the slow-moving atomic nuclei are replaced by the heavy quarks and the potential that describes the interaction of the positive nuclear charges and the surrounding negative electron clouds are

replaced by lattice QCD computed gluon-induced potentials (Juge, Kuti, and Morningstar, 1999). A first application of this approach was used to predict the masses of the lowest-lying charmonium hybrid and tetraquark mesons.

#### 4. Kinematically induced resonancelike mass peaks

While the classic signal for the presence of an unstable hadron resonance is a peak in the invariant mass distribution of its decay products, not all mass-spectrum peaks are genuine hadron states. Some can be produced by near-threshold kinematic effects. These include threshold “cusps” and anomalous triangle singularities.

*Threshold cusps:* Fig. 8(a) shows the three lowest-order diagrams for three-body decays  $Y \rightarrow \pi D \bar{D}^*$ . Consider the one-loop diagram, where  $D$  and  $\bar{D}^*$  elastically rescatter. If the two particles are in an  $S$  wave, the imaginary part of the scattering amplitude is zero for  $M(D\bar{D}^*) < (m_D + m_{\bar{D}^*})$  and abruptly rises at threshold as (Bugg, 2011; Blitz and Lebed, 2015; Swanson, 2016)

$$\text{Im}T(s) \propto g^2 \rho(s), \quad (1)$$

where  $g$  is the coupling constant and  $\rho(s)$  is the phase-space factor. In order to eventually terminate the growth of  $\rho(s)$  before  $\text{Im}T$  increases to an unphysically large value, it has to be attenuated by a hadronic form factor  $F(s)$  in which case

$$\rho(s) = \frac{2k}{\sqrt{s}} F(s), \quad (2)$$

where  $k$  is the momentum of one of the particles in the two-particle rest frame. For  $T(s)$  to be analytic, it must have a real part of the form

$$\text{Re}T(s) = \frac{1}{\pi} P \int_{s_{\text{thresh}}}^{\infty} \frac{ds' g^2(s') \rho(s')}{s' - s}, \quad (3)$$

where  $P$  denotes the principal value integral and  $s_{\text{thresh}}$  is the mass-squared at threshold. The resulting  $|T|$  has a very sharp, cusplike structure that peaks slightly above the  $M = \sqrt{s_{\text{thresh}}}$  threshold; this peak originates from kinematics and has nothing to do with any resonant structure in the  $D\bar{D}^*$  two-body system. The  $M(D\bar{D}^*)$  behavior of  $|T|$  and its real and imaginary parts is shown in Fig. 8(b). Guo *et al.* (2015) argued that genuine cusp effects are small, and that the cusp-based models (Bugg, 2011; Blitz and Lebed, 2015; Swanson, 2016), which described the significant near-threshold peaks in the experimental data, enhanced the cusp effect by introduction of *ad hoc*, nonanalytic form factors in the coupling constant  $g \rightarrow g(s)$  in Eq. (1), which invalidates the approach.

*Anomalous triangle singularity:* In three-body decays, diagrams that contain internal triangles, as illustrated in Fig. 8(c), may contribute. Landau (1959) showed that this diagram becomes singular when the three virtual particles that form the triangle are all simultaneously on the mass shell. This is called the anomalous triangle singularity (ATS). In kinematic regions where the conditions for this singularity are satisfied (Coleman and Norton, 1965), resonancelike peaking structures that have nothing to do with true particle resonances

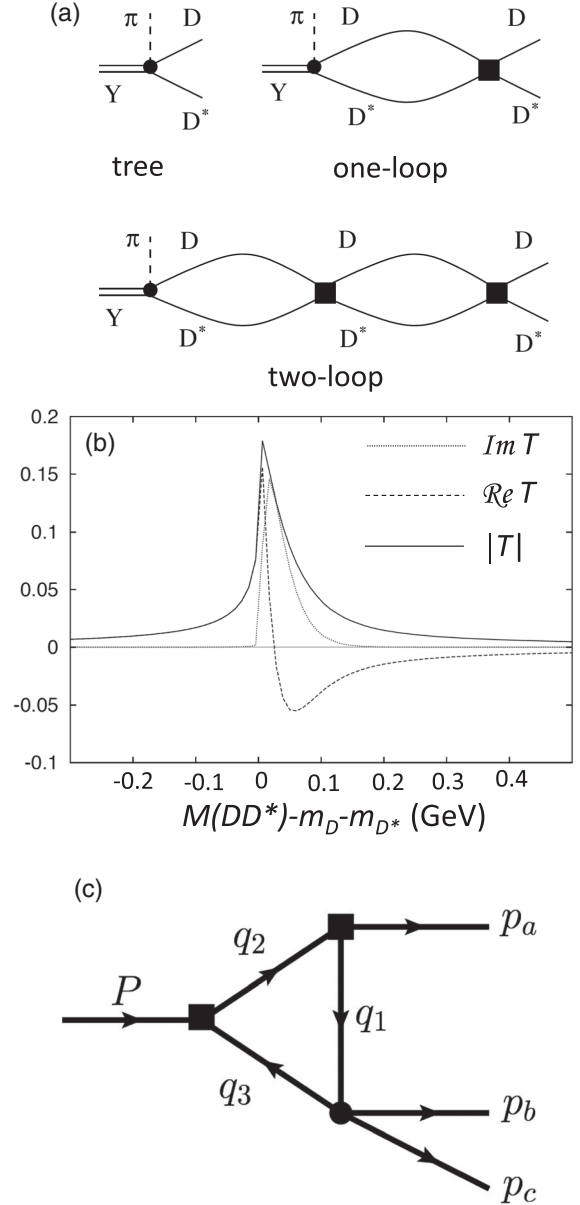


FIG. 8. (a) Low order diagrams that describe a three-body decay process  $Y \rightarrow \pi D \bar{D}^*$  scattering near the  $\sqrt{s} = m_D + m_{\bar{D}^*}$  threshold. From Guo *et al.*, 2015. (b) The scattering amplitude near threshold. The dotted curve is  $\text{Im}T$ , the dashed curve is  $\text{Re}T$ , and the solid curve is  $|T|$ . Adapted from Swanson, 2015. (c) A three-body decay with an internal triangle. This diagram is singular when the three virtual particles that form the triangle are all simultaneously on the mass shell.

can be produced. It has been shown that, if the rescattering is purely elastic, the effect of the triangle singularity integrates to zero in the Dalitz plot projections (Schmid, 1967). However, in the case of many coupled channels, this theorem applies to the sum of intensities of all of them, thus the Dalitz plot projections to individual channels can produce mass peaks (Szczepaniak, 2016). Properties of the ATS and methods for distinguishing ATS-induced mass peaks from genuine resonances have been discussed by Szczepaniak (2015), Liu, Oka, and Zhao (2016), and Pilloni *et al.* (2017).

### C. Lattice QCD

In QCD, information about the mass of a hadron  $H$  is encoded in the correlation function  $C_H(t)$  of the hadron creation operator  $\mathcal{O}_H$  evaluated at different times  $C_H(t) = \langle \Omega | \mathcal{O}_H^\dagger(t) \mathcal{O}_H(0) | \Omega \rangle$  (Wagner *et al.*, 2013). Here the state  $H$  is created from the vacuum  $|\Omega\rangle$  at time  $t = 0$  and propagates until time  $t$  when it is annihilated. The operator  $\mathcal{O}_H(t)$  is a suitable composition of quark and gluon field operators, e.g., for a pion, which is a pseudoscalar  $u\bar{d}$  state, it is  $\mathcal{O}_\pi(t) = \int d^3r \bar{u}(\mathbf{r}, t) \gamma_5 d(\mathbf{r}, t)$ , where  $d(\mathbf{r}, t)$  and  $\bar{u}(\mathbf{r}, t)$  are the  $\bar{d}$ - and  $u$ -quark creation operators. The integration extends over all possible spatial configurations of the quark and gluon fields. To avoid the oscillating behavior of the correlator in real time, the integration is performed in the Euclidean space-time where the time coordinate is imaginary. The hadron mass is determined from the correlation function's asymptotic exponential behavior  $C_H(t) \propto \exp(-m_H t)$ .

The path integral is impossible to solve analytically. A major conceptual breakthrough occurred when Wilson (1974) proposed that long-distance QCD could be digitized by transcribing the relevant integrals to a lattice of discrete space-time points, where quark fields placed at lattice sites interact with each other by interconnected gluon links. The resulting equations are solved numerically by using Monte Carlo techniques to generate random samples of all possible configurations.

The difficulty with this approach is that realistic lattice QCD (LQCD) computations require extreme computational resources, much beyond those that were available when Wilson first proposed his ideas. Ideally, the lattice should be several fermi in extent in order to fully contain a hadron while the lattice spacing must be small enough to minimize discretization errors. With a lattice of 32 sites in each of the four dimensions, there are  $32^4 \approx 10^6$  lattice sites. With quark fields restricted to just two quark flavors,  $u$  and  $d$ , each with a real and an imaginary part, with three colors and four spin components, plus 32 gluon degrees of freedom (8 color  $\times$  4 spin), the dimension of the integral is  $32^4 \times (2 \times 24 + 32) \approx 10^8$ .

Wilson's dream is now becoming a reality thanks to the relentless, Moore's lawlike advance in high-performance computing. Systems capable of providing hundreds of teraflop/sr by exploiting large-scale parallel programming techniques with calculations running cooperatively across thousands of processors are now available (Blum *et al.*, 2013).<sup>10</sup> This, coupled with major advances in LQCD algorithms [see Orginos and Richards (2015) for a recent review], has resulted in a number important recent results related to hadron masses.

For example, the QCDSF Collaboration (Bietenholz *et al.*, 2011) reported a lattice calculation of the masses of hadrons composed of  $u$ ,  $d$ , and  $s$  quarks, ranging from the  $\eta$  meson to the  $\Omega^-$  baryon using only the charged pion and kaon masses and a combination of the  $p$ ,  $\Sigma$ , and  $\Xi$  masses as inputs; the

<sup>10</sup>One teraflop/sr is defined as the number of floating-point operations performed in a year by a computer that sustains  $1 \times 10^{12}$  operations per second.

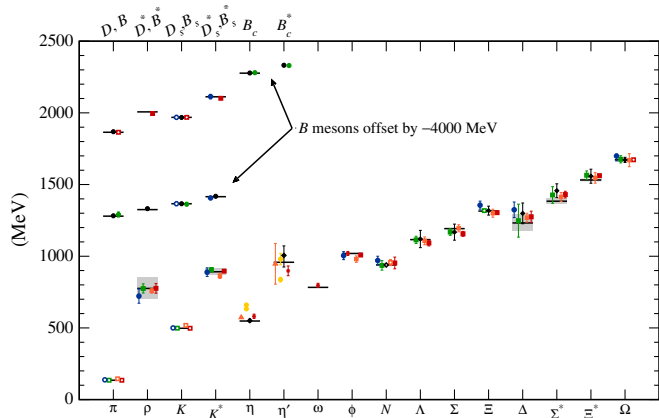


FIG. 9. The LQCD hadron spectrum from MILC (Aubin *et al.*, 2004; Bazavov *et al.*, 2010), PACS-CS (Aoki *et al.*, 2009), BMW (Durr *et al.*, 2008), QCDSF (Bietenholz *et al.*, 2011), RBC and UKQCD (Christ *et al.*, 2010), Hadron Spectrum (Dudek *et al.*, 2011), UKQCD (Gregory *et al.*, 2012), Fermilab-MILC (Bernard *et al.*, 2011), HPQCD (Gregory *et al.*, 2011), and Mohler and Woloshyn (2011). The  $b$ -flavored meson masses are offset by  $-4000$  MeV. Horizontal bars (gray boxes) denote experimentally measured masses (widths). From Kronfeld, 2012.

only tunable parameters are the quark masses and the coupling constant  $\alpha_s$ . Recent results for mesons and baryons are shown in Fig. 9, where there is good agreement with the established values.

To date, because of computing-power constraints, most LQCD computations ignore isospin violations and set the  $u$ - and  $d$ -quark masses equal. However, precision lattice results on QCD-generated isospin violations are now being realized. Borsanyi *et al.* (2015) reported a lattice-based, *ab initio* computation of the (1.293 MeV) neutron-proton mass difference that results from the competition between electromagnetic and QCD-induced isospin-breaking effects<sup>11</sup> with an accuracy of 300 keV. They also determined mass splittings in the  $\Sigma$ ,  $\Xi$ ,  $D$ , and  $\Xi_{cc}$ <sup>12</sup> isospin multiplets with precision that is better, in some cases, than that of the currently available experimental measurements, as shown in Fig. 10.

The spectrum of mesons containing one charmed quark, or a charmed-anticharmed pair, was recently computed on the lattice by Cichy, Kalinowski, and Wagner (2016). To tune the valence quark masses they used experimental values of the masses of electrically neutral and charged  $\pi$ ,  $K$ , and  $D$

<sup>11</sup>The calculation reported by Borsanyi *et al.* (2015) found a QCD contribution to  $m_n - m_p$  that is  $2.52 \pm 0.49$  times larger than that from the (opposite-sign) electromagnetic effect. The magnitude of this QCD contribution has a large existential significance; an increase or decrease by as little as  $\sim 20\%$  would have dire consequences on nature's ability to support life (Wilczek, 2015).

<sup>12</sup>The  $\Xi_{cc}$  is a candidate for a doubly charmed  $ccq$  baryon with mass  $M = 3820 \pm 1.0$  MeV that was reported by the SELEX experiment (Mattson *et al.*, 2002; Ocherashvili *et al.*, 2005) but was not confirmed by other experiments (Aaij *et al.*, 2013c; Aubert *et al.*, 2006d; Chistov *et al.*, 2006). The LHCb group recently reported a  $12\sigma$  signal for a  $\Xi_{cc}$  candidate at a lower mass of  $3621.4 \pm 0.8$  MeV (Aaij *et al.*, 2017e).

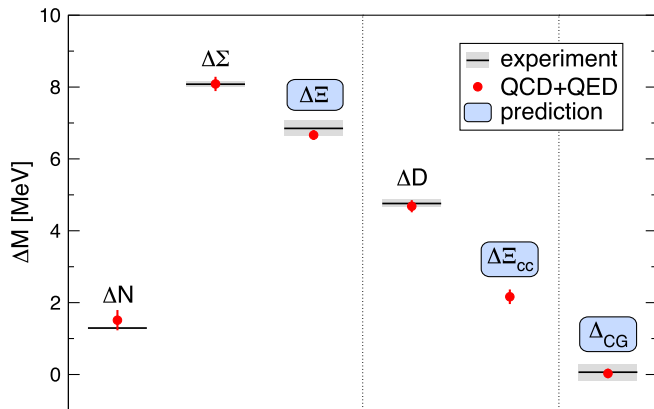


FIG. 10. Results of the lattice computations of  $\Delta N = m_n - m_p$ ,  $\Delta\Sigma = m_{\Sigma^-} - m_{\Sigma^+}$ ,  $\Delta\Xi = m_{\Xi^-} - m_{\Xi^0}$ ,  $\Delta D = m_{D^+} - m_{D^0}$ , and  $\Delta\Xi_{cc} = m_{\Xi_{cc}^{++}} - m_{\Xi_{cc}^+}$  isospin mass splittings, and a test of the Coleman-Glashow relation (Coleman and Glashow, 1961)  $\Delta_{CG} \equiv \Delta M_N - \Delta M_\Sigma - \Delta M_\Xi = 0$ . The horizontal lines are the experimental values and the gray shaded regions represent the experimental error. The computed precision for the quantities with labels in blue shaded boxes is better than that of current measurements. From Borsanyi *et al.*, 2015.

mesons. Using a variety of quark-antiquark meson creation operators they were able to determine the masses of the lowest-lying  $1S$  and  $1P$  charmonium states with levels of precision that are in the range 0.2%–0.8%. Cichy, Kalinowski, and Wagner (2016) also successfully verified the masses of several charm mesons with the exception of the  $D_{s0}^*(2317)$  and  $D_{s1}(2460)$  (see Sec. IV), which have masses close to two-meson thresholds and, thus, require more advanced techniques (Leskovec *et al.*, 2015), as discussed in Sec. IV.

The Hadron Spectrum Collaboration (Liu *et al.*, 2012) did a comprehensive study of the spectrum of excited charmonium mesons with masses up to 4.5 GeV that included possible  $c\bar{c}$ -gluon hybrid states. They found that the lightest  $c\bar{c}$ -gluon hybrids are a  $0^{-+}$  pseudoscalar with  $M \approx 4195$  GeV: a  $1^{-+}$  exotic with  $M \approx 4215$  MeV and a  $1^{--}$  vector with  $M \approx 4285$  MeV. One of the nonstandard mesons discussed in this review is the  $Y(4260)$  vector state that is considered by some to be a promising candidate for a  $1^{--}$  hybrid state. (This is discussed in Sec. V.C.) It will be interesting to see what happens to the LQCD-computed mass value when calculations extended to three-particle resonances (Hansen and Sharpe, 2014, 2015; Briceno, Hansen, and Sharpe, 2016) become feasible in the next decades. Determining the highly excited resonance spectra has recently become possible thanks to a technique proposed by Luscher (1991).

Recently, attempts to address questions related to possible quarkoniumlike, four-quark mesons have been reported. For example, in order to get insight into the structure of the  $X(3872)$ , a candidate nonstandard meson with mass very near the  $D\bar{D}^*$  threshold [i.e.,  $M(X(3872)) \approx m_D + m_{D^*}$ ] and discussed in Sec. V.A, Padmanath, Lang, and Prelovsek (2015) made a LQCD study that included standard  $c\bar{c}$  charmonium,  $D\bar{D}^*$  meson-meson, and diquark-diantiquark operators, 22 in total, that allowed the particle to be a superposition of all three configurations. Their result indicated

the presence of a  $c\bar{c}$  and a meson-meson ( $D\bar{D}^*$ ) component, but with no sign of a diquark-diantiquark component, leading them to the conclusion that a QCD tetraquark interpretation of the  $X(3872)$  was disfavored. Bicudo *et al.* (2016) considered the possible existence of bound states in the  $\bar{b}\bar{b}ud$  four-quark systems with a net beauty flavor of  $B = 2$ . Their first exploratory simulations found signs of a state with a binding energy of  $-90_{-36}^{+43}$  MeV, i.e., about  $2\sigma$  from zero. This was followed up by more precise calculations; see Francis *et al.* (2017) and references therein. For a review of the searches of resonances with LQCD, see Briceno, Dudek, and Young (2017).

Lattice QCD efforts in the area of nonstandard hadron spectroscopy, while still in their infancy, are very encouraging. With the order-of-magnitude increase in the available computing power expected during the next decade (Blum *et al.*, 2013) and continued advances in the sophistication of the algorithms that will be used to extract physics information from the improved configurations, LQCD seems to be on the verge of becoming a powerful tool for deriving a theoretical understanding of the recently discovered states and for providing important guidance for future experiments.

### III. HEAVY FLAVOR EXPERIMENTS

The results reviewed here come from experiments that operate at vastly different energies. At the low-energy extreme is the BESIII experiment at the Institute of High Energy Physics in Beijing that operates at the BEPCII  $e^+e^-$  collider and can access c.m. energies between 2 and 4.6 GeV. At the high-energy extreme are the ATLAS, CMS, and LHCb experiments operating at the LHC  $pp$  collider at CERN, with c.m. energies that are more than 3 orders of magnitude higher, i.e., 7 to 13 TeV. In between are the now defunct BABAR and Belle  $e^+e^-$   $B$ -factory experiments and, earlier, the CLEO experiment that all ran at c.m. energies near 10 GeV, and the CDF and D0 experiments at the 1.96 TeV Tevatron  $p\bar{p}$  collider.

The low-energy  $e^+e^-$  experiments have the advantage of clean experimental environments and the ability to exploit energy-momentum-conservation constraints to help extract signals from complex final states, including those containing  $\gamma$  rays and  $\pi^0$  mesons. However, the relevant production cross sections are at the few nanobarn level and, even with the high luminosities achieved by BEPCII and the  $B$  factories, event rates are low. In contrast, the high-energy experiments at hadron colliders enjoy charm particle production cross sections of a few millibarns and beauty particle cross sections of the order of a 100  $\mu\text{b}$ , so large event samples can be accumulated. The charmed and beauty particles are usually highly boosted, thereby producing decay vertices that are well separated from the production point and experimentally quite distinct. This makes it possible to isolate very clean samples of events, but only for all-charged-particle final states. Final states containing neutral particles suffer from severe combinatorial backgrounds and low detection efficiency.

Many of the early contributions to this research were from the BABAR (Aubert *et al.*, 2002) and Belle (Abashian *et al.*, 2002) experiments that operated at the PEP-II (PEP-II, 1993)

and KEKB (Kurokawa and Kikutani, 2003)  $e^+e^- B$  factories, respectively, between 1999 and 2010. These facilities accumulated data at and near  $E_{c.m.} = 10.58$  GeV to study matter-antimatter asymmetries ( $CP$  violations) in the decays of  $B$  mesons and to validate the Kobayashi-Maskawa mechanism for  $CP$  violation (Kobayashi and Maskawa, 1973).

The total cross section for  $e^+e^- \rightarrow$  hadrons at energies that were accessed by the  $B$ -factory colliders is shown in Fig. 11(b). There are three narrow peaks, called the  $\Upsilon(1S)$ ,  $\Upsilon(2S)$ , and  $\Upsilon(3S)$ , at c.m. energies of 9.46, 10.02, and 10.36 GeV, respectively. These are the three lowest spin-triplet  $S$ -wave bottomonium ( $b\bar{b}$ ) states. Since they are below the  $E_{c.m.} = 2m_B = 10.56$  GeV open-bottom threshold and, thus, not able to decay into a  $B$  and a  $\bar{B}$  meson pair, their primary decay channel is via  $b$ -quark  $\bar{b}$ -quark annihilation into gluons. Since this is an “OZI-suppressed” process,<sup>13</sup> the three below-threshold bottomonium states have natural widths that are less than 100 keV and much smaller than the colliders’ c.m. energy spreads, which are typically  $\sim 6$  MeV. The fourth peak, the  $\Upsilon(4S)$ , with a peak mass of 10.58 GeV, can decay to  $B\bar{B}$  meson pairs and has a natural width of  $\Gamma(\Upsilon(4S)) \approx 20$  MeV and is distinctly broader than the c.m. energy spread. Most of the data taking by both  $B$ -factory experiments occurred at a c.m. energy corresponding to the peak mass of the  $\Upsilon(4S)$  resonance.

The BEPCII  $e^+e^-$  collider (Gu *et al.*, 2003) in Beijing and its associated BESIII experiment (Ablikim *et al.*, 2010) started operation in 2008 and covers the c.m. energy range between 2.0 and 4.6 GeV, which includes the thresholds for producing  $\tau^+\tau^-$  lepton and  $c\bar{c}$  quark pairs. The  $c\bar{c}$  system has two narrow  $J^{PC} = 1^{--}$  resonances below the  $E_{c.m.} = 2m_D = 3.73$  GeV open-charm threshold: the  $J/\psi$  and the  $\psi'$  [the latter is often denoted as  $\psi(2S)$  or  $\psi(3686)$ ]. The first  $1^{--}$  resonance above that threshold is the  $\psi(3770)$ , which decays almost exclusively into  $D\bar{D}$  final states. Figure 11(a) shows  $\sigma(e^+e^- \rightarrow$  hadrons) for energies that are accessible at the BEPCII collider.

As is clear from the cross-section plot in Fig. 11(b),  $e^+e^-$  annihilations with c.m. energies between 9.4 and 10.8 GeV, the energy range that was accessible to *BABAR* and *Belle*, are good sources of particles containing  $b$  quarks and  $b\bar{b}$ -quark pairs. In addition,  $e^+e^-$  collisions in this energy range also produce relatively large numbers of particles containing  $c$  quarks and  $c\bar{c}$ -quark pairs. The processes involved are illustrated in Fig. 12 and described in the following.

*Charmed quark production in B-meson decays:*  $\bar{B}$  mesons have a  $b\bar{q}$  quark content ( $\bar{q} = \bar{u}$  or  $\bar{d}$ ), a mass of 5.28 GeV, and a lifetime of approximately 1.5 ps. In  $E_{c.m.} = 10.58$  GeV  $e^+e^-$  collisions they are produced in  $B\bar{B}$  pairs that are nearly at rest and with no accompanying particles. The primary decay mechanism is the weak interaction transition  $b \rightarrow c$  with the emission of a virtual  $W^-$  boson. In about 15% of these decays, the  $W^-$  materializes as a  $\bar{c}$  and an  $s$  quark. Figure 12(a) illustrates this process for the cases where the  $s$  quark

<sup>13</sup>The suppression of strong interaction processes in which no quark lines connect the initial to the final state is known as the Okubo-Zweig-Iizuka (OZI) rule (Okubo, 1963; Zweig, 1964; Iizuka, 1966).

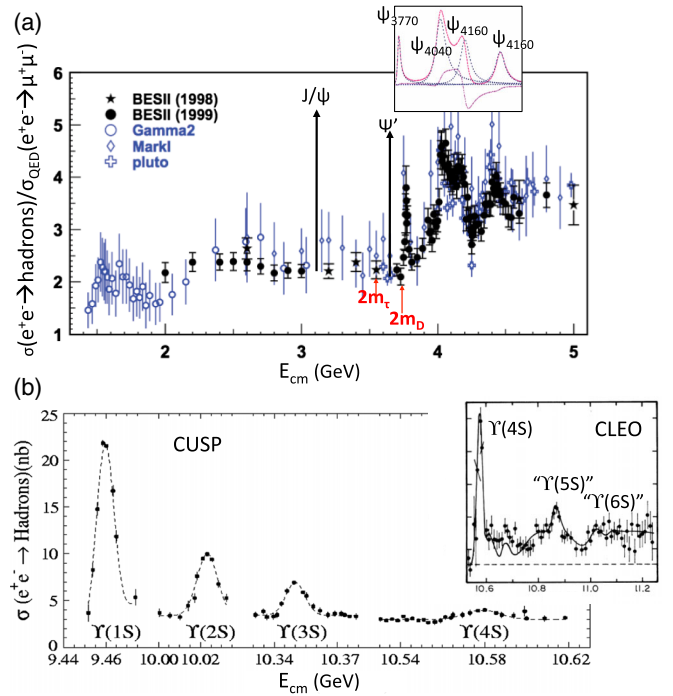


FIG. 11. (a) Total cross-section measurements for  $e^+e^-$  annihilation into hadronic final states in units of the QED cross section  $\sigma_{\text{QED}}(e^+e^- \rightarrow \mu^+\mu^-) = 86.8 \text{ nb/s}(\text{GeV}^2)$  (Augustin *et al.*, 1975; Bacci *et al.*, 1981; Criegee and Knies, 1982; Bai *et al.*, 2000, 2002). The inset shows the results of a fit to the measurements in the 3.6 to 4.6 GeV energy interval that identifies the  $1^{--}$  charmonium states in this region (Ablikim *et al.*, 2007). (b) Measurements of  $\sigma(e^+e^- \rightarrow$  hadrons) in the 9.45 to 10.62 GeV energy region from CUSP (Rice *et al.*, 1982). The inset shows measurements between 10.55 and 11.5 GeV from CLEO (Besson *et al.*, 1985).

combines with the spectator  $\bar{q}$  to form a  $K$  meson. In these events the system recoiling against the  $K$  meson contains a  $c\bar{c}$  quark pair and, to the extent that the original  $\bar{q}$  quark is a passive spectator to the decay process (the “factorization approximation”) (Beneke *et al.*, 1999), the  $c\bar{c}$  pair has  $J^{PC}$  quantum numbers of  $0^{++}$ ,  $1^{--}$ , and  $1^{++}$ , which finds support in the experimental results (Aubert *et al.*, 2006b). Sizable corrections to the factorization approximation may occur.

Since the  $B$  mesons are produced in pairs with no accompanying particles, the c.m. energy of each meson is  $E_{c.m.}/2$ , which is precisely known from the operating conditions of the collider. This provides two powerful and weakly correlated experimental signatures for identifying events of interest:  $\Delta E_{c.m.} \equiv E_{c.m.}/2 - \sum_i E_i^* = 0$  and  $M_{bc} \equiv \sqrt{(E_{c.m.}/2)^2 - |\sum_i \vec{p}_i^*|^2} = m_B$ , where  $E_i^*$  and  $\vec{p}_i^*$  are the c.m. energy and three-momentum of the  $i$ th decay product of the  $B$  meson candidate. The experimental resolutions for  $\Delta E_{c.m.}$  and  $M_{bc}$  depend upon the decay mode that is under consideration; typical rms values are 10–15 MeV for  $\Delta E_{c.m.}$  and 2.5–3 MeV for  $M_{bc}$ . For a more detailed discussion of these variables and an improved definition of  $M_{bc}$  for asymmetric  $e^+e^-$  colliders, see Sec. VII.1.1.2 of Bevan *et al.* (2014).

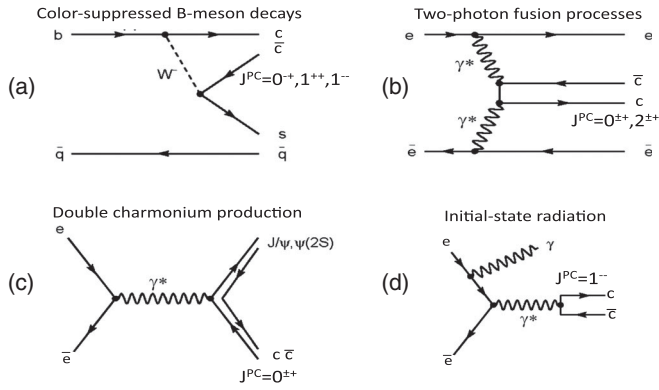


FIG. 12. Processes that produce  $c\bar{c}$  pairs in  $e^+e^-$  collisions near  $E_{c.m.} = 10.6$  GeV: (a)  $B \rightarrow K(c\bar{c})$  decays, (b) two-photon fusion processes, (c)  $e^+e^-$  annihilation into  $c\bar{c}c\bar{c}$ , and (d) initial state radiation.

The  $X(3872)$ , the first of the nonstandard  $XYZ$  meson candidates to be seen, was discovered by Belle as a narrow peak in the  $\pi^+\pi^-J/\psi$  invariant mass distribution for  $B \rightarrow K\pi^+\pi^-J/\psi$  decays (Choi *et al.*, 2003). Figure 13 shows the  $M_{bc}$ ,  $\Delta E_{c.m.}$ , and  $M(\pi^+\pi^-J/\psi)$  distributions for  $B^- \rightarrow K^-X(3872)$ ;  $X(3872) \rightarrow \pi^+\pi^-J/\psi$  event candidates, where the events in each plot are selected from the signal peak regions of the other two distributions. The background under the signal peaks is mainly combinatorial, i.e., where one of the tracks assigned to the reconstructed  $B$  meson is, in fact, a decay product of the accompanying  $\bar{B}$ . The  $X(3872)$  is discussed in detail in Sec. V.A.

*Two-photon fusion processes:* In the two-photon fusion process, both the incoming  $e^-$  and  $e^+$  radiate photons that subsequently interact via the diagram shown in Fig. 12(b). In this process, the quark-antiquark pair is produced with a probability that is proportional to  $e_q^4$ , where  $e_q$  is the quark charge; since  $e_c = 2/3$ , this favors  $c\bar{c}$  production. This process is dominated by events where both of the incoming photons are nearly real ( $q^2 \approx 0$ ), in which case both the  $e^+$  and  $e^-$  scatter at very small angles and are undetectable. For these “untagged” events the net transverse momentum  $p_T$  of the  $c\bar{c}$  system’s decay products is very small, and this provides an important experimental signature. The allowed  $J^{PC}$  quantum numbers for  $c\bar{c}$  systems produced via this process are restricted to  $0^{\pm++}$  and  $2^{\pm++}$ . The conventional  $\chi'_{c2}$  ( $2^3P_2$ ) charmonium state was first seen by Belle (Uehara *et al.*, 2006) as a distinct peak near 3930 MeV in the  $D\bar{D}$  invariant mass distribution in selected, low  $p_T$   $\gamma\gamma \rightarrow D\bar{D}$  candidate events.

*Double charmonium production:* Prior to the operation of the  $B$  factories, computations based on NRQCD predicted that prompt inclusive  $J/\psi$  production in continuum  $e^+e^-$  annihilation events at  $E_{c.m.} \approx 10$  GeV would be dominated by  $e^+e^- \rightarrow J/\psi g$  and  $e^+e^- \rightarrow J/\psi gg$  processes, where  $g$  denotes a gluon, and that  $e^+e^- \rightarrow J/\psi c\bar{c}$  processes would account for no more than 10% of the inclusive  $J/\psi$  production rate (Berezhnoy and Likhoded, 2004). One of the surprises from the  $B$  factories was the Belle observation that the  $e^+e^- \rightarrow J/\psi c\bar{c}$  process is, in fact, the dominant mechanism

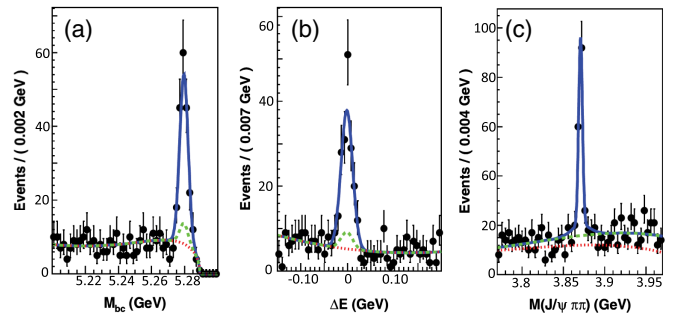


FIG. 13. (a)  $M_{bc}$ , (b)  $\Delta E_{c.m.}$ , and (c)  $M(\pi^+\pi^-J/\psi)$  distributions for  $B^- \rightarrow K^-\pi^+\pi^-J/\psi$  decays. The narrow  $\pi^+\pi^-J/\psi$  mass peak in (c) is the  $X(3872)$  signal. From Choi *et al.*, 2011.

for prompt  $J/\psi$  production, accounting for approximately 60% of the total rate for these events (Pakhlov *et al.*, 2009). Charge conjugation invariance requires that the  $c\bar{c}$  system recoiling against the  $J/\psi$  have even charge conjugation parity.<sup>14</sup> Figure 14(a) shows Belle’s measured distribution of masses recoiling from the  $J/\psi$  in inclusive  $e^+e^- \rightarrow J/\psi + X$  production, with clear peaks corresponding to the  $\eta_c$ ,  $\chi_{c0}$ , and  $\eta'_{c1}$ , the well-established  $1^1S_0$ ,  $1^3P_0$ , and  $2^1S_0$  charmonium states, respectively (Abe *et al.*, 2007). In addition, there is a distinct peak  $X(3940)$  that cannot be identified with any known charmonium state.

The established charmonium states seen in Fig. 14(a) all have even charge conjugation and zero angular momentum ( $J = 0$ ). The absence of signals for the  $\chi_{c1}$  and  $\chi_{c2}$ , which are in the same mass range and have even  $C$ , provides some circumstantial evidence that the  $e^+e^- \rightarrow J/\psi + (c\bar{c})$  production process favors  $(c\bar{c})$  systems with  $J = 0$ .

*Initial state radiation:* In  $e^+e^-$  colliders, the initial state  $e^+$  or  $e^-$  occasionally radiates a high-energy  $\gamma$  and the  $e^+$  and  $e^-$  subsequently annihilate at a correspondingly reduced c.m. energy  $E'_{c.m.} = E_{c.m.}\sqrt{1-x}$ , where  $x = 2E_\gamma/E_{c.m.}$  is the fraction of the radiating beam particle’s c.m. energy that is carried off by the photon.  $B$ -factory experiments typically operate at  $E_{c.m.} = 10.58$  GeV and, when an  $E_\gamma \approx 4.5$  GeV  $\gamma$  is radiated, the  $e^+e^-$  annihilation occurs at a c.m. energy of  $E'_{c.m.} \approx 4$  GeV, which is in the  $c\bar{c}$  threshold region. As a result,  $e^+e^-$  collisions at  $E_{c.m.} = 10.58$  GeV can directly produce  $1^{--}$   $c\bar{c}$  states in association with a single high-energy  $\gamma$ . Advantages of measurements that exploit this initial state radiation (ISR) process are that they can be made parasitically with other measurements and a broad range of reduced energies can be accessed at the same time. Although ISR is a higher-order QED process and, thus, suppressed, the very high luminosities provided by the  $B$ -factory colliders have made it a valuable research tool. Figure 14(b) shows the invariant mass distribution from BABAR for  $\pi^+\pi^-J/\psi$  events produced in association with a high-energy  $\gamma$  (Aubert *et al.*, 2005a). In this measurement, the ISR  $\gamma$  was not detected and, instead, its existence was established by selecting events with

<sup>14</sup>Two charmonium states with the same  $C$  parity can be produced in two-photon annihilation processes, but these are suppressed relative to single-photon annihilation by a factor of  $(\alpha_{\text{QED}}/\alpha_s)^2$  (Bodwin, Lee, and Braaten, 2003).

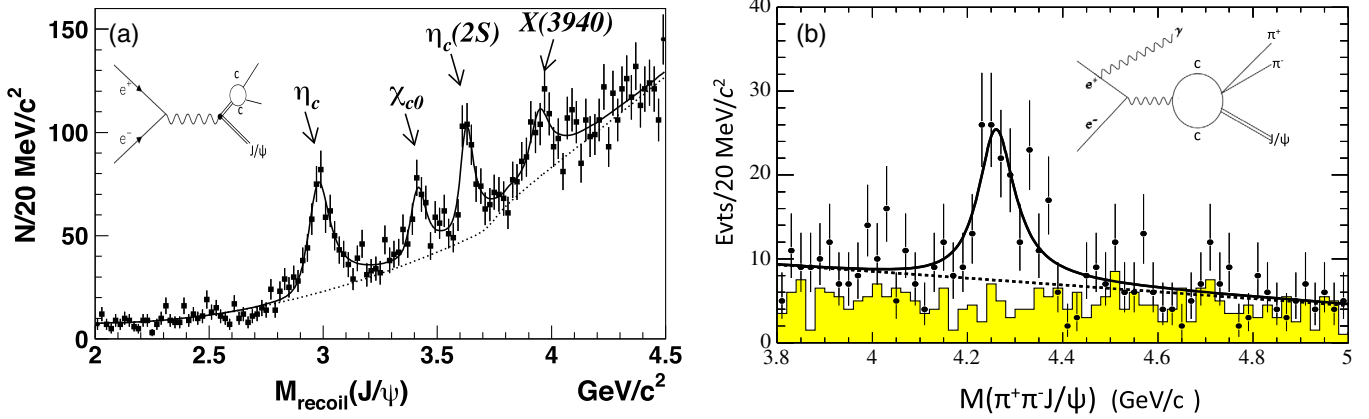


FIG. 14. (a) The distribution of masses recoiling from the  $J/\psi$  in inclusive  $e^+e^- \rightarrow J/\psi X$  events. From Abe *et al.*, 2007. (b) The  $\pi^+\pi^-J/\psi$  invariant mass distribution for  $e^+e^- \rightarrow \gamma_{\text{ISR}}\pi^+\pi^-J/\psi$  events. From Aubert *et al.*, 2005a.

a missing mass  $M_{\text{miss}}$  consistent with zero, where  $M_{\text{miss}} \equiv \sqrt{(E_{\text{c.m.}} - \sum_i E_i^*)^2 - |\sum_i \vec{p}_i^*|^2}$  and  $E_i^*$  and  $\vec{p}_i^*$  are the c.m. energy and three-momentum of the  $i$ th detected particle. The  $\pi^+\pi^-J/\psi$  mass distribution in Fig. 14(b) is dominated by an unexpected distinct peak near 4.26 GeV that *BABAR* called the  $Y(4260)$ . Its production from a single virtual photon ensures that the  $J^{PC}$  quantum numbers of the  $Y(4260)$  must be the same as those of the photon, i.e.,  $1^{--}$ . There are no unassigned  $1^{--}$  charmonium states near 4260 MeV and the  $Y(4260)$  cannot be a conventional  $c\bar{c}$  meson. The  $Y(4260)$  is discussed in detail in Sec. V.C.

For  $J^{PC} = 1^{--}$  states such as the  $Y(4260)$ , the BESIII experiment near the  $\tau$ -charm threshold region has the advantage that they can be directly produced in  $e^+e^-$  annihilation, e.g.,  $e^+e^- \rightarrow Y(4260) \rightarrow \pi^+\pi^-J/\psi$ , with no ISR photons and their associated luminosity penalty.

By working with exclusive events near threshold, and exploiting the possibility of applying energy and momentum kinematic constraints that improve resolution and signal to noise, the BESIII experiment is uniquely able to isolate events with complex final states. This provides opportunities that are not available to  $B$ -factory and hadron-collider experiments that are mostly restricted to studies of processes that include a final-state  $J/\psi$  or  $\psi'$  that decays to a pair of leptons. This is because dilepton events are experimentally distinct, simple to reconstruct, and have low combinatorial backgrounds. In contrast, the BESIII experiment routinely isolates clean signals of charmonium states that only decay to complex multihadron final states and are plagued by large combinatorial backgrounds in  $B$ -factory and hadron-collider environments. For example, BESIII has made studies of reactions that have an  $\eta_c$  and/or an  $h_c$  in the final state, by selecting and reconstructing complex, multihadron final states.<sup>15</sup>

<sup>15</sup>The  $\eta_c$  is the  $0^{-+}$  spin-singlet hyperfine partner of the  $J/\psi$  and the  $h_c$  is the  $1^{+-}$  spin-singlet partner of the  $(\chi_{c0}, \chi_{c1}, \chi_{c2})$   $P$ -wave spin triplet of  $c\bar{c}$  states. Although the existence of the  $h_c$  was predicted in 1974, it remained undiscovered until 30 years later, when it was found in  $\psi' \rightarrow \pi^0 h_c$  decays by the CLEO experiment (Rosner *et al.*, 2005).

This capability is illustrated by a recent BESIII study of the  $e^+e^- \rightarrow \pi^+\pi^-h_c$  process at c.m. energies in the vicinity of the  $Y(4260)$  peak, in which they detected the  $h_c$  via its decay to  $h_c \rightarrow \gamma\eta_c$  (Fig. 15), which is its dominant decay mode with a branching fraction of  $51\% \pm 6\%$  (Patrignani *et al.*, 2016). To accomplish this, they selected  $e^+e^- \rightarrow \pi^+\pi^-h_c$  events, where the candidate  $\eta_c$  mesons were reconstructed in one of 16 different exclusive hadronic decay channels, and applied conservation of energy and momentum constraints. With this relatively clean  $e^+e^- \rightarrow \pi^+\pi^-h_c$  event sample, the BESIII experiment discovered a narrow enhancement in the  $\pi^\pm h_c$  invariant mass distribution that is a candidate for an electrically charged charmoniumlike four-quark state, called the  $Z_c(4020)$  (Ablikim *et al.*, 2013b), as discussed in Sec. VI.B. Reconstruction of events with an  $h_c$  in the final state has never been accomplished in  $B$ -factory or hadron-collider experiments.

The BESIII experiment is scheduled to continue to run until 2025, with some minor upgrades to the detector and the BEPCII collider. There are serious discussions in China (Zhao *et al.*, 2016) and Russia (Bondar *et al.*, 2013) about the possibility of a new facility in the charm quark threshold

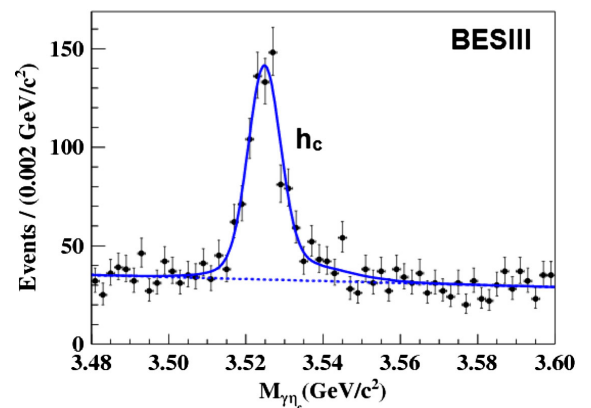


FIG. 15. The projection of events with  $\gamma\pi^+\pi^-$  recoil mass near the  $\eta_c$  mass onto  $\gamma\eta_c$  mass for  $e^+e^- \rightarrow \pi^+\pi^-\gamma\eta_c$  candidate events in BESIII. From Ablikim *et al.*, 2013b.



energy region with a luminosity of the order of  $10^{35} \text{ cm}^{-2} \text{ s}^{-1}$ , a 2-order-of-magnitude increase over that of BEPCII.

SuperKEKB is a major upgrade to the KEKB facility with the ambitious goal of a factor of 40 increase in instantaneous luminosity (to  $8 \times 10^{35} \text{ cm}^{-2} \text{ s}^{-1}$ ) that will start operation in late 2017 with a targeted total integrated luminosity of  $50\,000 \text{ fb}^{-1}$  (50 inverse attobarns) by about 2025 (Ohnishi *et al.*, 2013). BelleII is an upgraded version of the Belle detector that is being constructed by a large international collaboration to exploit the physics opportunities provided by SuperKEKB (Aushev *et al.*, 2010a). While the main emphasis of the BelleII program is on searches for new, beyond the standard model physics processes, a high-sensitivity program of studies of hadron spectroscopy is planned (Bondar, Mizuk, and Voloshin, 2017).

The CDF (Acosta *et al.*, 2004) and D0 (Abazov *et al.*, 2004) experiments at the Tevatron, which collided  $p\bar{p}$  at 1.96 TeV c.m. energy, were the first to confirm Belle’s observation of the  $X(3872)$ . They made the important observations that characteristics of  $X(3872)$  production in hadron collisions were very similar to those of the  $\psi'$ , including strong signals for prompt production (Fig. 16). This is a strong indication the  $X(3872)$  and  $\psi'$  production mechanisms are the same. This is discussed further in Sec. V.A.

In the proper time distribution for  $X(3872) \rightarrow \pi^+\pi^-J/\psi$  vertex positions CDF found that most of the  $X(3872)$  production in  $p\bar{p}$  collisions was due to prompt QCD processes; only  $16\% \pm 5\%$  of the signal is from displaced vertices that are characteristic of open-bottom-particle decays (Bauer, 2005). The displaced-vertex fraction for  $\psi'$  production is somewhat larger,  $28\% \pm 1\%$ , but comparable. In 2009, with an order-of-magnitude larger data set, CDF reported the most precise single mass measurement to date,  $M(X(3872)) = 3871.61 \pm 0.16(\text{stat}) \pm 0.19(\text{syst}) \text{ MeV}$  (Fig. 17). This mass value is indistinguishable from the  $D^0\bar{D}^{*0}$  threshold mass  $m_{D^0} + m_{D^{*0}} = 3871.68 \pm 0.10 \text{ MeV}$  (Patrignani *et al.*, 2016),

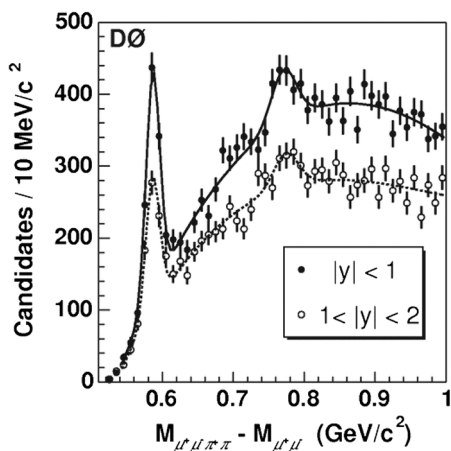


FIG. 16. The  $\Delta M = M(\pi^+\pi^-\mu^+\mu^-) - M(\mu^+\mu^-)$  distributions for central events (solid points) and end-cap events (open circles). The similarity between the relative signal yields in the  $X(3872)$  and  $\psi'$  peaks indicates that the production mechanism for the two states has similar dependence on pseudorapidity ( $|y|$ ). From Abazov *et al.*, 2004.

with high precision; this is one of the most striking properties of the  $X(3872)$ .

The latest generation of high- $p_T$   $pp$  hadron-collider experiments at the LHC, ATLAS (Aad *et al.*, 2008), and CMS (Chatrchyan *et al.*, 2008) are producing complementary results on the production of exotic hadrons. For example, CMS has measured the  $p_T$  dependence of the prompt  $X(3872)$  production cross section (Chatrchyan *et al.*, 2013a) and found it to be about a factor of 4 below an NRQCD-based theoretical prediction (Artoisenet and Braaten, 2010). CMS (Chatrchyan *et al.*, 2013b) and ATLAS (Aad *et al.*, 2015) have also performed measurements of the inclusive  $\pi^+\pi^-\Upsilon(1S)$  mass distribution at a c.m. energy of 8 TeV in search for bottomoniumlike counterparts of the  $X(3872)$  or  $Y(4260)$ . No dramatic signals were found, but the sensitivity of these searches was not very high. Cross section times branching-fraction upper limits for new state production that are  $\sim 6.5\%$  of the  $\Upsilon(2S) \rightarrow \pi^+\pi^-\Upsilon(1S)$  production were established (Chatrchyan *et al.*, 2013a); this is about the same as the CMS measured ratio for  $X(3872) \rightarrow \pi^+\pi^-J/\psi$  and  $\psi' \rightarrow \pi^+\pi^-J/\psi$  production:  $6.6\% \pm 0.7\%$  (Chatrchyan *et al.*, 2013a).

The LHCb experiment is the first hadron-collider experiment that is dedicated to heavy-flavor physics. Its detector (Alves *et al.*, 2008; Aaij *et al.*, 2015a) is a single-arm forward spectrometer that captures heavy-quark production cross sections that are comparable to those in the high- $p_T$ , central detectors at LHC, but concentrated in a compact solid angle near the forward direction ( $0.8^\circ < \theta < 15.4^\circ$ ). Because of this concentration, a much smaller number of electronic channels are required and, thus, there is a smaller data record for each event. As a result, the LHCb data acquisition system can record events at a higher frequency than the high- $p_T$  detectors; the LHCb recorded data at a 5 kHz rate in run I (2011–2012)

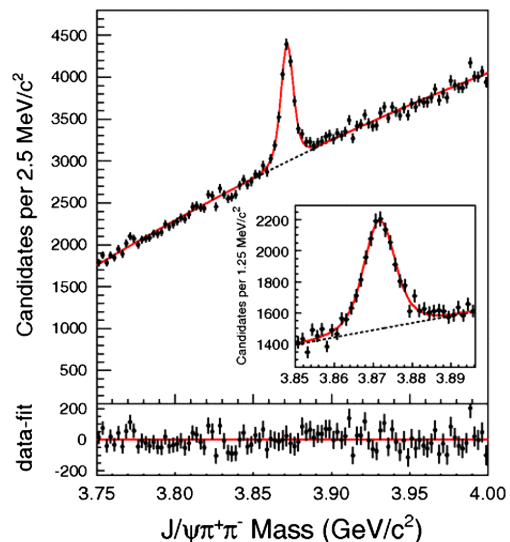


FIG. 17. The data points in the upper panel show the invariant mass distribution for  $X(3872) \rightarrow \pi^+\pi^-J/\psi$  candidates in the CDF detector. The solid curve shows the result of an unbinned likelihood fit and the dashed curve shows the background component. The lower panel shows the fit residuals. From Aaltonen *et al.*, 2009b.

and 12.5 kHz in run II (2015–present), which are about a factor of 5 higher than the corresponding rates for the ATLAS and CMS detectors. Furthermore, in contrast with the central detectors, most of the trigger bandwidth is dedicated to heavy-flavor physics and includes dimuon events with low transverse momentum thresholds and purely hadronic events that have secondary decay vertices that are well separated from the  $pp$  collision points. The price of these capabilities is a limit on the tolerable instantaneous luminosity of  $4 \times 10^{32} \text{ cm}^{-2} \text{ s}^{-1}$ , which is almost 2 orders of magnitude lower than the maximum values that the LHC is capable of delivering. This makes the CMS and ATLAS experiment competitive in detection of some  $B$  decays to simple final states with muon pairs. The LHCb detector is equipped with two ring-imaging Cherenkov (RICH) detectors that provide good suppression of pion backgrounds for final states that include kaons and protons. The central detectors at the LHC and Tevatron lack efficient hadron identification and, thus, have to cope with high backgrounds in such channels.

The production cross sections for heavy flavors at the LHC are 3 orders of magnitude larger than those at the  $e^+e^- B$  factories. Even after correcting for the smaller reconstruction efficiencies and shorter accumulated beam time, the run-I LHCb data samples of  $B$  decays to  $J/\psi$  and light hadrons are an order of magnitude larger than those accumulated during the ten-year operating lifetimes of the  $B$  factories. The signal purity is even slightly better than in  $BABAR$  or Belle, thanks to the long visible lifetimes of the lightest open-bottom-flavored hadrons. The identification of tracks produced from a displaced vertex reduces combinatorial backgrounds associated with additional particles produced in the primary  $pp$  collisions as well as those from the decays of the companion bottom-flavored hadron. The large signal sample enabled the LHCb group to make the first determination of  $X(3872)$ 's  $J^{PC}$  quantum numbers (Aaij *et al.*, 2013a, 2015d), confirm the  $Z(4430)^+$  structure (Aaij *et al.*, 2014b, 2015b), and demonstrate its consistency with a Breit-Wigner (BW) resonance hypothesis by means of an Argand diagram (Aaij *et al.*, 2014b). Recently, LHCb has performed the first amplitude analysis of  $B^+ \rightarrow J/\psi \phi K^+$  decays that made the first determination of the quantum numbers of the  $X(4140)$  and established the existence of three other  $J/\psi \phi$  mass peaks: the  $X(4274)$ ,  $X(4500)$ , and  $X(4700)$  (Aaij *et al.*, 2017a, 2017d). An advantage of collecting data at a hadronic collider is the simultaneous accumulation of large  $B$ ,  $B_s$ ,  $B_c$ , and  $\Lambda_b^0$  data sets, as opposed to  $B$  factories, where  $B_s$  samples require dedicated data runs, and  $B_c$  mesons and  $\Lambda_b^0$  baryons are not accessible. The large sample of  $\Lambda_b$  events in LHCb's run-I data sample led to the discovery of pentaquarklike  $J/\psi p$  mass structures  $P_c(4450)^+$  and  $P_c(4380)^+$  in  $\Lambda_b^0 \rightarrow J/\psi p K^-$  decays (Aaij *et al.*, 2015c).

LHCb is equipped with an electromagnetic calorimeter. However,  $\gamma$  ray and  $\pi^0$  reconstruction efficiencies are much lower than in the  $e^+e^-$  experiments and, because of the lack of vertex information, combinatorial backgrounds for photons are large. Nevertheless, exploration of channels with one  $\gamma$  ray, or  $\pi^0$  or  $\eta$  is possible. For example, Fig. 18 shows LHCb signals for  $\gamma J/\psi$  and  $\gamma \psi'$  decays of the  $X(3872)$ . These data

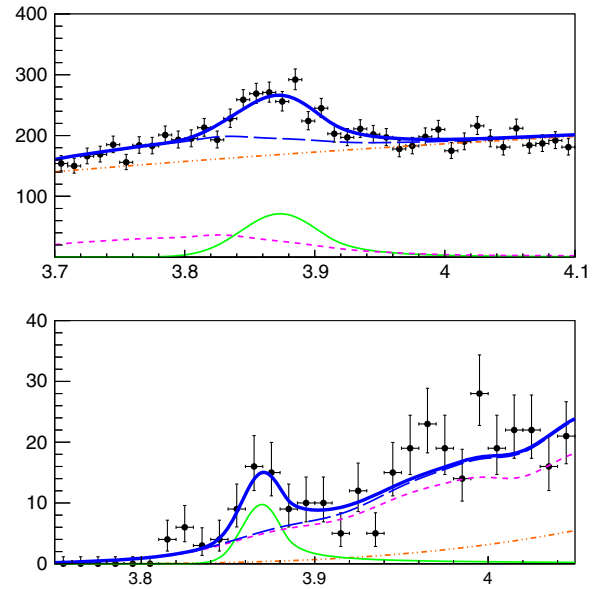


FIG. 18. The upper (lower) panel shows the  $M(J/\psi\gamma)$  [ $M(\psi'\gamma)$ ] distribution for events with  $M(J/\psi\gamma K^+)$  [ $M(\psi'\gamma K^+)$ ] within  $3\sigma$  of  $m_{B^+} = 5.28 \text{ GeV}$ . From Aaij *et al.*, 2014a.

were used to provide the most precise measurement to data of the branching-fraction ratio (Aaij *et al.*, 2014a)

$$\frac{\mathcal{B}(X(3872) \rightarrow \gamma\psi')}{\mathcal{B}(X(3872) \rightarrow \gamma J/\psi)} = 2.46 \pm 0.70, \quad (4)$$

which is an important quantity for distinguishing between different theoretical interpretations of the  $X(3872)$ .

All of the LHCb results on hadron spectroscopy that have been published to date have been based on analyses of run-I data, i.e., with integrated luminosities as high as  $3 \text{ fb}^{-1}$  at  $E_{\text{c.m.}}(pp) = 7\text{--}8 \text{ TeV}$ . The on-going run II is expected to conclude in 2018 with an additional  $8 \text{ fb}^{-1}$  of integrated luminosity collected mostly at  $E_{\text{c.m.}}(pp) = 13 \text{ TeV}$ , where the heavy-flavor production cross sections are about a factor of 2 higher (Aaij *et al.*, 2016d). A major upgrade of the LHCb detector is currently in preparation (Bediaga *et al.*, 2012), which will allow collecting data at  $2 \times 10^{33} \text{ cm}^{-2} \text{ s}^{-1}$  starting around 2021. About  $50 \text{ fb}^{-1}$  of integrated luminosity is expected by 2030. A second major upgrade is under consideration, which would allow data taking with an instantaneous luminosity of  $2 \times 10^{34} \text{ cm}^{-2} \text{ s}^{-1}$  with the goal of a final data sample corresponding to  $300 \text{ fb}^{-1}$  by the end of LHC operations.

#### IV. HEAVY-LIGHT EXOTIC HADRON CANDIDATES

The quark model (Godfrey and Isgur, 1985; Godfrey and Moats, 2016) predicts a rich spectrum of heavy-light mesons containing a heavy quark  $Q$  and a light antiquark  $\bar{q} = \bar{u}, \bar{d}, \bar{s}$ . In contrast to quarkonium, where the states are best characterized by the  $Q\bar{Q}$  spin  $S$  and the relative orbital angular momentum  $L$ , the heavy-light  $Q\bar{q}$  mesons are expected to be best described by  $\vec{J}_q$ , the orbital angular momentum  $\vec{L}_q$  plus

the spin  $\vec{s}_q$  of the light quark, since the heavy-quark spin interactions are suppressed by its large mass.

For  $S$ -wave  $Q\bar{q}$  systems,  $j_q = 1/2$  and there are two meson states, one with  $J^P = 0^-$  and the other with  $J^P = 1^-$ , corresponding to antiparallel and parallel  $\vec{j}_q$  and  $\vec{s}_Q$  configurations. For  $P$ -wave systems,  $j_q$  can be either  $1/2$  or  $3/2$ , and two doublets of meson states are expected: one for  $j_q = 1/2$  that contains a  $J^P = 0^+$  and  $1^+$  meson, and the other for  $j_q = 3/2$  with a  $J^P = 1^+$  and a  $2^+$  meson.

In the charm quark sector ( $Q = c$ ) the nonstrange ( $\bar{q} = \bar{u}, \bar{d}$ )  $S$ -wave states are the well-established pseudoscalar  $D$  and vector  $D^*$  isospin doublets. The corresponding strange ( $\bar{q} = \bar{s}$ ) mesons are the  $D_s^+$  and  $D_s^{*+}$  isospin singlets. The ‘‘hyperfine’’ mass splitting  $m_{1^-} - m_{0^-}$  for the  $D^* - D$  and  $D_s^* - D_s$  are nearly equal; for both systems it is about 140 MeV (Patrignani *et al.*, 2016).

The  $P$ -wave  $D$  mesons, which are hard to produce and tend to be wide and overlapping, are difficult to study experimentally. For example, in the  $\bar{q} = \bar{u}, \bar{d}$  system, the  $j_q = 1/2, J^P = 0^+$   $D_0(2400)$  meson and the  $j_q = 1/2, J^P = 1^+$   $D_1(2430)$  meson have  $\sim 300$  MeV natural widths and their properties have only recently been established (Abe *et al.*, 2004; Link *et al.*, 2004; Aubert *et al.*, 2009a). In the  $j_s = 3/2$   $c\bar{s}$  system, the very narrow ( $\Gamma = 0.92 \pm 0.05$  MeV)  $D_{s1}(2536)$  meson and the relatively narrow ( $\Gamma = 17 \pm 4$  MeV)  $D_{s2}^*(2573)$  meson were well established in the 1990s but, prior to the operation of  $B$  factories, the  $j_s = 1/2, 0^+$  and  $1^+$  states had still not been identified. According to the quark model, these states were expected to have masses above the  $m_{D^{(*)}} + m_K$  threshold and it was suspected that strong decays to  $DK$  and  $D^*K$  final states made them wide and difficult to see.

One of the biggest surprises from the  $B$  factories was the  $BABAR$  discovery of a very narrow state decaying to  $D_s\pi^0$  with mass near 2317 MeV produced in inclusive  $e^+e^- \rightarrow D_s^+\pi^0 + X$  interactions. CLEO quickly confirmed the  $BABAR$   $D_{s0}^*(2317)$  discovery and reported the observation of a second narrow state decaying to  $D_s^*\pi^0$  with mass near 2460 MeV that is now called the  $D_{s1}(2460)$  (Besson *et al.*, 2003). The Belle experiment established the production of both states in exclusive  $B \rightarrow \bar{D}D_{sJ}$  decays, observed the  $D_{s1}(2460) \rightarrow D_s^*\gamma$  decay mode, and established the spin parity of the  $D_{s1}(2460)$  to be  $J^P = 1^+$  (Krokovny *et al.*, 2003).

The latest world-average results for their masses and 95% C.L. upper limits on their natural widths are (Patrignani *et al.*, 2016)

$$\begin{aligned} D_{s0}^*(2317): & \quad M = 2317.7 \pm 0.6 \text{ MeV}, & \quad \Gamma < 3.8 \text{ MeV}, \\ D_{s1}(2460): & \quad M = 2459.5 \pm 0.6 \text{ MeV}, & \quad \Gamma < 3.5 \text{ MeV}. \end{aligned} \quad (5)$$

Since the  $J^P = 1^+$  quantum numbers of the  $D_{s1}(2460)$  match those expected for the  $P$ -wave  $j_s = 1/2$   $1^+$  state, and the mass  $D_{s1} - D_{s0}^*$  mass splitting  $141.8 \pm 0.8$  MeV closely matches the hyperfine splitting measured in the  $S$ -wave systems, a natural interpretation of these two states is that they are the ‘‘missing’’  $P$ -wave  $j_s = 1/2$   $0^+$  and  $1^+$   $c\bar{s}$  states. Since the  $D_{s0}^*(D_{s1})$  mass is below the  $DK$  ( $D^*K$ ) mass threshold, it can

TABLE IV. Comparison of the masses of the low-lying  $D_s$  ( $c\bar{s}$ ) and charged  $D$  ( $c\bar{d}$ ) meson states. Here the  $D_{s0}^*(2317)$  and the  $D_{s1}(2460)$  are identified with the  $P$ -wave,  $0^+$   $j_q = 1/2$  and  $1^+$   $j_q = 3/2$  mesons, respectively. The masses are from Patrignani *et al.* (2016).

$L$	$j_q$	$J^P$	$m(c\bar{d})$ (MeV)	$m(c\bar{s})$ (MeV)	$m_{c\bar{s}} - m_{c\bar{d}}$ (MeV)
0	1/2	$0^-$	$1869.6 \pm 0.1$	$1968.3 \pm 0.1$	$98.7 \pm 0.1$
		$1^-$	$2010.3 \pm 0.1$	$2112.1 \pm 0.4$	$101.7 \pm 0.4$
1	1/2	$0^+$	$2318 \pm 29$	$2317.7 \pm 0.6$	$0.3 \pm 29$
		$1^+$	$2430 \pm 36$	$2449.5 \pm 0.1$	$30 \pm 36$
	3/2	$1^+$	$2423.2 \pm 2.4$	$2335.1 \pm 0.6$	$111.9 \pm 2.4$
		$2^+$	$2464.3 \pm 1.6$	$2571.9 \pm 0.8$	$107.6 \pm 1.8$

decay only via isospin-violating processes, which accounts for its small width.<sup>16</sup>

However, their masses, which are much lower than quark model expectations for  $P$ -wave  $c\bar{s}$  states,<sup>17</sup> are a puzzle. This is illustrated in Table IV, where masses of  $c\bar{d}$  mesons are compared with those of the corresponding  $c\bar{s}$  mesons. The  $c\bar{s} - c\bar{d}$  mass differences for the  $S$ -wave  $0^-$  and  $1^-$  mesons are both very close to 100 MeV, as is also the case for the  $1^+$  and  $2^+$   $j_q = 3/2$   $P$ -wave mesons. In the quark model, the corresponding  $c\bar{d}$  and  $c\bar{s}$  mesons have the same configurations, and the  $\approx 100$  MeV mass difference reflects the  $s$  and  $d$  quark mass difference.

This is not the case for the  $D_{s0}^*(2317)$  and  $D_{s1}(2460)$  mesons, if they are taken to be the  $j_q = 1/2$  and  $j_q = 3/2$   $P$ -wave mesons, in which case the masses of the  $c\bar{s}$  and  $c\bar{d}$  systems are nearly equal, in spite of the  $s$ - and  $d$ -quark mass differences. This puzzling behavior led to speculation that these states may contain four-quark components, either in a QCD tetraquark arrangement or as moleculelike structure formed from  $D$  and  $K$  mesons.

In the tetraquark picture (Cheng and Hou, 2003; Terasaki, 2003; Bracco *et al.*, 2005; Maiani *et al.*, 2005), the  $D_{s0}^*(2317)$  could be a  $[cq][\bar{s}\bar{q}]$  state, in which case a rich spectrum of similar states is expected to exist. In particular, there should be electrically neutral and doubly charged partners. A  $BABAR$  study of  $D_s^+\pi^\pm$  systems produced in  $e^+e^-$  annihilations found no states in the  $D_{s0}^*(2317)$  mass region in either channel (Aubert *et al.*, 2006a) and Belle reported upper limits on the production of neutral or doubly charged partner states in  $B \rightarrow \bar{D}D_s^+\pi^\pm$  that are an order of magnitude below isospin-based predictions, making the tetraquark option implausible (Choi *et al.*, 2015).

The  $D_{s0}^*$  and  $D_{s1}$  lie about 40 MeV below the  $DK$  and  $D^*K$  mass thresholds, respectively, suggesting that they might be  $DK^{(*)}$  molecules (Barnes, Close, and Lipkin, 2003), or mixtures of a  $DK^{(*)}$  molecule and a conventional  $c\bar{s}$  meson (Browder, Pakvasa, and Petrov, 2004). The idea that the  $D_{s0}^*(2317)$  and  $D_{s1}(2460)$  may be  $DK^{(*)}$  bound states was

<sup>16</sup>A  $0^+$  assignment for the  $D_{s0}^*$  is supported by the absence of any evidence for  $D_{s0}^* \rightarrow D_s\gamma$  decays.

<sup>17</sup>A recent quark calculation of the masses of the  $j_q = 1/2$   $P$ -wave  $c\bar{s}$  mesons finds 2484 MeV for the  $0^+$  and 2549 MeV for the  $1^+$  states (Godfrey and Moats, 2016).

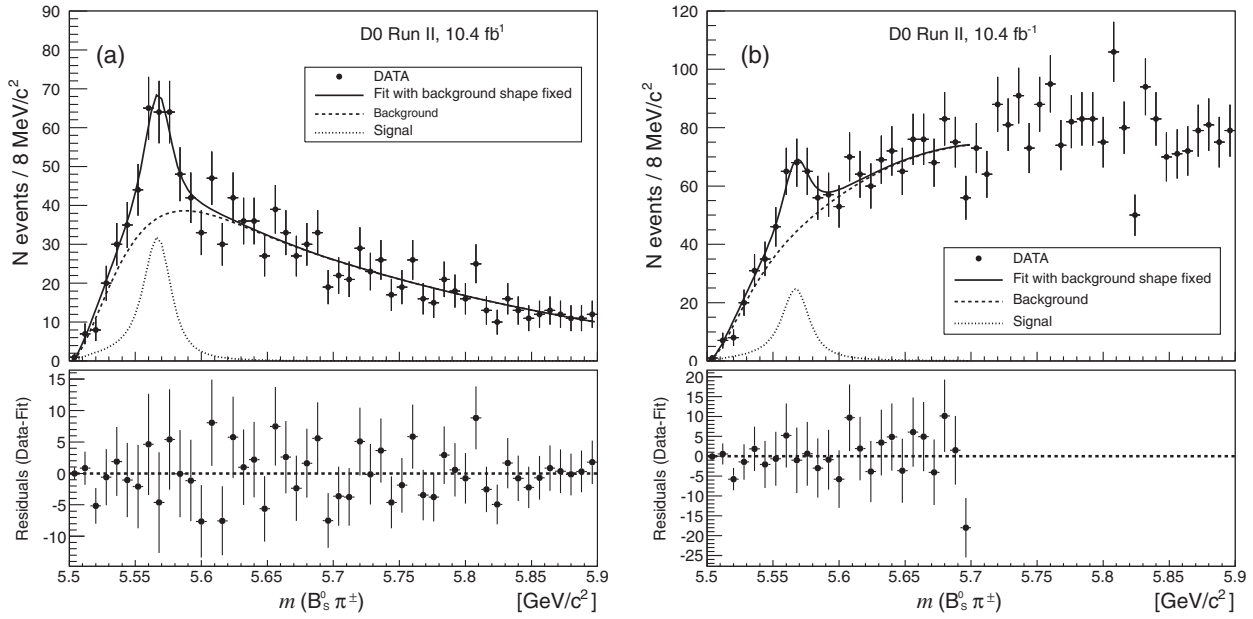


FIG. 19. The  $M(B_s^0\pi^\pm)$  distribution together with the background distribution (dashed curve) and fit results (solid curve) for events (a) with and (b) without the application of the  $B_s^0 - \pi^\pm$  opening angle requirement. From [Abazov et al., 2016](#).

studied with lattice QCD by [Leskovec et al. \(2015\)](#). They examined the  $J^P = 0^+$  and  $1^+$  states that are produced when  $DK$  and  $D^*K$  scattering operators are included with the standard  $c\bar{s}$  meson operators. The analysis established the existence of below-threshold poles with binding energies consistent with  $D_{s0}^*(2317)$  and  $D_{s1}(2460)$ .

Recently the D0 Collaboration reported evidence for a possible four-quark state that decays to  $B_s^0\pi^\pm$ , where the  $B_s^0$  decays via  $B_s^0 \rightarrow J/\psi\phi$  ([Abazov et al., 2016](#)). In the analysis, 5500 reconstructed  $B_s^0 \rightarrow J/\psi\phi$  decay candidates were paired with a charged particle that was assumed to be a pion. Multiple entries for a single event, which occur when more than one pion candidate passes the track selection criteria, were suppressed by limiting the angular separation of the  $B_s^0$  candidate and the charged track. The resultant  $B_s^0\pi^\pm$  invariant mass spectrum, shown in Fig. 19(a), has a narrow structure that is approximately 60 MeV above the  $m_{B_s} + m_\pi$  threshold.

The solid curve in Fig. 19(a) shows the results of a fit that uses a resolution-broadened BW line shape to represent a signal (dotted curve) plus an incoherent background modeled by an empirical shape that was determined from  $B_s^0$ -mass sideband events (for non- $B_s^0$  background) and Monte Carlo (MC) simulated inclusive  $B_s^0$  production events (for combinatorial backgrounds associated with real  $B_s^0$  mesons). The fitted mass and width of the peak, which the D0 group called the  $X(5568)$ , are  $M = 5567.8 \pm 2.9(\text{stat})_{-1.9}^{+0.9}(\text{syst})$  MeV and  $\Gamma = 21.9 \pm 6.4(\text{stat})_{-2.5}^{+5.0}(\text{syst})$  MeV. The signal significance, including look-elsewhere and systematic-uncertainty effects, is  $5.1\sigma$ . The  $X(5568)$  signal is also evident in the  $B_s^0\pi^\pm$  spectrum without the pion direction restriction, shown in Fig. 19(b), albeit with reduced significance. The ratio of the number of  $B_s$  mesons that originate from  $X(5568)$  decays to all  $B_s$  mesons is determined for the D0 acceptance to be  $\rho_X^{D0} = (8.1 \pm 2.4)\%$ .

In an alternative approach, they extracted a  $B_s^0\pi^\pm$  signal by performing fits of the number of  $B_s^0$  events in the  $J/\psi\phi$  mass distribution in 20-MeV intervals of  $M(B_s^0\pi^\pm)$ . The results of that fit confirm that the observed signal is due to events with genuine  $B_s^0$  mesons and eliminates the possibility that some non- $B_s^0$  process may mimic the signal.

To confirm the production of the  $X(5568)$  with an independent sample, D0 studied events in which the  $B_s^0$  meson decayed semileptonically ([Zieminska et al., 2017](#)). Decays  $B_s^0 \rightarrow \mu^\mp D_s^\pm X$ , where  $X$  denotes a neutrino possibly accompanied by mesons, are much more abundant than the exclusive decay  $B_s^0 \rightarrow J/\psi\phi$ . The mass resolution is worse due to the presence of the undetected neutrino, but it is possible to select events where this effect is minimized by requiring that the  $D_s$  meson and the muon account for a large fraction of the  $B_s^0$  momentum. The data show an excess over the simulated background at the mass expected from events produced by the decay  $X(5568) \rightarrow B_s^0\pi^\pm$  with  $B_s^0 \rightarrow J/\psi\phi$ , as seen in Fig. 20, thereby providing a confirmation of the results of [Abazov et al. \(2016\)](#). The combined significance of the signal in the two channels is 5.7 standard deviations.

The LHCb group searched for  $X(5568)$  production in  $pp$  collisions at  $E_{\text{c.m.}} = 7\text{--}8$  TeV ([Aaij et al., 2016b](#)). With 44 000  $B_s^0 \rightarrow J/\psi\phi$  and 65 000  $B_s^0 \rightarrow D_s^- \pi^+$  reconstructed events and a superior signal-to-background ratio, no peaking structure in the  $B_s^0\pi^\pm$  invariant mass distribution is observed in the  $X(5568)$  mass region (see the left panel of Fig. 21). Upper limits on  $\rho_X^{\text{LHCb}}$  of  $< 1.2\%$  ( $< 2.4\%$ ) for  $p_T(X) > 5$  GeV ( $> 10$  GeV) are established at the 95% C.L. In addition, the CMS group found no sign of an  $X(5568)$  peak in a preliminary analysis of a 48 000 event sample of reconstructed  $B_s^0 \rightarrow J/\psi\phi$  decays and reported an upper limit of  $\rho_X^{\text{CMS}} < 3.9\%$  at the 95% C.L. ([Sirunyan et al., 2017](#)) (see the right panel of Fig. 21).

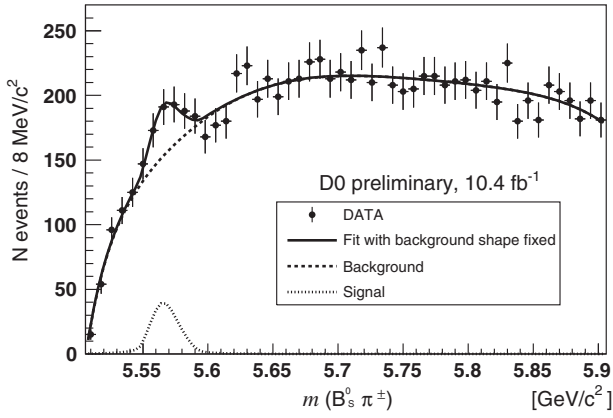


FIG. 20. The invariant mass distribution  $M(B_s^0\pi^\pm)$  for the  $B_s^0 \rightarrow D_s\mu X$  event sample with the results of the fit superimposed. From Zieminska *et al.*, 2017.

No satisfactory theoretical description of the  $X(5568)$  structure has yet been proposed (Burns and Swanson, 2016; Esposito, Piloni, and Polosa, 2016; Guo, Meißner, and Zou, 2016; Yang, Wang, and Meißner, 2017). If confirmed, this state would be comprised of two quarks and two antiquarks of four different flavors:  $b$ ,  $s$ ,  $u$ , and  $d$ . Such a state might be a tightly bound  $B_d^0 - K^\pm$  molecule or a  $[bd] - [\bar{s}\bar{u}]$  tetraquark. However, the low mass of the  $X(5568)$ , about 200 MeV below both the  $B_d^0 K^\pm$  threshold and the three-quark ( $bsu$ )  $\Xi_b$  baryon, disfavors both of these interpretations. A lattice QCD study of the  $B_s\pi$  scattering (Lang, Mohler, and Prelovsek, 2016) does not support the existence of a  $J^P = 0^+$  state with the  $X(5568)$  parameters.

## V. NEUTRAL EXOTIC HADRON CANDIDATES

### A. $X(3872)$

The first quarkoniumlike candidate for a nonstandard hadron to be seen was the  $X(3872)$ , which was found by

Belle (Choi *et al.*, 2003) as an unexpected narrow peak in the  $\pi^+\pi^-J/\psi$  invariant mass distribution in  $B \rightarrow K\pi^+\pi^-J/\psi$  decays shown in Fig. 22(a). It is experimentally well established, having been seen and studied by a number of experiments (Abazov *et al.*, 2004; Acosta *et al.*, 2004; Aubert *et al.*, 2005c; Aaij *et al.*, 2012a; Chatrchyan *et al.*, 2013a; Ablikim *et al.*, 2014d; Aaboud *et al.*, 2017). Its most intriguing feature is its mass: the 2016 PDG world-average value is  $M(X(3872)) = 3871.69 \pm 0.17$  MeV, which at current levels of precision is indistinguishable from the  $D^0\bar{D}^{*0}$  mass threshold  $m_{D^0} + m_{D^{*0}} = 3871.68 \pm 0.10$  MeV (Patrignani *et al.*, 2016); the difference is  $\delta m_{00} \equiv (m_{D^0} + m_{D^{*0}}) - M(X(3872)) = -0.01 \pm 0.20$  MeV. Whether this close proximity of the  $X(3872)$  to the  $D^0\bar{D}^{*0}$  mass threshold is a coincidence or a feature of hadron dynamics is an issue that has attracted considerable interest. The  $X(3872)$  is also quite narrow; Belle has reported a 90% C.L. upper limit on its total width of  $\Gamma < 1.2$  MeV (Choi *et al.*, 2011). In addition to the production in  $B \rightarrow X(3872)K$  decays, the  $X(3872)$  state was also observed in  $B \rightarrow X(3872)K\pi$  decays (Bala *et al.*, 2015).

The radiative decay process  $X(3872) \rightarrow \gamma J/\psi$  was measured by BABAR (Aubert *et al.*, 2006c) and Belle (Bhardwaj *et al.*, 2011) to have a branching fraction that is  $0.24 \pm 0.05$  of that for the  $\pi^+\pi^-J/\psi$  mode. This, plus BABAR (Aubert *et al.*, 2009b) and LHCb (Aaij *et al.*, 2014a) reports of strong evidence for  $X(3872) \rightarrow \gamma\psi'$  decays [see Fig. 18(b)], establishes the charge conjugation parity of the  $X(3872)$  as even ( $C = +$ ), in which case the  $\pi^+\pi^-$  system in the  $X \rightarrow \pi^+\pi^-J/\psi$  decay process must be from  $\rho^0 \rightarrow \pi^+\pi^-$  decay. This is consistent with  $\pi^+\pi^-$  line-shape measurements done by CDF (Abulencia *et al.*, 2006), Belle (Choi *et al.*, 2011), and CMS (Chatrchyan *et al.*, 2013a). The  $\pi^+\pi^-$  line shape measured by Belle is shown in Fig. 22(b).

In their 3  $\text{fb}^{-1}$  run-I data sample, the LHCb experiment detected a  $1011 \pm 38$  event signal for the decay chain  $B^+ \rightarrow K^+X(3872)$ ;  $X(3872) \rightarrow \pi^+\pi^-J/\psi$ ;  $J/\psi \rightarrow \mu^+\mu^-$  on a small background as shown in Fig. 23(a). In an amplitude

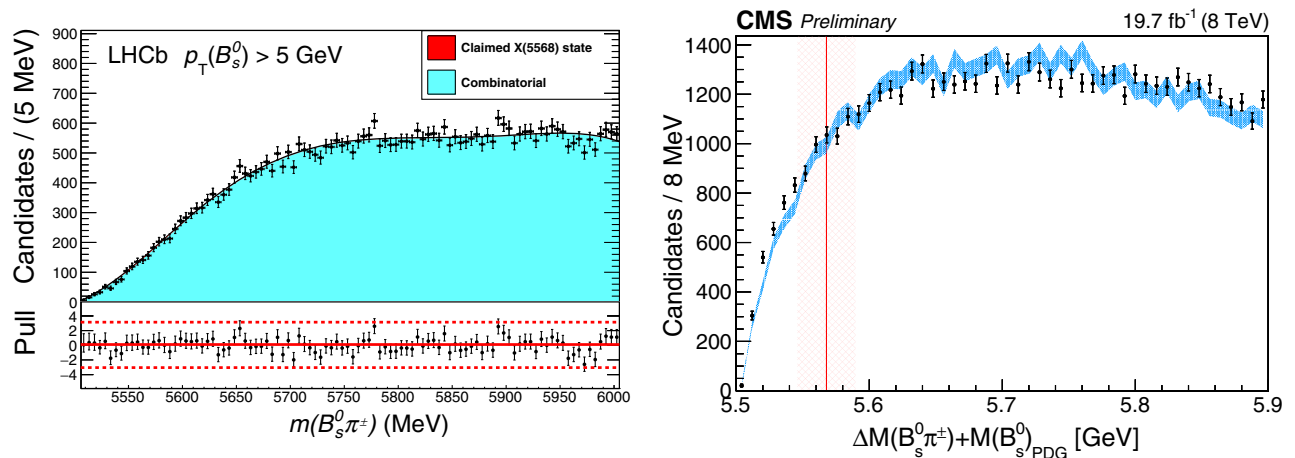


FIG. 21. The  $B_s^0\pi^\pm$  distributions (points with error bars) observed by (left) the LHCb [from Aaij *et al.* (2016b)] and by (right) the CMS [from Sirunyan *et al.* (2017)]. The LHCb plot shows the result of a fit of an  $X(5568)$  signal (not visible) included on top of the combinatorial background. The continuous blue band in the CMS plot is the distribution observed for the  $B_s^0$ -mass sideband data. The vertical red band illustrates the  $M_X \pm \Gamma_X$  region of the  $X(5568)$  state claimed by D0.

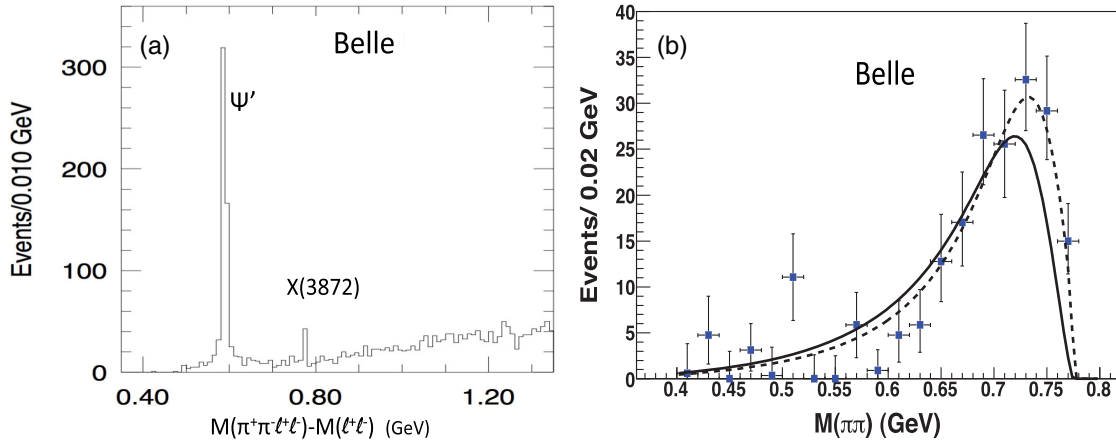


FIG. 22. (a) The  $M(\pi^+\pi^-\ell^+\ell^-) - M(\ell^+\ell^-)$  distribution for  $B \rightarrow K\pi^+\pi^-\ell^+\ell^-$  events with  $|M(\ell^+\ell^-) - m_{J/\psi}| < 20$  MeV. From Choi *et al.*, 2003. (b) The  $\pi^+\pi^-$  invariant mass distribution for  $X(3872) \rightarrow \pi^+\pi^-J/\psi$  events in Belle (Choi *et al.*, 2003). The curves show results of fits to a  $\rho \rightarrow \pi^+\pi^-$  line shape including  $\rho - \omega$  interference (Choi *et al.*, 2011). The dashed (solid) curve is for even (odd)  $X(3872)$  parity

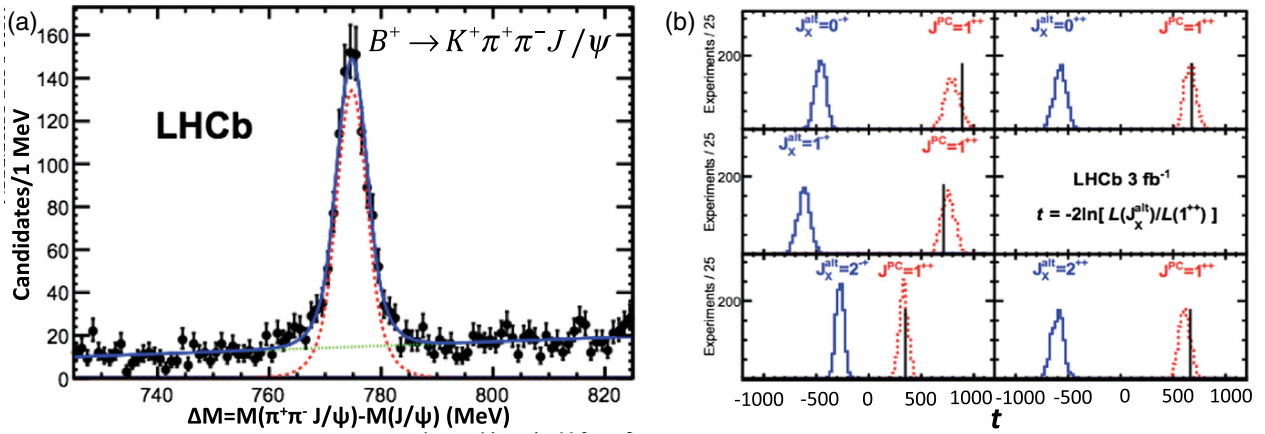


FIG. 23. (a) The  $M(\pi^+\pi^-J/\psi) - m_{J/\psi}$  distribution for  $B^+ \rightarrow K^+\pi^+\pi^-J/\psi$  events. (b) Distributions of  $t \equiv -2 \ln[\mathcal{L}^{\text{alt}}/\mathcal{L}^{1^{++}}]$  for simulated experiments for alternative  $J^{PC}$  hypotheses (solid blue histograms) and  $1^{--}$  (dashed red histograms). The vertical lines show the values of  $t$  determined from the data. Similar results for  $J^{PC} = 3^{\pm+}$  and  $4^{\pm+}$  are not shown. From Aaij *et al.*, 2015d.

analysis based on the angular correlations among the five final-state particles in these events, the LHCb group found that the  $J^{PC} = 1^{++}$  quantum number hypothesis had the highest likelihood value (Aaij *et al.*, 2013a, 2015d). They evaluated the significance of the  $1^{++}$  assignment using the likelihood ratio  $t \equiv -2 \ln[\mathcal{L}^{\text{alt}}/\mathcal{L}^{1^{++}}]$  as a test variable, where  $\mathcal{L}^{1^{++}}$  is the likelihood for the  $1^{++}$  hypothesis and  $\mathcal{L}^{\text{alt}}$  is that for an alternative. (With this definition, positive values of  $t$  favor  $1^{++}$ .) The solid blue (dashed red) histograms in Fig. 23(b) show  $t$  value distributions for ensembles of MC experiments generated with alternative and  $1^{++}$   $J^{PC}$  values,<sup>18</sup> with the  $t$  value determined for the real data indicated by vertical black lines. The experimental results favor the  $1^{++}$  hypotheses over all alternative even- $C$   $J^{PC}$  assignments with  $J \leq 4$  by a wide margin; in all comparisons the statistical significance of the

$1^{++}$  assignment, determined from the distributions for the ensembles of MC experiments, is more than  $16\sigma$ .

The only available  $1^{++}$  standard charmonium level that is expected to have a mass near 3872 MeV is the  $2^3P_1$   $c\bar{c}$  state, commonly known as the  $\chi_{c1}(2P)$  or  $\chi'_{c1}$ . However, for a number of reasons, the assignment of the  $X(3872)$  as the  $\chi'_{c1}$  charmonium state has been deemed “improbable” (Eichten, Lane, and Quigg, 2006). Among these are the  $X(3872)$  mass and width values and the apparent isospin violation in its discovery decay channel  $X(3872) \rightarrow \rho J/\psi$ .

*Mass:* The  $\chi'_{c2}$ , the  $J = 2$  spin-multiplet partner of the  $\chi'_{c1}$ , was identified by Belle in 2006 as a distinct peak in the  $\gamma\gamma \rightarrow D\bar{D}$  cross section at  $3927 \pm 3$  MeV, with an angular distribution that is characteristic of a  $D$ -wave  $D\bar{D}$  meson system and a production rate that is consistent with charmonium model expectations for the  $2^3P_2$   $c\bar{c}$  state (Uehara *et al.*, 2006). BABAR confirmed this observation in 2010 (Aubert *et al.*, 2010) and found properties that are consistent with those reported by Belle. There is general agreement in the quarkonium community that the identification of the Belle peak as

<sup>18</sup>The experiments are generated with numbers of signal and background events that fluctuate around those in the experimental data according to the observed statistical errors.

the  $\chi'_{c2}$  is reliable (Brambilla *et al.*, 2011). If, with this assignment for the  $\chi'_{c2}$ , the  $X(3872)$  is identified as the  $\chi'_{c1}$ , the  $\chi'_{c2} - \chi'_{c1}$  mass splitting would be  $\delta M_{2-1}(2P) = 56 \pm 3$  MeV and larger than the measured splitting for the  $1P$  states:  $\delta M_{2-1}(1P) = 46.5 \pm 0.1$  MeV. This conflicts with  $c\bar{c}$  potential model expectations that  $\delta M_{2-1}(n_r, P)$  decreases with increasing radial quantum  $n_r$  (Godfrey and Isgur, 1985; Barnes, Godfrey, and Swanson, 2005). For  $c\bar{c}$  states above the threshold for decays into open-charmed  $D\bar{D}$  and  $D\bar{D}^*$  mesons, potential model calculations should be modified to include the effects of intermediate on-mass-shell open-charmed-meson loops. These effects have been estimated by three groups using three different approaches (Eichten, Lane, and Quigg, 2004; Li and Chao, 2009; Wang, Yang, and Ping, 2014); all three of these analyses predict that  $\delta M_{2-1}(2P)$  decreases to values that are even lower than potential model expectations, contrary to what the  $X(3872) = \chi'_{c1}$  assignment would imply.

*Width:* The Belle group's upper limit  $\Gamma(X(3872)) < 1.2$  MeV is only slightly higher than the measured width of the  $1P$   $\chi_{c1}$  state,  $\Gamma(\chi_{c1}) = 0.84 \pm 0.04$  MeV (Patrignani *et al.*, 2016). However, since the  $X(3872)$  has a number of allowed decay channels that are not accessible to the  $\chi_{c1}$ , including the  $X(3872) \rightarrow \rho J/\psi$  discovery mode and the order of magnitude stronger  $D^0\bar{D}^{*0}$  mode that is discussed below, these are expected to be reflected in a substantially larger total width for the  $X(3872)$ , if it were in fact, the  $\chi'_{c1}$  (Eichten, Lane, and Quigg, 2004).

*Isospin violation:* Since standard charmonium states contain no constituent  $u$  or  $d$  quarks, they necessarily have zero isospin. On the other hand, since the  $\rho$  meson is an isovector, the  $\rho J/\psi$  decay final state has isospin  $I = 1$ , and the  $\chi'_{c1} \rightarrow \rho J/\psi$  decay process violates isospin and should be strongly suppressed and an unlikely discovery mode for a charmonium state (Eichten, Lane, and Quigg, 2006).

These reasons, plus the close correspondence between its mass and the  $m_{D^0} + m_{D^{*0}}$  threshold, led to considerable speculation that the substructure of the  $X(3872)$  is more complex than that of a simple  $c\bar{c}$  charmonium state (Tornqvist, 2003).

An interesting question about the  $X(3872)$  is the value of its isospin. Explicit evidence for strong isospin violation in  $X(3872)$  decays came from observations by both Belle (Abe *et al.*, 2005) and BABAR (del Amo Sanchez *et al.*, 2010a) of the  $X(3872) \rightarrow \omega J/\psi$  decay mode<sup>19</sup> with a branching fraction that is nearly equal to that for  $\rho J/\psi$ ; the PDG average is  $\mathcal{B}(X(3872) \rightarrow \omega J/\psi) / \mathcal{B}(X(3872) \rightarrow \pi^+ \pi^- J/\psi) = 0.8 \pm 0.3$  (Patrignani *et al.*, 2016). Since  $M_{X(3872)} - m_{J/\psi} \approx 775$  MeV, the upper kinematic boundary for the mass of the  $\pi^+ \pi^-$  system is right at the peak mass of the  $\rho$  resonance and  $\sim 7$  MeV below  $m_\omega$ . Thus, while the decay  $X(3872) \rightarrow \rho J/\psi$  is kinematically allowed to proceed through nearly the entire low-mass side of the  $\rho$  resonance,  $X(3872) \rightarrow \omega J/\psi$  can proceed only via a small fraction of the low-mass tail of the  $\omega$  peak. These considerations imply a kinematic suppression of the amplitude for  $X(3872) \rightarrow \omega J/\psi$  decays relative to the  $\rho J/\psi$  channel by a factor of about  $\sim 4$ , in which case the near

equality of the  $\rho J/\psi$  and  $\omega J/\psi$  decay rates implies that an  $I = 0$  assignment is favored (Suzuki, 2005), but a sizable isovector component in the  $X(3872)$  wave function is still allowed. If the  $X(3872)$  had  $I = 1$ , it would have charged partners. Searches for narrow, charged partners of the  $X(3872)$  decaying into  $\rho^\pm J/\psi$  by BABAR (Aubert *et al.*, 2005b) and Belle (Choi *et al.*, 2011) set branching ratio limits that are well below expectations based on isospin conservation. These results suggest that the  $X(3872)$  is mostly an isospin singlet and that the  $\rho J/\psi$  decay mode violates isospin symmetry.

The  $X(3872) \rightarrow D^0\bar{D}^{*0}$  decay mode has been observed by both Belle (Aushev *et al.*, 2010c) and BABAR (Aubert *et al.*, 2008c) with a measured branching fraction that is  $9.9 \pm 2.3$  times that for the  $\pi^+ \pi^- J/\psi$  channel [see Figs. 24(a) and 24(b)]. The  $J^{PC} = 1^{++}$  quantum number assignment implies that the  $X(3872)$  couples to a  $D^0\bar{D}^{*0}$  pair in an  $S$  and/or  $D$  wave and, because the  $D^0\bar{D}^{*0}$  system is right at threshold, the  $S$  wave can be expected to be dominant. In this case some general and universal theorems apply (Braaten and Hammer, 2006; Braaten and Lu, 2007; Coito, Rupp, and van Beveren, 2013; Polosa, 2015). One consequence of these theorems is that, independently of its dynamical origin, the  $X(3872)$  should exist for a significant fraction of the time as a  $D^0\bar{D}^{*0}$  moleculelike state (either bound or virtual) with a size comparable to its scattering length  $a_{00} = \hbar / \sqrt{\mu |\delta m_{00}|}$ , where  $\mu$  is the  $D^0\bar{D}^{*0}$  reduced mass. The limited experimentally allowed range for nonzero  $\delta m_{00}$  values implies that the mean  $D^0 - \bar{D}^{*0}$  separation has to be large:  $a_{00} \geq 7$  fm. Although the  $X(3872)$  mass is well below the  $D^+ D^{*-}$  mass threshold, it is expected to exist for a smaller fraction of the time as a  $D^+ D^{*-}$  moleculelike state. The extent of the  $D^+ D^{*-}$  configuration, for which  $\delta m_{+-} = (m_{D^+} - m_{D^{*-}}) - M(X(3872)) = 8.2$  MeV and  $a_{+-} \approx 2$  fm, is much different. The very different properties of the  $D^0\bar{D}^{*0}$  and  $D^+ D^{*-}$  configurations ensure that the  $X(3872)$  isospin is not precisely defined<sup>20</sup> as was first pointed out by Tornqvist (2004).

One diagnostic of the nature of  $X(3872)$  is the relative strength of the  $\gamma\psi'$  and  $\gamma J/\psi$  decay modes (Swanson, 2004a). The preference for  $\gamma\psi'$  over  $\gamma J/\psi$ , as indicated in Eq. (4), is in accord with expectations for a  $1^{++}$  charmonium, where the  $\chi'_{c1}$  and the  $\psi'$  have the same radial wave function and the  $\chi'_{c1} \rightarrow \gamma\psi'$   $E1$  transition is favored over that for  $\gamma J/\psi$ , which are “hindered” (Barnes, Godfrey, and Swanson, 2005) by the mismatch between the orthogonal initial- and final-state radial wave functions.<sup>21</sup> In contrast, in models in which the  $X(3872)$  is a pure molecular state, the  $\gamma\psi'$  decay channel is strongly suppressed relative to that for  $\gamma J/\psi$  (Swanson, 2004b; Dong *et al.*, 2011).

Another diagnostic that has been proposed is the nature of its prompt production in high-energy hadron collisions (Bignamini *et al.*, 2009). As discussed in Sec. III, the hadron-collider

<sup>20</sup>Since  $|I = 1; I_3 = 0\rangle = [|D^0\bar{D}^{*0}\rangle + |D^+ D^{*-}\rangle] / \sqrt{2}$  and  $|I = 0; I_3 = 0\rangle = [|D^0\bar{D}^{*0}\rangle - |D^+ D^{*-}\rangle] / \sqrt{2}$ , a well-defined  $I = 1$  or  $0$  state implies equal  $D^0\bar{D}^{*0}$  and  $D^+ D^{*-}$  content.

<sup>21</sup>In this case the  $2P$ - $1S$  overlap integral is only nonzero because the final-state  $1S$  radial wave function is boosted relative to that for the initial-state  $1P$  state.

<sup>19</sup>The  $\omega$  meson and, thus, the  $\omega J/\psi$  final state, have zero isospin.

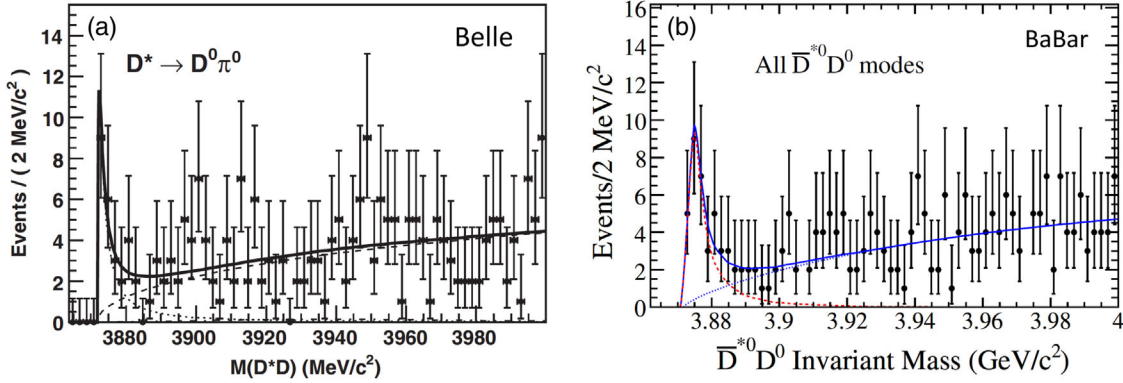


FIG. 24.  $M(D^0\bar{D}^{*0})$  distributions from  $B \rightarrow KD^0\bar{D}^{*0}$ . (a) From Belle. From [Aushev et al., 2010c](#). (b) From BABAR. From [Aubert et al., 2008c](#). The peaks near threshold are the signals  $X(3872) \rightarrow D^0\bar{D}^{*0}$  decays.

experiments see strong signals for prompt  $X(3872)$  production in  $E_{c.m.} = 1.96$  TeV  $p\bar{p}$  collisions at the Tevatron ([Abazov et al., 2004](#); [CDFII Collaboration, 2004](#)), and in  $pp$  collisions at  $E_{c.m.} = 7$  ([Chatrchyan et al., 2013a](#)) and 8 TeV ([Aaboud et al., 2017](#)) collisions at the LHC. In each of these experiments, the measured properties of  $X(3872)$  production are quite similar to those for the  $\psi'$  aside from an overall scale factor of about one-tenth, as illustrated in Fig. 25, where ATLAS measurements of the transverse momentum ( $p_T$ ) dependence of prompt  $\psi'$  and  $X(3872)$  production are shown as solid black and red circles, respectively ([Aaboud et al., 2017](#)).

If the  $X(3872)$  is a composite  $D\bar{D}^*$  moleculelike object, as suggested by the closeness of its mass to the  $m_{D^0} + m_{D^{*0}}$  threshold, one would expect that its production properties in prompt, high-energy hadron collisions would be less like those of the  $\psi'$  and more like those of known composite objects, such as light nuclei or hypernuclei. In the absence of any direct measurements of light nuclei and hypernuclei production in 7–8 TeV  $pp$  collisions, [Esposito, Guerrieri, Maiani et al. \(2015\)](#) extrapolated measurements from the ALICE experiment ([Adam et al., 2016a, 2016b](#)) of inclusive deuteron,  ${}^3\text{He}$ , and hypertriton  ${}^3_\Lambda H$  production cross sections in Pb-Pb collisions [with nucleon-nucleon c.m. energies of  $E_{c.m.}(NN) = 2.76$  TeV], to  $pp$  collisions at 7 TeV by means of a Glauber-model calculation. These are included in Fig. 25 where the associated curves are results of fits to the commonly used blast-wave-model functions for particle production in high-energy heavy ion collisions ([Schnedermann, Sollfrank, and Heinz, 1993](#)).

In the Glauber model, the nucleons inside heavy ions interact independently, and multinucleon, collective effects are ignored. The blue dash-dotted curve shows the [Esposito, Guerrieri, Maiani et al. \(2015\)](#) estimate for how the hypertriton extrapolation and fit would change if large collective effects were included. The extrapolations from Pb-Pb measurements to  $pp$  collisions and the blast-wave model are approximate and likely to be wrong by large factors. However, the differences between these extrapolations and the measured  $X(3872)$   $p_T$  dependence are many orders of magnitude too large to be accounted for by refinements in the models.

The BESIII experiment reported  $X(3872)$  production in the process  $e^+e^- \rightarrow \gamma\pi^+\pi^-J/\psi$  at c.m. energies in the region of the  $Y(4260)$  charmoniumlike resonance peak ([Ablikim et al., 2014d](#)). The  $X(3872)$  was detected via its  $\pi^+\pi^-J/\psi$  decay

channel; a  $\pi^+\pi^-J/\psi$  invariant mass distribution summed over the data at four energy points is shown in Fig. 26(a), where a  $6.3\sigma$  peak at the mass of the  $X(3872)$  is evident. Figure 26(b) shows the energy dependence of the  $X(3872)$  production rate where there is some indication that the observed signal is associated with the  $Y(4260)$ . Assuming that  $Y(4260) \rightarrow \gamma X(3872)$  decays are the source of this signal, and using the PDG lower limit  $\mathcal{B}(X(3872) \rightarrow \pi^+\pi^-J/\psi) > 0.026$  ([Patrignani et al., 2016](#)), BESIII determines

$$\frac{\mathcal{B}(Y(4260) \rightarrow \gamma X(3872))}{\mathcal{B}(Y(4260) \rightarrow \pi^+\pi^-J/\psi)} > 0.05,$$

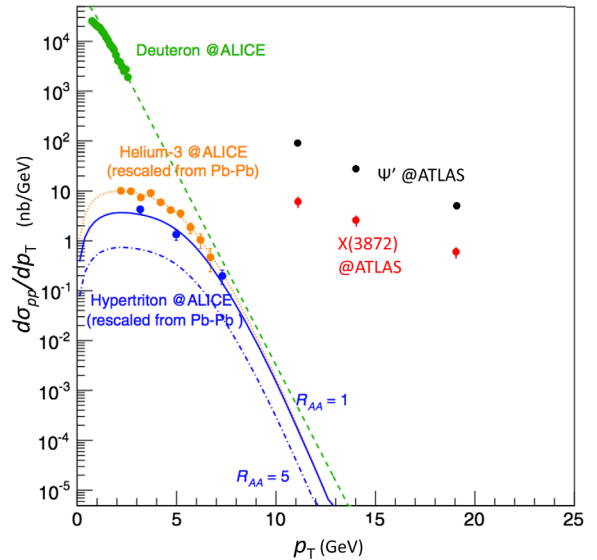


FIG. 25. Differential cross sections for particle production vs  $p_T$  at the LHC. The solid red (black) circles are ATLAS measurements of prompt  $X(3872)$  ( $\psi'$ ) production in  $E_{c.m.} = 8$  TeV  $pp$  collisions ([Aaboud et al., 2017](#)). Results for deuteron (green),  ${}^3\text{He}$  (orange), and  ${}^3_\Lambda H$  (blue) are extrapolations of ALICE Pb-Pb measurements at  $E_{c.m.}(NN) = 2.76$  to  $E_{c.m.}(pp) = 7$  TeV using a Glauber model. Adapted from [Esposito, Guerrieri, Maiani et al., 2015](#). The associated curves are the results of fits of the blast-wave model ([Schnedermann, Sollfrank, and Heinz, 1993](#)) expectations in the absence of any corrections for multinucleon collective effects. The blue dash-dotted curve is the extrapolated result for  ${}^3_\Lambda H$  when collective effects are included.



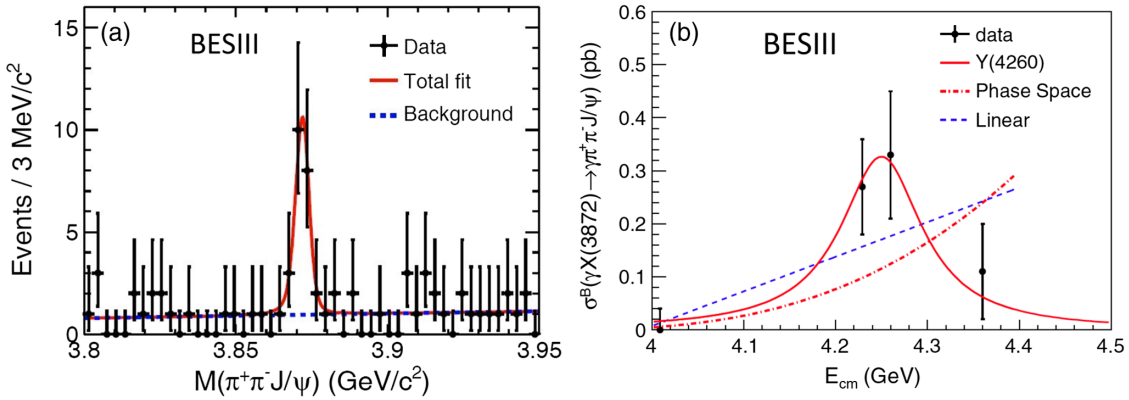


FIG. 26. (a) The data points show the BESIII experiment's  $M(\pi^+\pi^-J/\psi)$  distribution for  $e^+e^- \rightarrow \gamma\pi^+\pi^-J/\psi$  events at energies near the  $Y(4260)$  resonance. The fitted peak has a mass and width of  $M = 3871.9 \pm 0.7$  MeV and  $\Gamma = 0.0^{+1.7}_{-0.0}$  MeV ( $< 2.4$  MeV), which are in good agreement with the PDG world-average values for the  $X(3872)$ . (b) The energy dependence of the BESIII  $\sigma(e^+e^- \rightarrow \gamma X(3872)) \times \mathcal{B}(X(3872) \rightarrow \pi^+\pi^-J/\psi)$  measurement. The solid curve is the  $Y(4260)$  line shape fitted to the data; the dashed curves show phase-space and linear production model expectations. From Ablikim *et al.*, 2014d.

which is substantial and suggests that there is some commonality in the nature of the  $Y(4260)$ ,  $X(3872)$ , and  $Z_c(3900)$ .<sup>22</sup>

### B. $X(3915)$

After finding the  $X(3872)$  in  $B \rightarrow K\rho J/\psi$  decays, Belle studied  $B \rightarrow K\omega J/\psi$  decay, where in a data sample containing 275M  $B\bar{B}$  meson pairs they observed a prominent, near-threshold enhancement in the  $\omega J/\psi$  invariant mass distribution shown in Fig. 27(a) (Choi *et al.*, 2005). Belle fitted this enhancement with an  $S$ -wave BW resonance shape and found a mass and width for this peak, which they originally named the  $Y(3940)$ , of  $M = 3943 \pm 17$  MeV and  $\Gamma = 87 \pm 24$  MeV. The Belle result was confirmed by *BABAR* with a data sample containing 383M  $B\bar{B}$  meson pairs (Aubert *et al.*, 2008b) and, later, with *BABAR*'s final, 467M  $B\bar{B}$ -meson-pair data sample (del Amo Sanchez *et al.*, 2010a). *BABAR*'s fits to the data yielded lower mass and width values:  $M = 3919 \pm 4$  MeV and  $\Gamma = 31 \pm 11$  MeV. With their full data sample, *BABAR* was able to resolve an  $X(3872) \rightarrow \omega J/\psi$  contribution to the enhancement [see the inset in the upper panel of Fig. 27(b)]. The weighted averages of the Belle and *BABAR* results are  $M = 3920 \pm 4$  and  $\Gamma = 41 \pm 10$  MeV.

An  $\omega J/\psi$  mass peak with similar mass and width on a very small background was reported by Belle in the two-photon process  $\gamma\gamma \rightarrow \omega J/\psi$  and shown in Fig. 28(a) (Uehara *et al.*, 2010). The *BABAR* group subsequently observed a very similar peak (Lees *et al.*, 2012c) in the same process with mass and width values that were in good agreement with those reported by Belle [see Fig. 28(b)]. The weighted averages of the Belle and *BABAR* measurements are  $M = 3917.4 \pm 2.4$  MeV and  $\Gamma = 14 \pm 6$  MeV. The close agreement between the masses determined for the  $Y(3940) \rightarrow \omega J/\psi$  peak in  $B \rightarrow K\omega J/\psi$  decays and the  $X(3915) \rightarrow \omega J/\psi$  signal seen in  $\gamma\gamma \rightarrow \omega J/\psi$  production, and the similar values of the widths suggest that these are two different production

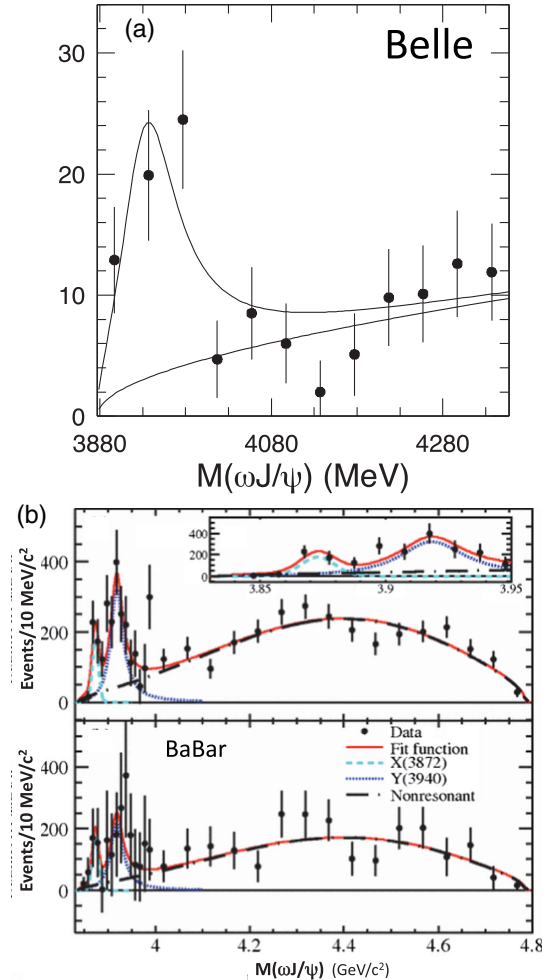


FIG. 27.  $X(3915) \rightarrow \omega J/\psi$  signals in  $B \rightarrow K\omega J/\psi$  decays. (a) From Belle. From Choi *et al.*, 2005. (b) From *BABAR*. From del Amo Sanchez *et al.*, 2010a. In the latter, the upper panel shows results for  $B^+ \rightarrow K^+\omega J/\psi$  and the lower panel shows those for  $B^0 \rightarrow K_S\omega J/\psi$ . The inset in the upper panel shows an expanded view of the low end of the  $\omega J/\psi$  mass scale, where the smaller, low-mass peak is due to the  $X(3872) \rightarrow \omega J/\psi$  and the larger, higher-mass peak is the  $X(3915) \rightarrow \omega J/\psi$  signal.

<sup>22</sup>The  $Y(4260)$  meson is discussed in Sec. V.C and the  $Z_c(3900)$  is discussed in Sec. VI.

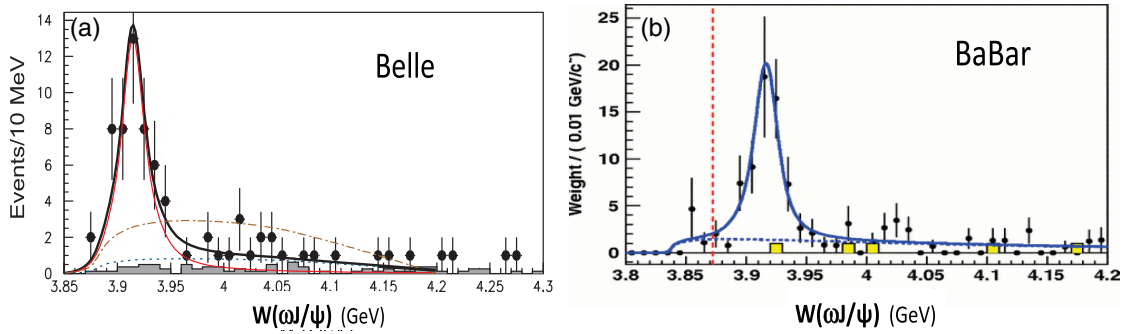


FIG. 28.  $X(3915) \rightarrow \omega J/\psi$  signals in  $\gamma\gamma \rightarrow \omega J/\psi$  fusion reactions. (a) From Belle. From Uehara *et al.*, 2010. (b) From BABAR. From Lees *et al.*, 2012c. The bold solid curves are results of fits with a BW resonance shape to represent the signal and a smooth function of  $p^*$  to represent the background, where  $p^*$  is the  $J/\psi$  momentum in the  $\gamma\gamma$  c.m. system. The dash-dotted curve in (a) is the result of a fit with no BW resonance term; the dashed vertical line in (b) indicates the location of  $W = 3872$  MeV. The shaded histograms show the non- $J/\psi$  background estimated from events in the  $J/\psi$  mass sidebands.

mechanisms for the same state. In the following we assume this to be the case and refer to this state as the  $X(3915)$ . The PDG tables (Patrignani *et al.*, 2016) list the results from both channels as a single entry with average mass and width values of

$$\begin{aligned} M(X(3915)) &= 3918.4 \pm 1.9 \text{ MeV}, \\ \Gamma(X(3915)) &= 20.0 \pm 5.0 \text{ MeV}. \end{aligned} \quad (6)$$

### 1. Is the $X(3915)$ the $\chi_{c0}$ charmonium state?

BABAR performed a spin-parity analysis with their  $\gamma\gamma \rightarrow \omega J/\psi$  events that favored a  $J^{PC} = 0^{++}$  quantum number assignment. Based on this result, they identified the  $X(3915)$  as a candidate for the  $2^3P_0$  charmonium state, commonly known as the  $\chi'_{c0}$ , and the PDG classified the  $X(3915)$  as the  $\chi'_{c0}$  in the 2014 Meson Summary Tables (Olive *et al.*, 2014). However, although BABAR's preferred  $J^{PC} = 0^{++}$  values match expectations for the  $\chi'_{c0}$ , other properties of the  $X(3915)$  make it a poor candidate for the  $2^3P_0$  charmonium state (Guo and Meissner, 2012; Wang, Yang, and Ping, 2014; Olsen, 2015). The mass is too high; the  $\chi'_{c2} - X(3915)$  mass splitting  $\delta M_{2-0}(2P) = 8.8 \pm 3.2$  MeV is only 6% of the  $1P$  splitting:  $\delta M_{2-0}(1P) = 141.5 \pm 0.3$  MeV in strong contradiction with theoretical expectations (Eichten, Lane, and Quigg, 2004; Li and Chao, 2009; Wang, Yang, and Ping, 2014). Another peculiarity of the  $X(3915) = \chi'_{c0}$  assignment is the lack of any experimental evidence for  $X(3915) \rightarrow D\bar{D}$  decays and the apparent strength of the  $X(3915) \rightarrow \omega J/\psi$  discovery mode, which conflicts with expectations that  $\chi_{c0} \rightarrow D\bar{D}$  would be a strongly favored *fall-apart* mode and  $\chi'_{c0} \rightarrow \omega J/\psi$  an OZI-rule-violating process that is expected to be strongly suppressed (Okubo, 1963; Zweig, 1964; Iizuka, 1966).

Zhou, Xiao, and Zhou (2015) added to the controversy by pointing out that the BABAR spin-parity analysis that ruled out the  $J^{PC} = 2^{++}$  hypothesis assumed the dominance of the helicity-2 amplitude over that for helicity 0. Their reanalysis of the BABAR angular distributions showed that when a helicity-0 amplitude is included, a  $J^{PC} = 2^{++}$  assignment cannot be ruled out and made an argument that identifies

the  $X(3915)$  as the  $\chi'_{c2}$  charmonium state. However, their argument for the  $X(3915) = \chi'_{c2}$  assignment ignores the consequences of  $X(3915)$  production in  $B \rightarrow K\omega J/\psi$  decays. For example, since the *total* branching fraction  $\mathcal{B}(B^+ \rightarrow K^+\chi_{c2}(1P)) = (1.1 \pm 0.4) \times 10^{-5}$  is smaller than the product of branching fractions

$$\mathcal{B}(B^+ \rightarrow K^+X(3915)) \times \mathcal{B}(X \rightarrow \omega J/\psi) = 3.0_{-0.7}^{+0.9} \times 10^{-5}, \quad (7)$$

the  $X(3915) = \chi'_{c2}$  assignment implies a  $B^+ \rightarrow K^+\chi'_{c2}$  partial decay width that is substantially larger than that for  $B^+ \rightarrow K^+\chi_{c2}$ , which is contrary to models for  $B$ -meson decays to charmonium states, where these widths are expected to be proportional to the square of the  $c\bar{c}$  wave function at the origin, which decreases with increasing radial quantum number (Bodwin *et al.*, 1992).

On the other hand, the  $X(3915) \rightarrow \omega J/\psi$  signals seen in  $B$  decays and in  $\gamma\gamma$  production may be unrelated. More data and separate spin-parity determinations for the  $\omega J/\psi$  systems produced in  $B \rightarrow K\omega J/\psi$  and  $\gamma\gamma \rightarrow \omega J/\psi$  processes and with fewer assumptions are needed. At present, the situation remains confused, as evidenced by the 2016 edition of the PDG report, which no longer identifies this as the  $\chi'_{c0}$  and has reverted to calling this state the  $X(3915)$  (Patrignani *et al.*, 2016). Recently Belle reported the observation of an alternative  $\chi'_{c0}$  candidate, the  $X^*(3860)$ , with none of the problems associated with the  $X(3915) = \chi'_{c0}$  assignment (Chilikin *et al.*, 2017). This is discussed in Sec. V.E.

### 2. Is the $X(3915)$ a $c\bar{c}s\bar{s}$ four-quark state?

The most parsimonious interpretation of existing data is to assume that the  $\omega J/\psi$  peaks seen in  $B$  decays and  $\gamma\gamma$  production are due to the same state. In that case, the most likely  $J^{PC}$  assignment is  $0^{++}$ , and the mass and strength of the  $\omega J/\psi$  decay channel and absence of any evidence for a significant  $D\bar{D}$  decay mode rule against its identification as a  $c\bar{c}$  charmonium state. The mass is 18.2 MeV below the  $2m_{D_s}$  threshold, and this suggests that it may contain a significant  $c\bar{c}s\bar{s}$  component, in either a  $D_s^+D_s^-$  moleculelike configuration (Li and Voloshin, 2015), a  $[\bar{c}s][cs]$  tetraquark (Lebed and

Polosa, 2016), or a mixture of the two. In any of these pictures, the  $D\bar{D}$  decay mode would strictly violate the OZI rule, while the  $\omega$  meson's small, but non-negligible  $s\bar{s}$  content (Benayoun *et al.*, 1999) would partially mitigate the  $\omega J/\psi$  mode's violation of the rule and an  $\omega J/\psi$  decay width that is comparable or greater than that for  $D\bar{D}$  would not be *a priori* ruled out. For a  $c\bar{c}s\bar{s}$  combination configured as either a moleculelike or a tetraquark arrangement, the decay mode least affected by OZI suppression would be  $X(3915) \rightarrow \eta\eta_c$  and this could be expected to be a dominant decay mode. However, Belle searched for this mode, saw no significant signal, and established a (90% C.L.) product branching-fraction upper limit (Vinokurova *et al.*, 2015):

$$\mathcal{B}(B^+ \rightarrow K^+ X(3915)) \times \mathcal{B}(X \rightarrow \eta\eta_c) < 4.7 \times 10^{-5}. \quad (8)$$

Since this limit is not very stringent, it is difficult to draw a definite conclusion from it. A comparison of it with the  $\omega J/\psi$  measurement given in Eq. (7) indicates that, in spite of Belle's null result, the partial decay width for  $X(3915) \rightarrow \eta\eta_c$  could still be larger than that for  $\omega J/\psi$  by as much as a factor of  $\approx 2$ . The expectation that the  $\eta\eta_c$  partial width should be large is only qualitative and our limited level of understanding of these processes precludes the ability of making a reliable quantitative estimate of just how large it should be. Because of this, the absence of an  $\eta\eta_c$  mode would probably only be fatal to the  $c\bar{c}s\bar{s}$  quark assignment if its partial width was shown to be definitely much smaller than that for  $\omega J/\psi$  decays.<sup>23</sup>

### 3. Discussion

Since it is relatively narrow and is seen as clear signals in both  $B$ -meson decays and  $\gamma\gamma$  fusion reactions, the  $X(3915)$  is one of the most intriguing of the XYZ exotic meson candidates. However, significant progress in our understanding of its underlying nature will probably not be forthcoming until larger data samples are available in future experiments such as BelleII (Abe *et al.*, 2010). With the order-of-magnitude larger event samples that are expected for BelleII, we can expect definitive  $J^{PC}$  determinations and measurements of, or more stringent limits on, the strengths of the  $D\bar{D}$  and  $\eta\eta_c$  decay channels for both the  $B$ -meson decay and  $\gamma\gamma$ -fusion production modes. The LHCb experiment has demonstrated the ability to detect  $\omega$  mesons in  $B$  decays (Aaij *et al.*, 2013b) and should also be able to probe the  $X(3915)$  quantum numbers.

#### C. $Y(4260)$ and other $J^{PC} = 1^{--}$ states

After the discovery of the  $X(3872)$  in  $\pi^+\pi^- J/\psi$  decays and before its  $J^{PC} = 1^{++}$  quantum number assignment was established, the BABAR group considered the possibility that it might be a  $1^{--}$  vector state and searched for its direct production in the initial-state-radiation process  $e^+e^- \rightarrow \gamma_{\text{ISR}} \pi^+\pi^- J/\psi$  (Aubert *et al.*, 2005d). They did not see an  $X(3872)$  signal and were able to conclude that the  $X(3872)$ 's  $J^{PC}$  quantum numbers were not  $1^{--}$ . They did see, however, an unexpected strong accumulation of events with  $\pi^+\pi^- J/\psi$

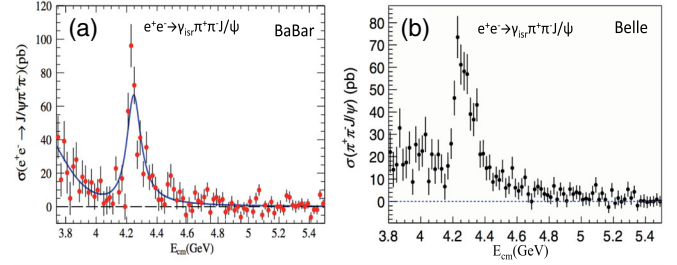


FIG. 29. (a) The data points show the Born cross sections for  $e^+e^- \rightarrow \pi^+\pi^- J/\psi$ , measured via the initial-state radiation process  $e^+e^- \rightarrow \gamma_{\text{ISR}} \pi^+\pi^- J/\psi$  by BABAR. The curve shows results of a fit that used a single BW resonance to represent the  $Y(4260)$  resonance plus a linear background term. From Lees *et al.*, 2012b. (b) Belle measurements of the same cross sections. From Liu *et al.*, 2013.

invariant masses that peaked near 4.26 GeV, shown in Fig. 14(b), that they called the  $Y(4260)$  (Aubert *et al.*, 2005a). Subsequent BABAR measurements (Lees *et al.*, 2012b) of the “Born” cross sections<sup>24</sup> for  $e^+e^- \rightarrow \pi^+\pi^- J/\psi$  at c.m. energies near the  $Y(4260)$  mass peak, using their full data set, are shown in Fig. 29(a). This peak was quickly confirmed by CLEO (Coan *et al.*, 2006) and Belle (Yuan *et al.*, 2007). The most recent Belle measurements (Liu *et al.*, 2013) of  $\sigma(e^+e^- \rightarrow \pi^+\pi^- J/\psi)$  in the  $Y(4260)$  region, based on their full data set, are shown in Fig. 29(b), where the similarity with the BABAR measurements is apparent. The weighted average of the mass and width values determined by BABAR, CLEO, and Belle from fits of a single BW resonance line shape to the  $Y(4260)$  peak in their data are (Patrignani *et al.*, 2016)

$$\begin{aligned} M(Y(4260)) &= 4251 \pm 9 \text{ MeV}, \\ \Gamma(Y(4260)) &= 120 \pm 12 \text{ MeV}. \end{aligned} \quad (9)$$

The excess of events near 4 GeV in their  $\pi^+\pi^- J/\psi$  cross-section measurements was attributed by Belle to an additional possible resonance that they called the  $Y(4008)$  (Yuan *et al.*, 2007; Patrignani *et al.*, 2016), but a similar excess was not observed by BABAR (Lees *et al.*, 2012b) and was not confirmed by recent BESIII results (Ablikim *et al.*, 2017c).

The production mode of the  $Y(4260)$  ensures that its  $J^{PC}$  quantum numbers are the same as those of the photon, i.e.,  $1^{--}$ . Its discovery decay mode  $Y(4260) \rightarrow \pi^+\pi^- J/\psi$  provides strong evidence that its constituents contain a  $c\bar{c}$  quark pair. However, all of the  $1^{--}$   $c\bar{c}$  charmonium levels with mass below 4500 MeV have already been assigned to well-established  $1^{--}$  resonances that are seen in the total cross section for  $e^+e^- \rightarrow$  hadrons between 2.6 and 4.6 GeV (Bai *et al.*, 2000, 2002) [see the inset in Fig. 11(a)]. In addition, even though its mass is well above all of the  $D^{(*)}\bar{D}^{(*)}$  open-charmed-meson mass thresholds, there is no evidence for its decay to pairs of open-charmed mesons in the inclusive

<sup>24</sup>Born cross sections are cross sections that correspond to the lowest-order Feynman diagram and are determined by “radiatively correcting” observed cross sections for higher-order QED effects such as initial-state radiation and vacuum polarization.

<sup>23</sup>This issue is discussed by Li and Voloshin (2015).

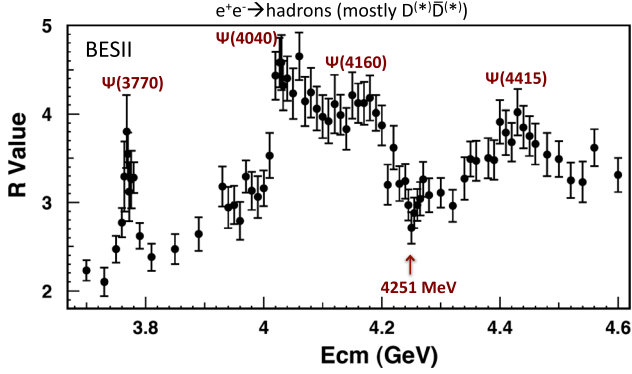


FIG. 30. Measurements of the ratio  $R = \sigma_{\text{tot}}(e^+e^- \rightarrow \text{hadrons}) / \sigma_{\text{QED}}(e^+e^- \rightarrow \mu^+\mu^-)$ , where  $\sigma_{\text{QED}}(e^+e^- \rightarrow \mu^+\mu^-) = 86.85 \text{ nb}/s$  ( $s$  in  $\text{GeV}^2$ ). The structures above  $R \approx 2$  are attributed to the indicated  $1^{--}$  charmonium mesons decaying to  $D\bar{D}$ ,  $D\bar{D}^*$  open-charmed, or  $D^*\bar{D}^*$  final states. The expected position for a  $Y(4260)$  signal, indicated by an arrow, is located at a local minimum in the measured cross section. From [Bai et al., 2002](#).

$e^+e^- \rightarrow \text{hadrons}$  total cross section. BESII measurements of  $\sigma_{\text{tot}}(e^+e^- \rightarrow \text{hadrons})$  at c.m. energies between 3.7 and 4.6 GeV, shown in Fig. 30, exhibit considerable structure that is primarily due to the production and decay to pairs of open-charmed mesons of the established  $1^{--}$   $\psi(3770)$ ,  $\psi(4040)$ ,  $\psi(4160)$ , and  $\psi(4415)$  charmonium states. The strong signals for these states in  $\sigma_{\text{tot}}(e^+e^- \rightarrow \text{hadrons})$  plus their absence in the  $M(\pi^+\pi^-J/\psi)$  invariant mass distributions shown in Figs. 29(a) and 29(b) reflect the expected strong dominance of fall-apart decays to open-charmed-meson pairs over OZI-rule-suppressed decays to hidden-charm final states that is characteristic of above-open-charm-threshold charmonium states. In contrast, the absence of any sign of  $Y(4260)$  decays to charmed mesons in  $\sigma_{\text{tot}}(e^+e^- \rightarrow \text{hadrons})$  plus its strong signal in the  $\pi^+\pi^-J/\psi$  decay channel is opposite to expectations for charmonium. As a result, there has been considerable theoretical speculation that the  $Y(4260)$  might be some kind of a multiquark meson or a  $c\bar{c}$ -gluon hybrid state ([Brambilla et al., 2011](#); [Guo, Yépez-Martínez, and Szczepaniak, 2014](#); [Maiani et al., 2014](#)).

A *BABAR* search for  $Y(4260) \rightarrow \pi^+\pi^-\psi'$  decays in  $e^+e^- \rightarrow \pi^+\pi^-\psi'$  events resulted in the  $\pi^+\pi^-\psi'$  invariant mass distribution shown in Fig. 31(a), where there is a strong peaking of events near 4320 MeV on a nearly negligible background ([Aubert et al., 2007](#)). This peak is not compatible with the measured mass and width of the  $Y(4260)$ , as indicated by the dashed curve in the figure. A subsequent study of the same reaction with a larger data sample by Belle confirmed the *BABAR* observation, albeit at a somewhat higher mass near 4360 MeV as shown in Fig. 31(b) ([Wang et al., 2007](#)). The current PDG values for the mass and width of this peak, called the  $Y(4360)$ , are ([Patrignani et al., 2016](#))

$$\begin{aligned} M(Y(4360)) &= 4346 \pm 6 \text{ MeV}, \\ \Gamma(Y(4360)) &= 102 \pm 12 \text{ MeV}. \end{aligned} \quad (10)$$

In addition, Belle observed a second distinct  $\pi^+\pi^-\psi'$  invariant mass peak near 4660 MeV that is evident in

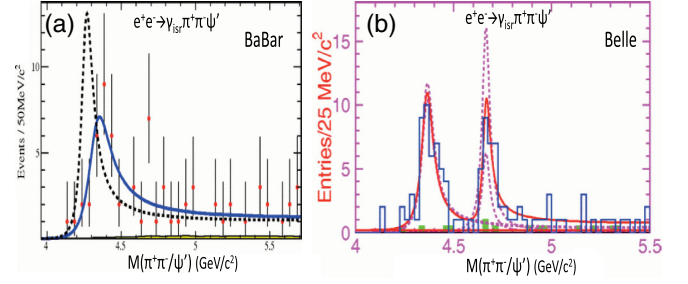


FIG. 31. (a) The data points show the  $\pi^+\pi^-\psi'$  invariant mass distribution for  $e^+e^- \rightarrow \gamma_{\text{ISR}}\pi^+\pi^-\psi'$  events in *BABAR*. The solid curve shows results of a fit that used a single-BW resonance to represent the signal plus a linear background term. The dashed curve shows the results of a fit with mass and width constrained to the  $Y(4260)$  values. From [Aubert et al., 2007](#). (b) The blue histogram shows the corresponding results from Belle. The solid curve shows the results of a fit that uses two interfering BW amplitudes, one with mass near 4360 MeV and the other near 4660 MeV. The dashed curves show the individual resonance contributions from two equally good fits that have different interference phases. From [Wang et al., 2007](#).

Fig. 31(b), an observation that was confirmed by *BABAR* ([Lees et al., 2014](#)). In addition, Belle also reported a peak with similar mass and width in the  $\Lambda_c^+\Lambda_c^-$  invariant mass in  $e^+e^- \rightarrow \gamma_{\text{ISR}}\Lambda_c^+\Lambda_c^-$  events ([Pakhlova et al., 2008](#)). The PDG average of the Belle and *BABAR* mass and width measurements of this second peak, called the  $Y(4660)$ , are ([Patrignani et al., 2016](#))

$$\begin{aligned} M(Y(4660)) &= 4643 \pm 9 \text{ MeV}, \\ \Gamma(Y(4660)) &= 72 \pm 11 \text{ MeV}. \end{aligned} \quad (11)$$

### 1. BESIII as a “ $Y(4260)$ factory”

The *BABAR* and Belle results on the  $Y(4260)$ ,  $Y(4360)$ , and  $Y(4660)$  all relied on production of these states via the ISR process illustrated in Fig. 12(d) and discussed in Sec. III. This process has the advantage of sampling many  $e^+e^-$  c.m. energies at once, but is limited by a severe, order  $\alpha_{\text{QED}}$ , luminosity penalty associated with the radiation of a hard photon. For detailed studies of these states, the BESIII experiment has the advantage of operating at and near c.m. energies corresponding to the  $Y(4260)$  and  $Y(4360)$  peaks, thereby functioning as a “ $Y$  factory.” In this mode of operation, large event samples can be accumulated near the peaks of these resonances. On the other hand, line-shape measurements of the resonance parameters and the separation of resonance signals from underlying nonresonant backgrounds require time-consuming energy-by-energy scans.

BESIII’s first data-taking run in this energy range accumulated a  $525 \text{ pb}^{-1}$  data sample at 4260 MeV in which they found  $1477 \pm 43 \pi^+\pi^-J/\psi$  events that included  $307 \pm 48$  events of the type  $e^+e^- \rightarrow \pi^\mp Z_c(3900)^\pm$ ;  $Z_c(3900)^\pm \rightarrow \pi^\pm J/\psi$ , where the  $Z_c(3900)^\pm$  is a relatively narrow, resonance-like structure with nonzero electric charge that is discussed in Sec. VI. BESIII subsequently did a scan of measurements around the  $Y(4260)$  and  $Y(4360)$  peaks, including relatively high statistics points at  $E_{\text{c.m.}} = 4230$ ,

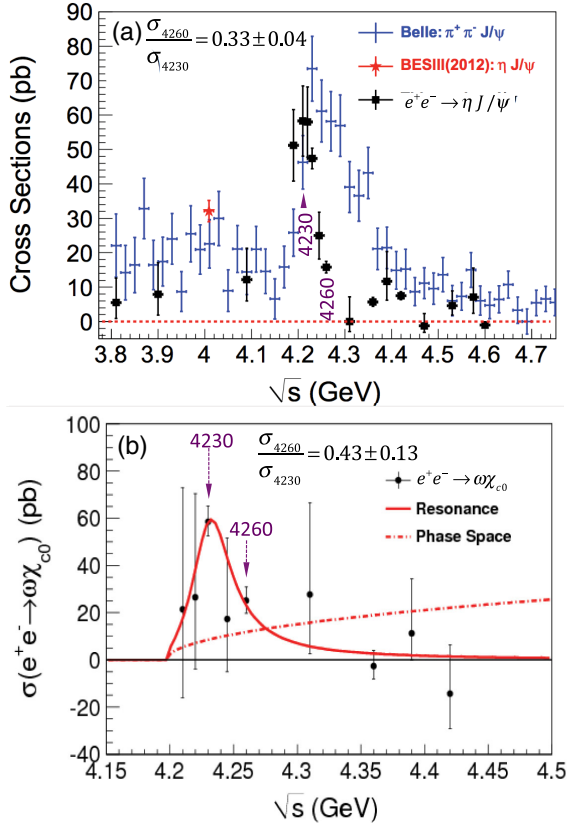


FIG. 32. (a) Cross-section measurements for  $e^+e^- \rightarrow \eta J/\psi$  from BESIII shown as black points. For comparison, Belle isr measurements of the  $e^+e^- \rightarrow \pi^+\pi^-J/\psi$  cross section over the same energy range are shown as blue crosses (Liu *et al.*, 2013). The red star indicates a previous BESIII  $\eta J/\psi$  cross-section measurement near the peak of the  $\psi(4040)$  charmonium state (Ablikim *et al.*, 2012). Adapted from Ablikim *et al.*, 2015c. (b) The data points show BESIII measurements of the cross section for  $e^+e^- \rightarrow \omega\chi_{c0}$ . The solid curve shows the result of a fit of a threshold-constrained BW resonance shape to the data. The dash-dotted curve indicates what a phase-space-only distribution would be like. From Ablikim *et al.*, 2015g.

4260, and 4360 MeV.<sup>25</sup> With these data, BESIII measured the cross sections for  $e^+e^- \rightarrow \eta J/\psi$  shown in Fig. 32(a) (Ablikim *et al.*, 2015c) and  $e^+e^- \rightarrow \omega\chi_{c0}$  shown in Fig. 32(b) (Ablikim *et al.*, 2015g).

Figure 32(a) includes a comparison of BESIII's  $e^+e^- \rightarrow \eta J/\psi$  cross sections with Belle isr results for  $\sigma(e^+e^- \rightarrow \pi^+\pi^-J/\psi)$  (Liu *et al.*, 2013), where it is evident that the peak seen in the  $\eta J/\psi$  channel is much narrower than Belle's  $Y(4260) \rightarrow \pi^+\pi^-J/\psi$  peak. The  $\omega\chi_{c0}$  cross section [Fig. 32(b)] shows a behavior that is similar to that for  $\eta J/\psi$ . The red curve in this figure is the result of a fit of a threshold-constrained BW resonance to the  $\omega\chi_{c0}$  data points, which returns mass and width values  $M_{\omega\chi_{c0}} = 4230 \pm 10$  MeV and

<sup>25</sup>The three “high luminosity” data samples have integrated luminosities of 1047 pb<sup>-1</sup> at 4230 MeV, 827 pb<sup>-1</sup> at 4260 MeV, and 540 pb<sup>-1</sup> at 4360 MeV. The other points have luminosities of about 50 pb<sup>-1</sup>.

$\Gamma_{\omega\chi_{c0}} = 38 \pm 12$  MeV that are a poor match to the PDG values for the  $Y(4260)$  given in Eq. (9). The absence of any constraining  $\eta J/\psi$  data points on the lower side of the peak, i.e., between  $M(\eta J/\psi) = 4100$  and 4200 MeV, precluded BESIII from doing a meaningful fit for a  $\eta J/\psi$  line shape. Instead they characterized the shapes of the  $\eta J/\psi$  and  $\omega\chi_{c0}$  peaks by the ratio of their cross sections at the high-statistics  $E_{c.m.} = 4230$  and 4260 MeV data points:

$$R_{4230}^{4260}(f) = \frac{\sigma_{4260}^{4260}(e^+e^- \rightarrow f)}{\sigma_{4230}^{4260}(e^+e^- \rightarrow f)},$$

where they found good agreement  $R_{4230}^{4260}(\eta J/\psi) = 0.33 \pm 0.04$  and  $R_{4230}^{4260}(\omega\chi_{c0}) = 0.43 \pm 0.13$ .

The evident incompatibility of the narrow structures in the  $e^+e^- \rightarrow \eta J/\psi$  and  $e^+e^- \rightarrow \omega\chi_{c0}$  cross sections with the broad  $Y(4260) \rightarrow \pi^+\pi^-J/\psi$  peak prompted BESIII to map out the  $E_{c.m.}$  energy region in the vicinity of the  $Y(4260)$  with two additional, independent data sets (Ablikim *et al.*, 2017c). One consists of 19 high luminosity data runs with at least 40 pb<sup>-1</sup>/point between  $E_{c.m.} = 3773$  and 4599 MeV. The other consists of 60 “low-luminosity” energy-scan data runs with 7–9 pb<sup>-1</sup>/point between  $E_{c.m.} = 3882$  and 4567 MeV. Figures 33(a) and 33(b) show  $e^+e^- \rightarrow \pi^+\pi^-J/\psi$  cross-section measurements from the high- and low-luminosity data scans, respectively, where it is evident that the line shape of the “ $Y(4260)$ ” peak is not well described by a single-BW

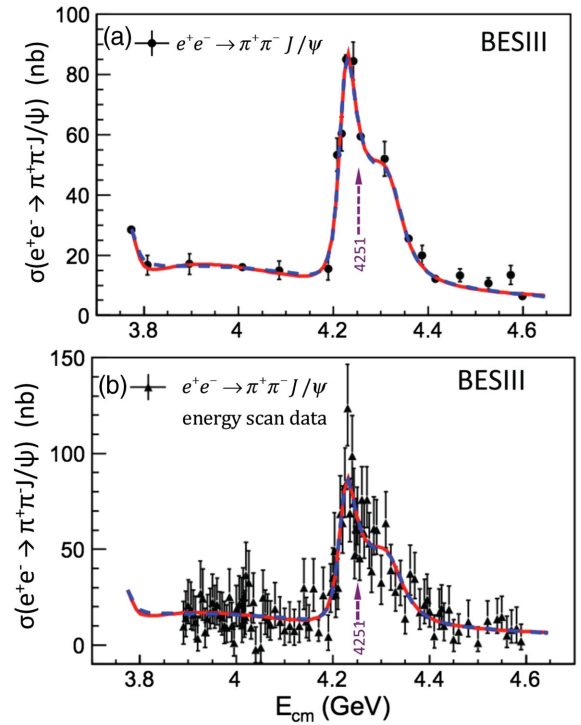


FIG. 33. BESIII measurements of the cross section for  $e^+e^- \rightarrow \pi^+\pi^-J/\psi$  for (a) the “high luminosity” and (b) the “low luminosity” scan data. Dashed arrows in both plots indicate the “ $Y(4260)$ ” mass value from the PDG-2016 average of results based on single-BW resonance fits to pre-2016 measurements given in Eq. (9). Adapted from Ablikim *et al.*, 2017c.

resonance function. The curves in the figures show the results from fits to the data in both plots with two interfering BW resonance amplitudes that provides mass and width values of

$$\begin{aligned} M_1 &= 4222 \pm 4 \text{ MeV}, & \Gamma_1 &= 44 \pm 5 \text{ MeV}, \\ M_2 &= 4320 \pm 13 \text{ MeV}, & \Gamma_2 &= 101_{-22}^{+27} \text{ MeV}, \end{aligned} \quad (12)$$

where the statistical and (smaller) systematic errors are added in quadrature. The simplest interpretation of these results is that the first peak is the  $Y(4260)$ , which has a significantly lower mass and narrower width than the  $B$ -factory-measured values that are given in Eq. (9), and that the second peak is due to a  $\pi^+\pi^-J/\psi$  decay mode of the  $Y(4360)$  resonance, with slightly lower mass and narrower width values than those determined from the  $\pi^+\pi^-\psi'$  decay mode listed in Eq. (10).

BESIII measurements of the energy dependence of the cross section for  $e^+e^- \rightarrow \pi^+\pi^-h_c$  with the same two data sets (Ablikim *et al.*, 2017a) are shown in Fig. 34. The solid red curve in the figure shows the results of a fit to the measurements with a coherent sum of two BW amplitudes. The parameters determined from the fit are

$$\begin{aligned} M_1 &= 4218 \pm 4 \text{ MeV}, & \Gamma_1 &= 66 \pm 9 \text{ MeV}, \\ M_2 &= 4392 \pm 6 \text{ MeV}, & \Gamma_2 &= 140 \pm 16 \text{ MeV}, \end{aligned} \quad (13)$$

where the statistical and (smaller) systematic errors are added in quadrature. The lower-mass BW term, shown in the figure as a dashed green line, has a fitted mass and width that is consistent with the  $M \approx 4220$  MeV peak seen in  $\eta J/\psi$ ,  $\omega\chi_{c0}$ , and  $\pi^+\pi^-J/\psi$ . No evidence for the higher-mass  $\pi^+\pi^-h_c$  peak is seen in the  $\eta J/\psi$  or  $\omega\chi_{c0}$  channels and its measured parameters are inconsistent with those of the  $Y(4360)$ , for both the  $\pi^+\pi^-J/\psi$  and  $\pi^+\pi^-\psi'$  channels.

## 2. Discussion

The  $Y(4260)$  and the other, higher-mass  $1^{--}$  states have attracted considerable attention; the *BABAR* (Aubert *et al.*,

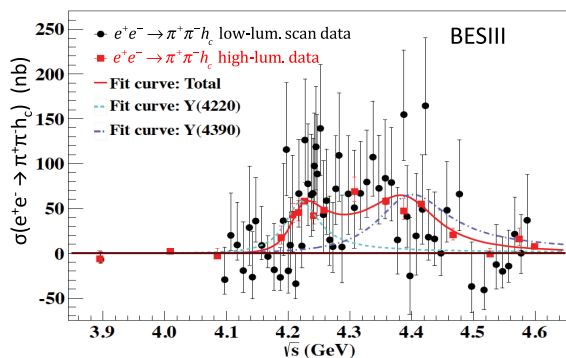


FIG. 34. The data points show BESIII measurements of the cross section for  $e^+e^- \rightarrow \pi^+\pi^-h_c$ , where the  $h_c$  was detected via its  $h_c \rightarrow \gamma\eta_c$  decay mode with the  $\eta_c$  reconstructed in one of 16 exclusive multihadron decay channels. The solid black dots are from the low-luminosity-scan and the solid red squares are from the high-luminosity-scan points. The solid red curve shows the results of a fit to the data with a coherent sum of two interfering BW amplitudes discussed in the text. From Ablikim *et al.*, 2017a.

2005a, 2007) and Belle (Wang *et al.*, 2007) papers reporting their discoveries rank among these experiments most highly cited papers. Most of the theoretical discussions to date have been focused on  $Y(4260)$  mass and width parameters that were determined from single-BW fits to isr line shapes shown in Fig. 29. However, the recent measurements of the  $e^+e^- \rightarrow \eta J/\psi$ ,  $\omega\chi_{c0}$ , and  $\pi^+\pi^-h_c$  cross sections, shown in Figs. 32 and 34, respectively, and precise results for  $e^+e^- \rightarrow \pi^+\pi^-J/\psi$  shown in Fig. 33, demonstrate that the single-resonance assumption that was used to determine the mass and width values given in Eq. (9) was too naive and the values that were derived are not reliable. The older results based on single-peak fits to  $\pi^+\pi^-J/\psi$  mass distribution ought to be ignored and the  $Y(4260)$  label probably should be retired. Averaging the mass and width determinations in  $\pi^+\pi^-J/\psi$ ,  $\pi^+\pi^-h_c$ , and  $\omega\chi_{c0}$  channels, we obtain

$$\begin{aligned} M(Y(4220)) &= 4222 \pm 3 \text{ MeV}, \\ \Gamma(Y(4220)) &= 48 \pm 7 \text{ MeV}, \end{aligned} \quad (14)$$

where the error on the width was scaled up to account for mild disagreements between the different channels.

Some theoretical papers interpreted the  $Y(4260)$  as a bound state of a  $D$  meson and a  $\bar{D}_1(2420)$ , a  $J^P = 1^+$   $P$ -wave excitation of the  $D$  meson with mass 2421 MeV and width  $\Gamma = 27.4$  MeV (Ding, 2009a; Wang, Hanhart, and Zhao, 2013). For the Eq. (9) mass value for the  $Y(4260)$ , this implied a  $D\bar{D}_1$  binding energy of  $\approx 35$  MeV, which is somewhat larger than typical values for nuclear systems that are bound by Yukawa meson-exchange forces. With the lower, Eq. (14) value for the  $Y(4220)$  mass, the implied  $D\bar{D}_1$  binding energy nearly doubles to 66 MeV, which suggests that the  $D\bar{D}_1$  molecule interpretation should be reevaluated. Others have proposed that the  $Y(4260)$  might be a  $c\bar{c}$ -gluon hybrid meson (Close and Page, 2005; Kou and Pene, 2005; Zhu, 2005). A lattice QCD calculation (with pion mass  $\sim 400$  MeV) found a candidate for a  $1^{--}$  hybrid state at a mass of  $4285 \pm 14$  MeV that they suggested as a possible interpretation for the  $Y(4260)$  (Liu *et al.*, 2012). A large radiative width of the  $Y(4260)$  would be at odds with the hybrid interpretation, and this calls for improved measurements of the  $e^+e^- \rightarrow \gamma X(3872)$  (Ablikim *et al.*, 2014d) cross section in the relevant mass range, to correlate it better with the observed  $Y$  structures and to extract their absolute radiative branching ratios.

## D. $X(4140)$ and other $J/\psi\phi$ structures

Studies of mass structures in  $J/\psi\phi$  have a vivid and controversial history that involves a number of experiments as summarized in Tables V and VI. The relative ease of triggering on  $J/\psi \rightarrow \mu^+\mu^-$  decays, supplemented with the distinctively narrow  $\phi \rightarrow K^+K^-$  mass peak, provides a relatively clean signature, even in hadron-collider experiments with no hadron identification capabilities. The history started in 2008, when the CDF Collaboration presented  $3.8\sigma$  evidence for a near-threshold  $J/\psi\phi$  mass peak in  $B^+ \rightarrow J/\psi\phi K^+$  decays, shown in Fig. 35(a), with mass  $M = 4143 \pm 3$  MeV

TABLE V. Results related to the  $X(4140) \rightarrow J/\psi\phi$  mass peak, first observed in  $B^+ \rightarrow J/\psi\phi K^+$  decays. The first (second) significance quoted for [Abazov et al. \(2015\)](#) is for the nonprompt (prompt) production components (the mass and width were determined from the nonprompt sample). The unpublished results are shown in italics.

Year	Experiment luminosity	$B \rightarrow J/\psi\phi K$ yield	Mass (MeV)	$X(4140)$ peak Width (MeV)	Significance
2008	CDF $2.7 \text{ fb}^{-1}$ ( <a href="#">Aaltonen et al., 2009a</a> )	$58 \pm 10$	$4143.0 \pm 2.9 \pm 1.2$	$11.7^{+8.3}_{-5.0} \pm 3.7$	$3.8\sigma$
2009	<i>Belle</i> ( <a href="#">Brodzicka, 2009</a> )	$325 \pm 21$	<i>4143.0 fixed</i>	<i>11.7 fixed</i>	<i>1.9\sigma</i>
2011	CDF $6.0 \text{ fb}^{-1}$ ( <a href="#">Aaltonen et al., 2017</a> )	$115 \pm 12$	$4143.4^{+2.9}_{-3.0} \pm 0.6$	$15.3^{+10.4}_{-6.1} \pm 2.5$	$5.0\sigma$
2011	LHCb $0.37 \text{ fb}^{-1}$ ( <a href="#">Aaij et al., 2012b</a> )	$346 \pm 20$	4143.4 fixed	15.3 fixed	$1.4\sigma$
2013	CMS $5.2 \text{ fb}^{-1}$ ( <a href="#">Chatrchyan et al., 2014</a> )	$2480 \pm 160$	$4148.0 \pm 2.4 \pm 6.3$	$28^{+15}_{-11} \pm 19$	$5.0\sigma$
2013	D0 $10.4 \text{ fb}^{-1}$ ( <a href="#">Abazov et al., 2014</a> )	$215 \pm 37$	$4159.0 \pm 4.3 \pm 6.6$	$19.9 \pm 12.6^{+1.0}_{-8.0}$	$3.0\sigma$
2014	<i>BABAR</i> ( <a href="#">Lees et al., 2015</a> )	$189 \pm 14$	4143.4 fixed	15.3 fixed	$1.6\sigma$
2016	LHCb $3.0 \text{ fb}^{-1}$ ( <a href="#">Aaij et al., 2017d</a> )	$4289 \pm 151$	$4146.5 \pm 4.5^{+4.6}_{-2.8}$	$83 \pm 21^{+21}_{-14}$	$8.4\sigma$
2015	D0 $10.4 \text{ fb}^{-1}$ ( <a href="#">Abazov et al., 2015</a> )	$p\bar{p} \rightarrow J/\psi\phi \dots$	$4152.5 \pm 1.7^{+6.2}_{-5.4}$	$16.3 \pm 5.6 \pm 11.4$	$5.7\sigma$ (4.7 $\sigma$ )

TABLE VI. Results related to  $J/\psi\phi$  mass structures heavier than the  $X(4140)$  peak.

Year	Experiment luminosity	$B \rightarrow J/\psi\phi K$ yield	Mass (MeV)	$X(4274\text{--}4700)$ peaks(s) Width (MeV)	Significance
2011	CDF $6.0 \text{ fb}^{-1}$ ( <a href="#">Aaltonen et al., 2017</a> )	$115 \pm 12$	$4274.4^{+8.4}_{-6.7} \pm 1.9$	$32.3^{+21.9}_{-15.3} \pm 7.6$	$3.1\sigma$
2011	LHCb $0.37 \text{ fb}^{-1}$ ( <a href="#">Aaij et al., 2012b</a> )	$346 \pm 20$	4274.4 fixed	32.3 fixed	
2013	CMS $5.2 \text{ fb}^{-1}$ ( <a href="#">Chatrchyan et al., 2014</a> )	$2480 \pm 160$	$4313.8 \pm 5.3 \pm 7.3$	$38^{+30}_{-15} \pm 16$	
2013	D0 $10.4 \text{ fb}^{-1}$ ( <a href="#">Abazov et al., 2014</a> )	$215 \pm 37$	$4328.5 \pm 12.0$	30 fixed	
2014	<i>BABAR</i> ( <a href="#">Lees et al., 2015</a> )	$189 \pm 14$	4274.4 fixed	32.3 fixed	$1.2\sigma$
2016	LHCb $3.0 \text{ fb}^{-1}$ ( <a href="#">Aaij et al., 2017d</a> )	$4289 \pm 151$	$4273.3 \pm 8.3^{+17.2}_{-3.6}$	$56 \pm 11^{+8}_{-11}$	$6.0\sigma$
			$4506 \pm 11^{+12}_{-15}$	$92 \pm 21^{+21}_{-20}$	$6.1\sigma$
			$4704 \pm 10^{+14}_{-24}$	$120 \pm 31^{+42}_{-33}$	$5.6\sigma$
2010	<i>Belle</i> ( <a href="#">Shen et al., 2010</a> )		$\gamma\gamma \rightarrow J/\psi\phi$	$4350.6^{+4.6}_{-5.1} \pm 0.7$	$13^{+18}_{-9} \pm 4$

and width  $\Gamma = 11.7^{+9.1}_{-6.2}$  MeV that is called the  $X(4140)$  ([Aaltonen et al., 2009a](#)).<sup>26</sup>

A conventional  $c\bar{c}$  charmonium state with this mass would be able to decay to a variety of open-charmed-meson pair final states via allowed fall-apart decays and have an expected width that is much higher than CDF's measured value for the  $X(4140)$ . Moreover, the observed  $J/\psi\phi$  decay mode would be OZI suppressed for charmonium-state decays and expected to have an undetectably small branching fraction. Because of these conflicts with charmonium-model-based expectations, the CDF observation triggered considerable interest. It was suggested that the  $X(4140)$  structure could be a molecular state ([Albuquerque, Bracco, and Nielsen, 2009](#); [Branz, Gutsche, and Lyubovitskij, 2009](#); [Ding, 2009b](#); [Liu and Ke, 2009](#); [Liu and Zhu, 2009](#); [Molina and Oset, 2009](#); [Wang, Liu, and Zhang, 2009](#); [Zhang and Huang, 2010](#); [X. Chen et al., 2015](#); [Karliner and Rosner, 2016a](#)), a tetraquark state ([Drenska, Faccini, and Polosa, 2009](#); [Stancu, 2010](#); [Anisovich et al., 2015](#); [Wang and Tian, 2015](#); [Lebed and Polosa, 2016](#)), a hybrid state ([Mahajan, 2009](#); [Wang, 2009](#)), or a rescattering effect ([Liu, 2009](#); [Swanson, 2015](#)).

A analysis of  $B^+ \rightarrow J/\psi\phi K^+$  decays by the LHCb Collaboration, based on a fraction of their run-I data sample ([Aaij et al., 2012b](#)), found no evidence for a narrow

$X(4140)$ -like peak and set an upper limit on its production that was in  $2.4\sigma$  tension with the CDF results ([Aaltonen et al., 2017](#)). Belle ([Brodzicka, 2009](#); [Shen, 2010](#)) (unpublished) and *BABAR* ([Lees et al., 2015](#)) searches for a narrow  $X(4140)$  state did not confirm its presence, but the limits that they set were not in serious conflict with the CDF measurements. In 2014, an  $X(4140) \rightarrow J/\psi\phi$ -like signal with mass and width values consistent with the CDF results and a statistical significance of  $5\sigma$ , shown in Fig. 35(b), was reported in  $B^+ \rightarrow J/\psi\phi K^+$  decays by the CMS Collaboration ([Chatrchyan et al., 2014](#)). Also in 2014, D0 reported the  $M(J/\psi\phi)$  distribution shown in Fig. 36(a), where there is  $3\sigma$  evidence for a narrow  $X(4140)$ -like structure, but with a mass  $4159 \pm 8$  MeV that was about 2 standard deviations higher than the CDF value ([Abazov et al., 2014](#)). In addition, D0 reported a  $4.7\sigma$  signal for prompt  $X(4140)$  production in  $E_{\text{c.m.}} = 1.96$  TeV  $p\bar{p}$  collisions as shown in Fig. 36(b) ([Abazov et al., 2015](#)). The BESIII Collaboration did not find evidence for  $X(4140) \rightarrow J/\psi\phi$  in  $e^+e^- \rightarrow \gamma X(4140)$  and set upper limits on its production cross sections at c.m. energies of 4.23, 4.26, and 4.36 GeV ([Ablikim et al., 2015a](#)).

In an unpublished update to their  $B^+ \rightarrow J/\psi\phi K^+$  analysis ([Aaltonen et al., 2017](#)), the CDF Collaboration presented  $3.1\sigma$  evidence for a second relatively narrow  $J/\psi\phi$  mass peak near  $4274 \pm 8$  MeV, an observation that has also received considerable attention in the literature ([Finazzo, Nielsen, and Liu, 2011](#); [He and Liu, 2011](#)). There are signs of a second  $J/\psi\phi$

<sup>26</sup>In the literature, this is sometimes referred to as the  $Y(4140)$ .

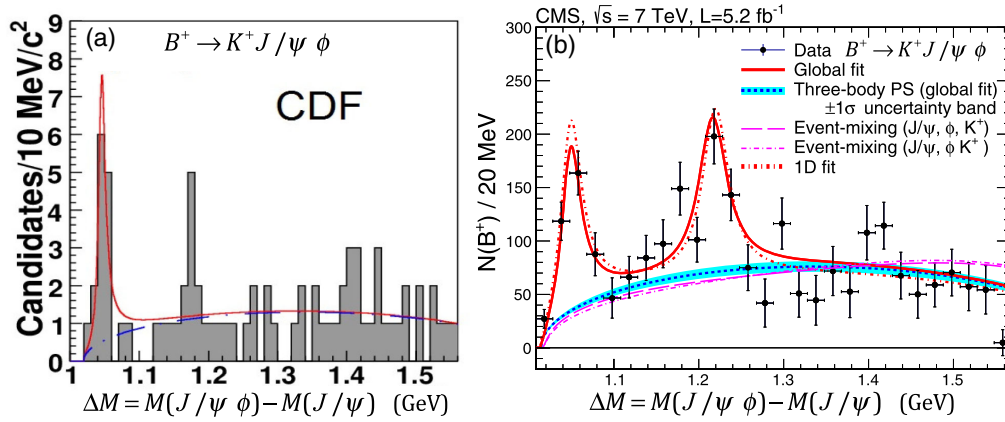


FIG. 35. (a) The  $\Delta M = M(J/\psi\phi) - M(J/\psi)$  distribution for a 58 event sample of candidate  $B^+ \rightarrow J/\psi\phi K^+$  decays from the CDF experiment. The histogram shows the data and the red curve shows the result of a fit with a BW signal shape and a three-body phase-space term to represent the nonresonant background. From [Aaltonen et al., 2009a](#). (b) The corresponding plot for a 2.5 K event sample of candidate  $B^+$  decays from the CMS experiment. Here the fit includes two BW signal shapes, one for the  $X(4140)$  and the other for the enhancement near  $\Delta M \approx 1.22$  GeV. From [Chatrchyan et al., 2014](#).

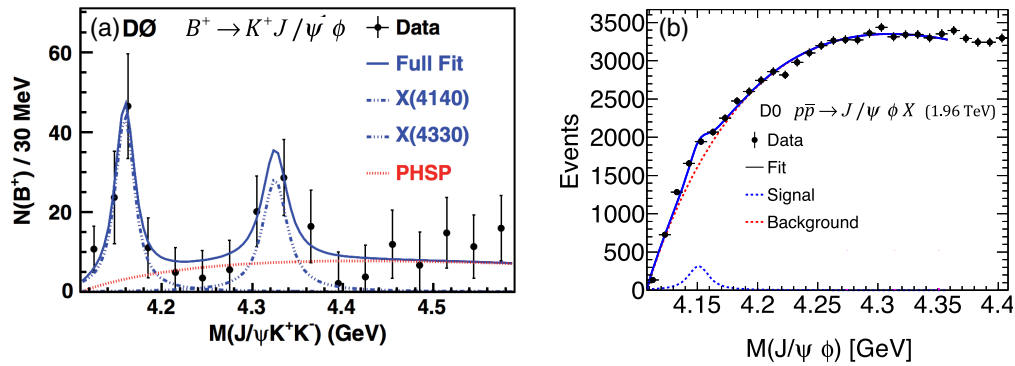


FIG. 36. (a) The  $M(J/\psi\phi)$  distribution for a 215 event sample of candidate  $B^+ \rightarrow J/\psi\phi K^+$  decays. The solid blue curve is the result of a fit with two BW signal shapes and a three-body phase-space term to represent the nonresonant background. From [Abazov et al., 2014](#). (b) The distribution of invariant masses for prompt  $J/\psi\phi$  combinations produced in inclusive  $p\bar{p} \rightarrow J/\psi\phi X$  reactions. From [Abazov et al., 2015](#).

mass peak in the CMS distribution shown in Fig. 35(b), but at a mass of  $4314 \pm 5$  MeV, which is 3.2 standard deviations higher than the CDF value; no statistical significance of this structure is reported ([Chatrchyan et al., 2014](#)). There is some hint of a second peak near 4330 MeV in the D0  $J/\psi\phi$  mass distribution shown in Fig. 36(a), but with a small,  $\sim 1.7\sigma$  significance. The Belle Collaboration saw  $3.2\sigma$  evidence for a narrow  $J/\psi\phi$  peak at  $4351 \pm 5$  MeV in two-photon collisions, which implies  $J^{PC} = 0^{++}$  or  $2^{++}$  and found no evidence for  $X(4140)$  in the same analysis ([Shen et al., 2010](#)).

### 1. The six-dimensional LHCb amplitude analysis

All the analyses mentioned had limited data sets and were based on simple  $J/\psi\phi$  mass fits, with a Breit-Wigner shape to represent the signal and an incoherent background described by an *ad hoc* functional shape (usually a three-body  $B^+ \rightarrow J/\psi\phi K^+$  phase-space distribution). While the  $M(\phi K)$  distribution in this decay process has been observed to be featureless, several resonant contributions from  $K^* \rightarrow K\phi$  excitations are expected. The first amplitude analysis of

$B^+ \rightarrow J/\psi\phi K^+$  decays that was capable of separately resolving possible  $K^{*+} \rightarrow \phi K^+$  and  $X \rightarrow J/\psi\phi$  resonances was recently reported by the LHCb Collaboration. This was based on a nearly background-free sample of  $B^+ \rightarrow J/\psi\phi K^+$  decays that was larger than that for any of the previous analyses ([Aaij et al., 2017a, 2017d](#)). In this analysis, it was found that the data across the full, six-dimensional (6D) phase space of invariant masses and decay angles spanned by the five final-state particles could not be described by a model that contains only excited kaon states that decay into  $\phi K$ ; an acceptable description of the data was obtained only when four coherent  $X \rightarrow J/\psi\phi$  peaking structures were included. The  $K^{*+}$  amplitude model determined from the analysis that included the four  $J/\psi\phi$  resonant structures is consistent with expectations based on the quark model and previous experimental  $K^{*+} \rightarrow \phi K^+$  resonance results.

Figure 37 shows the  $J/\psi\phi$  invariant mass distribution from the 4.3 K reconstructed  $B^+ \rightarrow J/\psi\phi K^+$  decays in the LHCb run-II data sample with the projected results from the 6D fit superimposed as a red histogram with error bars. There is no narrow  $J/\psi\phi$  mass peak just above the kinematic threshold as



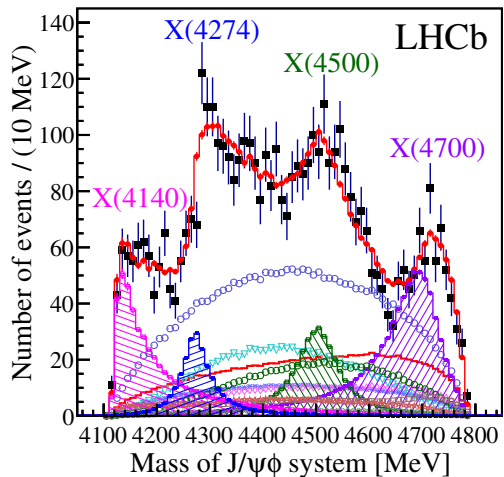


FIG. 37. The solid black squares with error bars show the distribution of  $J/\psi\phi$  invariant masses in the LHCb experiment's 4.3 K event sample of candidate  $B^+ \rightarrow J/\psi\phi K^+$  decays. The non- $B$ -decay background estimate is shown by the lower red histogram. Projection of the six-dimensional amplitude fit with the four  $X \rightarrow J/\psi\phi$  resonance terms shown as hatched histograms plus contributions from a  $X \rightarrow J/\psi\phi$  nonresonant amplitude (open blue circles) and  $K^{*+} \rightarrow \phi K^+$  excitations is shown by the solid-line red histogram with error bars. From Aaij *et al.*, 2017a, 2017d.

first reported by CDF. Instead, a broad enhancement with a mass  $M = 4146.5 \pm 4.5_{-2.8}^{+4.6}$  MeV that is consistent with the  $X(4140)$  values from CDF and CMS, but with a width  $\Gamma = 83 \pm 21_{-14}^{+21}$  MeV that is substantially broader than the CDF value<sup>27</sup> is observed with high ( $8.4\sigma$ ) significance. The  $J^{PC}$  quantum numbers of this structure are determined from the LHCb fit to be  $1^{++}$ ; other hypotheses are ruled out with a significance of  $5.7\sigma$  or more. The  $1^{++}$  quantum number assignment has an important impact on possible interpretations for the  $X(4140)$ , in particular, it rules out the  $0^{++}$  or  $2^{++}$   $D_s^{*+}D_s^{*-}$  molecular models proposed by Albuquerque, Bracco, and Nielsen (2009), Branz, Gutsche, and Lyubovitskij (2009), Ding (2009b), Liu and Zhu (2009), Molina and Oset (2009), Zhang and Huang (2010), and X. Chen *et al.* (2015). It was suggested that a below- $J/\psi\phi$  threshold  $D_s^{\pm}D_s^{*\mp}$  kinematically induced cusp (Swanson, 2015; Karliner and Rosner, 2016a) may be responsible for the observed  $X(4140)$  structure [see Appendix D in Aaij *et al.* (2017a)], although the cusp model used in this analysis is theoretically controversial as discussed in Sec. II.B.4.

The PDG's 2017 update to Patrignani *et al.* (2016) lists an average of all published measurements (Aaltonen *et al.*, 2009a; Abazov *et al.*, 2014, 2015; Chatrchyan *et al.*, 2014) of the  $X(4140)$  parameters as its mass  $4146.8 \pm 2.5$  MeV and width  $19_{-7}^{+8}$  MeV. The evolution of the  $Z(4430)^+$  mass and width determination (Choi *et al.*, 2008; Mizuk *et al.*, 2009; Chilikin *et al.*, 2013), discussed in Sec. VI.A.4, provides the valuable lesson that a one-dimensional fit to a mass

<sup>27</sup>This should be considered “tension,” rather than disagreement since the CDF and LHCb results differ by  $2.7\sigma$ .

distribution of a resonance peak, together with an *ad hoc* assumption about the background shape and its incoherence, is prone to yield biased mass and width results and underestimated systematic errors. Therefore, in Table I we list mass and width values that are based only on the results from the full amplitude analysis (Aaij *et al.*, 2017d), since this is the only one that resolved various background contributions and added them coherently to the signal amplitude.

The analysis also established the existence of the  $X(4274)$  structure with  $M = 4273.3 \pm 8.3_{-3.6}^{+17.2}$  MeV at the  $6\sigma$  significance level and with quantum numbers that were determined to be  $1^{++}$  at the  $5.8\sigma$  level. No proposed molecular bound state or cusp model can account for these  $X(4274)$   $J^{PC}$  values. A hybrid charmonium state in this mass region would have  $J^{PC} = 1^{-+}$  (Mahajan, 2009; Wang, 2009). Most models that interpret the  $X(4140)$  as a tetraquark state predicted that the  $J^{PC}$  values of the next higher-mass state to be different from  $1^{++}$  (Drenska, Faccini, and Polosa, 2009; Anisovich *et al.*, 2015; Wang and Tian, 2015; Lebed and Polosa, 2016; Maiani, Polosa, and Riquer, 2016). An exception is a tetraquark model implemented by Stancu (2010) that not only correctly assigned  $1^{++}$  to the  $X(4140)$ , but also predicted a second  $1^{++}$  state at a mass that is not much higher than that of the  $X(4274)$ . A lattice QCD calculation with diquark operators found no evidence for a  $1^{++}$  tetraquark below 4.2 GeV (Padmanath, Lang, and Prelovsek, 2015). However, given that not all dynamical effects were simulated, this calculation probably does not rule them out.

In addition, the LHCb analysis, which was the first high-sensitivity investigation of the high  $J/\psi\phi$  mass region, uncovered three significant  $0^{++}$  contributions: a  $0^{++}$  non-resonant term plus two, previously unseen  $0^{++}$  resonances, the  $X(4500)$  (with  $6.1\sigma$  significance) and the  $X(4700)$  (with  $5.6\sigma$  significance). The  $0^{++}$  quantum numbers of these states are established with significances of more than  $4\sigma$ . Wang, Liu, and Zhang (2009) predicted a virtual  $D_s^{*+}D_s^{*-}$  state at  $4.48 \pm 0.17$  GeV.

None of the  $J/\psi\phi$  structures observed in  $B$  decays are consistent with the state seen in two-photon collisions by the Belle Collaboration (Shen *et al.*, 2010).

## 2. Charmonium assignments for the $J/\psi\phi$ states?

The main reason that the  $X(4140)$  attracted a lot of interest was the narrow width reported by the early measurements. However, the widths determined from the LHCb analysis are larger, ranging between 56 and 120 MeV, depending on the  $J/\psi\phi$  peak, and these cannot *a priori* be considered to be too narrow to be charmonium states. The  $X(4140)$  and  $X(4274)$  both have quantum numbers that match the  $\chi_{c1}(3P)$  state, and their masses are in the range of potential model predictions for this state (Godfrey and Isgur, 1985; Barnes, Godfrey, and Swanson, 2005; Li, Meng, and Chao, 2009; Chen, 2016; Lu and Dong, 2016; Ortega *et al.*, 2016).

The dominant  $\chi_{c1}(3P)$  decay modes are expected to be to  $D\bar{D}^*$ ,  $D^*\bar{D}^*$ , and  $D_s\bar{D}_s^*$ , final states with total width predictions that range from low values near 30 MeV (Barnes, Godfrey, and Swanson, 2005; Ortega *et al.*, 2016) to values of 58 MeV (Chen, 2016). Given the considerable theoretical uncertainties of these predictions, either the  $X(4140)$  or the

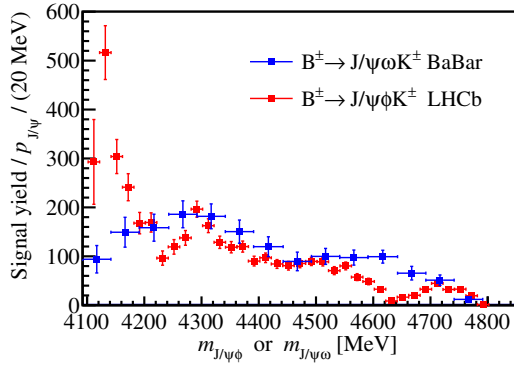


FIG. 38. The efficiency-corrected and background-subtracted  $J/\psi\phi$  invariant mass spectrum for  $B^+ \rightarrow J/\psi\phi K^+$  decays (red light points) from LHCb (Aaij *et al.*, 2017a, 2017d) and the  $J/\psi\omega$  mass spectrum for  $B^+ \rightarrow J/\psi\phi K^+$  decays (blue dark points) from BABAR (Lees *et al.*, 2015), where the signal yields (in arbitrary units) have been divided by the  $J/\psi$  momentum in the  $X$  rest frame to account for phase-space differences. The two distributions are normalized to have equal areas for masses above the  $J/\psi\phi$  threshold.

$X(4274)$  can be considered as a candidate for the  $\chi_{c1}(3P)$  state. The  $X(4500)$  and the  $X(4700)$  have been suggested as candidates for the  $\chi_{c0}(4P)$  and  $\chi_{c0}(5P)$  states, since they lie in the predicted mass and width ranges for these states (Lu and Dong, 2016; Ortega *et al.*, 2016). These higher charmonium states would have a large number of allowed decay modes to open charm mesons but, unfortunately, there are no published measurements of mass spectra in the relevant mass ranges for  $B \rightarrow D_{(s)}^{(*)}\bar{D}_{(s)}^* K$  decays.

Naively, one expects the couplings of the  $\chi_{cJ}(nP)$  states to  $J/\psi\phi$  and to  $J/\psi\omega$  to be very similar, with the rate for the latter being enhanced by the larger phase space that is available for the lighter states and the relative ease of producing light  $u\bar{u}$  or  $d\bar{d}$  quark pairs that comprise the  $\omega$  from the vacuum compared to that for more massive  $s\bar{s}$  pairs that comprise the  $\phi$ . The  $J/\psi\omega$  mass spectrum in  $B \rightarrow J/\psi\omega K$  decays measured by the BABAR Collaboration (Lees *et al.*, 2015) does not show any structures resembling the  $J/\psi\phi$  mass peaks, as illustrated in Fig. 38, which argues against a charmonium interpretation for any state among the  $X(4140)$ ,  $X(4274)$ ,  $X(4500)$ , and  $X(4700)$ .

### E. $X^*(3860)$ , $X(3940)$ , and $X(4160)$

As discussed in Sec. III, the  $X(3940)$  was first seen by Belle (Abe *et al.*, 2007) as an unexpected peak in the distribution of masses  $[M_{\text{recoil}}(J/\psi)]$  recoiling against a  $J/\psi$  in inclusive  $e^+e^- \rightarrow J/\psi X$  annihilation at  $E_{\text{c.m.}} \approx 10.6$  GeV shown in Fig. 14(a). In this figure, there are four distinct peaks: the lower three are due to the exclusive processes  $e^+e^- \rightarrow J/\psi\eta_c$ ,  $e^+e^- \rightarrow J/\psi\chi_{c0}$ , and  $e^+e^- \rightarrow J/\psi\eta'_c$ . The fourth peak, near 3940 MeV, cannot be associated with any known or expected charmonium state and has been named the  $X(3940)$ . The curve shows results of a fit that includes four BW line shapes, three for the established  $\eta_c$ ,  $\chi_{c0}$ , and  $\eta_c(2S)$  charmonium states plus a fourth one to accommodate the unexpected peak near

3940 MeV. From the fit, the mass of the fourth state was found to be  $M = 3943 \pm 6$  MeV, and a limit on the total width of  $\Gamma \leq 52$  MeV was established.

Belle did subsequent studies of the exclusive processes  $e^+e^- \rightarrow J/\psi D^{(*)}\bar{D}^{(*)}$  decays in the same energy region, where to compensate for the low detection efficiency for  $D$  and  $D^*$  mesons a partial reconstruction technique was used that required the reconstruction of the  $J/\psi$  and only one  $D$  or  $D^*$  meson, and the presence of the undetected  $\bar{D}$  or  $\bar{D}^*$  was inferred from energy-momentum conservation. With this technique, Belle found a strong signal for  $X(3940) \rightarrow D\bar{D}^*$  (Pakhlov *et al.*, 2008) plus two other states: the  $X^*(3860) \rightarrow D\bar{D}$  (Chilikin *et al.*, 2017) and  $Y(4160) \rightarrow D^*\bar{D}^*$  (Pakhlov *et al.*, 2008). Although these three states have not been confirmed by any other experiment, the significance of the Belle observations in all three cases is above the  $5\sigma$  level and we briefly discuss them here.

### 1. $X^*(3860) \rightarrow D\bar{D}$ , an alternative $\chi_{c0}(2P)$ candidate?

Figure 39(a) shows the distribution of masses recoiling against a detected  $J/\psi$  and  $D$  meson in  $e^+e^- \rightarrow J/\psi D + X$  annihilation events collected in Belle at c.m. energies at and near 10.58 GeV. There two peaks are apparent, one centered at  $M_{\text{recoil}}(J/\psi D) = m_D$ , corresponding to exclusive  $e^+e^- \rightarrow J/\psi D\bar{D}$  events and the other centered at  $m_{D^*}$ , corresponding to exclusive  $e^+e^- \rightarrow J/\psi D\bar{D}^*$  events (Chilikin *et al.*, 2017). Figure 39(b) shows the  $D\bar{D}$  invariant mass distribution for the pairs in the exclusive  $J/\psi D\bar{D}$  event sample, where there is a strong peaking at small masses. Fits to the data with a variety of nonresonant-model amplitudes were unable to describe the data over the four-dimensional phase space spanned by the final-state particles. For each choice of nonresonant amplitude, an additional, coherent BW amplitude was needed. The mass and width of the BW resonance determined from the best fit to the data [shown in Fig. 39(b) as a solid blue histogram] are  $M = 3862_{-32-13}^{+26+40}$  MeV and  $\Gamma = 201_{-67-82}^{+154+88}$  MeV. The  $J^{PC} = 0^{++}$  quantum number hypothesis gives the best fit to the data and was favored over the  $2^{++}$  hypothesis by  $2.5\sigma$ . The mass,  $0^{++}$  quantum numbers and strong  $D\bar{D}$  decay mode of the  $X^*(3860)$  all match well to expectations for the  $\chi_{c0}(2P)$  charmonium state, making it a superior candidate for this assignment than the  $X(3915)$ .

### 2. $X(3940) \rightarrow D\bar{D}^*$

Figure 40(a) shows the  $D\bar{D}^*$  invariant mass distribution for  $e^+e^- \rightarrow J/\psi DX$  annihilation events where  $M_{\text{recoil}}(J/\psi D)$  is in the  $\bar{D}^*$  peak (Pakhlov *et al.*, 2008). Here the hatched histogram is the non- $J/\psi$  and/or non- $D$ -meson background determined from  $J/\psi$  and  $D$ -meson mass sideband events. The inset shows the background-subtracted  $M(D\bar{D}^*)$  distribution, which is dominated by a near-threshold peak. A fit of a BW resonance to these data, shown as a solid curve in the figure, returns a mass and width of  $M = 3942 \pm 9$  MeV and  $\Gamma = 37_{-17}^{+27}$  MeV, values that are consistent with results for the  $X(3940)$  determined from the inclusive  $e^+e^- \rightarrow J/\psi X$  missing mass distribution (Abe *et al.*, 2007).

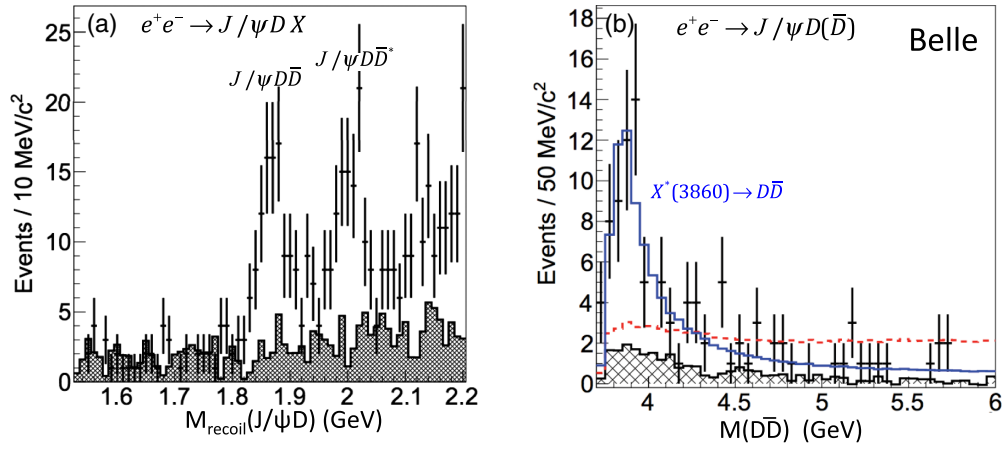


FIG. 39. (a) The distribution of masses recoiling from a reconstructed  $J/\psi$  and  $D$  meson in  $e^+e^- \rightarrow J/\psi DX$  annihilation at and near  $E_{c.m.} = 10.58$  GeV. The two peaks correspond to exclusive  $e^+e^- \rightarrow J/\psi D\bar{D}$  and  $J/\psi D\bar{D}^*$  events. The shaded histogram indicates the background level determined from the  $J/\psi$  and  $D$  mass sidebands. (b) The  $D\bar{D}$  invariant mass distribution for the exclusive  $e^+e^- \rightarrow J/\psi D\bar{D}$  events. The solid blue histogram is the result of a fit with a BW resonant amplitude plus a coherent nonresonant background. The red dashed histogram is the fit result when only a nonresonant amplitude is included. From [Chilikin et al., 2017](#).

### 3. $X(4160) \rightarrow D^* \bar{D}^*$

Figure 40(b) shows the  $D^* \bar{D}^*$  invariant mass distribution for  $e^+e^- \rightarrow J/\psi D^* X$  annihilation events where  $M_{\text{recoil}}(J/\psi D^*)$  is in the  $\bar{D}^*$  mass region. Here the mass-sideband-estimated non- $J/\psi$  and/or non- $D^*$ -meson backgrounds are very small. The curve shows the result of a fit to a single-BW resonance term plus a phase-space-like background. The fitted mass and width for this peak, which is called the  $X(4160)$ , is  $M = 4156 \pm 27$  MeV and  $\Gamma = 139_{-65}^{+113}$  MeV ([Pakhlov et al., 2008](#)).

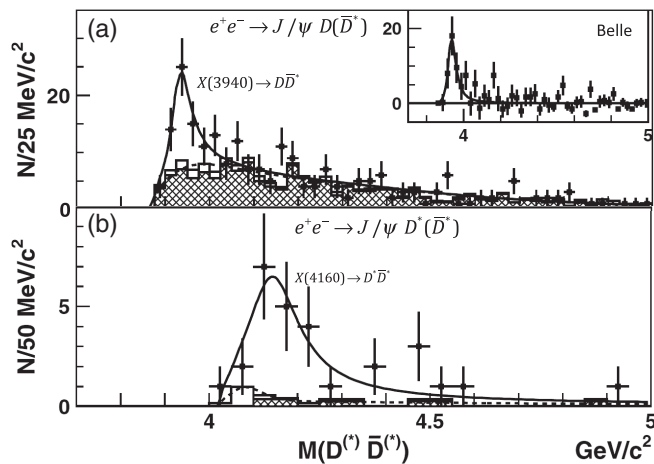


FIG. 40. (a) The  $M(D\bar{D}^*)$  distribution for  $e^+e^- \rightarrow J/\psi D\bar{D}^*$  events where the  $J/\psi$  and  $D$  meson are reconstructed and the four-momentum of the undetected  $\bar{D}^*$  meson is inferred from energy-momentum conservation ([Pakhlov et al., 2008](#)). The hatched histogram is the non- $J/\psi$  and/or non- $D$  meson background determined from the  $J/\psi$  and  $D$ -meson mass sidebands. The curve shows the results of the fit to the  $X(3940)$  resonance described in the text. (b) The  $M(D^* \bar{D}^*)$  distribution for exclusive  $e^+e^- \rightarrow J/\psi D^* \bar{D}^*$  events. The curve is the result of the fit for the  $X(4160)$ . From [Abe et al., 2007](#).

### 4. Discussion

Neither the  $X(3940)$  nor the  $X(4160)$  show up in the  $D\bar{D}$  invariant mass distribution for exclusive  $e^+e^- \rightarrow J/\psi D\bar{D}$  at the same energies. Also, as mentioned, the absence of signals for any of the known nonzero spin charmonium states in the inclusive spectrum of Fig. 14(a) provides circumstantial evidence for  $J=0$  assignments for the  $X(3940)$  and  $X(4160)$ . If the  $X(3940)$  has  $J=0$ , its  $D\bar{D}^*$  decay mode ensures that its  $J^{PC}$  quantum numbers are  $0^{-+}$ . If the  $X(4160)$  has  $J=0$  the absence of any sign of  $X(4160) \rightarrow D\bar{D}$  decay supports a  $0^{-+}$  assignment for this state as well. In both cases, the measured masses are far below expectations for the only available unassigned  $0^{-+}$  charmonium levels: the  $\eta_c(3S)$  and  $\eta_c(4S)$ . Since there are no strong reasons to doubt the generally accepted identifications of the  $\psi(4040)$  peak seen in the inclusive cross section for  $e^+e^- \rightarrow \text{hadrons}$  as the  $\psi(3S)$  and the  $\psi(4415)$  peak as the  $\psi(4S)$  ([Bai et al., 2002](#)), these assignments would imply hyperfine  $n_r^3S - n_r^1S$  mass splittings that increase from the measured value of  $47.2 \pm 1.2$  MeV for  $n_r = 2$  ([Patrignani et al., 2016](#)) to  $\sim 100$  MeV for  $n_r = 3$  and  $\sim 250$  MeV for  $n_r = 4$  ([Chao, 2008](#)). This pattern conflicts with expectations from potential models, where hyperfine splittings are proportional to the square of the  $c\bar{c}$  radial wave function at  $r=0$  and decrease with increasing  $n_r$  ([Godfrey and Isgur, 1985](#)); this is the main reason that the  $X(3940)$  and  $X(4160)$  are considered candidates for nonstandard charmoniumlike hadrons.

## VI. CHARGED NONSTANDARD HADRON CANDIDATES

Distinguishing neutral candidates for nonstandard mesons that decay into quarkonia states from excitations of conventional  $Q\bar{Q}$  states is a complex task that can be fraught with ambiguities. In contrast, charged quarkoniumlike candidates are explicitly nonstandard and the only outstanding issues concern the nature of their internal dynamics. Candidates for

both charmoniumlike and bottomoniumlike charged states are discussed in this section.

### A. $Z(4430)^+$ and similar structures in $B$ decays

#### 1. The $Z(4430)^+ \rightarrow \psi'\pi^+$ in $B \rightarrow \psi'\pi^+K$ decays

The first established candidate for a charged charmoniumlike state dates back to 2007, when the  $Z(4430)^+$  was observed by the Belle Collaboration as a peak in the invariant mass of the  $\psi'\pi^+$  system in  $\bar{B} \rightarrow \psi'\pi^+K$  decays (Choi *et al.*, 2008) ( $K = K_s^0$  or  $K^-$ ). The BABAR experiment, with a data sample containing a similar number of  $B \rightarrow \psi'\pi^+K$  decay events, did not find strong evidence for a  $Z(4430)^+$  signal that could not be attributed to reflections from various kaon excitations decaying to  $K\pi^+$  that were analyzed in a model-independent way (Aubert *et al.*, 2009c). However, the BABAR results were not sensitive enough to directly contradict the Belle observation. Subsequently, the Belle Collaboration reanalyzed their data with an amplitude model that combined coherent  $K\pi^+$  and  $\psi'\pi^+$  resonant contributions to fit to the data distribution across a two-dimensional  $[M^2(K\pi) \text{ vs } M^2(\psi'\pi)]$  Dalitz plane (Mizuk *et al.*, 2009). This was later refined to include two additional kinematic variables that were angles that describe  $\psi' \rightarrow \ell^+\ell^-$  decays (Chilikin *et al.*, 2013). Both analyses reaffirmed Belle's original claim for a significant  $Z(4430)^+$  signal, albeit with a substantially larger mass and total width than the values given in the initial Belle report, which was based on a naive fit to the  $\psi'\pi^+$  mass distribution. The latter, four-dimensional amplitude analyses favored a  $J^P = 1^+$  spin parity of the  $Z(4430)^+$  over other possible  $J^P$  assignments at the  $3.4\sigma$  level.

The existence of the  $Z(4430)^+$  structure was independently confirmed in 2014 (with  $13.9\sigma$  significance) by the LHCb experiment (Aaij *et al.*, 2014b), which was based on a four-dimensional analysis of a  $\bar{B}^0 \rightarrow \psi'\pi^+K^-$  event sample that was an order of magnitude larger than those used in the Belle and BABAR experiments (see Fig. 41, upper panel). The LHCb amplitude analysis yielded results that were consistent with the Belle determination, including the confirmation of the  $J^P = 1^+$  assignment, but in this case at the  $9.7\sigma$  level. The average of the Belle and LHCb mass and width values are (Patrignani *et al.*, 2016)

$$\begin{aligned} M(Z(4430)) &= 4478_{-81}^{+15} \text{ MeV}, \\ \Gamma(Z(4430)) &= 181 \pm 31 \text{ MeV}. \end{aligned} \quad (15)$$

The large event sample enabled the LHCb group to measure the  $1^+$   $Z(4430)^+$  amplitude's dependence on  $\psi'\pi^+$  mass independently of any assumptions about the resonance line shape. The resulting "Argand diagram" of the real versus imaginary parts of the  $1^+$  amplitude, shown in Fig. 42 (left), shows a nearly circular, counterclockwise motion with an abrupt change in the amplitude phase at the peak of its magnitude that is characteristic of a BW resonance amplitude. This diagram rules out an interpretation of the  $Z(4430)$  peak as being due to the effects of a rescattering process proposed by Pakhlov and Uglov (2015) that predicted a clockwise phase motion. Since other rescattering mechanisms or

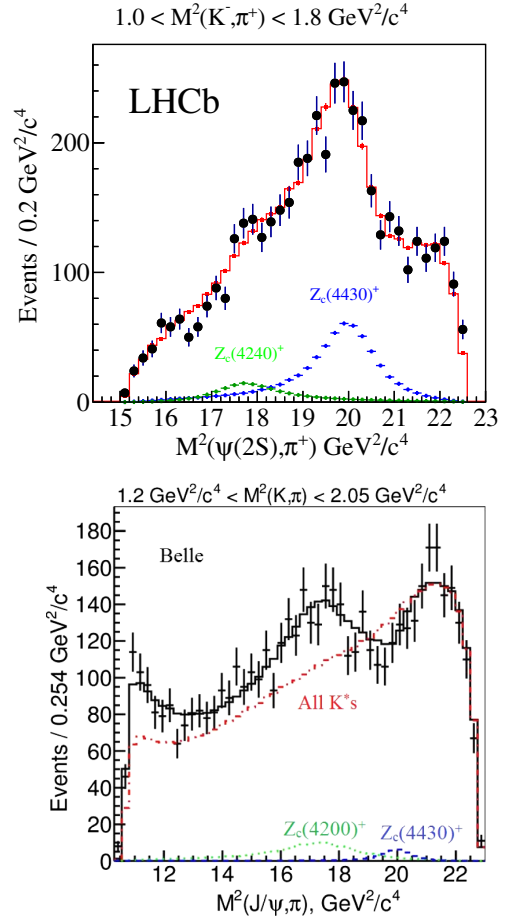


FIG. 41. The points with errors show distributions of (upper)  $M^2(\psi'\pi^+)$  in  $\bar{B}^0 \rightarrow \psi'\pi^+K^-$  decays from LHCb [from Aaij *et al.* (2014b)] and (lower)  $M^2(J/\psi\pi^+)$  in  $\bar{B}^0 \rightarrow J/\psi\pi^+K^-$  from Belle [from Chilikin *et al.* (2014)]. Here only events with  $K^-\pi^+$  invariant masses that are between the  $K^*(892)^0$  and  $K_2^*(1430)^0$  resonances are included in order to suppress contributions from the  $K\pi$  channel. Projections of four-dimensional amplitude fits that include coherent contributions from kaon excitations and two  $Z^+$  terms are superimposed as solid line histograms. The individual  $Z^+$  terms are shown as blue and green points; the dashed red curve in the Belle plot shows the projection of all the  $K^-\pi^+$  terms combined.

coupled-channel cusps could produce a counterclockwise phase motion similar to that of a BW resonance, higher statistics studies of the Argand diagram are needed to probe the amplitude dependence on mass at a level of detail that is fine enough to distinguish a resonance pole from other types of meson-meson interactions.

The LHCb Collaboration also performed an analysis of their  $\bar{B}^0 \rightarrow \psi'\pi^+K^-$  events using a  $K^-\pi^+$  model-independent approach (Aaij *et al.*, 2015b) similar to the one that was earlier performed by the BABAR Collaboration (Aubert *et al.*, 2009c). This approach yielded conclusive results that demonstrate the requirement for non- $K\pi$  contributions to  $\bar{B}^0 \rightarrow \psi'\pi^+K^-$  decays at the  $8\sigma$  level, as shown in Fig. 43. While this approach demonstrates the need for contributions from a non- $K\pi$  source in the  $Z(4430)^+$  mass region, it does not provide any independent way to extract any of the characteristics of

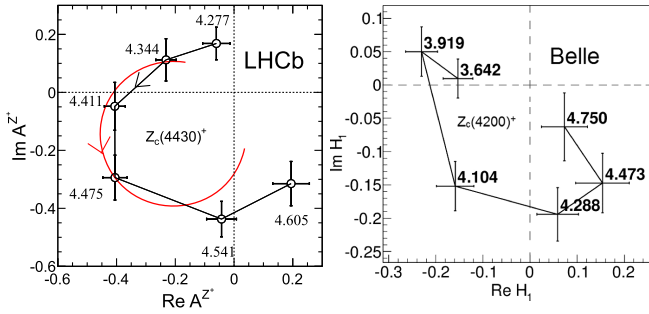


FIG. 42. Fitted values of the real and imaginary parts of the amplitude for (left)  $Z(4430)^+ \rightarrow \psi'\pi^+$  signal [from Aaij *et al.* (2014b)] and (right)  $Z(4200)^+ \rightarrow J/\psi\pi^+$  signal [from Chilikin *et al.* (2014)], for six  $M^2(\psi, \pi^+)$  bins of equal width that span the resonance. The solid red curve in the LHCb plot shows the pattern expected for a Breit-Wigner resonance amplitude. Units are arbitrary.

these contributions; for this, an amplitude analysis approach is necessary.

## 2. The $Z(4200)^+ \rightarrow J/\psi\pi^+$ in $\bar{B}^0 \rightarrow J/\psi\pi^+K^-$ decays

The Belle Collaboration performed an amplitude analysis of  $\bar{B}^0 \rightarrow J/\psi\pi^+K^-$  decays (Chilikin *et al.*, 2014) and found that in this channel too, the data could not be well described solely with contributions from the  $K\pi$  channel. A satisfactory fit was obtained only after contributions from two  $J/\psi\pi^+$  resonances were included: one corresponding to a very broad  $1^+$   $Z(4200)^+$  state with width  $\Gamma = 370 \pm 70_{-132}^{+70}$  MeV, mass  $4196_{-29}^{+31} +_{-13}^{+17}$  MeV, and a significance of  $6.2\sigma$ , and the second corresponding to  $J/\psi\pi$  decay mode of the  $Z(4430)$ . The analysis showed that the  $Z(4200)$  interferes destructively with the  $Z(4430)^+ \rightarrow J/\psi\pi^+$  amplitude, producing a dip in the  $M^2(J/\psi\pi^+)$  distribution near the  $Z(4430)$  peak mass, as shown in Fig. 41 (lower panel). In the analysis, the mass and width of the  $Z(4430) \rightarrow J/\psi\pi^+$  BW amplitude were fixed at the values determined from the  $\psi'\pi^+$  analysis. The statistical significance (not including systematic errors) of the  $Z(4430) \rightarrow J/\psi\pi^+$  amplitude was determined to be  $5.1\sigma$ , and the magnitude of the  $Z(4430) \rightarrow J/\psi\pi$  term was found to be much smaller than that for  $Z(4430) \rightarrow \psi'\pi$  in spite of the larger available phase space. The  $Z(4200)^+$  state awaits independent confirmation, although some indication for it in  $\psi(2S)\pi^+$  decays may have been seen in the LHCb  $B \rightarrow \psi'\pi K$  analysis (Aaij *et al.*, 2014b), where they reported evidence for a state in this mass region with either  $0^-$  or  $1^+$  quantum numbers that is shown by the green points in Fig. 41 (upper panel).<sup>28</sup>

The Belle Collaboration presented Argand diagrams for the  $J^P = 1^+$   $J/\psi\pi^+$  amplitude for two helicity amplitudes. One of them, shown in Fig. 42 (right panel), displays a nearly

<sup>28</sup>Using a  $0^-$  hypothesis, the LHCb obtained a mass of  $4239 \pm 18_{-10}^{+45}$  MeV and a width of  $220 \pm 47_{-74}^{+108}$  MeV, which are consistent with the Belle results but cannot be averaged with them since they are obtained using different  $J^P$  assignments. For the  $1^+$  hypothesis, LHCb reported only a width  $660 \pm 150$  MeV and that without a systematic uncertainty.

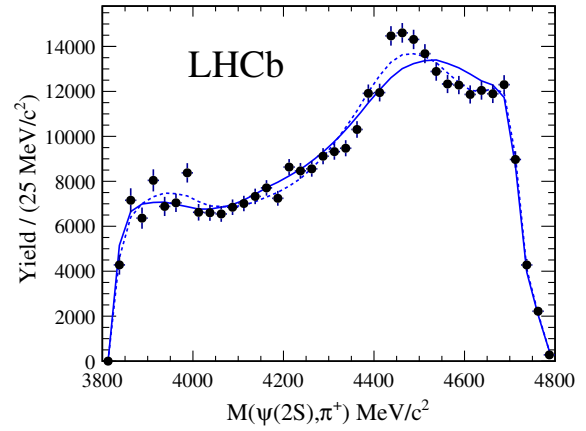


FIG. 43. The dots with error bars show background-subtracted and efficiency-corrected  $M(\psi'\pi^+)$  distribution for  $\bar{B}^0 \rightarrow \psi'\pi^+K^-$  events. The solid (dashed) blue lines correspond to contributions from the  $K^-\pi^+$  channel for a maximum-allowed angular momentum of  $J_{\max} = 2$  ( $J_{\max} = 3$ ). Since the lightest known  $J = 3$  resonance, the  $K_3^-(1780)$ , is already beyond the kinematically allowed  $K\pi$  mass limit for  $\bar{B} \rightarrow \psi'\pi K$  decay, no plausible contribution from the  $K\pi$  channel can account for the shape of the  $M(\psi'\pi)$  distribution in the  $Z(4430)^+$  mass region. From Aaij *et al.*, 2015b.

circular phase motion that is consistent with expectations for a BW resonance amplitude.

## 3. Charged $\chi_{c1}\pi^+$ resonances in $\bar{B}^0 \rightarrow \chi_{c1}\pi^+K^-$ decays

The Belle Collaboration also reported evidence for charged  $\chi_{c1}\pi^+$  resonances in a two-dimensional [ $M^2(K\pi)$  vs  $M^2(\chi_{c1}\pi)$ ] Dalitz plot analysis of  $\bar{B}^0 \rightarrow \chi_{c1}\pi^+K^-$  decays. The data could not be fitted with resonances in the  $K\pi$  channel only and was best described when two  $\chi_{c1}\pi^+$  resonances, the

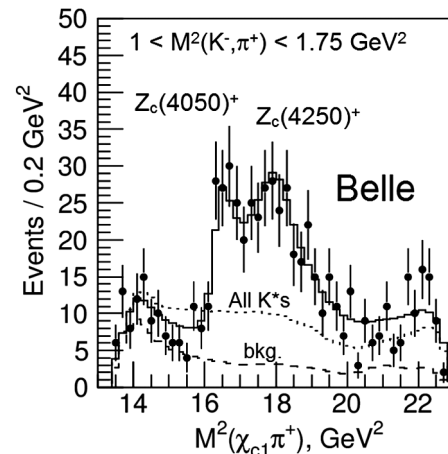


FIG. 44. The points with error bars show the  $M^2(\chi_{c1}\pi^+)$  distribution in  $\bar{B}^0 \rightarrow \chi_{c1}\pi^+K^-$  decays. The projection of a two-dimensional amplitude fit that included kaon excitations and two  $Z^+$  terms are superimposed as a solid line histogram. The dotted line corresponds to all  $K^-\pi^+$  terms combined and the non- $B$  and/or non- $\chi_{c1}$  background contribution is shown by the dashed line. From Mizuk *et al.*, 2008.

$Z(4050)^+$  and  $Z(4250)^+$ , were included, as shown in Fig. 44 (Mizuk *et al.*, 2008). *BABAR* saw an enhancement in the same mass region, but could account for it with reflections from  $K\pi^+$  resonances analyzed with the model-independent method (Lees *et al.*, 2012a); their results neither confirmed nor contradicted the Belle results. These two candidate  $\chi_{c1}\pi^+$  resonant states still await independent confirmation and a complete amplitude analysis that spans all six dimensions of the decay phase space and determines their quantum numbers.

#### 4. Discussion

The neutral  $X(3872)$ ,  $X(3915)$ , and  $Y(4260)$  charmonium-like states discussed in Sec. V showed up as distinct, relatively narrow peaks on a small background. In these cases, fitting the peaks with simple BW line shapes and ignoring the effects of possible signal interference with a coherent components of the nonresonant backgrounds were reasonable approximations. However, for the charged charmonium states discussed in this section, this approximation is no longer valid. Here, since the states are broad and contributions from coherent nonresonant processes are substantial, interference effects distort the signal line shape to such an extent that they no longer resemble that of a standard BW resonance peak.

This is illustrated for the case of the LHCb group's  $Z(4430)^+ \rightarrow \psi'\pi^+$  analysis (Aaij *et al.*, 2014b) in Fig. 45, where the black data points show the  $M^2(\psi'\pi^+)$  distribution for all of their selected  $\bar{B}^0 \rightarrow \psi'\pi^+K^-$  events (with no  $K\pi$  mass selection). The solid red histogram shows the results of the final LHCb four-dimensional fit that included a  $Z(4430)^+$  amplitude and the upper blue points show that fit's results with all the terms involving the  $Z(4430)^+ \rightarrow \psi'\pi^+$  removed. The difference between the red histogram and the upper blue points is the total  $Z^+$  contribution to the fit, including effects of interference with amplitudes in the  $K\pi$  channel. The shape of the total  $Z^+$  contribution is much different than that of the

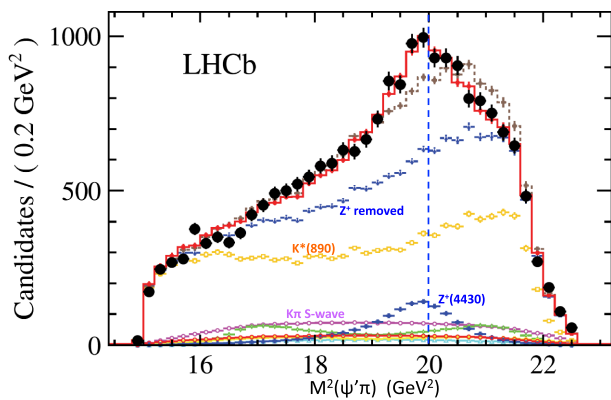


FIG. 45. The black points show the  $M^2(\psi'\pi^+)$  distribution for all of the LHCb  $\bar{B}^0 \rightarrow \psi'\pi^+K^-$  events. The solid red histogram is the projection of the four-dimensional fit that includes the  $Z(4430)^+$  amplitude and the dashed brown histogram shows the best fit that was found with no  $\psi'\pi^+$  resonances. Contributions from individual fit components are shown, with the dominant ones labeled. The upper blue points show the final fit results with the  $Z^+$  terms removed. The vertical dashed blue line indicates the fitted  $Z^+$  resonance mass value. Adapted from Aaij *et al.*, 2014b.

$Z^+$  term alone, shown as the lower blue points, because of strong interference effects that are constructive on the low-mass side of the  $Z^+$  resonance and switch to destructive at higher masses, reflecting the abrupt phase change that occurs at the peak of a BW resonance amplitude. The Belle group's original  $Z(4430)^+$  results were based on a naive BW line-shape fit to the visible peak, which corresponds only to the lower lobe of the actual pattern. As a result, they reported low values for the mass and width (Choi *et al.*, 2008).

While the presence of coherent nonresonant processes complicates the extraction of resonance signals, it provides the possibility of measuring the signal amplitude's phase motion across the resonance (see Fig. 42), thereby providing valuable information that would otherwise be inaccessible.

#### B. Charged $Z_b^+$ and $Z_c^+$ states produced in $e^+e^-$ processes

##### 1. The $Z_b$ charged bottomoniumlike mesons

The large  $Y(4260) \rightarrow \pi^+\pi^-J/\psi$  signal discovered in the charmonium mass region by *BABAR* motivated a Belle search for similar behavior in the bottomonium system (Hou, 2006). This uncovered anomalously large  $\pi^+\pi^-\Upsilon(n_rS)$  ( $n_r = 1, 2, 3$ ) production rates that peak around  $E_{c.m.}(e^+e^-) = 10.89$  GeV as shown in the upper three panels of Fig. 46 (Santel *et al.*, 2016). This peak energy is close to a peak in the  $e^+e^- \rightarrow b\bar{b}$  cross section near  $E_{c.m.} \approx 10.87$  GeV, shown in the lower

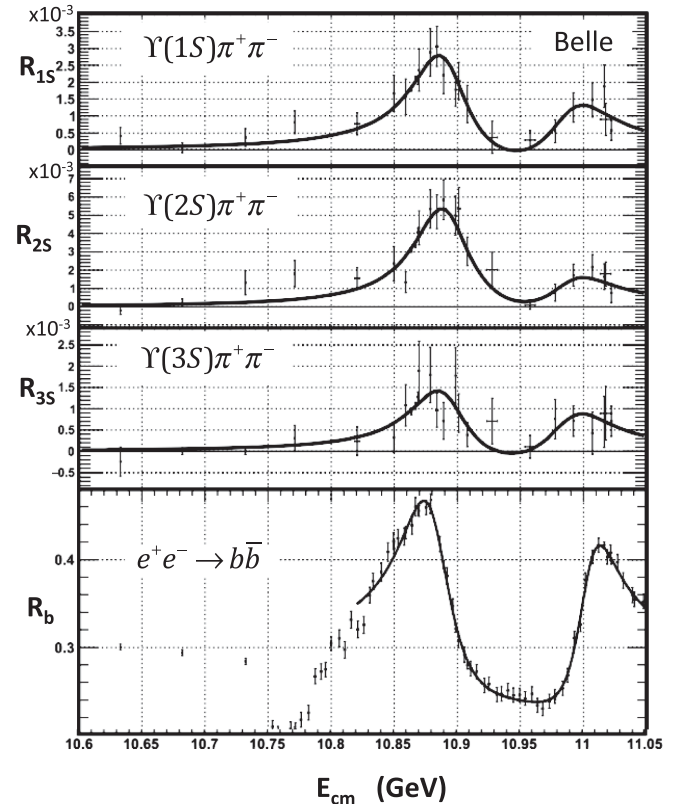


FIG. 46. Cross sections for  $e^+e^- \rightarrow \pi^+\pi^-\Upsilon(n_rS)$  (upper) ( $n_r = 1, 2, 3$ ) and (lower)  $e^+e^- \rightarrow b\bar{b}$  in units of the Born QED cross section for  $e^+e^- \rightarrow \mu^+\mu^-$  [ $\sigma_{\text{QED}}(e^+e^- \rightarrow \mu^+\mu^-) = 4\pi\alpha^2/3E_{c.m.}^2$ ] in the vicinity of the  $\Upsilon(5S)$  resonance. From Santel *et al.*, 2016.

panel of Fig. 46, that is usually associated with the conventional  $\Upsilon(5S)$  bottomonium meson.

If the peaks in the  $\pi^+\pi^-\Upsilon(n_rS)$  cross sections are attributed to  $\Upsilon(5S)$  decays, it implies  $\Upsilon(5S) \rightarrow \pi^+\pi^-\Upsilon(n_rS)$  ( $n_r = 1, 2, 3$ ) partial widths that are 2 orders of magnitude larger than theoretical predictions (Chen *et al.*, 2008), and the measured values of the  $\Upsilon(4S)$  decay widths to  $\pi^+\pi^-\Upsilon(1S, 2S)$  (Patrignani *et al.*, 2016).<sup>29</sup> This suggests that either the peak in the  $e^+e^-$  annihilation cross section near  $E_{c.m.} = 10.87$  GeV that has long been identified as the  $\Upsilon(5S)$   $b\bar{b}$  bottomonium state (Besson *et al.*, 1985) is not a standard  $b\bar{b}$  meson but instead a  $b$ -quark-sector equivalent of the  $Y(4260)$  (Ali *et al.*, 2010), or there is an overlap of the conventional  $\Upsilon(5S)$  with a nearby  $b$ -quark-sector equivalent of the  $Y(4260)$ , or the  $\Upsilon(5S)$  experiences some dynamical effects that have little or no influence on the  $\Upsilon(4S)$ . We follow the PDG and refer to this peak as the  $\Upsilon(10860)$ .

Belle accumulated a large sample of data at and near the energy of the  $\Upsilon(10860)$  mass peak [ $E_{c.m.}(e^+e^-) = 10.866$  GeV] in order to investigate the source of this anomaly,  $121.4 \text{ fb}^{-1}$  in total. Figure 47(a) shows the distribution of masses recoiling against all of the  $\pi^+\pi^-$  pairs in these events (Adachi *et al.*, 2012). The combinatorial background is large—there are typically  $10^6$  entries in each 1 MeV bin—and the statistical errors are small ( $\sim 0.1\%$ ). The data were fit piecewise with sixth-order polynomials and the residuals from the fits are shown in the lower panel of Fig. 47(b), where in addition to peaks at the  $\Upsilon(1S)$ ,  $\Upsilon(2S)$ , and  $\Upsilon(3S)$  masses and some expected reflections there are unambiguous signals for the  $h_b(1P)$  and  $h_b(2P)$ , the  $1^1P_1$  and  $2^1P_1$  bottomonium states. This was the first observation of these two elusive levels (Adachi *et al.*, 2012). One puzzle is that the  $\pi^+\pi^-h_b(m_rP)$ , ( $m_r = 1, 2$ ) final states are produced at rates that are nearly the same as those for  $\pi^+\pi^-\Upsilon(n_rS)$  ( $n_r = 1, 2, 3$ ), even though the  $\Upsilon(5S) \rightarrow \pi^+\pi^-h_b$  transition requires a heavy-quark spin flip that is expected to result in a strong suppression (Bondar *et al.*, 2011).

Figure 48(a) shows the  $\pi^+\pi^-h_b$  yields versus the maximum  $h_b\pi^\pm$  invariant mass for (upper)  $h_b = h_b(1P)$  and (lower)  $h_b = h_b(2P)$ , where it can be seen that essentially all of the  $\pi^+\pi^-h_b$  events are associated with the production of an  $h_b\pi$  system with an  $M(h_b\pi)$  value near either 10610 or 10650 MeV (Bondar *et al.*, 2012). Studies of fully reconstructed  $\pi^+\pi^-\Upsilon(n_rS)$ , ( $n_r = 1, 2, 3$ )  $\Upsilon(n_rS) \rightarrow \ell^+\ell^-$  events in the same data sample found  $\Upsilon(n_rS)\pi$  mass peaks at the same masses in the  $M_{\max}(\Upsilon(n_rS)\pi)$  distributions for all three narrow  $\Upsilon(n_rS)$  states; these are shown in the three panels of Fig. 48(b). Here the fractions of  $\pi^+\pi^-\Upsilon(n_rS)$  events in the two peaks are substantial— $\sim 6\%$  for the  $\Upsilon(1S)$ ,  $\sim 22\%$  for the  $\Upsilon(2S)$ , and  $\sim 43\%$  for the  $\Upsilon(3S)$ —but, unlike the case for

<sup>29</sup>For example, the PDG average value of  $\Upsilon(4S)$  branching fraction to  $\pi^+\pi^-\Upsilon(1S)$  measurements is  $\mathcal{B}(\Upsilon(4S) \rightarrow \pi^+\pi^-\Upsilon(1S)) = (8.1 \pm 0.6) \times 10^{-5}$  (Patrignani *et al.*, 2016). In contrast, the Belle measurement for the peak near 10.86 GeV is more than 50 times larger,  $\mathcal{B}(\Upsilon(10860) \rightarrow \pi^+\pi^-\Upsilon(1S)) = (5.3 \pm 0.6) \times 10^{-3}$  (Chen *et al.*, 2010).

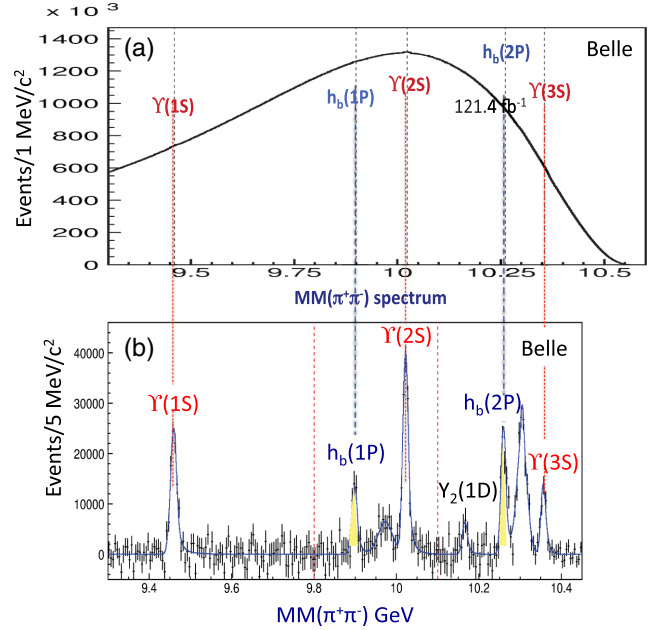


FIG. 47. (a) Distribution of masses recoiling against  $\pi^+\pi^-$  pairs at c.m. energies near 10.87 GeV and (b) residuals from piecewise fits to the data with smooth polynomials. The  $h_b(1P)$  and  $h_b(2P)$  peaks, shaded in yellow (light gray), were the first observations of these two states. From Adachi *et al.*, 2012.

the  $\pi^+\pi^-h_b(m_rP)$  channels, they account only for a fraction of the anomalous  $\pi^+\pi^-\Upsilon(n_rS)$  event yield (Garmash *et al.*, 2015). Thus, the production and decays of the two  $Z_b$  states can explain some, but not all of the anomalously large  $\Upsilon(5S) \rightarrow \pi^+\pi^-\Upsilon(1S, 2S, 3S)$  decay rates. The fitted values of the peak masses (indicated by the vertical dashed lines in each panel of Fig. 48) and widths in all five channels are consistent with each other; the weighted average mass and width values of the two peaks, named the  $Z_b(10610)$  and  $Z_b(10650)$ , are

$$\begin{aligned} Z_b(10610): M_1 &= 10607 \pm 2 \text{ MeV}, \\ \Gamma_1 &= 18.4 \pm 2.4 \text{ MeV}, \\ Z_b(10650): M_2 &= 10652 \pm 2 \text{ MeV}, \\ \Gamma_2 &= 11.5 \pm 2.2 \text{ MeV}, \end{aligned} \quad (16)$$

respectively. A Belle study of  $\pi^0\pi^0\Upsilon(n_rS)$  ( $n_r = 1, 2, 3$ ) found a  $6.5\sigma$  signal for the neutral  $Z_b(10610)^0$  isospin partner state with a mass  $M(Z_b(10610)^0) = 10609 \pm 6$  MeV and a production rate that is consistent with isospin-based expectations (Krokovny *et al.*, 2013).

The  $Z_b(10610)$  mass is only  $2.6 \pm 2.2$  MeV above the  $m_B + m_{B^*}$  mass threshold and the  $Z_b(10650)$  mass is only  $2.0 \pm 1.6$  MeV above  $2m_{B^*}$ . Dalitz plot analyses of the  $\pi^+\pi^-\Upsilon(n_rS)$  final states establish  $J^P = 1^+$  quantum number assignments for both states (Garmash *et al.*, 2015). The close proximity of the  $Z_b(10610)$  and  $Z_b(10650)$  to the  $B\bar{B}^*$  and  $B^*\bar{B}^*$  thresholds, respectively, and the  $J^P = 1^+$  quantum number assignment suggests that they may be virtual  $S$ -wave moleculelike states (Bondar *et al.*, 2011).

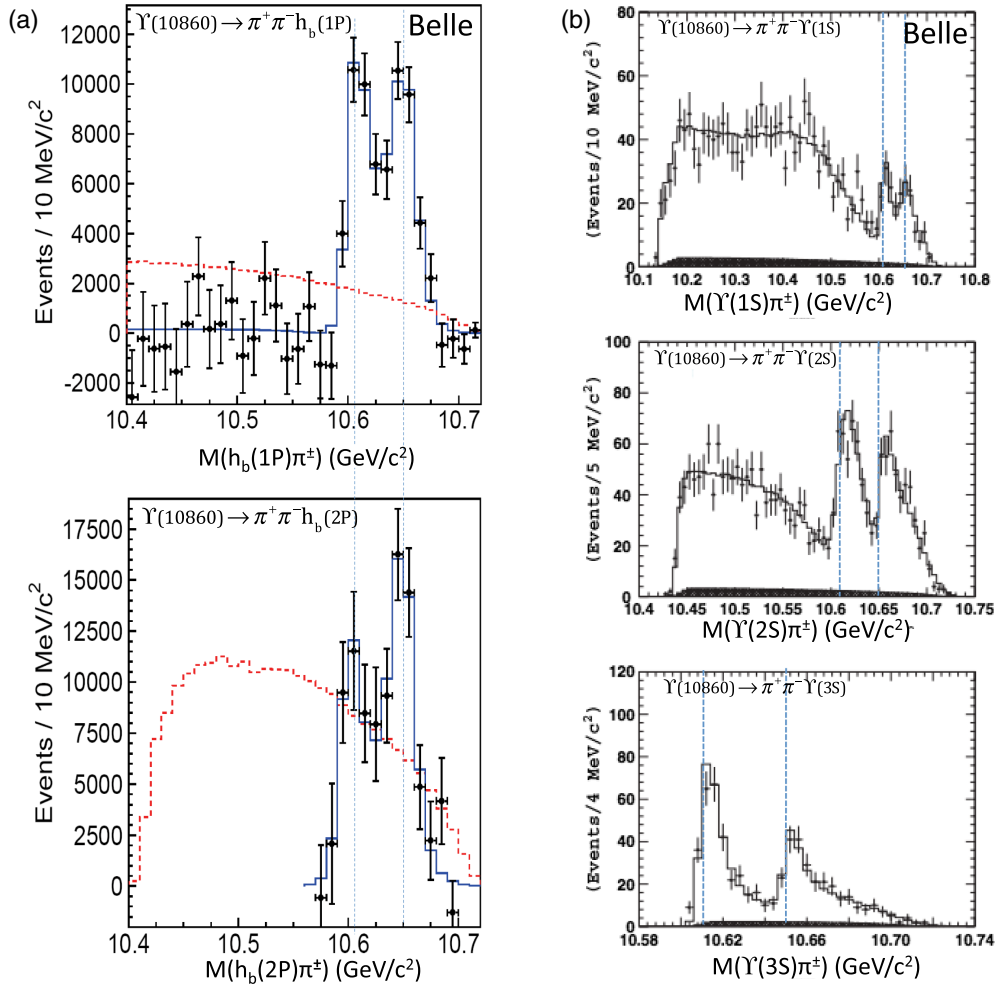


FIG. 48. (a) Invariant mass distributions for (upper)  $h_b(1P)\pi^+$  and (lower)  $h_b(2P)\pi^+$  from  $e^+e^- \rightarrow \pi^+\pi^-h_b(n_rP)$  events. (b) Invariant mass distributions for (upper)  $Y(1S)\pi^+$ , (center)  $Y(2S)\pi^+$ , and (lower)  $Y(3S)\pi^+$  in  $e^+e^- \rightarrow \pi^+\pi^-Y(n_rS)$  events. The vertical dashed lines in each panel indicate the mass values given in Eq. (16). From Bondar *et al.*, 2012.

The  $B^{(*)}\bar{B}^*$  molecule picture is supported by a Belle study of  $Y(10860) \rightarrow \pi B^{(*)}\bar{B}^*$  final states in the same data sample (Garmash *et al.*, 2016), where the pion and one  $B$  meson is reconstructed and the presence of the accompanying  $\bar{B}$  and the distinction between  $\pi B\bar{B}^*$  and  $\pi B^*\bar{B}^*$  are inferred from energy-momentum conservation; the  $B\bar{B}^*$  and  $B^*\bar{B}^*$  invariant masses are inferred from the pion momentum. The data points in Figs. 49(a) and 49(b) show the  $B\bar{B}^*$  and  $B^*\bar{B}^*$  invariant mass distributions, respectively, where the background, mostly from continuum  $e^+e^- \rightarrow c\bar{c}$  events and estimated from events where the pion charge and the flavor of the detected  $B$  meson do not match, is shown as hatched histograms.

The  $M(B\bar{B}^*)$  distribution [Fig. 49(a)] has a distinct peak near the mass of the  $Z_b(10610)$  and the  $M(B^*\bar{B}^*)$  distribution [Fig. 49(b)] peaks at the  $Z_b(10650)$  mass. Fits to the data with various combinations of  $Z_b$  BW amplitudes, both with and without a coherent nonresonant phase-space term, are shown as curves in the figures. In these fits, the masses and widths of the BW amplitudes are fixed at the values given in Eq. (16). The default fit, shown as short dashed curves, uses only a  $Z_b(10610) \rightarrow B\bar{B}^*$  amplitude for the  $B\bar{B}^*$  [Fig. 49(a)] fit and a

$Z_b(10650) \rightarrow B^*\bar{B}^*$  amplitude for the  $B^*\bar{B}^*$  [Fig. 49(b)] fit and gives an adequate description of the data. Other variations include phase space only (dotted), single BW amplitudes plus phase space (dash-dotted), and two BW amplitudes plus phase space (long dashed) do not make any significant improvements.

From the default fit, the branching-fraction values  $\mathcal{B}(Z_b(10610) \rightarrow B^+\bar{B}^{*0} + \bar{B}^0B^{*+}) = (86 \pm 3)\%$  and  $\mathcal{B}(Z_b(10610) \rightarrow B^{*+}\bar{B}^{*0}) = (74 \pm 6)\%$  are inferred. The  $B^{(*)}\bar{B}^*$  fall-apart modes are stronger than the sum total of the  $\pi^+Y(n_rS)$  and  $\pi^+h(m_rP)$  modes, but only by factors of  $\sim 6$  for the  $Z_b(10610)$  and  $\sim 3$  for the  $Z_b(10650)$ . The measured branching fraction for  $Z_b(10650) \rightarrow B\bar{B}^*$  is consistent with zero. These patterns, where  $B\bar{B}^*$  decays dominate for the  $Z_b(10610)$  and  $B^*\bar{B}^*$  decays are dominant for the  $Z_b(10650)$ , are consistent with expectations for moleculelike structures (Karliner and Rosner, 2015), which were proposed even before these states were observed (Liu *et al.*, 2008, 2009). A tetraquark interpretation of these states (Ali *et al.*, 2015) was also made before their discovery (Karliner and Lipkin, 2008).



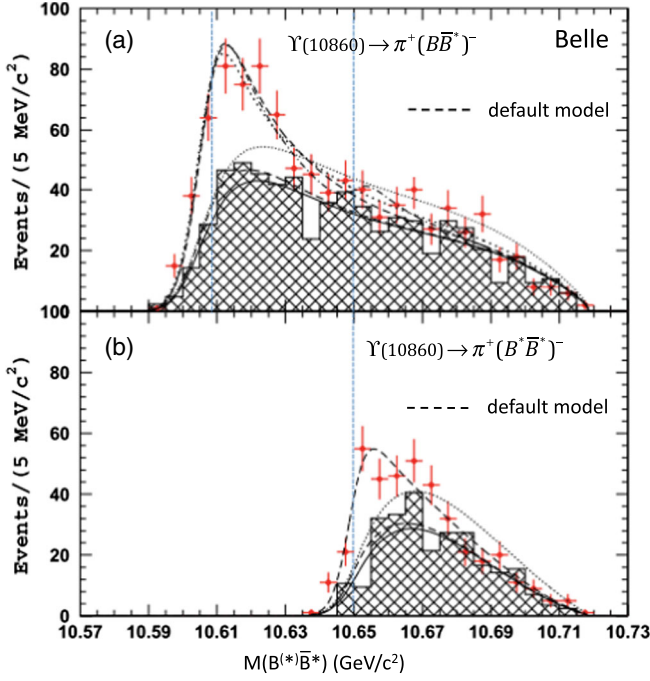


FIG. 49. (a) The  $M(B\bar{B}^*)$  distribution for  $\pi^+ B\bar{B}^*$  events and (b) the  $M(B^*\bar{B}^*)$  distribution for  $\pi^+ B^*\bar{B}^*$  events. The short dashed curves show results of fits with only a  $Z_b(10610) \rightarrow B\bar{B}^*$  contribution to (a) and a  $Z_b(10650) \rightarrow B^*\bar{B}^*$  contribution to (b). The other curves and the hatched (background) histograms are described in the text. From Garmash *et al.*, 2016.

## 2. The $Z_c$ charged charmoniumlike mesons

As discussed in the previous section, the discovery in the  $c$ -quark sector of the unexpected  $Y(4260) \rightarrow \pi^+\pi^-J/\psi$  signal in the initial-state-radiation process  $e^+e^- \rightarrow \gamma_{\text{ISR}}\pi^+\pi^-J/\psi$  at  $E_{\text{c.m.}} \approx 10.6$  GeV motivated Belle to look for possible related anomalies in  $e^+e^- \rightarrow \pi^+\pi^-Y(n_rS)$  ( $n_r = 1, 2, 3$ ) reactions near  $E_{\text{c.m.}} = 10.86$  GeV. This resulted in the discovery of anomalously high transition rates for what was presumed to be the  $Y(5S)$  charmonium state to  $\pi^+\pi^-Y(1S, 2S, 3S)$ , as shown in the top three panels of Fig. 46 (Chen *et al.*, 2010). Further investigations of these anomalies led to the discovery of the  $Z_b(10610)$  and  $Z_b(10650)$  charged bottomoniumlike states. These discoveries in the  $b$ -quark sector prompted the BESIII group to take data with the BEPCII collider operating at  $E_{\text{c.m.}} = 4.26$  GeV, to see if there were  $c$ -quark sector equivalents of the  $Z_b$  states produced in the decays of the  $Y(4260)$ .

The  $Z_c(3900)$ : Fig. 50 shows the distribution of the largest of the  $\pi^+J/\psi$  and  $\pi^-J/\psi$  invariant mass combinations in  $Y(4260) \rightarrow \pi^+\pi^-J/\psi$  events in a 525  $\text{pb}^{-1}$  BESIII data sample accumulated at  $E_{\text{c.m.}} = 4.260$  GeV (Ablikim *et al.*, 2013a). Here a distinct peak, called the  $Z_c(3900)$ , is evident near 3900 MeV. A fit using a BW amplitude to represent the  $\pi^\pm J/\psi$  mass peak and an incoherent phase-space-like function to represent the nonresonant background gives a mass and width of  $M(Z_c(3900)) = 3899.0 \pm 6.1$  MeV and  $\Gamma(Z_c(3900)) = 46 \pm 22$  MeV, which is  $\sim 24$  MeV above the  $m_{D^{*+}} + m_{\bar{D}^0}$  (or  $m_{D^+} + m_{\bar{D}^{*0}}$ ) threshold. The  $Z_c(3900)$  was observed by Belle in isr data at about the same time (Liu *et al.*, 2013).

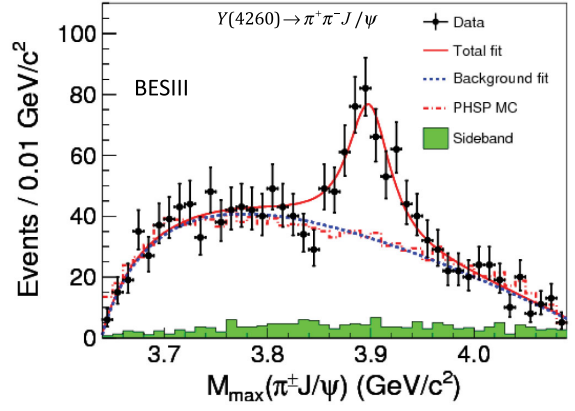


FIG. 50. Distribution of the larger of the two  $\pi^\pm J/\psi$  masses in  $e^+e^- \rightarrow \pi^+\pi^-J/\psi$  events collected in the BESIII detector at  $E_{\text{c.m.}} = 4.260$  GeV. The filled histogram shows the level of the non- $J/\psi$  background, which is determined from  $J/\psi$  mass sideband events. From Ablikim *et al.*, 2013a.

A subsequent BESIII study of the  $D^0D^{*-}$  systems produced in  $e^+e^- \rightarrow \pi^+D^0D^{*-}$  final states in the same data sample (Ablikim *et al.*, 2014b) found the very strong near-threshold peak in the  $D^0D^{*-}$  and invariant mass distribution shown in Fig. 51(a). The solid curve in the figure shows the results of a fit to the data with a threshold-modified BW amplitude to represent the peak and an incoherent phase-space-like function to represent the background. The same analysis found a similar peak in the  $D^-D^{*0}$  invariant mass distribution in  $e^+e^- \rightarrow \pi^+D^-D^{*0}$  events. The masses and widths from the two channels are consistent and their average values are  $M = 3883.9 \pm 4.5$  MeV and  $\Gamma = 24.8 \pm 12$  MeV.

Since the mass is  $\approx 2\sigma$  lower than the  $Z_c(3900)$  mass reported in Ablikim *et al.* (2013a), BESIII cautiously named this  $D\bar{D}^*$  state the  $Z_c(3885)$ . In the mass determinations of both the  $Z_c(3885)$  and  $Z_c(3900)$ , effects of possible interference with a coherent component of the nonresonant background are ignored, an approximation that can bias mass measurements by amounts comparable to the resonance widths, and this effect could account for the different mass values. Thus, we consider it highly likely that the  $Z_c(3885)$  is the  $Z_c(3900)$  in a different decay channel. If this is the case, the partial width for  $Z_c(3900) \rightarrow D\bar{D}^*$  decays is  $6.2 \pm 2.9$  times larger than that for  $J/\psi\pi^+$ , which is small compared to open-charm versus hidden-charm decay-width ratios for established charmonium states above the open-charm threshold, such as the  $\psi(3770)$  and  $\psi(4040)$ , where corresponding ratios are measured to be more than an order of magnitude larger (Patrignani *et al.*, 2016). On the other hand, this ratio is similar to the properties of the  $X(3872)$  and  $Z_b$  states.

The strong  $Z_c(3885) \rightarrow D\bar{D}^*$  signal enabled the BESIII group to determine its  $J^P$  quantum numbers from the dependence of its production on  $\theta_\pi$ , the bachelor pion production angle relative to the beam direction in the  $e^+e^-$  c.m. system. For  $J^P = 0^-$ ,  $dN/d|\cos\theta_\pi|$  should go as  $\sin^2\theta_\pi$ ; for  $1^-$  it should follow  $1 + \cos^2\theta_\pi$ , and for  $1^+$  it should be flat ( $0^+$  is forbidden by parity). Figure 51(b) shows the efficiency-corrected  $Z_c(3885)$  signal yield as a function of  $|\cos\theta_\pi|$ , together with expectations for  $J^P = 0^+$  (dashed red),  $1^-$

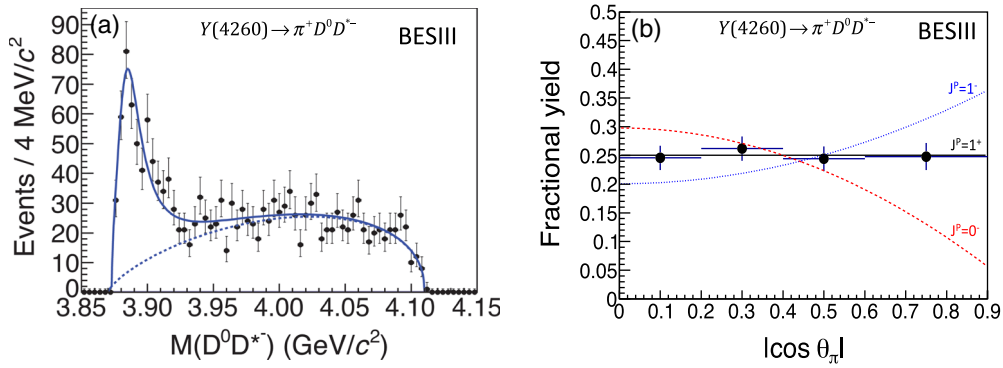


FIG. 51. (a) The  $D^0 D^{*0}$  invariant mass distribution in  $e^+e^- \rightarrow \pi^+ D^0 D^{*0}$  events collected in the BESIII detector at  $E_{\text{c.m.}} = 4.260$  GeV. The solid curve shows the result of a fit to the data points with a threshold-modified BW amplitude plus an incoherent phase-space-like background (dashed curve). (b) The efficiency-corrected  $Z_c(3885)$  production angle distribution compared to expectations for different  $J^P$  quantum number assignments. From [Ablikim et al., 2014b](#).

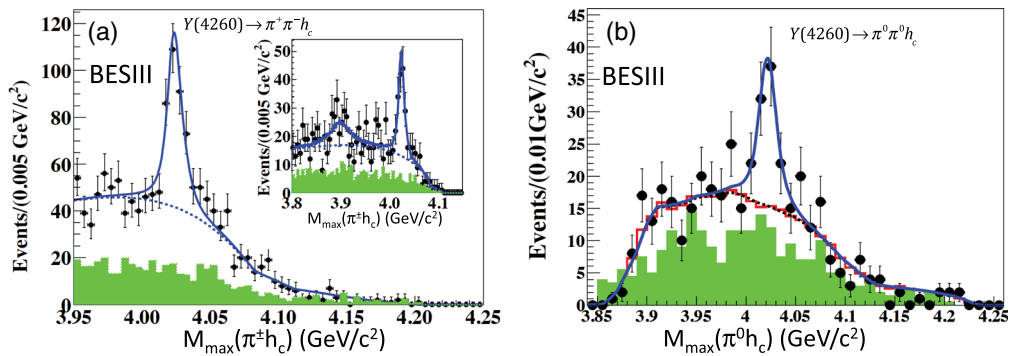


FIG. 52. (a) The distribution of the larger of the two  $\pi^\pm h_c$  masses in  $e^+e^- \rightarrow \pi^+ \pi^- h_c$  events collected in the BESIII detector at  $E_{\text{c.m.}} = 4.260$  and  $4.360$  GeV. The inset shows a larger  $M(\pi h_c)$  that includes the  $Z_c(3900)$  mass region. From [Ablikim et al., 2013b](#). (b) The  $M_{\text{max}}(\pi^0 h_c)$  distribution for  $e^+e^- \rightarrow \pi^0 \pi^0 h_c$  events. The filled histograms show the level of the non- $h_c$  background determined from  $h_c$  mass sideband events. The curves are described in the text. From [Ablikim et al., 2014c](#).

(dotted blue), and  $J^P = 1^+$ . The  $J^P = 1^+$  assignment is clearly preferred and the  $0^-$  and  $1^-$  assignments are ruled out with high confidence.

BESIII also reported neutral counterparts of the  $Z_c(3900)$  in the  $\pi^0 J/\psi$  channel in  $e^+e^- \rightarrow \pi^0 \pi^0 J/\psi$  events ([Ablikim et al., 2015f](#)), and the  $D^+ D^{*0}$  and  $D^0 \bar{D}^{*0}$  channels in  $e^+e^- \rightarrow \pi^0 (D \bar{D}^*)^0$  events ([Ablikim et al., 2015e](#)), with mass and width values that are in good agreement with the charged  $Z_c(3900)$  state measurements. The relative signal yields in the charged and neutral channels are consistent with expectations based on isospin conservation.

*The  $Z_c(4020)$ :* With data accumulated at the peaks of the  $Y(4260)$ ,  $Y(4360)$ , and nearby energies, BESIII made a study of  $\pi^+ \pi^- h_c(1P)$  final states ([Ablikim et al., 2013b](#)). Exclusive  $h_c(1P)$  decays were detected via the  $h_c \rightarrow \gamma \eta_c$  transition, where the  $\eta_c$  was reconstructed in 16 exclusive hadronic decay modes. With these data, BESIII observed a distinct peak near 4020 MeV in the  $M_{\text{max}}(\pi^\pm h_c)$  distribution that is shown in Fig. 52(a). A fit to this peak, which the BESIII group called the  $Z_c(4020)^+$ , with a signal BW amplitude (assuming  $J^P = 1^+$ ) plus a smooth background, returns a  $\sim 9\sigma$  significance signal with a mass of  $M(Z_c(4020)) = 4022.9 \pm 2.8$  MeV—about 5 MeV above  $m_{D^{*+}} + m_{\bar{D}^{*0}}$ —and a width of  $\Gamma(Z_c(4020)) = 7.9 \pm 3.7$  MeV.

The inset in Fig. 52(a) shows the result of including a  $Z_c(3900)^+ \rightarrow \pi^+ h_c$  term in the fit. In this case, a marginal  $\sim 2\sigma$  signal for  $Z_c(3900)^+ \rightarrow \pi^+ h_c$  is seen to the left of the  $Z_c(4020)$  peak. This translates into an upper limit on the branching fraction for  $Z_c(3900)^+ \rightarrow \pi^+ h_c$  decay that is less than that for  $Z_c(3900)^+ \rightarrow \pi^+ J/\psi$  by a factor of 5.

BESIII also observed the neutral isospin partner of the  $Z_c(4020)$  ([Ablikim et al., 2014c](#)). The  $M_{\text{max}}(\pi^0 h_c)$  distribution for  $e^+e^- \rightarrow \pi^0 \pi^0 h_c$  events in the same data set used for the  $Z_c(4020)^\pm$ , shown in Fig. 52(b) looks qualitatively like the  $M_{\text{max}}(\pi^\pm h_c)$  distribution with a distinct peak near 4020 MeV. A fit to the data that includes a BW term with a width fixed at the value measured for the  $Z_c(4020)^+$  and floating mass returns a mass of  $4023.9 \pm 4.4$  MeV; this and the signal yield are in good agreement with expectations based on isospin symmetry.

A study of  $e^+e^- \rightarrow D^{*+} \bar{D}^{*0} \pi^-$  events in the  $E_{\text{c.m.}} = 4.260$  GeV data sample using a partial reconstruction technique that only required the detection of the bachelor  $\pi^-$ , the  $D^+$  from the  $D^{*+} \rightarrow \pi^0 D^+$  decay and one  $\pi^0$ , from either the  $D^{*+}$  or the  $\bar{D}^{*0}$  decay, to isolate the process and measure the  $D^{*+} \bar{D}^{*0}$  invariant mass ([Ablikim et al., 2014a](#)). The signal for real  $D^{*+} \bar{D}^{*0} \pi^-$  final states is the distinct peak near

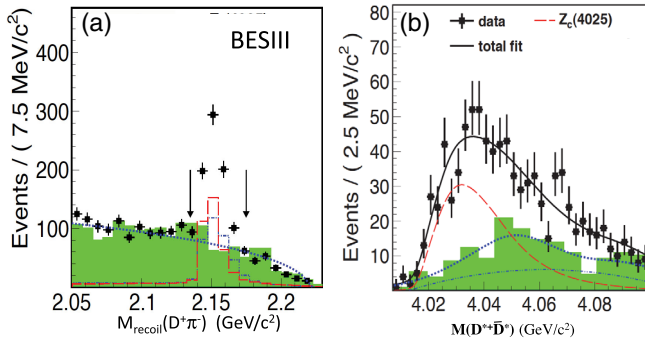


FIG. 53. (a) Distribution of masses recoiling against the reconstructed  $\pi^-$  and  $D^+$  in  $e^+e^- \rightarrow \pi^-(D^*\bar{D}^*)^+$  events collected in the BESIII detector at  $E_{c.m.} = 4.260$  GeV. The peak near 2.15 GeV corresponds to  $e^+e^- \rightarrow \pi^-(D^{*+}\bar{D}^{*0})^+$  signal events. (b) The  $M(D^{*+}\bar{D}^{*0})$  distribution inferred from the  $\pi^-$  momentum for signal events. The filled histograms show the level of the combinatorial background determined from events where the reconstructed pion and  $D$  meson have the same electric charge. The curves are described in the text. From Ablikim *et al.*, 2014a.

2.15 GeV in the distribution of masses recoiling from the reconstructed  $D^+$  and  $\pi^-$ , shown in Fig. 53(a). The measured  $D^*\bar{D}^*$  invariant mass distribution for events in the 2.15 GeV peak and inferred from the  $\pi^-$  momentum is shown as the data points in Fig. 53(b). Here the strong near-threshold peaking behavior cannot be well described by a phase-space-like distribution, shown as a dash-dotted blue curve, or by combinatorial background, which is determined from wrong-sign events in the data (i.e., events where the pion and charged  $D$  meson have the same sign) that are shown as the shaded histogram. The solid black curve shows the results of a fit to the data points that includes an efficiency weighted  $S$ -wave BW function (long dashes), the combinatorial background shape (short dashes) scaled to measured non- $D^{*+}\bar{D}^{*0}\pi^-$  background level under the signal peak in Fig. 53(a), and a phase-space term (dash-dotted). The fit returns a  $13\sigma$  signal with mass and width  $M = 4026.3 \pm 4.5$  MeV and  $\Gamma = 24.8 \pm 9.5$  MeV, values that agree within errors to those measured for the  $Z_c(4020)^+ \rightarrow \pi^+h_c$  channel. Although BESIII cautiously calls this  $(D^*\bar{D}^*)^+$  signal the  $Z_c(4025)$ , we consider this to likely be another decay mode of the  $Z_c(4020)$ .

A neutral  $D^*\bar{D}^*$  state with a mass and width that are consistent with the  $Z_c(4025)^+$  was seen by BESIII in  $e^+e^- \rightarrow \pi^0(D^*\bar{D}^*)^0$  events (Ablikim *et al.*, 2015d).

The  $Z_c(4020) \rightarrow D^*\bar{D}^*$  and  $\pi^-h_c$  signal yields reported in Ablikim *et al.* (2014a) and Ablikim *et al.* (2013b), respectively, imply a partial width for  $Z_c(4020) \rightarrow D^*\bar{D}^*$  that is larger than that for  $Z_c(4020) \rightarrow \pi h_c$ , but only by a factor of  $12 \pm 5$ , not by the large factors that are characteristic of conventional charmonium. In addition, there is no sign of  $Z_c(4020) \rightarrow D\bar{D}^*$  in Fig. 51(a), where there is a  $\sim 500$  event  $Z_c(3885) \rightarrow D^0D^{*-}$  signal. A recent BESIII study of  $Z_c(3900) \rightarrow D\bar{D}^*$  decays (Ablikim *et al.*, 2015b) set a 90% confidence level upper limit  $\mathcal{B}(Z_c(4020) \rightarrow D\bar{D}^*) < 0.13\mathcal{B}(Z_c(3885) \rightarrow D\bar{D}^*)$ . This absence of any evident signal for  $Z_c(4020) \rightarrow D\bar{D}^*$  suggests that the  $Z_c(4020) \rightarrow D\bar{D}^*$  partial width is considerably smaller

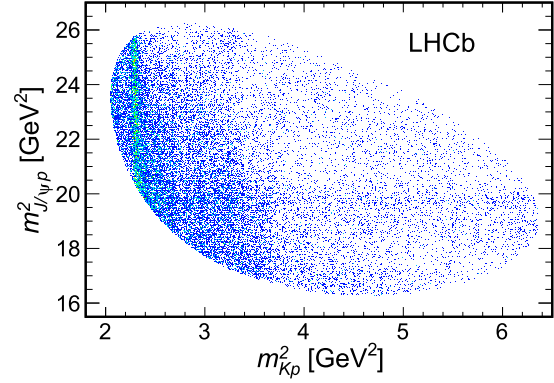


FIG. 54. Dalitz plot distribution for  $\Lambda_b^0 \rightarrow J/\psi p K^-$  decays. From Aaij *et al.*, 2015c.

than that for  $Z_c(4020) \rightarrow D^*\bar{D}^*$ , which mirrors the behavior of the two  $Z_b$  states and is suggestive of some relation to the  $Z_c(4020)$ 's proximity to the  $2m_{D^*}$  threshold.

Many similarities between the  $Z_c$  and  $Z_b$  states discovered in  $e^+e^-$  annihilations to  $\pi\pi$  plus a heavy quarkonium states can be taken as a reflection of heavy quark symmetry. However, there are also differences between them that await an explanation. While the  $Z_b(10610)$  and  $Z_b(10650)$  both decay to  $\pi Y(n_r S)$  and  $\pi h_b$ , the  $Z_c(4020)$  is not observed in  $\pi J/\psi$  and the  $Z_c(3900)$  is not observed in  $\pi h_c$ .<sup>30</sup> The latter is particularly difficult to accommodate in a purely molecular interpretation in which both  $Z_c$  states should copiously decay to  $\pi h_c$  (Esposito, Guerrieri, and Pilloni, 2015).

## VII. PENTAQUARK CANDIDATES

At the birth of the quark model, Gell-Mann (1964) and Zweig (1964) both suggested the possibility of particles built from more than the minimal quark content, including pentaquark baryons  $qqqq\bar{q}$ . Experimental searches for pentaquarks comprised of light flavors have a long and often controversial history summarized in Sec. I.C. No undisputed candidates have been found in over 50 years of searches, although unusual properties of some ordinary baryons, such as the  $\Lambda(1405)$ , are often attributed to mixing of  $qqq$  and  $qqqq\bar{q}$  systems.

In 2015, convincing evidence for pentaquarklike structures with a minimal quark content of  $uudc\bar{c}$  was reported by LHCb in a study of  $\Lambda_b^0 \rightarrow J/\psi p K^-$  ( $J/\psi \rightarrow \mu^+\mu^-$ ) decays (Aaij *et al.*, 2015c). In addition to contributions from many conventional  $\Lambda^* \rightarrow K^- p$  baryon resonances (with a quark content of  $uds$ ), the data contain a narrow peak in the  $J/\psi p$  mass distribution that is evident as a distinct horizontal band in the  $M^2(J/\psi p)$  vs  $M^2(K^- p)$  Dalitz plot shown in Fig. 54, and the distribution of  $J/\psi p$  invariant masses shown in Fig. 55(b).

In order to clarify the nature of this band, an amplitude analysis was performed that was modeled after the four-dimensional analysis of  $\bar{B}^0 \rightarrow \psi' \pi^+ K^-$  ( $\psi' \rightarrow \mu^+\mu^-$ ) that

<sup>30</sup>There is also possibly a different resonant  $\pi\psi'$  substructure in  $e^+e^- \rightarrow \pi^+\pi^-\psi'$  (Ablikim *et al.*, 2017b).

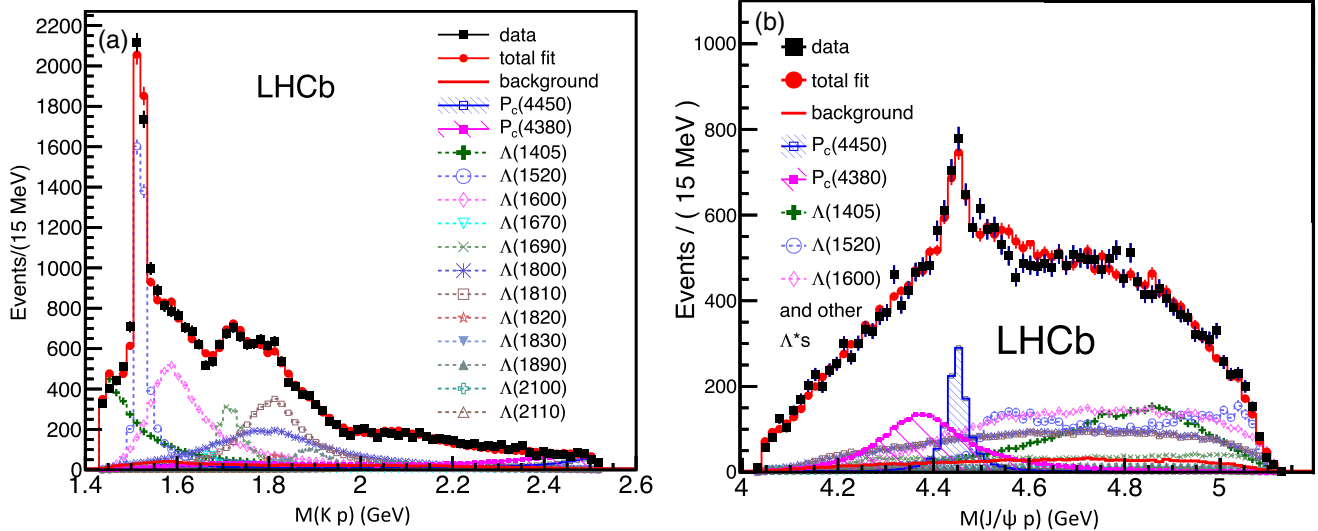


FIG. 55. Projections of the amplitude fit with  $P_c(4380)^+$  and  $P_c(4450)^+$  states included (red histogram) onto the (a)  $M(Kp)$  and (b)  $M(J/\psi p)$  distributions (black squares with error bars) in  $\Lambda_b^0 \rightarrow J/\psi p K^-$  event sample. Contributions from individual components of the fit are indicated as different color or line-style histograms as labeled. From Aaij *et al.*, 2015c.

the LHCb group used to study the  $Z(4430)^+ \rightarrow \psi' \pi^+$  charmoniumlike state as described in Sec. VI.A. Although the properties of the initial-state particles are quite different—the spin  $1/2$   $\Lambda_b$  versus the spin  $0$   $B$  meson—the final states for the two processes are very similar, with  $\pi^+$  being replaced by  $p$ . The signal statistics  $26\,000 \pm 170$  and the background level  $5.4\%$  are also comparable. A quasi-two-body amplitude model was used that was based on an isobar approximation (i.e., summing up coherent Breit-Wigner amplitudes) with the dynamics of the contributing decay processes parametrized by a helicity formalism. The amplitude fit spanned a kinematically complete, six-dimensional space of independent kinematic variables, including invariant masses  $M(Kp)$  and  $M(J/\psi p)$ , decay helicity angles ( $\theta$ ) of  $\Lambda_b$ ,  $J/\psi$ ,  $\Lambda^*$ , or pentaquark candidate  $P_c^+ \rightarrow J/\psi p$ , and angles between the decay planes.<sup>31</sup> For the  $K^- p$  channel, fourteen reasonably well-established  $\Lambda^*$  resonances were included with masses and widths set to their values given in the 2014 PDG tables (Olive *et al.*, 2014) and varied within their uncertainties when evaluating systematic errors. Their helicity couplings (between 1 and 6 complex numbers per resonance) were determined from the fit to the data. It was found that these  $\Lambda^*$  contributions taken by themselves fail to describe the data. It was necessary to add two nonstandard  $P_c^+ \rightarrow J/\psi p$  pentaquark contributions to the matrix element (ten free parameters per resonance) before the narrow structure seen in  $M(J/\psi p)$  could be reasonably well reproduced, as illustrated in Fig. 55.

The lower-mass state  $P_c(4380)^+$  has a fitted mass of  $4380 \pm 8 \pm 29$  MeV, width of  $205 \pm 18 \pm 86$  MeV, a fit fraction of  $(8.4 \pm 0.7 \pm 4.2)\%$ , and a significance of  $9\sigma$ . The higher-mass state  $P_c(4450)^+$  has a fitted mass of  $4449.8 \pm 1.7 \pm 2.5$  MeV, a much narrower width of

$39 \pm 5 \pm 19$  MeV, a fit fraction of  $(4.1 \pm 0.5 \pm 1.1)\%$ , and a significance of  $12\sigma$ .

The need for a second  $P_c^+$  state is visually more apparent in Fig. 56(b) that shows the  $M(J/\psi p)$  projections for large  $Kp$  invariant masses [ $M(Kp) \geq 2.0$  GeV], where contributions from  $\Lambda^*$  resonances are the smallest. Even though contributions from the two  $P_c^+$  states are most visible in this region, they interfere destructively in this part of the Dalitz plane, as is evident in the figure. In contrast, in the  $M(J/\psi p)$  projection at the other extreme of the Dalitz plane, at low  $Kp$  mass values [ $1.55 \leq M(Kp) \leq 1.70$  GeV] shown in Fig. 56(a), the interference between the two  $P_c^+$  states is constructive. High  $M(Kp)$  values correspond to  $\cos \theta_{p_c}$  values near  $+1$ , while low  $M(Kp)$  values correspond to  $\cos \theta_{p_c} \approx -1$ . The observed pattern, with interference that is constructive near  $\cos \theta_{p_c} \approx -1$  and destructive near  $\cos \theta_{p_c} \approx +1$ , can occur only between

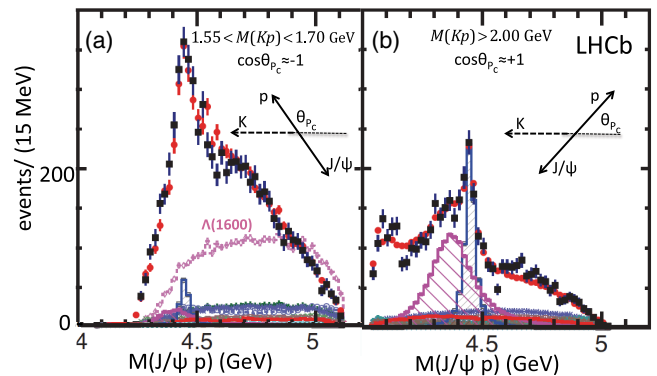


FIG. 56. Projections of the amplitude fit with  $P_c(4380)^+$  and  $P_c(4450)^+$  states included (solid red circles) onto the  $M(J/\psi p)$  invariant mass distributions from  $\Lambda_b^0 \rightarrow J/\psi p K^-$  events (black squares with error bars) with (a)  $1.55 \leq M(Kp) \leq 1.70$  GeV and (b)  $M(Kp) > 2.00$  GeV. The individual fit components are shown with the same color and line-style designations that are used in Fig. 55. Adapted from Aaij *et al.*, 2015c.

<sup>31</sup>The decay helicity angle is the angle between one of the decay products and the boost direction in the rest frame of the parent particle.

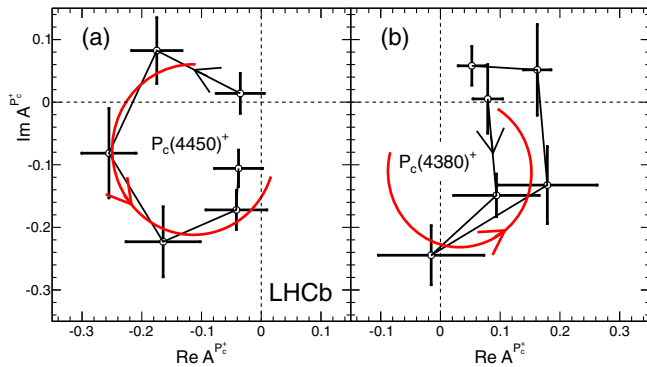


FIG. 57. Fitted values of the real and imaginary parts of the amplitudes of the (a)  $P_c(4450)^+$  and (b)  $P_c(4380)^+$  states for  $\Lambda_b^0 \rightarrow J/\psi p K^-$  shown in the Argand diagrams as connected points with the error bars (masses increase counterclockwise). The solid red curves are the predictions from the Breit-Wigner formula, with resonance masses and widths set to the nominal fit results and scaled to the displayed points. From Aaij *et al.*, 2015c.

odd and even partial waves, thereby indicating that the two  $P_c^+$  states must have opposite parities. A similar interference pattern is observed in the  $\cos\theta_{\Lambda^*}$  distribution [Fig. 7 in Aaij *et al.* (2015c)] that reflects the presence of parity doublets in the  $\Lambda^*$  spectrum. Unfortunately, the spins of the two  $P_c^+$  states were not uniquely determined. Within the statistical and systematic ambiguities,  $(3/2, 5/2)$  and  $(5/2, 3/2)$  combinations with either  $(-, +)$  or  $(+, -)$  parities are not well resolved. All other combinations are disfavored. There is a strong dependence of the data preference for the  $P_c^+$  spins on the  $\Lambda^*$  model used in the amplitude fit [see Sec. 13.1 in Jurik (2016)], and this calls for some caution in the interpretation of the observed  $P_c^+$  states until their quantum numbers are more firmly determined.

Argand diagrams for the two  $P_c^+$  states are shown in Fig. 57. These were obtained by replacing the Breit-Wigner amplitude for one of the  $P_c^+$  states at a time by a combination of independent complex amplitudes at six equidistant points in the  $\pm\Gamma_0$  range (interpolated in mass for continuity) that were fit to the data simultaneously with the other parameters of the full matrix element model. While the narrower  $P_c(4450)^+$  state shows the expected resonant behavior, the diagram for the  $P_c(4380)^+$  deviates somewhat from BW expectations. However, the statistical errors are large, especially for the broader  $P_c(4380)^+$  state.

The inclusion of additional  $\Lambda^*$  states beyond the well-established ones, of  $\Sigma^*$  excitations (expected to be suppressed), and of nonresonant contributions with a constant amplitude, did not remove the need for two pentaquark states in the model to describe the data. On the other hand,  $\Lambda^*$  spectroscopy is a complex subject, from both experimental and theoretical points of view. This was demonstrated by a recent reanalysis of  $\bar{K}N$  scattering data (Fernandez-Ramirez *et al.*, 2016) in which the  $\Lambda(1800)$  state, which was previously considered to be “well established,” is not seen, and where evidence for a few previously unidentified states is included. In fact, all theoretical models for  $\Lambda^*$  baryons (Capstick and Isgur, 1986; Loring, Metsch, and Petry, 2001; Melde, Plessas, and Sengl, 2008; Engel *et al.*, 2013; Faustov and Galkin,

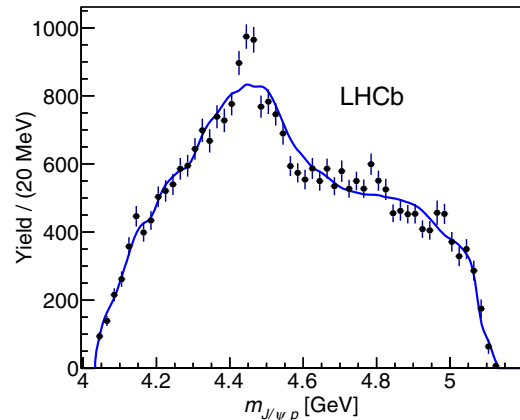


FIG. 58. The efficiency-corrected and background-subtracted distribution of  $M(J/\psi p)$  for the LHCb data, shown as black points with error bars, is compared with the best fit obtained using reflections based on the observed  $K^- p$  mass distribution and moments of the  $K^- p$  helicity angle patterns, shown as the solid blue curve. The possibility that the  $M(J/\psi p)$  distribution can be accommodated by any plausible reflections from the  $K^- p$  system is ruled out at the  $> 9\sigma$  level. Adapted from Aaij *et al.*, 2016a.

2015; Santopinto and Ferretti, 2015) predict a much larger number of higher-mass excitations than is established experimentally. The high density of predicted states, which are generally expected to have large widths, makes it difficult to identify individual states experimentally. Nonresonant contributions with a nontrivial  $K^- p$  mass dependence may also occur. Therefore, LHCb also inspected their data with an approach that is nearly independent of the way the  $K^- p$  contributions are modeled (Aaij *et al.*, 2016a). A representation of the Dalitz plane distribution was constructed using the measured  $M(Kp)$  distribution and Legendre polynomial moments of the cosine of the  $\Lambda^*$  helicity angle determined from the data as a function of  $M(Kp)$ . The maximal rank of the moments generated by the  $K^- p$  contributions alone cannot be higher than twice their largest total angular momentum. Since high-spin  $\Lambda^*$  states cannot significantly contribute at low  $M(Kp)$  values, high rank moments were excluded from the representation [see Figs. 1 and 3 in Aaij *et al.* (2016a)]. When projected onto the  $M(J/\psi p)$  axis of the Dalitz plane, this representation cannot describe the data as shown in Fig. 58. The disagreement was quantified to be at least at the  $9\sigma$  level and demonstrates that the hypothesis that  $K^- p$  contributions alone can generate the observed  $m_{J/\psi p}$  mass structure can be rejected with very high confidence without any assumptions about the number of  $K^- p$  contributions, their resonant or nonresonant character, or their mass shapes or interference phases. This establishes the presence of contributions either from nonstandard hadron channels or from rescattering effects of conventional ones. However, this approach says nothing about their characterization.

The LHCb Collaboration also inspected Cabibbo-suppressed decays  $\Lambda_b^0 \rightarrow J/\psi p \pi^-$  for signs of the  $P_c(4380)^+$  and  $P_c(4450)^+$  states (Aaij *et al.*, 2016c). The reconstructed  $\Lambda_b^0$  signal yield in this channel is more than an order of magnitude smaller and has a background fraction that is worse by a factor of 3 than the Cabibbo-favored mode, thereby

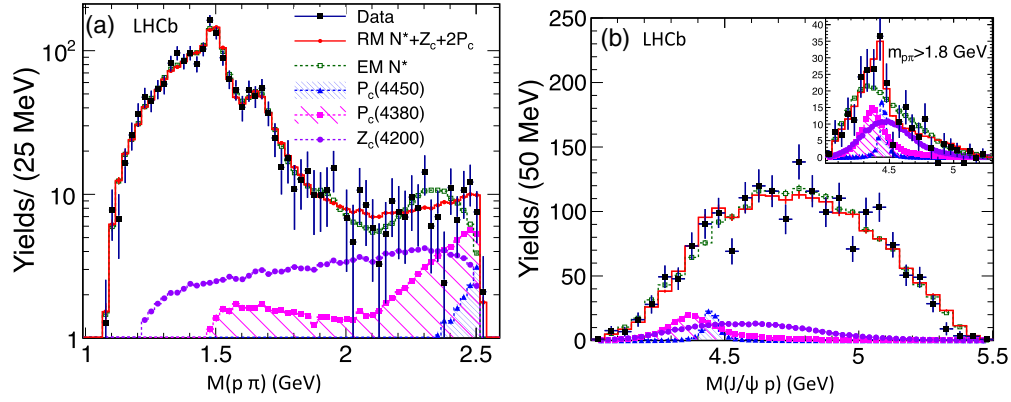


FIG. 59. Comparisons of projections of the amplitude fits (red histogram) onto (a)  $M(p\pi)$  and (b)  $M(J/\psi p)$  data distributions for  $\Lambda_b^0 \rightarrow J/\psi p \pi^-$  decays. The dashed green histogram shows the results of a fit with no nonstandard hadrons in the  $p\pi$  and  $J/\psi p$  channels. The inset in (b) shows the  $M(J/\psi p)$  fit-data comparison for events with  $M(p\pi) > 1.8$  GeV, where there is some hint of a  $P_c(4450)^+$  signal. Adapted from Aaij *et al.*, 2016c.

precluding the ability to perform an unconstrained search for  $J/\psi p$  states. Instead, the  $P_c^+$  parameters were fixed to the values measured in the  $\Lambda_b^0 \rightarrow J/\psi p K^-$  channel and varied within their uncertainties (including  $J^P$  ambiguities) in systematic studies. Only the production helicity couplings were allowed to be different (four free parameters per state). The possible presence of the  $Z_c(4200)^- \rightarrow J/\psi \pi^-$  resonance, observed by Belle in  $B^0 \rightarrow J/\psi \pi^- K^+$  decays, further complicates the amplitude analysis, adding ten free parameters even after its mass and width had been fixed to the measured values. Up to 14 known  $N^* \rightarrow p\pi^-$  resonances were included in the fit. As a result, even after neglecting contributions from higher orbital angular momenta in the  $N^*$  decays, there were as many as 106 free parameters in the six-dimensional fit to the relevant masses and helicity angles.

The analysis yielded  $3.1\sigma$  evidence for the summed presence of nonstandard [ $Z_c(4200)^-$ ,  $P_c(4380)^+$ , and  $P_c(4450)^+$ ] hadron contributions. The  $M(p\pi)$  and  $M(J/\psi p)$  projections of the fit are compared with the experimental data in Figs. 59(a) and 59(b), respectively. The inset in Fig. 59(b) shows the  $M(J/\psi p)$  projection for events with  $M(p\pi) > 1.8$  GeV, where there is some, but not very significant, indication of a  $P_c(4450)^+ \rightarrow J/\psi p$  signal. However, ambiguities between  $P_c^+$  and  $Z_c^-$  terms eliminate any ability to establish the presence of any individual nonstandard hadron contribution. As a result, these results failed to confirm any of these states, and more data are needed for more conclusive results.

## VIII. SUMMARY AND FUTURE PROSPECTS

Here we do not attempt to provide a detailed review of the successes and failures of the large variety of theoretical models that have been proposed as explanations of the nonstandard hadrons discussed in this review. For this we refer the interested reader to three recent and comprehensive discussions of these issues with somewhat different viewpoints (Chen *et al.*, 2016; Esposito, Pilloni, and Polosa, 2017; Lebed, Mitchell, and Swanson, 2017). Instead we provide our

experimentally oriented sense of where this field is at and where it is heading.

Experimentally, it seems remarkable that the number of charmoniumlike states above the  $D\bar{D}$  threshold that have unexpected properties, such as narrow total widths and/or relatively large decay rates to hidden-charm states in spite of the existence of easily accessible decay channels with open charm, is about double the number of known charmonium states in this mass range that conform to expected behavioral patterns (see Fig. 60). Clearly, the simple  $Q\bar{Q}$  model of charmonium, which works so well for states below the open-flavor threshold, fails at higher masses, and some new degrees of freedom have become relevant.

The high-mass bottomonium system is not as experimentally well explored as that for charmonium (Fig. 61). However, when explored with the same technique, i.e.,  $e^+e^-$  energy scans, it revealed anomalous states with apparently similar characteristics as those observed in the charmonium system, as expected from heavy-quark symmetry.

Finding and understanding these new degrees of freedom presents a great challenge to current theoretical models of hadronic structures.

## A. Theory

### 1. Molecules

We owe our existence to residual strong forces between nucleons, i.e., between individually confined, color-singlet groups of three quarks in baryons. The resulting nuclei support the rich diversity of atoms in nature. In the context of QCD, this binding resembles the binding of atoms in molecules by residual electromagnetic forces and, thus, nuclei can be pictured as baryon-baryon molecules. Nuclear physics provides good models for the molecular forces between nucleons, and it is natural to expect that meson-meson and meson-baryon combinations may also experience similar forces. But, since nuclear models are not based on direct derivations from the fundamental theory of strong interactions (QCD), it is not *a priori* known how strong the forces in these

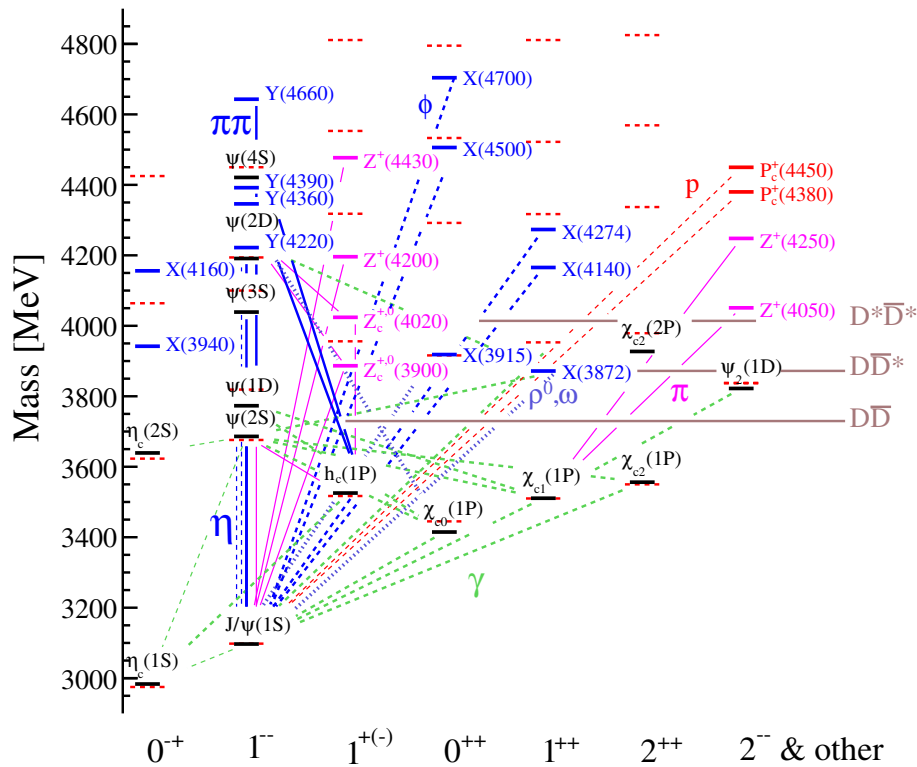


FIG. 60. The current status of the charmoniumlike spectrum. The dashed (red) horizontal lines indicate the expected states and their masses based on recent calculations (Barnes, Godfrey, and Swanson, 2005) based on the Godfrey-Isgur relativized potential model (Godfrey and Isgur, 1985), supplemented by the calculations in Lu and Dong (2016) for high radial excitations of the  $P$ -wave states. The solid (black) horizontal lines indicate the experimentally established charmonium states, with masses and spin-parity ( $J^{PC}$ ) quantum number assignments from Patrignani *et al.* (2016) and labeled by their spectroscopic assignment. The open-flavor decay channel thresholds are shown with longer solid (brown) horizontal lines. The candidates for exotic charmoniumlike states are also shown with shorter solid (blue or magenta) horizontal lines with labels reflecting their most commonly used names. All states are organized according to their quantum numbers given on horizontal axes. The last column includes states with unknown quantum numbers, the two pentaquark candidates, and the lightest charmonium  $2^{--}$  state. The lines connecting the known states indicate known photon or hadron transitions between them: dashed green are  $\gamma$  transitions (thick  $E1$ , thin  $M1$ ), solid magenta are  $\pi$ , thin (thick) dashed blue are  $\eta$  ( $\phi$ ), dashed red are  $p$ , dotted blue are  $\rho^0$  or  $\omega$ , and solid blue other  $\pi\pi$  transitions, respectively.

other, non-nucleon-nucleon, systems are, or if bound moleculelike meson-meson or meson-baryon combinations actually exist.

The 2003 Belle paper (Choi *et al.*, 2003) that reported the discovery of the  $X(3872) \rightarrow \pi^+\pi^-J/\psi$  emphasized two intriguing experimental features. One was the close proximity of the  $X(3872)$  mass and the  $D^0\bar{D}^{*0}$  mass threshold; at that time, the measurement precision of the  $X(3872)$  mass was  $\pm 0.8$  MeV and that of the PDG-2002 value world average for  $m_{D^0} + m_{D^{*0}}$  was  $\pm 1$  MeV (Hagiwara *et al.*, 2002) and  $\delta m_{00} = (m_{D^0} + m_{D^{*0}}) - M(X(3872)) = -0.9 \pm 1.3$  MeV. The second intriguing feature was the concentration of  $\pi^+\pi^-$  invariant masses near the  $\rho$  meson mass that was a strong indication that the decay violated isospin symmetry in a substantial way (Choi *et al.*, 2003).

Within a few weeks after the Belle results were made public, papers were posted by Tornqvist (2003) and Close and Page (2004) that pointed out that these mass and isospin-breaking properties were characteristic of expectations for a  $D\bar{D}^*$  molecular state. In fact, a  $J^{PC} = 1^{++}$ ,  $D\bar{D}^*$  bound state with mass near 3870 MeV had been predicted (and named) by Tornqvist (1994); inspired by its similarity to the deuteron,

Tornqvist called the state a deuson. As a result, at that time, experimenters and theorists expected that a thorough understanding of the underlying nature of the  $X(3872)$  would be a straightforward exercise and that they could look forward to exploring a rich spectroscopy of related deuson states, in both the charm quark and bottom quark sectors.

However, this optimism turned out to be short lived. As discussed in Sec. V.A, the CDF and D0 groups found the  $X(3872)$  was produced promptly in  $E_{c.m.} = 1.96$  TeV  $p\bar{p}$  annihilations with production cross sections and other characteristics that are similar to those for prompt  $\psi'$  production (Abazov *et al.*, 2004; CDFII Collaboration, 2004), while detailed computations for a loosely bound  $D\bar{D}^*$  composite showed that such similarities were highly unlikely (Bignamini *et al.*, 2009). Also, in the deuson picture, the  $X(3872)$  is primarily a  $D^0\bar{D}^{*0}$  bound state. Searches for other near-threshold  $D\bar{D}^*$  combinations, such as mostly  $D^+D^{*-}$  or  $D^0D^{*-}$  states, with the same  $J^{PC} = 1^{++}$  quantum numbers, came up empty (Aubert *et al.*, 2005b; Choi *et al.*, 2011). Another problem with the deuson idea is the large rate for  $X(3872) \rightarrow \gamma\psi(2S)$  reported by BABAR (Aubert *et al.*, 2009b) and LHCb (Aaij *et al.*, 2014a) [see Eq. (4)], which is expected

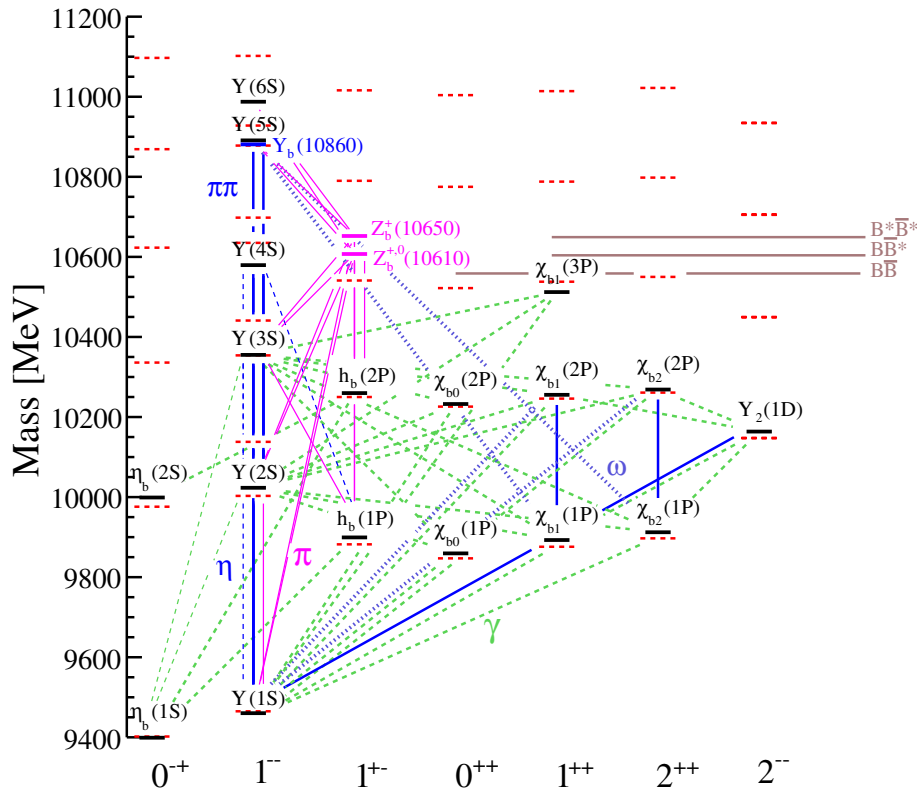


FIG. 61. The current status of the bottomoniumlike spectrum. The dashed (red) lines indicate the expected states and their masses based on recent calculations (Godfrey and Moats, 2015) based on the Godfrey-Isgur relativized potential model (Godfrey and Isgur, 1985). The solid (black) horizontal lines indicate the experimentally established charmonium states, with masses and spin-parity ( $J^{PC}$ ) quantum number assignments from Patrignani *et al.* (2016), and labeled by their spectroscopic assignment. The open-flavor decay channel thresholds are shown with longer solid (brown) horizontal lines. The candidates for exotic bottomoniumlike states are also shown with shorter solid (blue or magenta) horizontal lines with labels reflecting their most commonly used names. The known photon and hadron transitions are also indicated (see the caption of Fig. 60).

for the  $2^3P_1$  charmonium state but counter to predictions for molecules (Swanson, 2004b; Dong *et al.*, 2011).

At present and as pointed out by Braaten and Lu (2007), it seems likely that the  $X(3872)$  is a quantum mechanical mixture of a tightly bound  $c\bar{c}$  core in  $2^3P_1$  configuration and a moleculelike  $D\bar{D}^*$  combination. This idea was verified by detailed computations in Coito, Rupp, and van Beveren (2013) and Takeuchi, Shimizu, and Takizawa (2014); the latter found that the bulk of the  $D\bar{D}^*$  binding comes from the coupling between the  $c\bar{c}$  core and the  $D\bar{D}^*$  components and not much comes from the mutual attraction between the  $D$  and the  $\bar{D}^*$ , which is the key feature of deuson models. In this picture for the  $X(3872)$ , its prompt production in high-energy hadron collisions and radiative decays to the  $\psi'$  proceed via the  $c\bar{c}$  core component of the  $X(3872)$  and, thus, have characteristics that are similar to those expected for the  $\chi'_{c1}$ .

The bulk of the extensive theoretical literature on nonstandard hadrons is on molecular models (Braaten and Kusunoki, 2004; Pakvasa and Suzuki, 2004; Voloshin, 2004; Fleming *et al.*, 2007; Zhu, 2008; Gamermann and Oset, 2009; Molina and Oset, 2009; Zhang, Meng, and Zheng, 2009; Sun *et al.*, 2012; Wang, Hanhart, and Zhao, 2013; Polosa, 2015; Karliner and Rosner, 2016a; Guo *et al.*, 2018). In these, binding is provided by pion- and other light-meson

exchange forces. Since the binding provided by these forces is not expected to be very large, molecular states are expected to be near the masses of their constituent hadrons and have appropriate  $S$ -wave  $J^{PC}$  quantum numbers. This is the case for the  $Z_b(10610)$  and  $Z_b(10650)$ , which are within a few MeV of the  $B\bar{B}^*$  and  $B^*\bar{B}$  thresholds, respectively, and applies reasonably well to the  $Z_c(3900)$  and  $Z_c(4020)$ , which are 24 and 5 MeV above the  $D\bar{D}^*$  and  $D^*\bar{D}$  thresholds, respectively. However, the interpretation of these states as molecules is controversial. Peaks at masses that are slightly above threshold are dangerously similar to expectations for kinematically induced cusps (Bugg, 2011; Blitz and Lebed, 2015; Swanson, 2016) [see Fig. 8(b) and related text]. Anomalous triangle singularities are another mechanism that can produce above-threshold peaks that are not related to a physical resonance (Chen, Liu, and Matsuki, 2013). Moreover, unlike the  $X(3872)$ , no evidence for these states has been found in lattice QCD calculations (Prelovsek and Leskovec, 2013; Prelovsek *et al.*, 2015; Ikeda *et al.*, 2016; Lee *et al.*, 2014). On the other hand, detailed studies of the BESIII's  $Z_c(3900) \rightarrow J/\psi\pi$  and  $D\bar{D}^*$  signals (Guo *et al.*, 2015) and Belle's corresponding  $Z_b$  signals (Albaladejo *et al.*, 2016; Guo *et al.*, 2016; Pilloni *et al.*, 2017) show that the observed peaks can be identified as virtual states with associated poles in the complex scattering  $t$  matrices.



The  $J^P = 1^+ Z(4430)$  (now with a mass near 4478 MeV) has been proposed as a radial excitation of the  $Z_c(3900)$ , in a moleculelike  $D\bar{D}^*(2S)$  configuration (Ma *et al.*, 2014; Barnes, Close, and Swanson, 2015), where the  $D^*(2S)$  is the radial excitation of the  $D^*$ . Although the existence of the  $D^*(2S)$  has not been firmly established, the *BABAR* group reported a strong candidate for this state in the  $D^+\pi^-$  and  $D^{*+}\pi^-$  invariant mass distributions in inclusive  $e^+e^- \rightarrow D^{(*)+}\pi^-X$  reactions at  $E_{\text{c.m.}} = 10.58$  GeV (del Amo Sanchez *et al.*, 2010b); LHCb subsequently reported observations of  $D^{(*)}\pi$  invariant mass structures with peak and width values similar to *BABAR*'s that were produced in high-energy  $pp$  collisions (Aaij *et al.*, 2013d). The averages of the *BABAR* and LHCb mass and width measurements for this state, which is called the  $D_j^*(2600)$ , are  $2622 \pm 12$  MeV and  $104 \pm 20$  MeV, respectively (Patrignani *et al.*, 2016). If we assume  $D^*(2S) = D_j^*(2600)$ , the  $D\bar{D}^*(2S)$  ‘‘threshold’’ is at  $\approx 4490$  MeV, and  $\approx 12$  MeV above the  $Z(4430)$  mass. This association with a radially excited  $D^*$  meson may account for the observed preference for the  $Z(4430)$  to decay to  $\psi(2S)\pi$  over  $J/\psi\pi$  [recall that  $\psi' = \psi(2S)$ ]. The large  $D_j^*(2600)$  width could also explain the large  $Z(4430)$  width, although for such a broad constituent, it is not clear whether the molecular formalism still applies. Also, unlike the  $Z(4430)$  state, the  $Z_c(3900)$  state is not produced in  $B \rightarrow ZK$  decays (Chilikin *et al.*, 2014), which casts doubt on any model in which these two states have essentially the same internal structure, differing only by a radial excitation.

Molecules are not likely explanations for most of the other hidden-charm nonstandard mesons. For example, when the  $Y(4260)$  was first reported by *BABAR* with a mass of  $4259_{-10}^{+8}$  MeV, its interpretation as a  $D\bar{D}_1(2420)$  molecule with a binding energy of  $\approx 25$  MeV might have been plausible (Wang, Hanhart, and Zhao, 2013). But recent high-statistics measurements by BESIII have shown that single resonance fits to the  $Y(4260)$  were naive and the peak is, in fact, best fit by two resonances (see Fig. 33) with masses  $4220 \pm 4$  and  $4320 \pm 13$  MeV (Wang, Hanhart, and Zhao, 2013). This implies that the required  $D\bar{D}_1(2420)$  binding energy for the lower-mass peak would be much higher, at  $\approx 65$  MeV, while the higher-mass state would be unbound by  $\approx 35$  MeV, making a molecular interpretation for either component of this peak implausible.

The only relevant two-particle threshold with  $J^{PC} = 0^{++}$   $S$ -wave quantum numbers that is near the  $X(3915)$  meson is the  $D_s^+D_s^-$  threshold at 3937 MeV. However, since three-pseudoscalar-meson couplings are forbidden by parity plus rotation invariance,  $\pi$ -meson exchange forces, which provide the bulk of the binding for the deuteron, are not applicable.<sup>32</sup> Thus, there is no plausible deusonlike model that can account for the nature of the  $X(3915)$ . Likewise, before the LHCb group established the  $J^{PC}$  of the  $X(4140)$  resonance as  $1^{++}$ , there were a number of suggestions that it was an  $S$ -wave  $D_s^{*+}D_s^{*-}$  molecule ( $2m_{D_s^{*-}} = 4224$  MeV). But an  $S$ -wave  $D_s^{*+}D_s^{*-}$  system can have only  $J^{PC} = 0^{++}$  or  $2^{++}$  [since

$C = (-1)^{L+S}$ ] (Bondar, Mizuk, and Voloshin, 2017). The LHCb measurement (Aaij *et al.*, 2017d) rules out this possibility and, in addition, they reported three additional candidates for  $c\bar{c}s\bar{s}$  states: the  $X(4274)$ ,  $X(4500)$ , and  $X(4700)$ . None of these are close to the thresholds of any  $S$ -wave combinations of  $D_s$  excitations that would reproduce their measured quantum numbers.

Some have suggested that the narrow  $P_c(4450)$  pentaquark might be an  $S$ -wave,  $J^P = 3/2^-$  molecule comprised of a  $\Sigma_c$  baryon and a  $\bar{D}^*$  meson, with a binding energy of  $\approx 13$  MeV (Karliner and Rosner, 2015; Roca, Nieves, and Oset, 2015). This, taken alone, might be a reasonable suggestion. However, if the  $P_c(4450)$  is  $3/2^-$ , the LHCb data indicate that the  $P_c(4380)$  should be  $5/2^+$  (Aaij *et al.*, 2015c). The lightest meson-baryon combinations that can produce spin  $5/2$  in an  $S$  wave are  $p\chi_{c2}$  (for which  $\pi$ -exchange forces are not allowed) and  $\Sigma_c^*\bar{D}^*$ , with mass thresholds that are 115 and 145 MeV above the  $P_c(4380)$  mass, respectively. Moreover, the  $\sim 200$  MeV width of the lower-mass  $P_c(4380)$  state makes it pretty short lived for a molecular state with  $c$  and  $\bar{c}$  spatially separated into two different confining volumes, resulting in a small overlap of its wave function with the  $J/\psi$  state that is produced in its decay (Karliner, 2016). These thresholds are also too high to provide a plausible molecular explanation for the case where the  $J^P = 5/2^\pm$  assignment is associated with the heavier and narrower  $P_c(4450)$  peak. This is not only the case for a bound molecule interpretation, but also for cusp or triangle anomaly mechanisms, which require  $S$ -wave interactions to make significant contributions (Bayar *et al.*, 2016).

Thus, a reasonable conclusion is that while molecule models have relevance for some of the observed candidates, they are not the whole story.

## 2. Diquarks

QCD, which explains the existence of  $q\bar{q}$  mesons and  $qqq$  baryons, also predicts that the short-distance color force between two quarks in an  $S = 0$  diquark antitriplet state [see Fig. 6(b)] is attractive and one-half the strength of the attraction between a quark and an antiquark in a standard meson. Therefore, diquarks and antidiquarks are expected to play a strong role in shaping the spectroscopy of multi-quark hadrons, when pairs of quarks exist inside the confinement volume (Jaffe, 1977a).

Maiani *et al.* (2005) proposed that the  $X(3872)$  is formed from a symmetric combination of an  $S = 0$  and 1 diquark and antidiquark in a relative  $S$  wave:  $[cq]_{S=0}[\bar{c}\bar{q}]_{S=1} + [cq]_{S=1}[\bar{c}\bar{q}]_{S=0}$ , with  $q = u$  or  $d$ . This implies the existence of two nearly degenerate neutral states  $X_h$  and  $X_l$  that are mixtures of  $X_u = [cu][\bar{c}\bar{u}]$  and  $X_d = [cd][\bar{c}\bar{d}]$ , with a mass difference:

$$\begin{aligned} M(X_h) - M(X_l) &= 2(m_d - m_u) / \cos 2\theta \\ &= 7 \pm 2 \text{ MeV} / \cos 2\theta, \end{aligned} \quad (17)$$

where  $\theta$  is the mixing angle. Here an unequal mixture of the two states (i.e.,  $\theta \neq 45^\circ$ ) would generate isospin violation in  $X_h$  and  $X_l$  decays. Tetraquarks made out of diquarks must be compact due to the confinement of color, which naturally can explain the large  $X(3872)$  prompt production rate at hadron

<sup>32</sup>Single-pion exchange between a  $D_s^+$  and  $D_s^-$  violates isospin symmetry.

colliders. Moreover, this model predicted the existence of three additional states: two  $0^{++}$  states with lower-mass values and a  $2^{++}$  state at a higher mass. The production of two neutral  $X(3872)$  states differing in mass by an amount consistent with the Eq. (17) prediction was ruled for high-energy  $p\bar{p}$  production by CDF (Aaltonen *et al.*, 2009b) and for production in  $B$  meson decays by BABAR (Aubert *et al.*, 2008a) and Belle (Choi *et al.*, 2011). Compelling candidates for the predicted  $0^{++}$  and  $2^{++}$  states have yet to be identified. Similar to the case for molecular models, the significant  $X(3872) \rightarrow \gamma\psi(2S)$  rate relative to the  $X(3872) \rightarrow \gamma J/\psi(1S)$  decays is not naturally explained by the tetraquark model, unless it also includes mixing with the  $\chi_{c1}(2P)$  charmonium state or dynamical effects (Brodsky, Hwang, and Lebed, 2014) discussed below. In addition, unlike molecular models, the tetraquark picture does not offer natural explanations for the  $X(3872)$  mass coincidence with the  $D^0\bar{D}^{*0}$  threshold or its very narrow width. The latter led to a hybridized-tetraquark model, which explains the near-threshold states as an interplay between bound molecules and compact tetraquark states (Esposito, Pilloni, and Polosa, 2016).

Diquark interpretations have been proposed to explain most of the observed states. For example, in this model, the  $Y(4260)$  is a symmetric  $[cq]_{S=0}[\bar{c}\bar{q}]_{S=1}$  diquark-diantiquark combination, similar to the  $X(3872)$ , but in a relative  $P$  wave (Maiani *et al.*, 2014). The  $\approx 350$  MeV mass difference between the two states is consistent with the typical mass penalty that is associated with the addition of one unit of orbital angular momentum (see, e.g., Table IV) and the strong  $Y(4260) \rightarrow \gamma X(3872)$  transition reported by BESIII (Ablikim *et al.*, 2014d) would be an allowed electric dipole transition between the two related states (H. X. Chen *et al.*, 2015). Likewise the  $Z_c(3900)$  can be naturally accommodated as the *antisymmetric*,  $S$ -wave  $[cq]_{S=0}[\bar{c}\bar{q}']_{S=1}$  diquark-diantiquark combination, and the  $Z(4430)$  as its first radial excitation. The diquark picture also can explain states that molecular models have trouble with, such as the  $X(3915)$  (Lebed and Polosa, 2016) and the four states seen decaying to  $J/\psi\phi$  (Maiani, Polosa, and Riquer, 2016; Chen *et al.*, 2017), and provide a common origin for the  $P_c(4380)$  and  $P_c(4450)$  pentaquarks that can accommodate their opposite parities (Lebed, 2015; Maiani, Polosa, and Riquer, 2015).

These successes can be attributed to a larger number of degrees of freedom in strong color binding as compared to weak, Yukawa-type exchange forces. Orbital excitations between colored objects can reach higher spin states at lower masses. Slight changes in free parameters that describe the strength of the color forces can shift predicted masses to any value, while molecular models can accommodate structures only near hadron-hadron mass thresholds. However, the free parameters of diquark models are usually readjusted when moving from the description of one exotic hadron system to another, resulting in no single unified diquark model that can describe all of the observed states at once. The universal prediction of large prompt production rates for tightly bound tetraquarks and pentaquarks at hadron colliders is in some conflict with the reality that to date only the  $X(3872)$  and  $X(4140)$  states have been seen in this production mode (Bondar, Mizuk, and Voloshin, 2017).

One problem with the diquark picture is that, since the strong radial color force between the diquark and the diantiquark is universal, it has the same strength for  $q, q' = u, d, s$  independently of their flavor or spin state. Therefore, every successful application of the idea to an experimentally observed state carries with it predictions for a large number of related states that typically are not seen as was the case for the original diquark-diantiquark interpretation of the  $X(3872)$  discussed above. Another problem is that in this picture diquark separations are comparable to the diquark sizes, and there is nothing in the model to prevent fast fall-apart widths to individually confined mesons and baryons, thereby precluding the existence of narrow states.

Brodsky, Hwang, and Lebed (2014) addressed these problems with a scheme that creates separation between diquarks, severely restricts the number of observed states, and suppresses the superfluous ones. Their basic idea, which they call *dynamical diquarks*, is that at production the diquark and diantiquark move rapidly apart, a motion that is opposed by the increasingly stronger confinement force. By the time the motion stops, the diquark-diantiquark separation is large and there is no substantial overlap between the quarks in one and the antiquarks in the other. Hadronization of diquarks separated dynamically by this production mechanism depends on the overlap of the tails of the quark and antiquark wave functions and occurs only if this overlap is well matched to an accessible configuration of final-state hadrons. In this way the process has a complex and intricate dependence on the production mechanism and decay final states that suppresses all the unwanted states. But this comes at the cost of stripping the dynamical diquark picture of virtually all of its ability to predict the existence of additional states.

Baryons with heavy quarks are an interesting testing ground for diquark models. For example, in heavy-light-light-quark baryons, spin couplings of the heavy quark are expected to be suppressed by its heavy mass creating favorable conditions for formation of a light diquark  $[qq]Q$ . Since a good diquark would be in the same color state as  $\bar{q}$ , a mesonlike radial and orbital-angular-momentum excitation spectrum is expected for such a system. The known excitations of charmed and beauty baryons follow these predictions. For example, the LHCb has recently observed five narrow  $\Omega_c$  excitations (Aaij *et al.*, 2017c) that lie in the mass range of  $1P$  and  $2S$  states predicted by diquark models (Ebert, Faustov, and Galkin, 2011; Karliner and Rosner, 2017). Their masses extend to just below  $m_\Xi + m_D$ , which is the threshold for decays that leave the  $ss$  diquark intact. Therefore, their strong decays to  $\Xi_c^+ K^-$  require the disintegration of the  $ss$  diquark, which can explain their narrow widths (0.8–8.7 MeV) in spite of the fact that there is no OZI suppression.

In doubly heavy baryons, the heavy-quark pair is likely to form a diquark  $[QQ]q$  acting like an effective heavy antiquark. Using an approach based on this idea, Karliner and Rosner (2014) predicted with good precision the mass of the  $\Xi_{cc}^{++}$  baryon that was recently observed by LHCb (Aaij *et al.*, 2017e). They have extended this model to predict that the mass of the lightest  $1^+$   $[bb][\bar{u}\bar{d}]$  tetraquark system would be well below the threshold for decays to  $B^- \bar{B}^0 \gamma$  and therefore be stable under strong and electromagnetic decays (Eichten and

Quigg, 2017). The similar  $[bc][\bar{u}\bar{d}]$  tetraquark state is also likely to be stable, while  $[bc][\bar{u}\bar{d}]$  may be right below or right above the  $D^0 D^{*+}$  threshold. Almost the same predictions for these states were obtained a year earlier by Francis *et al.* (2017) employing LQCD calculations with diquark interpolators. Therefore, these are now perhaps the most firm theoretical predictions offering hope for unambiguously establishing the existence of diquark tetraquarks in not too distant future.

### 3. QCD hybrids

The existence of hybrid states is among the most intriguing predictions of QCD. The most striking experimental signature for QCD hybrids is the possible existence of mesons with exotic quantum numbers. However, since all the states discussed in this review have nonexotic quantum numbers, they do not include a smoking-gun candidate for a hybrid state. The state that has been most strongly promoted as a candidate for a  $c\bar{c}$ -gluon charmonium hybrid is the  $1^{--} Y(4260)$  (Close and Page, 2005; Kou and Pene, 2005; Zhu, 2005). However, this assignment is not unique, and this state is also considered to be a good QCD tetraquark candidate. Charmonium hybrids are expected to have strong decays to  $S$ -wave  $D^{(*)}\bar{D}^{**}$  final states, where  $D^{**}$  designates the  $P$ -wave charmed mesons described in Table IV. For the  $Y(4260)$ , the only possible accessible final state of this type would be  $D^*\bar{D}_0^*(2400)$ , where the  $D_0^*(2400)$  is a  $0^{++} D\pi$  resonance with mass and width  $M = 2318 \pm 29$  MeV and  $\Gamma = 267 \pm 40$  MeV. In principle, a high-statistics study of  $Y(4260) \rightarrow D^*\bar{D}\pi$  might see evidence for a  $D^*\bar{D}_0^*$  final state but, since it decays to  $D\pi$  in a  $S$  wave, it would probably be difficult to distinguish from a nonresonant background. As mentioned in Sec. V.C, the latest lattice QCD study of charmonium states has a lowest-mass  $1^{--}$  hybrid candidate at  $M = 4285 \pm 14$  MeV (Liu *et al.*, 2012). This is  $\approx 65$  MeV above the recent BESIII measurement of the  $Y(4260)$  mass ( $4220 \pm 4$  MeV). However, given that the LQCD calculations are missing simulations of couplings to the available decay channels, this difference should probably be considered small.

### 4. Hadrocharmonium

In the hadrocharmonium model, the strong preference for the  $Y(4260)$  [ $Y(4360)$ ] meson to decay to  $\pi^+\pi^-J/\psi$  ( $\pi^+\pi^-\psi'$ ) over the fall-apart  $D^{(*)}\bar{D}^{(*)}$  modes is accommodated by a meson structure that contains a color-singlet charmonium-state core surrounded by a light-quark excitation (Dubynskiy and Voloshin, 2008). In the case of the  $Y(4260)$  [ $Y(4360)$ ], this core state was taken to be the  $J/\psi$  ( $\psi'$ ). Since the  $J/\psi$  ( $\psi'$ ) state is present in its constituents, the  $Y(4260)$  [ $Y(4360)$ ] naturally prefers to decay to final states that include it. However this model had trouble with BESIII observations of substantial rates for  $Y(4260)$  and  $Y(4360)$  decays to  $\pi^+\pi^-h_c$  final states (Ablikim *et al.*, 2013b). In the  $J/\psi$  and  $\psi'$ , the  $c$  and  $\bar{c}$  quarks are in a spin-triplet state, while in the  $h_c$  they are in a spin-singlet. By themselves, the triplet and singlet cores cannot mix and a hadrocharmonium state should have strong rates for decays to one of them, but not both. In an attempt to fix this problem, the model was revised to include

two hadrocharmonium states, one with a spin-triplet core and one with a spin-singlet core, and these two states mix, producing the observed  $Y(4260)$  and  $Y(4360)$ , which now can both decay to singlet and triplet states with relative rates determined by the (unspecified) mixing angle (Li and Voloshin, 2014). But, subsequent to the appearance of this modification to the model, the BESIII group found that in the two resonance  $Y(4260) \rightarrow \pi^+\pi^-J/\psi$  structure shown in Fig. 33 (Ablikim *et al.*, 2017c), both resonant components have strong decay rates to  $\pi^+\pi^-J/\psi$ , while the latest BESIII  $\pi^+\pi^-h_c$  cross-section measurements (Ablikim *et al.*, 2017a), shown in Fig. 34, find a strong  $\pi^+\pi^-h_c$  decay rate for the lower-mass resonant component, but no signal for the higher-mass component. Even with the mixing, the hadrocharmonium model will have a hard time reproducing this decay pattern.

### 5. Kinematically induced resonancelike peaks

As mentioned in the discussion of molecular models, some have suggested that the  $Z_c$  and  $Z_b$  peaks are due to kinematic effects caused by the nearby  $D^{(*)}\bar{D}^*$  and  $B^{(*)}\bar{B}^*$  mass thresholds (Bugg, 2011; Chen, Liu, and Matsuki, 2013; Blitz and Lebed, 2015; Swanson, 2016). Others claim that the same data show that the peaks are associated with poles in the corresponding  $D^{(*)}\bar{D}^*$  or  $B^{(*)}\bar{B}^*$  scattering  $t$  matrix and, therefore, qualify as genuine physical states (Guo *et al.*, 2015, 2016). This seems to be a controversy that only more and higher-precision data can resolve. For example, although both mechanisms produce strong phase motion that can be displayed in Argand plots, the detailed mass dependence of this phase motion is distinctly different for the two models. Another suggestion requires the application of sophisticated coupled-channel data analysis techniques (Pilloni *et al.*, 2017). However, distinguishing between the two scenarios with either method will require large data samples, with increases over existing data sets by factors that approach 2 orders of magnitude. This would require at least a year-long dedicated BESIII run at energies near the  $Y(4260)$  peak and a long period of BelleII operation at the  $Y(10860)$  peak.

### 6. Comments

At this point, the challenges posed by the observed heavy quarkoniumlike states with unusual properties have not been answered well by any theory for hadronic states.

In general the successful theoretical work in this area has been reactive rather than predictive. Different approaches have had some success for some states but fail or are not applicable to others. This could be because the nonstandard hadrons that are observed are due to a variety of different, unrelated mechanisms, or that the actual underlying mechanism has not yet been discovered. The lack of good understanding of the nature of these states sheds doubt into our understanding of hadronic structures in general. Open-flavor thresholds in light hadron spectroscopy are usually right above the ground states of such systems and whatever mechanisms that are in play for above-open-flavor-threshold heavy quarkoniumlike hadrons are likely having a strong influence on light hadron spectroscopy.

More theoretical and experimental work is required in all areas of hadron spectroscopy to overcome this crisis.

## B. Experiment

To date, the progress in the field has mainly been driven by experiments. Even though Tornqvist proposed the existence of a  $J^{PC} = 1^{++}$  state with mass near the  $D\bar{D}^*$  threshold ten years before its discovery (Tornqvist, 1994), the  $X(3872)$ 's narrow width, close proximity to the  $D^0\bar{D}^{*0}$ , large isospin violation, and its strong production in  $B$ -meson decays and high-energy  $p\bar{p}$  collisions were surprises. Likewise, the discovery of the  $Y(4260)$  as a large peak in the  $e^+e^- \rightarrow \pi^+\pi^-J/\psi$  cross section with no hints of a corresponding signal in the open-charmed-meson channel was totally unexpected. Subsequent discoveries, in both the  $c$ -quark and  $b$ -quark sectors, were similarly unanticipated. New developments in this field have closely tracked increases in the size and improvements in the quality of the available data samples plus advances in the sophistication of analysis techniques. The discovery of the  $P_c(4380)$  and  $P_c(4450)$  pentaquarks was possible because of the unprecedentedly large sample of  $\Lambda_b$  decays that was accumulated by the LHCb experiment. Likewise, the two-resonance structure of the  $Y(4260)$  was seen by BESIII only because they had a larger data sample and better mass resolution than the earlier measurements. The clear demonstration of BW-amplitude-like phase motion for the  $Z(4430)$  meson and the  $P_c(4450)$  pentaquark was the result of complex, multidimensional amplitude analyses.

There are large differences in what we know about various candidate states. For some, such as the  $X(3872)$  and the  $Y(4260)$ , we know the quantum numbers and a number of decay modes, while for others we do not even know their quantum numbers. Even the ones with a lot of available information have important pieces of information that are unknown. For example, we still do not know the natural width of the  $X(3872)$  or whether its mass is above or below the  $m_{D^0} + m_{D^{*0}}$  mass threshold. We have not seen phase motion for the  $Y(4260)$ , or convincing phase motion for the  $P_c(4380)$ . While we learned a great deal about the nature of the  $X(3872)$  from the fact that it is produced promptly in high-energy  $p\bar{p}$  and  $pp$  collisions, we have only limited information about prompt hadroproduction of other states.

For experimental reasons, most of the states seen so far were first discovered in decay modes that include a  $J/\psi$  or a  $\psi'$  as the final state. Future experiments that access pairs of open-charm or beauty particles may uncover interesting dimensions of this spectroscopy that might give important clues about the underlying dynamics.

In addition to finding new states, it would be useful if our level of knowledge of all of the candidate states could be brought to the same high level as the currently best known ones. For example, multidimensional amplitude analyses of  $B \rightarrow KJ/\psi\omega$  and  $K\chi_{c1}\pi$  are needed to establish the  $J^{PC}$  quantum numbers of the  $X(3915)$ , and the  $Z(4050)^+$  and  $Z(4250)^+$ .

Fortunately there are powerful experiments that are currently running and producing important and unique results. For example,  $B \rightarrow K\chi_{c1}\pi$  and  $KJ/\psi\omega$  are accessible to the LHCb even with their existing data sample. Their recent discoveries of  $J/\psi\phi$  mesons and  $P_c$  pentaquarks were based

on analyses of their  $3\text{ fb}^{-1}$  run-I data sample that was accumulated at  $E_{\text{c.m.}}(pp) = 7$  and 8 TeV. In run II, which is now underway and will finish in 2018, they will accumulate an additional  $8\text{ fb}^{-1}$  at  $E_{\text{c.m.}}(pp) = 13$  TeV. Since the  $b$ -quark production cross section at 13 TeV is about twice that at 7 TeV (Aaij *et al.*, 2017b), the run-II data set will be equivalent to approximately 5 times that for run I. Thus, we can anticipate the discovery of additional states and significant improvements of existing results, including substantial improvements in the precision of the  $Z(4430)$  and  $P_c$  Argand plots. A LHCb detector upgrade in 2021 will enable it to accumulate higher luminosities. After that they expect that the total data sample accumulated by 2030 will be  $50\text{ fb}^{-1}$  [collected at  $E_{\text{c.m.}}(pp) = 14$  TeV]. The LHCb Collaboration is also discussing a major detector or luminosity upgrade after 2030 with an ultimate goal of  $300\text{ fb}^{-1}$ . Even larger integrated luminosities will be collected at the LHC by the CMS and ATLAS detectors. Therefore, it is expected that these experiments will also continue to contribute to advances in exotic hadron spectroscopy in spite of their lack of hadron identification and their more restrictive triggers.

BESIII is planning long data runs in the  $Y(4260)$  peak region during the next few years, and these should provide sufficient data to support studies of the phase motion across the  $Z_c$  peaks in  $Y(4260) \rightarrow \pi^+\pi^-J/\psi$  and  $\pi^+\pi^-h_c$  decay channels and enable amplitude analyses of  $Y(4260) \rightarrow \pi D^{(*)}\bar{D}^*$  decays. Long-term future BESIII running plans include high luminosity scans over the  $2m_D \leq E_{\text{c.m.}}(e^+e^-) \leq 2m_{\Lambda_c} + 50$  MeV range to completely map out  $c$ -quark production in the threshold region in a large assortment of decay channels.

The BelleII experiment will start physics operation in late 2017. The first year of running will be used to develop experience with machine operations without either the inner pixel or the silicon-strip vertex detector in place. Since this configuration has limited capabilities for doing  $B$ -meson physics, which is the main motivation for the project, operation at the  $Y(10860)$  and higher energies for detailed studies of the  $Z_b$  mesons and searches for possible additional states is planned (Bondar, Mizuk, and Voloshin, 2017). Over the anticipated ten-year operational lifetime of BelleII, a total data sample of  $50\text{ ab}^{-1}$  will be accumulated, mostly at  $E_{\text{c.m.}}(e^+e^-) = 10.58$  GeV. Thus, the final BelleII data sample will be a factor of 50 larger than the Belle data set. The strengths of BelleII, i.e., superior photon,  $\pi^0$ ,  $\omega$ , and  $\eta^{(\prime)}$  detection capabilities and higher absolute reconstruction efficiencies, are complementary to those of LHCb. High reconstruction efficiencies are especially essential for studies of  $D_{(s)}^{(*)}\bar{D}_{(s)}^{(*)}$  systems. In addition, the  $B$ -factory environment provides a unique opportunity for making precise measurements of inclusive branching fractions such as  $B^+ \rightarrow K^+ X_{c\bar{c}}$ ;  $X_{c\bar{c}} \rightarrow \text{anything}$  decays (Aubert *et al.*, 2006b), where  $X_{c\bar{c}}$  designates relatively narrow charmoniumlike states such as the  $X(3872)$  or  $X(3915)$ . Inclusive branching fractions are required input for converting product branching fraction and total width measurements into decay partial width values, which are usually the theoretically relevant quantities.

There are several current and future medium-energy experiments designed to explore nonstandard hadrons and

to provide information on the properties of the still enigmatic states complementary to  $e^+e^-$  and hadron-collider experiments.

The PANDA experiment (Lutz *et al.*, 2009) at the Facility for Antiproton and Ion Research in Germany, expected to start data taking in 2022, will study particles produced in collisions of an intense, nearly monoenergetic beam of antiprotons with nucleons or nuclei in the c.m. energy range from 2.5 to 5.5 GeV. By performing a mass scan in several steps across the  $X(3872)$  resonance, PANDA will measure the resonance line shape that is sensitive to the binding mechanism with an accuracy an order of magnitude better than currently available. To resolve the nature of the  $D_{s0}^*(2317)$ , PANDA will do precise measurements of its total width and branching fractions to different decay channels. The  $p\bar{p}$  initial state will provide access to possible states with exotic quantum numbers. Lattice QCD indicates that the lightest exotic  $c\bar{c}$  hybrid with  $J^{PC} = 1^{-+}$  has a mass that is near 4.2 GeV (Liu *et al.*, 2012) and will be accessible at PANDA.

Discovery and studies of properties of hybrid mesons are the primary goals of the GlueX (Al Gholul *et al.*, 2016) and CLAS12 (Burkert, 2008) photoproduction experiments at the Jefferson National Accelerator Facility (JLab). Soon after the discovery of the LHCb pentaquark candidates, it was suggested (Kubarovsky and Voloshin, 2015; Wang, Liu, and Zhao, 2015; Hiller Blin *et al.*, 2016; Karliner and Rosner, 2016b) that photoproduction on a nucleon would be a promising way to search for these states and to study their properties. Recently, a proposal (Meziani *et al.*, 2016) to study photoproduction of  $J/\psi$  near threshold in search for the  $P_c$  states was approved by JLab and designated as a “high-impact” activity.

### C. Final remark

The heavy-flavor, nonstandard hadrons discussed in this review have severely challenged existing ideas about the underlying structure of hadrons. The puzzles that they pose have intrigued theorists in both the particle and nuclear physics communities and experimenters at all of the world’s particle physics accelerator facilities. While they do not challenge QCD as the exact theory of strong interactions, they expose the phenomenological disconnect between its Lagrangian and types of structures it can produce at large distances, with possible implications to strongly coupled theories proposed as extensions of the standard model. Often in the history of physics, puzzles and their eventual resolution have produced important advances in our understanding of nature. We hope that this will ultimately be the case for the issues that are discussed here.

### ACKNOWLEDGMENTS

This work was supported by the Korean Ministry of Education, Science and Technology under Project Code IBS-R016-D1 and by the National Science Foundation (USA) Award No. 1507572. We thank Steven Gottlieb for reading the manuscript and providing a number of useful comments.

### REFERENCES

- Aaboud, M., *et al.* (ATLAS Collaboration), 2017, *J. High Energy Phys.* **01**, 117.
- Aad, G., *et al.* (ATLAS Collaboration), 2008, *J. Instrum.* **3**, S08003.
- Aad, G., *et al.* (ATLAS Collaboration), 2015, *Phys. Lett. B* **740**, 199.
- Aaij, R., *et al.* (LHCb Collaboration), 2012a, *Eur. Phys. J. C* **72**, 1972.
- Aaij, R., *et al.* (LHCb Collaboration), 2012b, *Phys. Rev. D* **85**, 091103.
- Aaij, R., *et al.* (LHCb Collaboration), 2013a, *Phys. Rev. Lett.* **110**, 222001.
- Aaij, R., *et al.* (LHCb Collaboration), 2013b, *Nucl. Phys. B* **867**, 547.
- Aaij, R., *et al.* (LHCb Collaboration), 2013c, *J. High Energy Phys.* **12**, 090.
- Aaij, R., *et al.* (LHCb Collaboration), 2013d, *J. High Energy Phys.* **09**, 145.
- Aaij, R., *et al.* (LHCb Collaboration), 2014a, *Nucl. Phys. B* **886**, 665.
- Aaij, R., *et al.* (LHCb Collaboration), 2014b, *Phys. Rev. Lett.* **112**, 222002.
- Aaij, R., *et al.* (LHCb Collaboration), 2015a, *Int. J. Mod. Phys. A* **30**, 1530022.
- Aaij, R., *et al.* (LHCb Collaboration), 2015b, *Phys. Rev. D* **92**, 112009.
- Aaij, R., *et al.* (LHCb Collaboration), 2015c, *Phys. Rev. Lett.* **115**, 072001.
- Aaij, R., *et al.* (LHCb Collaboration), 2015d, *Phys. Rev. D* **92**, 011102.
- Aaij, R., *et al.* (LHCb Collaboration), 2016a, *Phys. Rev. Lett.* **117**, 082002.
- Aaij, R., *et al.* (LHCb Collaboration), 2016b, *Phys. Rev. Lett.* **117**, 152003.
- Aaij, R., *et al.* (LHCb Collaboration), 2016c, *Phys. Rev. Lett.* **117**, 082003; **117**, 109902(E) (2016).
- Aaij, R., *et al.* (LHCb Collaboration), 2016d, *J. High Energy Phys.* **03**, 159; 2016, 09, 13(E).
- Aaij, R., *et al.* (LHCb Collaboration), 2017a, *Phys. Rev. D* **95**, 012002.
- Aaij, R., *et al.* (LHCb Collaboration), 2017b, *Phys. Rev. Lett.* **118**, 052002.
- Aaij, R., *et al.* (LHCb Collaboration), 2017c, *Phys. Rev. Lett.* **118**, 182001.
- Aaij, R., *et al.* (LHCb Collaboration), 2017d, *Phys. Rev. Lett.* **118**, 022003.
- Aaij, R., *et al.* (LHCb Collaboration), 2017e, *Phys. Rev. Lett.* **119**, 112001.
- Aaltonen, T., *et al.* (CDF Collaboration), 2009a, *Phys. Rev. Lett.* **102**, 242002.
- Aaltonen, T., *et al.* (CDF Collaboration), 2009b, *Phys. Rev. Lett.* **103**, 152001.
- Aaltonen, T., *et al.* (CDF Collaboration), 2017, *Mod. Phys. Lett. A* **32**, 1750139.
- Abashian, A., *et al.*, 2002, *Nucl. Instrum. Methods Phys. Res., Sect. A* **479**, 117.
- Abazov, V. M., *et al.* (D0 Collaboration), 2004, *Phys. Rev. Lett.* **93**, 162002.
- Abazov, V. M., *et al.* (D0 Collaboration), 2014, *Phys. Rev. D* **89**, 012004.
- Abazov, V. M., *et al.* (D0 Collaboration), 2015, *Phys. Rev. Lett.* **115**, 232001.
- Abazov, V. M., *et al.* (D0 Collaboration), 2016, *Phys. Rev. Lett.* **117**, 022003.
- Abe, K., *et al.* (Belle Collaboration), 2004, *Phys. Rev. D* **69**, 112002.

- Abe, K., *et al.* (Belle Collaboration), 2005, in Lepton and photon interactions at high energies. Proceedings, 22nd International Symposium, LP 2005, Uppsala, Sweden, [arXiv:hep-ex/0505037](https://arxiv.org/abs/hep-ex/0505037).
- Abe, K., *et al.* (Belle Collaboration), 2007, *Phys. Rev. Lett.* **98**, 082001.
- Abe, T., *et al.* (Belle-II Collaboration), 2010, [arXiv:1011.0352](https://arxiv.org/abs/1011.0352).
- Ablikim, M., *et al.* (BES Collaboration), 2008, *Phys. Lett. B* **660**, 315.
- Ablikim, M., *et al.* (BESIII Collaboration), 2010, *Nucl. Instrum. Methods Phys. Res., Sect. A* **614**, 345.
- Ablikim, M., *et al.* (BESIII Collaboration), 2012, *Phys. Rev. D* **86**, 071101.
- Ablikim, M., *et al.* (BESIII Collaboration), 2013a, *Phys. Rev. Lett.* **110**, 252001.
- Ablikim, M., *et al.* (BESIII Collaboration), 2013b, *Phys. Rev. Lett.* **111**, 242001.
- Ablikim, M., *et al.* (BESIII Collaboration), 2014a, *Phys. Rev. Lett.* **112**, 132001.
- Ablikim, M., *et al.* (BESIII Collaboration), 2014b, *Phys. Rev. Lett.* **112**, 022001.
- Ablikim, M., *et al.* (BESIII Collaboration), 2014c, *Phys. Rev. Lett.* **113**, 212002.
- Ablikim, M., *et al.* (BESIII Collaboration), 2014d, *Phys. Rev. Lett.* **112**, 092001.
- Ablikim, M., *et al.* (BESIII Collaboration), 2015a, *Phys. Rev. D* **91**, 032002.
- Ablikim, M., *et al.* (BESIII Collaboration), 2015b, *Phys. Rev. D* **92**, 092006.
- Ablikim, M., *et al.* (BESIII Collaboration), 2015c, *Phys. Rev. D* **91**, 112005.
- Ablikim, M., *et al.* (BESIII Collaboration), 2015d, *Phys. Rev. Lett.* **115**, 182002.
- Ablikim, M., *et al.* (BESIII Collaboration), 2015e, *Phys. Rev. Lett.* **115**, 222002.
- Ablikim, M., *et al.* (BESIII Collaboration), 2015f, *Phys. Rev. Lett.* **115**, 112003.
- Ablikim, M., *et al.* (BESIII Collaboration), 2015g, *Phys. Rev. Lett.* **114**, 092003.
- Ablikim, M., *et al.* (BESIII Collaboration), 2017a, *Phys. Rev. Lett.* **118**, 092002.
- Ablikim, M., *et al.* (BESIII Collaboration), 2017b, *Phys. Rev. D* **96**, 032004.
- Ablikim, M., *et al.* (BESIII Collaboration), 2017c, *Phys. Rev. Lett.* **118**, 092001.
- Abrams, G. S., *et al.*, 1974, *Phys. Rev. Lett.* **33**, 1453.
- Abulencia, A., *et al.* (CDF Collaboration), 2006, *Phys. Rev. Lett.* **96**, 102002.
- Achasov, N. N., A. V. Kiselev, and G. N. Shestakov, 2008, *Nucl. Phys. B, Proc. Suppl.* **181–182**, 169.
- Acosta, D., *et al.* (CDF Collaboration), 2004, *Phys. Rev. Lett.* **93**, 072001.
- Adachi, I., *et al.* (Belle Collaboration), 2012, *Phys. Rev. Lett.* **108**, 032001.
- Adam, J., *et al.* (ALICE Collaboration), 2016a, *Phys. Lett. B* **754**, 360.
- Adam, J., *et al.* (ALICE Collaboration), 2016b, *Phys. Rev. C* **93**, 024917.
- Albaladejo, M., F.-K. Guo, C. Hidalgo-Duque, and J. Nieves, 2016, *Phys. Lett. B* **755**, 337.
- Albuquerque, R. M., M. E. Bracco, and M. Nielsen, 2009, *Phys. Lett. B* **678**, 186.
- Al Ghoul, H., *et al.* (GlueX), 2016, *AIP Conf. Proc.* **1735**, 020001.
- Ali, A., C. Hambroek, I. Ahmed, and M. J. Aslam, 2010, *Phys. Lett. B* **684**, 28.
- Ali, A., J. S. Lange, and S. Stone, 2017, *Prog. Part. Nucl. Phys.* **97**, 123.
- Ali, A., L. Maiani, A. D. Polosa, and V. Riquer, 2015, *Phys. Rev. D* **91**, 017502.
- Alvarez-Ruso, L., 2010, in *Dressing hadrons. Proceedings, Mini-Workshop, Bled, Slovenia*, pp. 1–8, [arXiv:1011.0609](https://arxiv.org/abs/1011.0609).
- Alves, Jr., A. A., *et al.* (LHCb Collaboration), 2008, *J. Instrum.* **3**, S08005.
- Andrews, D., *et al.* (CLEO Collaboration), 1980, *Phys. Rev. Lett.* **44**, 1108.
- Anisovich, V. V., M. A. Matveev, A. V. Sarantsev, and A. N. Semanova, 2015, *Int. J. Mod. Phys. A* **30**, 1550186.
- Aoki, S., *et al.* (PACS-CS Collaboration), 2009, *Phys. Rev. D* **79**, 034503.
- Appelquist, T., and H. D. Politzer, 1975, *Phys. Rev. Lett.* **34**, 43.
- Artoisenet, P., and E. Braaten, 2010, *Phys. Rev. D* **81**, 114018.
- Aubert, B., *et al.* (BABAR Collaboration), 2002, *Nucl. Instrum. Methods Phys. Res., Sect. A* **479**, 1.
- Aubert, B., *et al.* (BABAR Collaboration), 2005a, *Phys. Rev. Lett.* **95**, 142001.
- Aubert, B., *et al.* (BABAR Collaboration), 2005b, *Phys. Rev. D* **71**, 031501.
- Aubert, B., *et al.* (BABAR Collaboration), 2005c, *Phys. Rev. D* **71**, 071103.
- Aubert, B., *et al.* (BABAR Collaboration), 2005d, *Phys. Rev. D* **71**, 052001.
- Aubert, B., *et al.* (BABAR Collaboration), 2006a, *Phys. Rev. D* **74**, 032007.
- Aubert, B., *et al.* (BABAR Collaboration), 2006b, *Phys. Rev. Lett.* **96**, 052002.
- Aubert, B., *et al.* (BABAR Collaboration), 2006c, *Phys. Rev. D* **74**, 071101.
- Aubert, B., *et al.* (BABAR Collaboration), 2006d, *Phys. Rev. D* **74**, 011103.
- Aubert, B., *et al.* (BABAR Collaboration), 2007, *Phys. Rev. Lett.* **98**, 212001.
- Aubert, B., *et al.* (BABAR Collaboration), 2008a, *Phys. Rev. D* **77**, 111101.
- Aubert, B., *et al.* (BABAR Collaboration), 2008b, *Phys. Rev. Lett.* **101**, 082001.
- Aubert, B., *et al.* (BABAR Collaboration), 2008c, *Phys. Rev. D* **77**, 011102.
- Aubert, B., *et al.* (BABAR Collaboration), 2009a, *Phys. Rev. D* **79**, 112004.
- Aubert, B., *et al.* (BABAR Collaboration), 2009b, *Phys. Rev. Lett.* **102**, 132001.
- Aubert, B., *et al.* (BABAR Collaboration), 2009c, *Phys. Rev. D* **79**, 112001.
- Aubert, B., *et al.* (BABAR Collaboration), 2010, *Phys. Rev. D* **81**, 092003.
- Aubert, J. J., *et al.* (E598 Collaboration), 1974, *Phys. Rev. Lett.* **33**, 1404.
- Aubin, C., C. Bernard, C. DeTar, J. Osborn, S. Gottlieb, E. B. Gregory, D. Toussaint, U. M. Heller, J. E. Hetrick, and R. Sugar, 2004, *Phys. Rev. D* **70**, 094505.
- Augustin, J. E., *et al.*, 1974, *Phys. Rev. Lett.* **33**, 1406.
- Augustin, J. E., *et al.*, 1975, *Phys. Rev. Lett.* **34**, 764.
- Aushev, T., *et al.*, 2010a, [arXiv:1002.5012](https://arxiv.org/abs/1002.5012).
- Aushev, T., *et al.* (Belle Collaboration), 2010b, *Phys. Rev. D* **81**, 031103.
- Aushev, T., *et al.* (Belle Collaboration), 2010c, *Phys. Rev. D* **81**, 031103.

- Bacci, C., *et al.*, 1981, *Nucl. Phys. B* **184**, 31.
- Bai, J. Z., *et al.* (BES Collaboration), 2000, *Phys. Rev. Lett.* **84**, 594.
- Bai, J. Z., *et al.* (BES Collaboration), 2002, *Phys. Rev. Lett.* **88**, 101802.
- Bala, A., *et al.* (Belle Collaboration), 2015, *Phys. Rev. D* **91**, 051101.
- Bander, M., G. L. Shaw, P. Thomas, and S. Meshkov, 1976, *Phys. Rev. Lett.* **36**, 695.
- Bardeen, W. A., H. Fritzsch, and M. Gell-Mann, 1972, in *Topical Meeting on the Outlook for Broken Conformal Symmetry in Elementary Particle Physics Frascati, Italy*, arXiv:hep-ph/0211388.
- Barnes, T., F. E. Close, and H. J. Lipkin, 2003, *Phys. Rev. D* **68**, 054006.
- Barnes, T., F. E. Close, and E. S. Swanson, 2015, *Phys. Rev. D* **91**, 014004.
- Barnes, T., S. Godfrey, and E. S. Swanson, 2005, *Phys. Rev. D* **72**, 054026.
- Bauer, G. (CDF Collaboration), 2005, *Int. J. Mod. Phys. A* **20**, 3765.
- Bayar, M., F. Aceti, F.-K. Guo, and E. Oset, 2016, *Phys. Rev. D* **94**, 074039.
- Bazavov, A., *et al.* (MILC Collaboration), 2010, *Rev. Mod. Phys.* **82**, 1349.
- Bediaga, I., *et al.* (LHCb Collaboration), 2012, “Framework TDR for the LHCb Upgrade: Technical Design Report,” Reports No. CERN-LHCC-2012-007, and No. LHCb-TDR-12.
- Benayoun, M., L. DelBuono, S. Eidelman, V. N. Ivanchenko, and H. B. O’Connell, 1999, *Phys. Rev. D* **59**, 114027.
- Beneke, M., G. Buchalla, M. Neubert, and C. T. Sachrajda, 1999, *Phys. Rev. Lett.* **83**, 1914.
- Berezhnoy, A. V., and A. K. Likhoded, 2004, *Yad. Fiz.* **67**, 778 [*Phys. At. Nucl.* **67**, 757 (2004)].
- Bernard, C., *et al.* (Fermilab Lattice, MILC Collaborations), 2011, *Phys. Rev. D* **83**, 034503.
- Besson, D., *et al.* (CLEO Collaboration), 1985, *Phys. Rev. Lett.* **54**, 381.
- Besson, D., *et al.* (CLEO Collaboration), 2003, *Phys. Rev. D* **68**, 032002; **75**, 119908(E) (2007).
- Bevan, A. J., *et al.* (Belle, BABAR Collaborations), 2014, *Eur. Phys. J. C* **74**, 3026.
- Bhardwaj, V., *et al.* (Belle Collaboration), 2011, *Phys. Rev. Lett.* **107**, 091803.
- Bicudo, P., K. Cichy, A. Peters, and M. Wagner, 2016, *Phys. Rev. D* **93**, 034501.
- Bietenholz, W., *et al.*, 2011, *Phys. Rev. D* **84**, 054509.
- Bignamini, C., B. Grinstein, F. Piccinini, A. D. Polosa, and C. Sabelli, 2009, *Phys. Rev. Lett.* **103**, 162001.
- Blitz, S. H., and R. F. Lebed, 2015, *Phys. Rev. D* **91**, 094025.
- Blum, T., *et al.*, 2013, in *Community Summer Study 2013: Snowmass on the Mississippi (CSS2013)* Minneapolis, MN, arXiv:1310.6087.
- Bodwin, G. T., E. Braaten, T. C. Yuan, and G. P. Lepage, 1992, *Phys. Rev. D* **46**, R3703.
- Bodwin, G. T., J. Lee, and E. Braaten, 2003, *Phys. Rev. Lett.* **90**, 162001.
- Bondar, A., *et al.* (Belle Collaboration), 2012, *Phys. Rev. Lett.* **108**, 122001.
- Bondar, A. E., A. Garmash, A. I. Milstein, R. Mizuk, and M. B. Voloshin, 2011, *Phys. Rev. D* **84**, 054010.
- Bondar, A. E., R. V. Mizuk, and M. B. Voloshin, 2017, *Mod. Phys. Lett. A* **32**, 1750025.
- Bondar, A. E., *et al.* (Charm-Tau Factory), 2013, *Yad. Fiz.* **76**, 1132 [*Phys. At. Nucl.* **76**, 1072 (2013)].
- Borsanyi, S., *et al.*, 2015, *Science* **347**, 1452.
- Braaten, E., 2013, *Phys. Rev. Lett.* **111**, 162003.
- Braaten, E., and H. W. Hammer, 2006, *Phys. Rep.* **428**, 259.
- Braaten, E., and M. Kusunoki, 2004, *Phys. Rev. D* **69**, 114012.
- Braaten, E., C. Langmack, and D. H. Smith, 2014, *Phys. Rev. D* **90**, 014044.
- Braaten, E., and M. Lu, 2007, *Phys. Rev. D* **76**, 094028.
- Bracco, M. E., A. Lozea, R. D. Matheus, F. S. Navarra, and M. Nielsen, 2005, *Phys. Lett. B* **624**, 217.
- Brambilla, N., A. Pineda, J. Soto, and A. Vairo, 2000, *Nucl. Phys. B* **566**, 275.
- Brambilla, N., *et al.*, 2011, *Eur. Phys. J. C* **71**, 1534.
- Brambilla, N., *et al.*, 2014, *Eur. Phys. J. C* **74**, 2981.
- Branz, T., T. Gutsche, and V. E. Lyubovitskij, 2009, *Phys. Rev. D* **80**, 054019.
- Briceno, R. A., J. J. Dudek, and R. D. Young, 2017, arXiv:1706.06223.
- Briceno, R. A., M. T. Hansen, and S. R. Sharpe, 2016, *Proc. Sci. LATTICE2016*, 115.
- Brodsky, S. J., D. S. Hwang, and R. F. Lebed, 2014, *Phys. Rev. Lett.* **113**, 112001.
- Brodzicka, J., 2009, *Conf. Proc.* **C0908171**, 299.
- Browder, T. E., S. Pakvasa, and A. A. Petrov, 2004, *Phys. Lett. B* **578**, 365.
- Bugg, D. V., 2011, *Europhys. Lett.* **96**, 11002.
- Burkert, V. D., 2008, in *CLAS 12 RICH Detector Workshop* Jefferson Lab, Newport News, Virginia, arXiv:0810.4718.
- Burns, T. J., and E. S. Swanson, 2016, *Phys. Lett. B* **760**, 627.
- Capstick, S., and N. Isgur, 1986, *Phys. Rev. D* **34**, 2809.
- CDFII Collaboration, 2004, “The lifetime distribution of  $X(3872)$  mesons produced in  $p\bar{p}$  collisions at CDF,” CDF note 7159.
- Chao, K.-T., 2008, *Phys. Lett. B* **661**, 348.
- Chatrchyan, S., *et al.* (CMS Collaboration), 2008, *J. Instrum.* **3**, S08004.
- Chatrchyan, S., *et al.* (CMS Collaboration), 2013a, *J. High Energy Phys.* **04**, 154.
- Chatrchyan, S., *et al.* (CMS Collaboration), 2013b, *Phys. Lett. B* **727**, 57.
- Chatrchyan, S., *et al.* (CMS Collaboration), 2014, *Phys. Lett. B* **734**, 261.
- Chen, D.-Y., 2016, *Eur. Phys. J. C* **76**, 671.
- Chen, D.-Y., X. Liu, and T. Matsuki, 2013, *Phys. Rev. D* **88**, 036008.
- Chen, H. X., L. Maiani, A. D. Polosa, and V. Riquer, 2015, *Eur. Phys. J. C* **75**, 550.
- Chen, H.-X., W. Chen, X. Liu, and S.-L. Zhu, 2016, *Phys. Rep.* **639**, 1.
- Chen, H.-X., E.-L. Cui, W. Chen, X. Liu, and S.-L. Zhu, 2017, *Eur. Phys. J. C* **77**, 160.
- Chen, K. F., *et al.* (Belle Collaboration), 2008, *Phys. Rev. Lett.* **100**, 112001.
- Chen, K. F., *et al.* (Belle Collaboration), 2010, *Phys. Rev. D* **82**, 091106.
- Chen, X., X. Lu, R. Shi, and X. Guo, 2015, arXiv:1512.06483.
- Cheng, H.-Y., and W.-S. Hou, 2003, *Phys. Lett. B* **566**, 193.
- Chilikin, K., *et al.* (Belle Collaboration), 2013, *Phys. Rev. D* **88**, 074026.
- Chilikin, K., *et al.* (Belle Collaboration), 2014, *Phys. Rev. D* **90**, 112009.
- Chilikin, K., *et al.* (Belle Collaboration), 2017, *Phys. Rev. D* **95**, 112003.
- Chistov, R., *et al.* (Belle Collaboration), 2006, *Phys. Rev. Lett.* **97**, 162001.
- Choi, S. K., *et al.* (Belle Collaboration), 2003, *Phys. Rev. Lett.* **91**, 262001.
- Choi, S.-K., *et al.* (Belle Collaboration), 2005, *Phys. Rev. Lett.* **94**, 182002.

- Choi, S. K., *et al.* (Belle Collaboration), 2008, *Phys. Rev. Lett.* **100**, 142001.
- Choi, S. K., *et al.*, 2011, *Phys. Rev. D* **84**, 052004.
- Choi, S. K., *et al.* (Belle Collaboration), 2015, *Phys. Rev. D* **91**, 092011; **92**, 039905(E) (2015).
- Christ, N. H., C. Dawson, T. Izubuchi, C. Jung, Q. Liu, R. D. Mawhinney, C. T. Sachrajda, A. Soni, and R. Zhou, 2010, *Phys. Rev. Lett.* **105**, 241601.
- Cichy, K., M. Kalinowski, and M. Wagner, 2016, *Phys. Rev. D* **94**, 094503.
- Close, F. E., and R. H. Dalitz, 1980, in *Workshop on Low-energy and Intermediate-energy Kaon-Nucleon Physics Rome, Italy*, p. 411.
- Close, F. E., and P. R. Page, 2004, *Phys. Lett. B* **578**, 119.
- Close, F. E., and P. R. Page, 2005, *Phys. Lett. B* **628**, 215.
- Coan, T. E., *et al.* (CLEO Collaboration), 2006, *Phys. Rev. Lett.* **96**, 162003.
- Coito, S., G. Rupp, and E. van Beveren, 2013, *Eur. Phys. J. C* **73**, 2351.
- Coleman, S., and R. E. Norton, 1965, *Nuovo Cimento* **38**, 438.
- Coleman, S. R., and S. L. Glashow, 1961, *Phys. Rev. Lett.* **6**, 423.
- Criegee, L., and G. Knies, 1982, *Phys. Rep.* **83**, 151.
- del Amo Sanchez, P., *et al.* (BABAR Collaboration), 2010a, *Phys. Rev. D* **82**, 011101.
- del Amo Sanchez, P., *et al.* (BABAR Collaboration), 2010b, *Phys. Rev. D* **82**, 111101.
- De Rujula, A., H. Georgi, and S. L. Glashow, 1977, *Phys. Rev. Lett.* **38**, 317.
- Diakonov, D., V. Petrov, and M. V. Polyakov, 1997, *Z. Phys. A* **359**, 305.
- Ding, G.-J., 2009a, *Phys. Rev. D* **79**, 014001.
- Ding, G.-J., 2009b, *Eur. Phys. J. C* **64**, 297.
- Dong, Y., A. Faessler, T. Gutsche, and V. E. Lyubovitskij, 2011, *J. Phys. G* **38**, 015001.
- Drenska, N. V., R. Faccini, and A. D. Polosa, 2009, *Phys. Rev. D* **79**, 077502.
- Dubynskiy, S., A. Gorsky, and M. B. Voloshin, 2009, *Phys. Lett. B* **671**, 82.
- Dubynskiy, S., and M. B. Voloshin, 2008, *Phys. Lett. B* **666**, 344.
- Dudek, J. J., R. G. Edwards, B. Joo, M. J. Peardon, D. G. Richards, and C. E. Thomas, 2011, *Phys. Rev. D* **83**, 111502.
- Durr, S., *et al.*, 2008, *Science* **322**, 1224.
- Dzierba, A. R., C. A. Meyer, and A. P. Szczepaniak, 2005, *J. Phys. Conf. Ser.* **9**, 192.
- Ebert, D., R. N. Faustov, and V. O. Galkin, 2011, *Phys. Rev. D* **84**, 014025.
- Eichten, E., K. Gottfried, T. Kinoshita, K. D. Lane, and T.-M. Yan, 1978, *Phys. Rev. D* **17**, 3090; **21**, 313(E) (1980).
- Eichten, E. J., K. Lane, and C. Quigg, 2004, *Phys. Rev. D* **69**, 094019.
- Eichten, E. J., K. Lane, and C. Quigg, 2006, *Phys. Rev. D* **73**, 014014; **73**, 079903(E) (2006).
- Eichten, E. J., and C. Quigg, 2017, [arXiv:1707.09575](https://arxiv.org/abs/1707.09575).
- Engel, G., C. Lang, D. Mohler, and A. Schaefer, 2013, *Phys. Rev. D* **87**, 074504.
- Esposito, A., A. L. Guerrieri, L. Maiani, F. Piccinini, A. Pilloni, A. D. Polosa, and V. Riquer, 2015, *Phys. Rev. D* **92**, 034028.
- Esposito, A., A. L. Guerrieri, F. Piccinini, A. Pilloni, and A. D. Polosa, 2015, *Int. J. Mod. Phys. A* **30**, 1530002.
- Esposito, A., A. L. Guerrieri, and A. Pilloni, 2015, *Phys. Lett. B* **746**, 194.
- Esposito, A., A. Pilloni, and A. D. Polosa, 2016, *Phys. Lett. B* **758**, 292.
- Esposito, A., A. Pilloni, and A. D. Polosa, 2017, *Phys. Rep.* **668**, 1.
- Faustov, R., and V. Galkin, 2015, *Phys. Rev. D* **92**, 054005.
- Feldman, G. J., *et al.*, 1975, *Phys. Rev. Lett.* **35**, 821; **35**, 1184(E) (1975).
- Fernandez-Ramirez, C., I. V. Danilkin, D. M. Manley, V. Mathieu, and A. P. Szczepaniak, 2016, *Phys. Rev. D* **93**, 034029.
- Finazzo, S. I., M. Nielsen, and X. Liu, 2011, *Phys. Lett. B* **701**, 101.
- Fleming, S., M. Kusunoki, T. Mehen, and U. van Kolck, 2007, *Phys. Rev. D* **76**, 034006.
- Francis, A., R. J. Hudspith, R. Lewis, and K. Maltman, 2017, *Phys. Rev. Lett.* **118**, 142001.
- Gamermann, D., and E. Oset, 2009, *Phys. Rev. D* **80**, 014003.
- Garmash, A., *et al.* (Belle Collaboration), 2015, *Phys. Rev. D* **91**, 072003.
- Garmash, A., *et al.* (Belle Collaboration), 2016, *Phys. Rev. Lett.* **116**, 212001.
- Gell-Mann, M., 1964, *Phys. Lett.* **8**, 214.
- Godfrey, S., and N. Isgur, 1985, *Phys. Rev. D* **32**, 189.
- Godfrey, S., and K. Moats, 2015, *Phys. Rev. D* **92**, 054034.
- Godfrey, S., and K. Moats, 2016, *Phys. Rev. D* **93**, 034035.
- Gokhroo, G., *et al.* (Belle Collaboration), 2006, *Phys. Rev. Lett.* **97**, 162002.
- Greenberg, O. W., 1964, *Phys. Rev. Lett.* **13**, 598.
- Gregory, E. B., A. C. Irving, C. M. Richards, and C. McNeile (UKQCD Collaboration), 2012, *Phys. Rev. D* **86**, 014504.
- Gregory, E. B., *et al.*, 2011, *Phys. Rev. D* **83**, 014506.
- Gross, D. J., and F. Wilczek, 1973, *Phys. Rev. Lett.* **30**, 1343.
- Gu, P. D., Y. Luo, Q. Qin, J. Q. Wang, S. Wang, G. Xu, and C. H. Yu, 2003, *ICFA Beam Dyn. Newslett.* **31**, 32 [[http://icfa-usa.jlab.org/archive/newsletter/icfa\\_bd\\_nl\\_31.pdf](http://icfa-usa.jlab.org/archive/newsletter/icfa_bd_nl_31.pdf)].
- Guo, F. K., C. Hanhart, Yu. S. Kalashnikova, P. Matuschek, R. V. Mizuk, A. V. Nefediev, Q. Wang, and J. L. Wynen, 2016, *Phys. Rev. D* **93**, 074031.
- Guo, F.-K., C. Hanhart, U.-G. Meißner, Q. Wang, Q. Zhao, and B.-S. Zou, 2018, following article, *Rev. Mod. Phys.* **90**, 015004.
- Guo, F.-K., C. Hanhart, Q. Wang, and Q. Zhao, 2015, *Phys. Rev. D* **91**, 051504.
- Guo, F.-K., and U.-G. Meißner, 2012, *Phys. Rev. D* **86**, 091501.
- Guo, F.-K., U.-G. Meißner, and B.-S. Zou, 2016, *Commun. Theor. Phys.* **65**, 593.
- Guo, P., T. Yépez-Martínez, and A. P. Szczepaniak, 2014, *Phys. Rev. D* **89**, 116005.
- Hagiwara, K., *et al.* (Particle Data Group), 2002, *Phys. Rev. D* **66**, 010001.
- Han, M. Y., and Y. Nambu, 1965, *Phys. Rev.* **139**, B1006.
- Hansen, M. T., and S. R. Sharpe, 2014, *Phys. Rev. D* **90**, 116003.
- Hansen, M. T., and S. R. Sharpe, 2015, *Phys. Rev. D* **92**, 114509.
- He, J., and X. Liu, 2011, [arXiv:1102.1127](https://arxiv.org/abs/1102.1127).
- He, Q., *et al.* (CLEO Collaboration), 2006, *Phys. Rev. D* **74**, 091104.
- Herb, S. W., *et al.*, 1977, *Phys. Rev. Lett.* **39**, 252.
- Hicks, K. H., 2012, *Eur. Phys. J. H* **37**, 1.
- Hiller Blin, A. N., C. Fernández-Ramírez, A. Jackura, V. Mathieu, V. I. Mokeev, A. Pilloni, and A. P. Szczepaniak, 2016, *Phys. Rev. D* **94**, 034002.
- Horn, D., and J. Mandula, 1978, *Phys. Rev. D* **17**, 898.
- Hou, W.-S., 2006, *Phys. Rev. D* **74**, 017504.
- Iizuka, J., 1966, *Prog. Theor. Phys. Suppl.* **37**, 21.
- Ikeda, Y., S. Aoki, T. Doi, S. Gongyo, T. Hatsuda, T. Inoue, T. Iritani, N. Ishii, K. Murano, and K. Sasaki (HAL QCD Collaboration), 2016, *Phys. Rev. Lett.* **117**, 242001.
- Isgur, N., R. Kokoski, and J. Paton, 1985, *Phys. Rev. Lett.* **54**, 869.
- Isgur, N., and J. E. Paton, 1983, *Phys. Lett. B* **124**, 247.
- Jaffe, R. L., 1977a, *Phys. Rev. D* **15**, 267.
- Jaffe, R. L., 1977b, *Phys. Rev. D* **15**, 281.



- Jaffe, R. L., 2005, *Phys. Rep.* **409**, 1.
- Jegerlehner, F., and A. Nyffeler, 2009, *Phys. Rep.* **477**, 1.
- Jones, L. W., 1977, *Rev. Mod. Phys.* **49**, 717.
- Juge, K. J., J. Kuti, and C. J. Morningstar, 1999, *Phys. Rev. Lett.* **82**, 4400.
- Jurik, N. P., 2016, "Observation of  $J/\psi$  p resonances consistent with pentaquark states in  $\Lambda_b^0 \rightarrow J/\psi K^- p$  decays," Ph.D. thesis (Syracuse University).
- Karliner, M., 2016, *Acta Phys. Pol. B* **47**, 117.
- Karliner, M., and H. J. Lipkin, 2008, [arXiv:0802.0649](https://arxiv.org/abs/0802.0649).
- Karliner, M., and J. L. Rosner, 2014, *Phys. Rev. D* **90**, 094007.
- Karliner, M., and J. L. Rosner, 2015, *Phys. Rev. Lett.* **115**, 122001.
- Karliner, M., and J. L. Rosner, 2016a, *Nucl. Phys. A* **954**, 365.
- Karliner, M., and J. L. Rosner, 2016b, *Phys. Lett. B* **752**, 329.
- Karliner, M., and J. L. Rosner, 2017, *Phys. Rev. D* **95**, 114012.
- Kobayashi, M., and T. Maskawa, 1973, *Prog. Theor. Phys.* **49**, 652.
- Kou, E., and O. Pene, 2005, *Phys. Lett. B* **631**, 164.
- Krokovny, P., *et al.* (Belle Collaboration), 2003, *Phys. Rev. Lett.* **91**, 262002.
- Krokovny, P., *et al.* (Belle Collaboration), 2013, *Phys. Rev. D* **88**, 052016.
- Kronfeld, A. S., 2012, *Annu. Rev. Nucl. Part. Sci.* **62**, 265.
- Kubarovsky, V., and M. B. Voloshin, 2015, *Phys. Rev. D* **92**, 031502.
- Kurokawa, S., and E. Kikutani, 2003, *Nucl. Instrum. Methods Phys. Res., Sect. A* **499**, 1.
- Landau, L. D., 1959, *Nucl. Phys.* **13**, 181.
- Lang, C. B., D. Mohler, and S. Prelovsek, 2016, *Phys. Rev. D* **94**, 074509.
- Lebed, R. F., 2015, *Phys. Lett. B* **749**, 454.
- Lebed, R. F., R. E. Mitchell, and E. S. Swanson, 2017, *Prog. Part. Nucl. Phys.* **93**, 143.
- Lebed, R. F., and A. D. Polosa, 2016, *Phys. Rev. D* **93**, 094024.
- Lee, S.-H., C. Detar, D. Mohler, and H. Na (Fermilab Lattice, MILC), 2014, *Proc. Sci. LATTICE2014*, 125.
- Lees, J. P., *et al.* (BABAR Collaboration), 2012a, *Phys. Rev. D* **85**, 052003.
- Lees, J. P., *et al.* (BABAR Collaboration), 2012b, *Phys. Rev. D* **86**, 051102.
- Lees, J. P., *et al.* (BABAR Collaboration), 2012c, *Phys. Rev. D* **86**, 072002.
- Lees, J. P., *et al.* (BABAR Collaboration), 2014, *Phys. Rev. D* **89**, 111103.
- Lees, J. P., *et al.* (BABAR Collaboration), 2015, *Phys. Rev. D* **91**, 012003.
- Leskovec, L., C. B. Lang, D. Mohler, S. Prelovsek, and R. M. Woloshyn, 2015, in 27th International Symposium on Lepton Photon Interactions at High Energy (LP15) Ljubljana, Slovenia, [arXiv:1511.04140](https://arxiv.org/abs/1511.04140).
- Li, B.-Q., and K.-T. Chao, 2009, *Phys. Rev. D* **79**, 094004.
- Li, B.-Q., C. Meng, and K.-T. Chao, 2009, *Phys. Rev. D* **80**, 014012.
- Li, X., and M. B. Voloshin, 2014, *Mod. Phys. Lett. A* **29**, 1450060.
- Li, X., and M. B. Voloshin, 2015, *Phys. Rev. D* **91**, 114014.
- Link, J. M., *et al.* (FOCUS Collaboration), 2004, *Phys. Lett. B* **586**, 11.
- Litke, A., *et al.* (Mark I Collaboration), 1973, *Phys. Rev. Lett.* **30**, 1189.
- Liu, L., G. Moir, M. Peardon, S. M. Ryan, C. E. Thomas, P. Vilaseca, J. J. Dudek, R. G. Edwards, B. Joo, and D. G. Richards (Hadron Spectrum), 2012, *J. High Energy Phys.* **07** 126.
- Liu, X., 2009, *Phys. Lett. B* **680**, 137.
- Liu, X., and H.-W. Ke, 2009, *Phys. Rev. D* **80**, 034009.
- Liu, X., Z.-G. Luo, Y.-R. Liu, and S.-L. Zhu, 2009, *Eur. Phys. J. C* **61**, 411.
- Liu, X., and S.-L. Zhu, 2009, *Phys. Rev. D* **80**, 017502.
- Liu, X.-H., M. Oka, and Q. Zhao, 2016, *Phys. Lett. B* **753**, 297.
- Liu, Y.-R., X. Liu, W.-Z. Deng, and S.-L. Zhu, 2008, *Eur. Phys. J. C* **56**, 63.
- Liu, Z. Q., *et al.* (Belle Collaboration), 2013, *Phys. Rev. Lett.* **110**, 252002.
- Loring, U., B. C. Metsch, and H. R. Petry, 2001, *Eur. Phys. J. A* **10**, 447.
- Lu, Q.-F., and Y.-B. Dong, 2016, *Phys. Rev. D* **94**, 074007.
- Luscher, M., 1991, *Nucl. Phys. B* **354**, 531.
- Lutz, M. F. M., *et al.* (PANDA Collaboration), 2009, [arXiv:0903.3905](https://arxiv.org/abs/0903.3905).
- Lyons, L., 1981, *Prog. Part. Nucl. Phys.* **7**, 157.
- Ma, L., X.-H. Liu, X. Liu, and S.-L. Zhu, 2014, *Phys. Rev. D* **90**, 037502.
- Mahajan, N., 2009, *Phys. Lett. B* **679**, 228.
- Maiani, L., F. Piccinini, A. D. Polosa, and V. Riquer, 2004, *Phys. Rev. Lett.* **93**, 212002.
- Maiani, L., F. Piccinini, A. D. Polosa, and V. Riquer, 2005, *Phys. Rev. D* **71**, 014028.
- Maiani, L., F. Piccinini, A. D. Polosa, and V. Riquer, 2014, *Phys. Rev. D* **89**, 114010.
- Maiani, L., A. D. Polosa, and V. Riquer, 2015, *Phys. Lett. B* **749**, 289.
- Maiani, L., A. D. Polosa, and V. Riquer, 2016, *Phys. Rev. D* **94**, 054026.
- Manohar, A. V., and M. B. Wise, 1993, *Nucl. Phys. B* **399**, 17.
- Manohar, A. V., and M. B. Wise, 2000, Cambridge Monogr. Part. Phys., Nucl. Phys., Cosmol. **10**, 1 [<http://inspirehep.net/record/538478/>].
- Mattson, M., *et al.* (SELEX Collaboration), 2002, *Phys. Rev. Lett.* **89**, 112001.
- Melde, T., W. Plessas, and B. Sengl, 2008, *Phys. Rev. D* **77**, 114002.
- Meyer, C. A., and E. S. Swanson, 2015, *Prog. Part. Nucl. Phys.* **82**, 21.
- Meyer, C. A., and Y. Van Haarlem, 2010, *Phys. Rev. C* **82**, 025208.
- Meziani, Z. E., *et al.*, 2016, [arXiv:1609.00676](https://arxiv.org/abs/1609.00676).
- Mizuk, R., *et al.* (Belle Collaboration), 2008, *Phys. Rev. D* **78**, 072004.
- Mizuk, R., *et al.* (Belle Collaboration), 2009, *Phys. Rev. D* **80**, 031104.
- Mohler, D., and R. M. Woloshyn, 2011, *Phys. Rev. D* **84**, 054505.
- Molina, R., and E. Oset, 2009, *Phys. Rev. D* **80**, 114013.
- Montanet, L., *et al.* (Particle Data Group) 1994, *Phys. Rev. D* **50**, 1173.
- Nakano, T., *et al.* (LEPS Collaboration), 2003, *Phys. Rev. Lett.* **91**, 012002.
- Necco, S., and R. Sommer, 2002, *Nucl. Phys. B* **622**, 328.
- Ocherashvili, A., *et al.* (SELEX Collaboration), 2005, *Phys. Lett. B* **628**, 18.
- Ohnishi, Y., *et al.*, 2013, *Prog. Theor. Exp. Phys.* **2013**, 03A011.
- Okubo, S., 1963, *Phys. Lett.* **5**, 165.
- Olive, K., *et al.* (Particle Data Group), 2014, *Chin. Phys. C* **38**, 090001.
- Olsen, S. L., 2015, *Phys. Rev. D* **91**, 057501.
- Orginos, K., and D. Richards, 2015, *J. Phys. G* **42**, 034011.
- Ortega, P. G., J. Segovia, D. R. Entem, and F. Fernández, 2016, *Phys. Rev. D* **94**, 114018.
- Padmanath, M., C. B. Lang, and S. Prelovsek, 2015, *Phys. Rev. D* **92**, 034501.
- Page, P. R., E. S. Swanson, and A. P. Szczepaniak, 1999, *Phys. Rev. D* **59**, 034016.

- Pakhlov, P., and T. Uglov, 2015, *Phys. Lett. B* **748**, 183.
- Pakhlov, P., *et al.* (Belle Collaboration), 2008, *Phys. Rev. Lett.* **100**, 202001.
- Pakhlov, P., *et al.* (Belle Collaboration), 2009, *Phys. Rev. D* **79**, 071101.
- Pakhlova, G., *et al.* (Belle Collaboration), 2008, *Phys. Rev. Lett.* **101**, 172001.
- Pakvasa, S., and M. Suzuki, 2004, *Phys. Lett. B* **579**, 67.
- Patrignani, C., *et al.* (Particle Data Group), 2016, *Chin. Phys. C* **40**, 100001.
- Pendlebury, J. M., *et al.*, 2015, *Phys. Rev. D* **92**, 092003.
- PEP-II, 1993, Reports No. SLAC-418, No. LBL-PUB-5379, No. CALT-68-1869, No. UCRL-ID-114055, and No. UCIRPA-93-01.
- Pilloni, A., C. Fernandez-Ramirez, A. Jackura, V. Mathieu, M. Mikhasenko, J. Nys, and A. P. Szczepaniak (JPAC Collaboration), 2017, *Phys. Lett. B* **772**, 200.
- Politzer, H. D., 1973, *Phys. Rev. Lett.* **30**, 1346.
- Polosa, A. D., 2015, *Phys. Lett. B* **746**, 248.
- Prelovsek, S., C. B. Lang, L. Leskovec, and D. Mohler, 2015, *Phys. Rev. D* **91**, 014504.
- Prelovsek, S., and L. Leskovec, 2013, *Phys. Lett. B* **727**, 172.
- Rice, E., *et al.*, 1982, *Phys. Rev. Lett.* **48**, 906.
- Roca, L., J. Nieves, and E. Oset, 2015, *Phys. Rev. D* **92**, 094003.
- Rosner, J. L., *et al.* (CLEO Collaboration), 2005, *Phys. Rev. Lett.* **95**, 102003.
- Santel, D., *et al.* (Belle Collaboration), 2016, *Phys. Rev. D* **93**, 011101.
- Santopinto, E., and J. Ferretti, 2015, *Phys. Rev. C* **92**, 025202.
- Schmid, C., 1967, *Phys. Rev.* **154**, 1363.
- Schnedermann, E., J. Sollfrank, and U. W. Heinz, 1993, *Phys. Rev. C* **48**, 2462.
- Schumacher, R. A., 2006, *AIP Conf. Proc.* **842**, 409.
- Shen, C., *et al.* (Belle Collaboration), 2010, *Phys. Rev. Lett.* **104**, 112004.
- Shen, C.-P., 2010, *Chin. Phys. C* **34**, 615.
- Sirunyan, A. M., *et al.* (CMS Collaboration), 2017, Report No. CMS-PAS-BPH-16-002 [arXiv:1712.06144].
- Stancu, F., 2010, *J. Phys. G* **37**, 075017.
- Sun, Z.-F., X. Liu, M. Nielsen, and S.-L. Zhu, 2012, *Phys. Rev. D* **85**, 094008.
- Suzuki, M., 2005, *Phys. Rev. D* **72**, 114013.
- Swanson, E. S., 2004a, *Phys. Lett. B* **598**, 197.
- Swanson, E. S., 2004b, *Phys. Lett. B* **588**, 189.
- Swanson, E. S., 2006, *Phys. Rep.* **429**, 243.
- Swanson, E. S., 2015, *Phys. Rev. D* **91**, 034009.
- Swanson, E. S., 2016, *Int. J. Mod. Phys. E* **25**, 1642010.
- Szczepaniak, A. P., 2015, *Phys. Lett. B* **747**, 410.
- Szczepaniak, A. P., 2016, *Phys. Lett. B* **757**, 61.
- Takeuchi, S., K. Shimizu, and M. Takizawa, 2014, *Prog. Theor. Exp. Phys.* **2014**, 123D01; **2015**, 079203(E) (2015).
- Terasaki, K., 2003, *Phys. Rev. D* **68**, 011501.
- Terasaki, K., 2004, “Charmed scalar mesons and related,” arXiv: hep-ph/0405146.
- 't Hooft, G., G. Isidori, L. Maiani, A. D. Polosa, and V. Riquer, 2008, *Phys. Lett. B* **662**, 424.
- Tornqvist, N. A., 1994, *Z. Phys. C* **61**, 525.
- Tornqvist, N. A., 2003, arXiv:hep-ph/0308277.
- Tornqvist, N. A., 2004, *Phys. Lett. B* **590**, 209.
- Trippe, T. G., *et al.* (Particle Data Group) 1976, *Rev. Mod. Phys.* **48**, S1; **48**, 497(E) (1976).
- Uehara, S., *et al.* (Belle Collaboration), 2006, *Phys. Rev. Lett.* **96**, 082003.
- Uehara, S., *et al.* (Belle Collaboration), 2010, *Phys. Rev. Lett.* **104**, 092001.
- Ueno, K., *et al.*, 1979, *Phys. Rev. Lett.* **42**, 486.
- Vinokurova, A., *et al.* (Belle Collaboration), **2015**, *J. High Energy Phys.* **06**, 132.
- Voloshin, M. B., 2004, *Phys. Lett. B* **579**, 316.
- Voloshin, M. B., and L. B. Okun, 1976, *Pis'ma Zh. Eksp. Teor. Fiz.* **23**, 369 [ [http://www.jetpletters.ac.ru/ps/1801/article\\_27526.pdf](http://www.jetpletters.ac.ru/ps/1801/article_27526.pdf)] [*JETP Lett.* **23**, 333 (1976)].
- Wagner, M., S. Diehl, T. Kuske, and J. Weber, 2013, “An introduction to lattice hadron spectroscopy for students without quantum field theoretical background,” arXiv:1310.1760.
- Wang, H., Y. Yang, and J. Ping, 2014, *Eur. Phys. J. A* **50**, 76.
- Wang, Q., C. Hanhart, and Q. Zhao, 2013, *Phys. Rev. Lett.* **111**, 132003.
- Wang, Q., X.-H. Liu, and Q. Zhao, 2015, *Phys. Rev. D* **92**, 034022.
- Wang, X. L., *et al.* (Belle Collaboration), 2007, *Phys. Rev. Lett.* **99**, 142002.
- Wang, X. L., *et al.* (Belle Collaboration), 2015, *Phys. Rev. D* **91**, 112007.
- Wang, Z.-G., 2009, *Eur. Phys. J. C* **63**, 115.
- Wang, Z.-G., Z.-C. Liu, and X.-H. Zhang, 2009, *Eur. Phys. J. C* **64**, 373.
- Wang, Z.-G., and Y.-F. Tian, 2015, *Int. J. Mod. Phys. A* **30**, 1550004.
- Weinstein, J. D., and N. Isgur, 1982, *Phys. Rev. Lett.* **48**, 659.
- Wilczek, F., 2015, *Nature (London)* **520**, 303.
- Wilson, K. G., 1974, *Phys. Rev. D* **10**, 2445.
- Wilczek, F., 2016, “Power Over Nature,” [http://www.edge.org/conversation/frank\\_wilczek-power-over-nature](http://www.edge.org/conversation/frank_wilczek-power-over-nature).
- Yang, Z., Q. Wang, and U.-G. Meissner, 2017, *Phys. Lett. B* **767**, 470.
- Yao, W.-M., *et al.*, 2006, *J. Phys. G* **33**, 1.
- Yuan, C. Z., *et al.* (Belle Collaboration), 2007, *Phys. Rev. Lett.* **99**, 182004.
- Zhang, J.-R., and M.-Q. Huang, 2010, *J. Phys. G* **37**, 025005.
- Zhang, O., C. Meng, and H. Q. Zheng, 2009, *Phys. Lett. B* **680**, 453.
- Zhao, Z., L. Luo, B. Zhang, and W. Xu, 2016, “Preliminary Concept and Key Technologies of HIEPA Accelerator,” *Proceedings of the 7th International Particle Accelerator Conference, (IPAC 2016): Busan, Korea* (CERN, Geneva, Switzerland).
- Zhou, Z.-Y., Z. Xiao, and H.-Q. Zhou, 2015, *Phys. Rev. Lett.* **115**, 022001.
- Zhu, S.-L., 2005, *Phys. Lett. B* **625**, 212.
- Zhu, S.-L., 2008, *Int. J. Mod. Phys. E* **17**, 283.
- Zieminska, D., *et al.* (D0 Collaboration), 2017, “Confirmation of the  $X(5568)$  with the semileptonic decay of  $B_s^0$ ,” D0 Note 6496-CONF.
- Zweig, G., 1964, “An  $SU_3$  model for strong interaction symmetry and its breaking,” Report No. CERN-TH-401.